WhiB-like developmental proteins and their iron-sulfur cluster dependent protein-protein interactions

A thesis submitted in part fulfilment for the degree of Doctor

of Philosophy.

2021

Melissa Y. Y. Stewart

University of East Anglia

Department of Chemistry

Declaration

I declare that the work contained in this thesis, submitted by me for the degree of Doctor of Philosophy, is my own original work, except where due reference is made to other authors, and has not been previously submitted by me for a degree at this or any other university.

Melissa Stewart

December 2020

Acknowledgements

Firstly, and most importantly I would like to thank my supervisor Prof. Nick Le Brun for all your support, mentoring and endless enthusiasm over the last four challenging, but thoroughly enjoyable years. I must also thank the members of my supervisory team at the John Innes Centre, Prof. Mark Buttner and Dr Matt Bush, who never failed to leave me full of new ideas and directions after each catch up. I would also like to thank the Norwich Research Park Doctoral Training Partnership and the BBSRC for this experience and for funding over the last 4 years.

For experiments, I am grateful to Dr Myles Cheesman for access to the CD spectrometer, Dr Nick Watmough for access to stopped flow instrumentation, Dr Matt Bush for help with EMSA experiments. Thank you also to Prof. Juan Fontecilla-Camps and Dr Yvain Nicolet for kindly hosting me in Grenoble, and Clara Rinaldi for helping me give crystallography a go.

A huge thank you to the residents of 2.24 for being so supportive and making every day entertaining, Dr Sophie Bennett, Lizzie Gray, Sam Piper, Dr Leon Jenner, Dr Justin Bradley and especially to Dr Jason Crack, for your patience, approachability and for knowing everything about everything.

Lastly, the warmest thank you to my family. Mum and dad for all your love and support. 我还要感谢的是我的爸爸及爷爷奶奶，你们为我的学习给予了巨大的鼓励和支持! And my favourite person, Edward, thank you for everything you do and for encouraging and supporting me every single day.

Abstract

WhiB-like (Wbl) proteins are iron-sulfur (Fe-S) cluster proteins unique to Actinobacteria. This work reports the characterisation of developmental Wbl proteins from *Streptomyces Venezuelae,* WhiB (*Sv*WhiB) and WhiD (*Sv*WhiD), along with biophysical studies of their iron- sulfur clusters and their protein-protein interactions. Like several Wbl proteins previously characterised, both *Sv*WhiB and *Sv*WhiD bind a [4Fe-4S] cluster that is sensitive to O_2, and, of the two the [4Fe-4S] *Sv*WhiB is particularly fragile. Both proteins also showed a distinctive high sensitivity to nitric oxide (NO). Kinetic studies revealed that *Sv*WhiD reacts in a concerted manner with ~9 NO per cluster. Characterisation studies also revealed that *Sv*WhiD exists in a monomer-dimer equilibrium associated with its unusual C-terminal extension. The mechanisms by which Wbl proteins function as transcriptional regulators has yet to be clearly demonstrated. In some cases, at least, this occurs via an interaction with another protein. Both *Sv*WhiB and *Sv*WhiD interact with domain 4 of the principal sigma factor of *Streptomyces*, σ^{HrdB} ($\sigma^{HrdB}{}_4$). Non-denaturing ESI-MS experiments was used to determine the dissociation constant (K_d) for the *Sv*WhiD-$\sigma^{HrdB}{}_4$ complex as ~0.7 µM, consistent with a relatively tight binding interaction. The complex formation was cluster dependent and a reaction with NO, which was complete at 8-10 NO molecules per cluster, resulted in dissociation of the Wbl: $\sigma^{HrdB}{}_4$ into the separate proteins. The *Sv*WhiD [4Fe-4S] cluster was significantly less sensitive to reaction with O_2 and NO when *Sv*WhiD was bound to $\sigma^{HrdB}{}_4$, consistent with protection of the cluster in the complex.

An interaction unique to WhiB is via a (non-Wbl) transcription factor called WhiA. Characterisation studies showed both *S. venezuelae* and *S. coelicolor* WhiA bind zinc, and that the zinc-bound form of *Sv*WhiA was responsible for direct interactions with DNA. *In vitro* EMSA studies confirmed direct binding of *Sv*WhiA to DNA, but also revealed the previously unobserved direct binding of *Sv*WhiB to the promoter regions of genes involved in sporulation initiation.

The additional study of an iron-sulfur cluster transcriptional regulator focused on RirA (Rhizobial iron regulator A), a global iron regulator in *Rhizobium*. RirA coordinates a [4Fe-4S] cluster via three conserved cysteines and has been shown to sense iron via a labile

fourth iron. An N8D RirA variant was generated based on the sequence of the previously structurally characterised NsrR, in which the fourth ligand is an aspartate residue. Strikingly, the N8D variant was found to have lost its iron sensing abilities but exhibited increased cluster stability in the presence of oxygen when compared to wild type RirA.

Contents

List of Figures

List of Tables

Abbreviations

Abs, A	Absorbance
Amp	Ampicillin
CD	Circular Dichroism
ChIP-seq	Chromatin Immunoprecipitation Sequencing
Da (kDa)	Dalton (kilodalton)
DNA	Deoxyribonucleic acid
DNIC	Dinitrosyl iron complex
DTT	Dithiothreitol
ε	Extinction coefficience (M^{-1} cm^{-1})
EDTA	Ethylenediaminetetraacetic acid
EMSA	Electromobility shift assay
EPR	Electron paramagnetic resonance
ESI-MS	Electrospray ionization mass spectroscopy
FAM	6-carboxyfluorescein
Fe	Iron
Fe-S	Iron-sulfur
FNR	Fumarate and nitrate reduction (regulator)
HEPES	4-(2-hydroxyethyl)-1-piperazineethanesulfonic acid
IPTG	Isopropyl-β-D-galactoside
IscR	Iron-sulfur cluster Regulator
Kan	Kanamycin

K_d	Dissociation constant
L (µL, mL)	Litre (microlitre, millilitre)
LB	Lysogeny broth
LC-MS	Liquid chromatography mass spectrometry
m (nm, µm, mm, cm)	Metre (nanometre, micrometre, millimetre, centimetre)
M (nM, µM, mM)	Mole (nanomole, micromole, millimole)
MS	Mass spectroscopy
Mw	Molecular weight
NsrR	Nitric oxide sensitive response regulator
NO	Nitric oxide
OD	Optical density
RBS	Roussin's Black Salt
RirA	Rhizobial iron regulator A
RNA	Ribonucleic acid
RNAP	Ribonucleic acid polymerase
Rpm	Revolutions per minute
RRE	Roussin's red ester
SDS-PAGE	Sodium dodecyl sulphate - polyacrylamide gel electrophoresis
TEMED	N,N,N',N'-tetra-methyl-ethylenediamine
Tris	Tris(hydroxymethyl)aminomethane
UV	Ultraviolet

UV-Vis	Ultraviolet- visible
V	Volt
v/v	Volume per volume
w/v	Weight per volume
Wbl	WhiB-like
WT	Wild type

Chapter 1. Introduction

1.1. *Streptomyces* developmental regulation

1.1.1. Overview of the *Streptomyces* life cycle

Streptomyces are a genus of soil-dwelling and filamentous Gram-positive bacteria with genomes of a relatively high GC content (~70%) compared to other bacteria such as *Escherichia coli* (*E.coli*) (~50%) [1]. The majority of antibiotics in use today are derived from *Streptomyces* and considerable research has sought to exploit the ability of *Streptomyces* to produce bioactive secondary metabolites like antifungals, antivirals, and especially antibiotics, with the aim of producing new therapeutic agents to combat the global issue of antibiotic resistance [2]. Being abundant in soil, *Streptomyces* not only produce secondary metabolites but also have key roles in soil ecology including mineralization and decomposition of organic matter.

Streptomyces undergo a complex and highly regulated life cycle [3-5] Research employing the model organisms, *S. coelicolor* and, more recently, *S. venezuelae,* has provided significant insight into the cell biological processes and regulatory networks involved [3]. First, spores germinate and undergo vegetative growth forming mycelial networks that scavenge nutrients, similar to that of filamentous fungi. The second stage is triggered by signals such as nutrient depletion, inducing the formation of multinuclear aerial hyphae that extend upwards away from the vegetative mycelium. During the third stage, sporulation is triggered. The multinuclear aerial hyphae are divided into long chains of uni-genomic spores that when mature are associated with a polyketide spore pigment (grey in *S. coelicolor* and dark green in *S. venezuelae*) (Figure 1.1).

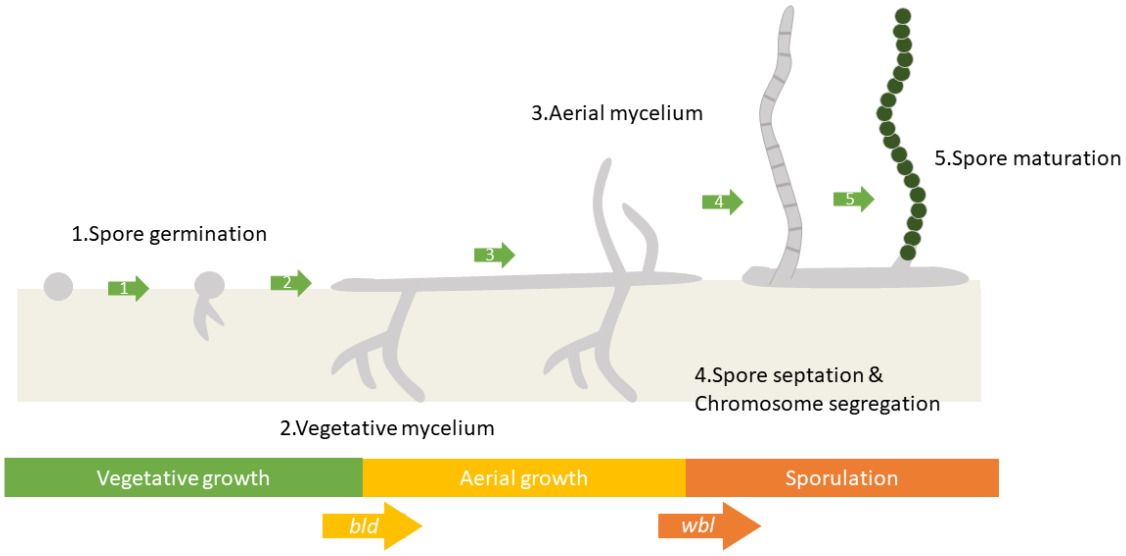

Figure 1.1 The *Streptomyces* developmental life cycle.

1. Germ tubes emerge from a single spore. 2. These germ tubes then grow by tip extension and branching to form a dense network of vegetative hyphae. 3. In response to certain environmentally adverse signals, aerial hyphae are formed. The *bld* gene products are required for the transition from vegetative growth to aerial hyphae formation. 4. The aerial hyphae then differentiate into chains of pre-spores. 5. Pre-spores then undergo maturation to form coloured, mature spores ready for dispersion. The *whi* gene products are required for the differentiation of aerial hyphae into mature spore chains.

1.1.2. *whi* and *bld* developmental mutations

Genes required for the process of differentiation in *Streptomyces* can be classified into two distinct groups based on their associated mutant phenotypes (Figure 1.1). “bld” mutations cause disruption during the earliest visible stage of morphological development, leading to the absence of a visible aerial mycelium and therefore *bld* mutants lack the characteristic “fuzzy” appearance of wild-type colonies [4]. *bld* mutants can themselves be categorised into two classes. Where *bld* genes encode developmental activators, such as AdpA (originally BldH), deletion blocks entry into early development,

preventing the formation of an aerial mycelium [6-8]. Where *bld* genes encode developmental repressors, such as the master regulator BldD, deletion bypasses the formation of the aerial mycelium and induces premature sporulation within the vegetative mycelium [3, 9-11].

Mutations in "*whi*" genes do not affect the formation of aerial hyphae but prevent differentiation into mature spores. A characteristic step of spore maturation is the production of a polyketide pigment, which gives the distinct colour of wild-type spores [5]. Therefore, whilst such mutant colonies have the characteristic "fuzzy" appearance, they remain white in colour. The WhiB-like (Wbl)-family proteins WhiB and WhiD, the focus of part of this thesis, are both developmental regulators encoded by *whi* genes[12, 13] .

The *whiB* gene is absolutely required for the transition from aerial growth to sporulation in *Streptomyces*. Interestingly, *whiB* and *whiA* mutants have identical phenotypes in both *S. coelicolor* and *S. venezuelae* [14, 15]. In line with this, WhiA and WhiB were subsequently shown to co-regulate the expression of the same set of genes in *S. venezuelae*, activating genes involved in chromosome segregation and cell division (e.g. *ftzZ*, *ftzW*, *ftzK*), as well as repressing those genes involved in aerial hyphae growth (e.g *filP*) [16]. Since WhiA is constitutively present throughout the *Streptomyces* life cycle [15], the decision to sporulate likely hinges upon WhiB, the expression of which is highly regulated.

Like the expression of many sporulation genes, the expression of *whiB* is first and foremost controlled by the master regulator BldD [12]. During vegetative growth and when bound to cyclic-di-GMP (c-di-GMP), BldD functions as a repressor of transcription [9, 10]. Aside from *whiB*, the BldD-c-di-GMP regulon contains many sporulation genes, including *bldM, bldN, whiG and ftsZ* [10, 11]. Such a developmental brake ensures that the expression of sporulation genes remains switched off during vegetative growth. Release of this brake occurs as c-di-GMP levels fall, leading to the derepression of BldD-c-di-GMP targets. *bldN* encodes a σ factor σ^{BldN} which mediates the expression of genes required for aerial growth, including *bldM* [17]. BldM in turn functions as a homodimeric

regulator, activating genes required for morphogenesis, including *whiB* [18]. Therefore, the release of BldD-mediated repression and subsequent BldM-mediated activation forms a key node in the control of *whiB* expression and, in turn, *Streptomyces* sporulation. Recently a second repressor of *whiB* was identified. Unlike BldD, BldO functions as a dedicated repressor of *whiB*. Deletion of either *bldD* (encoding the global brake) or *bldO* (encoding the dedicated brake) is sufficient to bypass the repression of *whiB* and promote premature sporulation during vegetative growth, thus the regulation of *whiB* expression is a concerted effort between the two repressor systems [19].

More recently, there has been further insight into the function of another *whi* gene, *whiG*, encoding the sporulation-specific σ factor σ^{WhiG}. The expression of *whiG* is coordinated via BldD-c-di-GMP-mediated repression and WhiAB-mediated activation [5, 12, 31]. However, σ^{WhiG} activity is also post-translationally controlled via an interaction with the anti-sigma factor RsiG (Gallagher et al., 2020). Significantly, structural studies reveal that the sigma-anti-sigma interaction is dependent upon c-di-GMP. Hence, a single molecule, c-di-GMP, functions post-translationally to control both the BldD and RsiG developmental brakes in *Streptomyces*. Following release of the c-di-GMP-RsiG brake, σ^{WhiG} controls the transcription of just two main target-genes, *whiH* and *whiI,* both of which encode key developmental regulators required for the later stages of sporulation that lead to the formation of mature spores [20, 21]. The overall sporulation cascade, including the key developmental regulators highlighted here and connections to the WhiA/WhiB pathway, is summarised in Figure 1.2.

1.1.3. Wbl proteins and their role in regulating sporulation

WhiB-like (Wbl) proteins are a family of Fe-S cluster proteins found uniquely in Actinobacteria [13, 22, 23]. Wbl proteins have been found to play crucial roles in diverse aspects of actinobacteria biology such as development, secondary metabolite production, and stress response [24]. Notably Wbl proteins are also involved in antibiotic resistance and virulence and survival of mycobacteria and corynebacteria, reflecting their roles during infection by human pathogens such as *Mycobacterium tuberculosis*, *Mycobacterium leprae* and *Corynebacterium diphtheriae* [25-28]. As the

name suggests, the Whi-regulator WhiB was the first member of the Wbl-family to be characterised, work conducted in *S. coelicolor [5, 29]*. Since then, a total of 14 Wbl proteins have been identified in *S. coelicolor*, 11 of which are encoded on the chromosome and 3 on the linear plasmid SCP1 [30, 31]. Analysis of Wbl protein sequences has revealed five distinct classes of Wbl proteins, largely conserved across the Actinobacteria [23]. Aside from morphological development, Wbl proteins play key roles in many aspects of *Streptomyces* biology. Namely, WblA is a down-regulator of antibiotic synthesis and is involved in the oxidative stress response, and WblC is implicated in antibiotic resistance [25, 32-36]. Three *Streptomyces* Wbl proteins: WhiB, WhiD and WblA are involved in the regulation of morphological differentiation.

Compared to WhiB, the role of the Wbl-family member WhiD in the regulation of differentiation is less well understood. Unlike *whiB* mutants, *whiD* mutants are able to sporulate but septation results in the formation of irregularly sized spores which are sensitive to heat, prone to lysis and show variability in cell wall deposition [37]. This suggests that WhiD functions later than WhiB in the sporulation cascade, regulating the placement of septa and maturation of subsequent spores.

The role of WblA appears complex as it functions to regulate both secondary metabolism and differentiation. In *S. coelicolor*, the *wblA* mutant phenotype is characterised by low spore production and a pink aerial mycelium, which arises from the lack of grey polyketide pigment production and the accumulation of two pigmented antibiotics, actinorhodin and undecylprodigiosin [35].

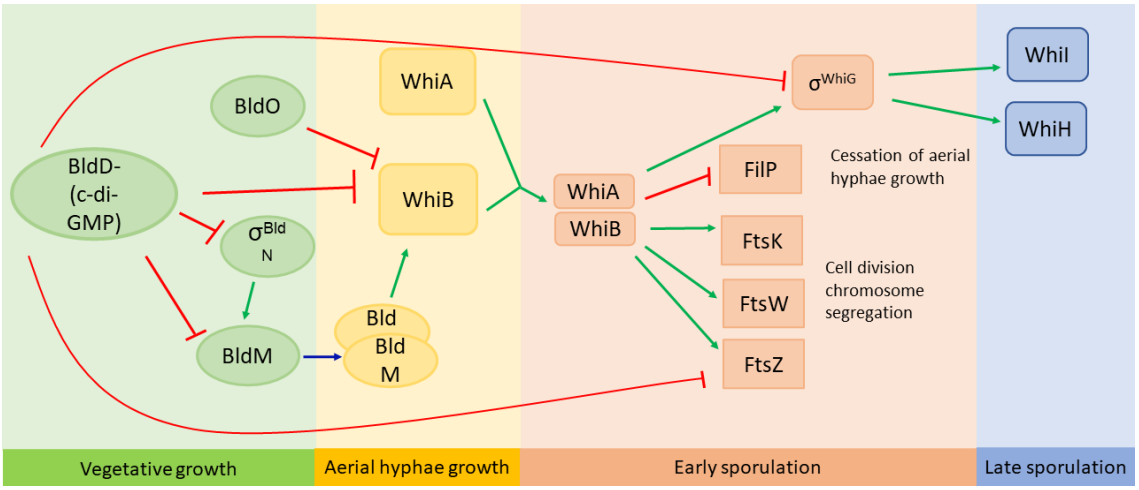

Figure 1.2. The sporulation regulatory network in *Streptomyces* focusing on WhiA and WhiB.

Initiation of differentiation requires the removal of the BldD-c-di-GMP repressor that functions to repress the expression of many genes including *bldN, bldM, whiB, whiG* and *ftsZ*. The initiation of sporulation requires the expression of *whiB* which depends upon the removal of the master BldD-brake and the dedicated BldO-brake. Subsequently, BldM (itself also repressed by BldD-c-di-GMP) functions to activate the expression of *whiB*. WhiB then functions in concert with WhiA (which is constitutively present) to co-initiate developmental cell division. WhiAB acts to further promote the sporulation cascade via activating σ^{WhiG} expression. Following release of the c-di-GMP-dependent RsiG-brake, σ^{WhiG}-dependent transcription of *whiI* and *whiH*, encoding regulators important in late sporulation, occurs. WhiAB also promotes the expression of various genes directly involved in cell division and chromosome segregation: *ftsK*, *ftsW* and *ftsZ*, as well as repressing the *filP* gene required for aerial hyphae growth.

1.1.4. *S. venezuelae* as a novel model organism for *Streptomyces* research

The study of differentiation in *Streptomyces*, including the role of Wbl proteins, has been aided by the use of an alternative model for the genus, *Streptomyces venezuelae*. *S. coelicolor* sporulates only on solid medium, and the differentiating aerial mycelium only makes up ~5% of the total biomass. The remaining 95% remains within the agar as vegetative mycelium. Significantly, unlike the classical model species *S. coelicolor*, *S. venezuelae* is able to sporulate both in liquid and on solid cultures [38]. This makes it much better suited to global "-omics"-related techniques such as chromatin immunoprecipitation sequencing (ChIP-seq) and RNA-seq enabling the effective characterisation of the regulatory networks that govern morphological development [3, 39-41]. Importantly, *S. ceolicolor* and *S. venezuelae* are closely related and the key features of the regulatory cascade that controls development are very likely to be the same. Notably, genes *whiA, whiB* and *whiD* are well conserved between the two species. In common with *S. coelicolor, S. venezuelae* also has 13+ genes encoding Wbl proteins within its genome [23].

1.2. Fe-S cluster proteins that regulate gene expression

1.2.1. Bacterial transcriptional regulation

Transcriptional regulators are proteins that modulate gene expression. Often this is done by binding of the regulatory protein to specific DNA motifs in the promoter region to activate transcription by recruiting the RNA polymerase (RNAP) through either direct protein interaction or altering DNA conformation to facilitate RNAP docking. Alternatively, they can bind to promoter regions and block RNA recruitment, thereby repressing transcription. In bacteria, another notable regulatory mechanism for transcription is the interaction with σ factors [42]. σ factors are unique to bacteria and are required for initiating transcription. They direct the core RNA polymerase to specific promoter elements and initiate DNA strand separation as the first step in the formation of the transcription bubble. A primary or "housekeeping" σ factor is essential for general transcription in exponentially growing cells. Under different conditions such as

morphological development, nutrient uptake, or stress responses, alternative σ factors are deployed to bind in a specified manner to promoters of genes appropriate for the stimulus [43]. Often when specific σ factors are not required, they are sequestered by proteins called anti- σ factors. Most σ factors are part of the σ^{70} family (named from their molecular weight), which consists of four subgroups (1, 2, 3 and 4) based on their structure and physiological functions. The domain conservations are summarised in Figure 1.3.

The housekeeping/ primary σ factor in *Streptomyces* is σ^{HrdB} [44]. The σ^{HrdB} regulon has been characterised in *S. coelicolor*. Interestingly, σ^{HrdB} is not only involved in essential gene expression, but also morphological differentiation and secondary metabolism. Notable genes include those encoding developmental Wbl proteins WhiB and WblA, as well as components of the cell division machinery FtsZ [44]. The *Streptomyces* genome usually encodes around 3 non-essential group 2 σ factors, which share high sequence similarity with σ^{HrdB} but with the absence of region 1.1: σ^{HrdA}, σ^{HrdC} and σ^{HrdD} [45]. Although the function of these alternative σ remains largely elusive, most studies have focused on σ^{HrdD}, which is suggested to be involved in stress response [43]. *S. venezuelae* possesses 2 alternative σ factors: σ^{HrdA} and σ^{HrdD} [43].

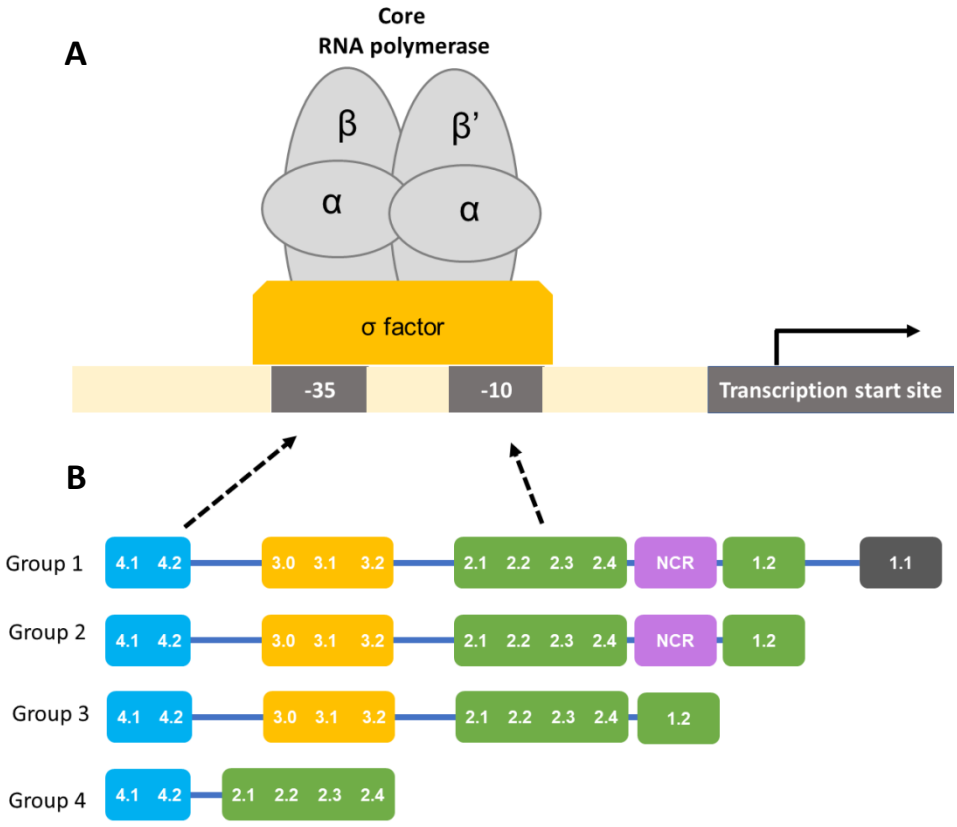

Figure 1.3 Domain organisation and promoter recognition of the σ^{70} family.

(A) representation of the organisation of the RNA polymerase transcription initiation complex. The σ factor binds to the -35 and -10 promoter regions with domains 4 and 2 respectively and recruits the core RNA polymerase. **(B)** domain organisation of σ factors from groups 1-4 with corresponding conserved structural domains as indicated and coloured. Domain 4 in blue, domain 3 in yellow, domain 2 in green, the non-conserved region is variable in size and is coloured purple, and domain 1 is in black.

1.2.2. Function and structure of Fe-S cluster proteins

Fe-S proteins were discovered in the 1960s but are amongst the most ancient protein cofactors. They are indispensable for sustaining many fundamental life processes such as nitrogen fixation, photosynthesis and respiration [46]. Fe-S cluster proteins have cofactors composed of iron and inorganic sulfide. Although mono-ferrodoxin type $[Fe(SR)_4]$ centres can be formed *in vitro* with only ferric iron and thiols and feature Fe-S

bonds, they are not strictly clusters. Within organisms much more complex Fe-S structures are found including, most commonly, [2Fe-2S] and [4Fe-4S] clusters. The Fe-S cluster biogenesis pathway is a complex and multistep process and highly conserved in all kingdoms of life. It is often more complex in eukaryotes in which Fe-S proteins must be produced and function in subcellular compartments such as the cytosol, nucleus, or in the mitochondrion [47, 48].

Typically, Fe-S proteins contain [4Fe-4S] or [2Fe-2S] clusters. The iron atoms in these clusters are present in either the + 2 or + 3 oxidation state and are tetrahedrally coordinated. The rhombic [2Fe-2S] cluster is composed of two iron ions bridged by two inorganic sulfides and is typically coordinated by four cysteine thiolate ligands. The [4Fe-4S] cluster can be visualised as two rhombic [2Fe-2S] clusters at 90 ° to each other, forming a cubane cluster. The cluster is linked again to the protein by four amino acid residues, this time lying at the vertices of a tetrahedron. [3Fe-4S] clusters are also sometimes observed, [3Fe-4S] clusters are often transient intermediates during cluster conversion from the removal of one iron from a [4Fe-4S] cluster [49, 50]. [3Fe-4S] cluster containing proteins also exist, although they are far less common than the cubic [4Fe-4S] cluster containing proteins. Examples can be found in [NiFe] hydrogenase, succinate dehydrogenase, and nitrate reductase, in which the [3Fe-4S] clusters are all involved in catalytic function via electron transfer [51-53]. Although coordinating ligands are usually cysteine thiolates, other amino acid side chains can be found such as histidine (N=), serine (R-O-) and aspartate (RCO_2-). Well characterised examples are the Rieske proteins which have [2Fe-2S] clusters coordinated by two cysteine and two histidine [54]. These common cluster structures are summarised in Figure 1.4. Complex Fe-S proteins can also utilise more than one type of Fe-S cluster and contain additional metal ions. Well characterised examples are found in the active site of nitrogenases. Nitrogenases contain two unique clusters, the P cluster ([8Fe-7S]) and the iron-molybdenum cofactor (FeMoco), which contains 7 Fe and one Mo connected by bridging sulfides, which facilitates the reduction of dinitrogen to ammonia [55, 56]. Some nitrogenases also use vanadium (V), or Fe in place of Mo but are found to be less efficient [55]. Another example of complex clusters can be found in [FeFe] hydrogenases, which catalyse both H_2 oxidation, and reduction of protons to molecular hydrogen. In [FeFe] hydrogenases,

a [4Fe-4S] cluster is directly bridged through a cysteine thiolate to a 2Fe subcluster in an arrangement called the H-cluster. The 2Fe sub-cluster is also coordinated by the non-protein ligands, carbon monoxide (CO), and cyanide (CN^-) groups [57].

This work focuses on Fe-S cluster proteins involved in transcriptional regulation of genes, which utilise their Fe-S clusters to sense different types of environmental stimuli and regulate gene transcription accordingly. This is further discussed in section 1.2.3. Aside from gene transcription, Fe-S cluster proteins perform a variety of roles in nature of which the most common is in electron transfer. Due to the ability of Fe-S clusters to delocalise electrons over both iron and sulfur. This was initially characterised in Fe-S cluster containing ferredoxins [58]. Fe-S clusters can act as catalytic centres. This may be redox driven, for example the iron hydrogenases catalyse the reversible oxidation of H_2 gas, allowing bacteria to use hydrogen as an energy source [59]. Fe-S clusters can also act as non-redox catalysts. For example, the [4Fe-4S] cluster in aconitase does not undertake redox activity, instead a hydroxyl-bound iron serves as a Lewis acid and catalyses the stereospecific isomerization of citrate to isocitrate via consecutive dehydration-hydration reactions [60]. Other clusters are redox inactive and play purely structural roles in proteins, such as those found in the DNA repair enzymes endonuclease III and MutY, in which the clusters control the structure of protein loops essential for recognition and repair of damaged DNA [61, 62]. Sulfur donation and radical formation are other examples of Fe-S cluster function. Biotin synthase is an S-adenosyl-L-methionine (SAM) radical enzyme that catalyses the conversion of dethiobiotin to biotin. Biotin synthase is a homodimeric protein in which each monomer consists of a [4Fe-4S] cluster which directly coordinates SAM and catalyses the production of the 5'deoxyadenosyl radical, which abstracts a hydrogen from dethiobiotin and forms a dethiobiotinyl C9 carbon radical [63]. Biotin synthase also consists of a [2Fe-2S] cluster, which then degrades and provides the sulfur for the generation of biotin [64].

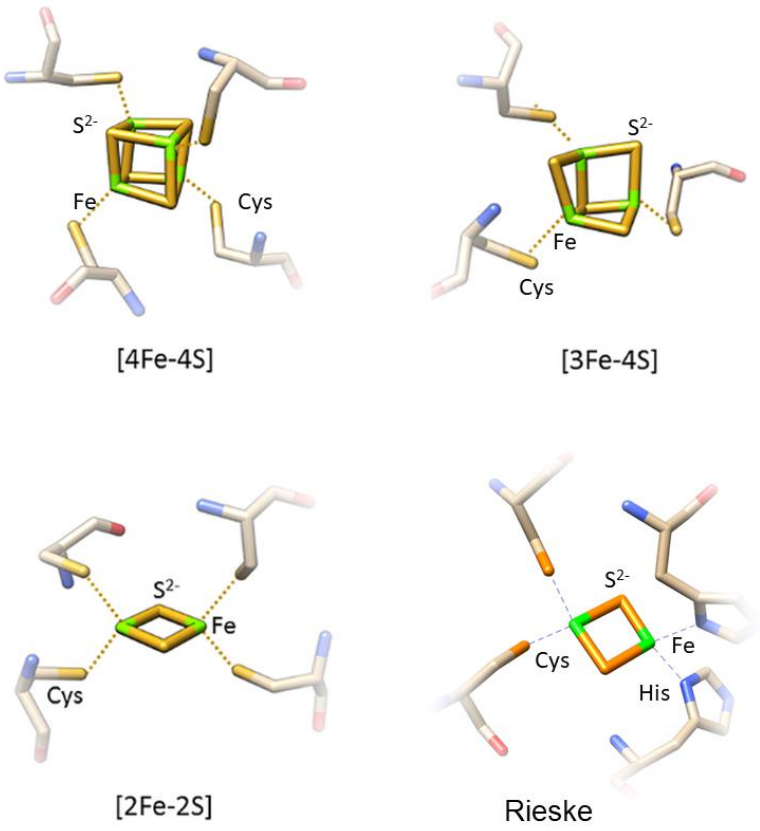

Figure 1.4 Common types of Fe-S clusters.

Clusters are composed of iron (green) and inorganic sulfide (orange). Coordinating cysteine and histidine ligands are labelled accordingly.

1.2.3. Bacterial Fe-S cluster proteins in transcription regulation

The precise nature of environmental sensing by an Fe-S cluster protein is highly variable. Fe-S clusters are redox sensitive, and some are susceptible to oxidation by O_2 and reactive oxygen species (ROS) such as superoxide (O_2^-) and hydrogen peroxide (H_2O_2). They are also prone to damage from reactive nitrogen species (RNS) such as nitric oxide (NO). The presence of ROS and RNS can be damaging in a cell, so stress responses are important and redox reactions underpin the mechanism of function for many Fe-S cluster regulators. Oxidative damage usually leads to cluster conversion and/or complete loss of cluster. This in turn likely results in a significant structural change in the corresponding protein which affects its ability to interact with DNA. The precise redox chemistry and sensitivities to the signal molecules is highly dependent upon the coordination environment of the cluster [65, 66]. Aside from O_2 and NO sensors, other characterised signals sensed by Fe-S regulators include Fe-S cluster availability, and iron availability [67].

Highlighted below are three well characterised examples of how Fe-S regulators sense different signalling molecules via their Fe-S cluster, thereby effecting gene transcription.

1.2.4. Examples of Fe-S transcriptional regulators

1.2.4.1. O_2 sensing – FNR

Fumarate and nitrate reduction (FNR) regulator of *E. coli* is one of the best characterised Fe-S cluster regulator proteins. It is the master regulator of the switch between aerobic and anaerobic metabolism in many bacteria. FNR is part of the cAMP receptor protein (CRP) superfamily and, like other members, it consists of two distinct domains [68]. In *E. coli* FNR, the N-terminal sensory domain has 4 conserved cysteines that bind a $[4Fe\text{-}4S]^{2+}$ cluster, which directly senses O_2 [50, 69, 70]. Under anaerobic conditions $[4Fe\text{-}4S]^{2+}$ FNR dimerises and allows the C-terminal DNA-binding domain to bind to target promoter regions [71, 72]. Holo-FNR acts bifunctionally to control the expression of >300 genes, as an activator of genes involved in anaerobic oxidation of carbon sources and reduction

of alternative terminal electron acceptors, and a repressor of genes specifically used in aerobic respiration [73, 74]. Upon exposure to oxygen, ESI-MS, spectroscopic and kinetic experiments showed that the $[4Fe\text{-}4S]^{2+}$ cluster forms a $[3Fe\text{-}4S]^{1+}$ cluster intermediate via oxidation of the cluster to an oxidation state, $[4Fe\text{-}4S]^{3+}$, and the immediate loss of Fe^{2+}. The transient $[3Fe\text{-}4S]^{1+}$ cluster intermediate subsequently ejects an Fe^{3+} and two sulfide ions to generate $[2Fe\text{-}2S]^{2+}$ FNR [75, 76]. Non-denaturing ESI-MS was recently employed to gain further insight into this step of the reaction and revealed the formation of a novel [3Fe-3S] cluster which results from the loss of one sulfide ion from $[3Fe\text{-}4S]^{1+}$ cluster, thus suggesting an oxidation state of $[3Fe\text{-}3S]^{3+}$. The $[2Fe\text{-}2S]^{2+}$ cluster then slowly degrades to apo -FNR [77]. [2Fe-2S] FNR becomes monomeric, and thus loses its DNA binding abilities [76]. Interestingly, Resonance Raman spectroscopy and LC-MS experiments showed that the cluster sulfides are oxidised to sulfanes. These can be incorporated into the cys-ion bonds that coordinate the [2Fe-2S] cluster as persulfides. Non-denaturing ESI-MS revealed that sulfide oxidation occurs at the same time as the formation of the [2Fe-2S] cluster and resulted in singly and doubly persulfide coordinated species [77]. This is significant because cysteine persulfides can act as a store of sulfur, which allows cluster repair to occur via a supply of only electrons and Fe^{2+}. This provides a method by which FNR acts as an oxygen sensitive regulator that tightly regulates transcription by continuously cycling between active [4Fe-4S] and inactive [2Fe-2S] and apo forms, with the dominant forms depending upon the level of O_2 present [77].

Although FNR is primarily a sensor of O_2, many Fe-S regulators can act upon multiple signals. *In vivo* studies showed that upon exposure to physiologically relevant concentrations of NO (~5 μM), FNR became inactive as multiple FNR-activated genes were downregulated, and FNR-repressed genes upregulated, including the *hmp* gene which encodes the bacterial flavohaemoglobin enzyme which is involved in detoxification of NO [78, 79]. Further studies using a semisynthetic FNR-dependant promoter showed that the amplitude of the response was ~4 fold lower for NO compared with O_2 [80]. Interestingly, *in vitro* studies showed that addition of NO to [4Fe-4S] FNR results in a rapid, multistep reaction resulting in iron-nitrosyl species, the rate of which was ~3 orders of magnitude greater than for O_2 [80]. The contrast between the

in vitro and *in vivo* sensitivity to O_2 and NO suggest that FNR is partially protected in the cell from NO by dedicated NO stress responses, likely involving another Fe-S transcription regulator, NsrR.

1.2.4.2. NO sensing: NsrR

NsrR is a global regulator belonging to the Rrf2 family of regulatory proteins. It functions in NO stress response in many bacteria [81]. In some bacteria it controls a complex network of genes. For example, in *E. coli* it has a regulon of over 60 genes, only some of which are involved in NO detoxification [82]. In contrast, *S. coelicolor* NsrR only regulates its own promoter, and two other genes, *hmpA1* and *hmpA2,* with binding tightest for *hmpA1*, followed by its own promoter, then *hmpA2*. *hmpA1* and *hmpA2* encode NO detoxifying flavohaemoglobins that convert NO to nitrate, or nitrous oxide in the presence and absence of O_2, respectively [82].

S. coelicolor NsrR binds a [4Fe-4S] cluster, coordinated by three cysteines and an aspartate residue [83]. In this form, holo-NsrR exhibits high affinity binding at an 11-bp inverted repeat sequence in the promoters of *hmpA1* and *hmpA2* and its own prometor [84]. Loss of the cluster to apo-NsrR results in loss of DNA binding. Furthermore, exposure to NO abolishes DNA binding [84]. Interestingly the response to NO is not uniform for all three genes, as binding of NsrR to the *hmpA2* gene promoter was found to be the most sensitive and was abolished upon the addition of only 2 NO per cluster. Binding to its own promoter was the least sensitive to NO [84].

1.2.4.3. Fe sensing: RirA

RirA is a global iron regulator found in bacteria including *Rhizobium* and other closely related rhizobial genera that induce nitrogen-fixing nodules on legumes [85, 86]. Rhizobia use many different iron sources and in *R. leguminosarum,* one iron source is the siderophore vicibactin (VB), which it both produces and imports. RirA belongs to the same Rrf2 family as NsrR and, as such, is a homodimeric Fe-S protein. In its [4Fe-4S]

bound form, RirA binds to the operator sequences known as “IRO boxes” [87]. In doing so it acts as a repressor of many genes involved in iron homeostasis, such as *vbsC* (involved in VB synthesis); *rpoI*, which encodes a σ factor needed for VB synthesis; and the two *fhuA* genes which encode the VB receptor [85, 87]. Upon exposure to low iron conditions, RirA loses its cluster to form apo-RirA via a transiently stable [2Fe-2S] cluster. [2Fe-2S] RirA exhibits much weaker DNA binding affinity, and apo-RirA cannot bind the IRO box at all [88]. Furthermore, in addition to its function as an iron sensor, RirA is also sensitive to O_2, apparently enabling it to integrate iron and O_2 signals in its response [88].

1.3. Wbl proteins: transcriptional regulators sensitive to NO and O_2

1.3.1. Structure of Wbl proteins

Wbl proteins are generally small proteins of 81-139 residues, with some exceptions which are larger (WblM, WblO and WblP). Universal sequence conservations include four conserved cysteines which bind a [4Fe-4S] cluster in the motif $Cx_nCx_2Cx_5C$, and a five residue motif (G[V/I]WGG), thought to be important for protein-protein interactions [23]. The first structure for the Wbl protein family was reported recently for *M. tuberculosis* WhiB1. This was largely facilitated by its particularly O_2-stable cluster. WhiB1 is a monomeric protein consisting of 3 conserved motifs: an N-terminal [4Fe-4S] cluster binding motif which contains the 4 conserved cysteines, a glycine-rich linker region which contains the (G[V/I]WGG) motif, and a C-terminal DNA binding AT-hook motif [89, 90]. The NMR structure revealed a four helix bundle, with four conserved cysteines located on helices 1,2 and 3 coordinating the [4Fe-4S] cluster. Between helix 3 and 4 is a loop containing the conserved G[V/I]WGG motif, in which the terminal glycine residues (G61 and G62) run along the face of the [4Fe-4S] cluster (Figure 1.5) [89].

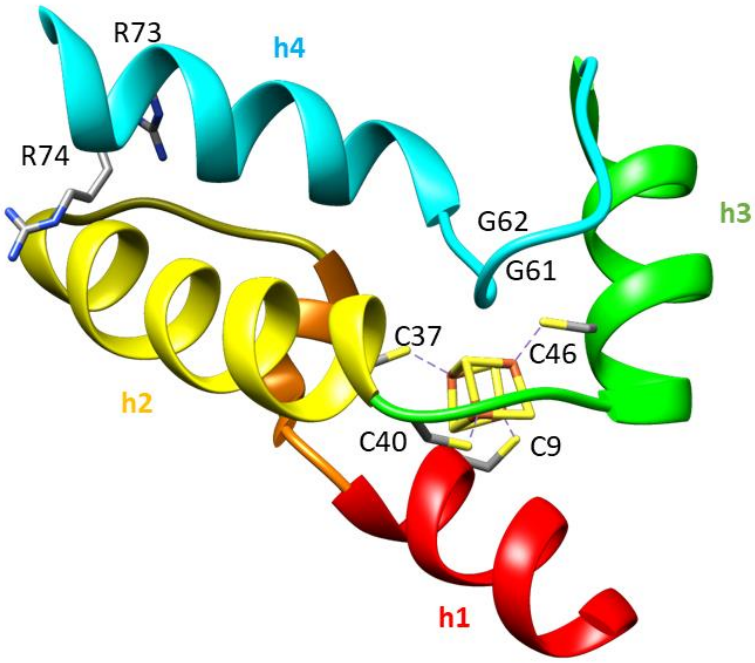

Figure 1.5 The structure of WhiB1 from *M. tuberculosis*.

Structure depicts four helices (labelled h1-h4) and the coordinated [4Fe-4S]. Coordinating cysteine residues are labelled (C9, C37, C40 and C46), The two conserved glycines, part of the G(V/I)WGG turn which run along the face of the [4Fe-4S] cluster, and the C-terminal arginine residues (R73 and R74) proposed for DNA interaction are also labelled. PDB ID: 5OAY.

1.3.2. Wbl proteins directly interact with DNA to regulate gene expression

The putative transcriptional regulatory activities of Wbl proteins have been confirmed by observations of direct binding of some Wbl proteins to promoters of target genes both *in vivo* and *in vitro.*

In vitro electrophoretic mobility shift assay (EMSA) studies of *M. tuberculosis* WhiB1 showed that the loss of cluster through exposure to O_2 or nitrosylation promotes binding to DNA via exposure of positively charged residues in the C-terminal helix, specifically R73 and R74 appear to be crucial for DNA binding *in vitro* (Figure 1.5) [89]. Apo-WhiB1 binds and represses transcription from its own promoter, as well as the promoter region of *groEL2*, an essential chaperonin, and the *espA* operon which encodes protein components for the secretion of the major virulence factor ESX-1 [89, 91]. Similarly, the WhiB4 [4Fe-4S] cluster is also dispensable as the oxidised apo-form is required for DNA binding. WhiB4 has been implicated in the oxidative stress response, and microarray analysis revealed WhiB4 regulates the expression of numerous antioxidant genes [27]. Furthermore, upon exposure to oxidative stress, disulfide-linked oligomerization via the cysteines activates its ability to facilitate genome condensation to protect DNA from oxidative damage [27, 92]. In line with this, ChIP-seq of WhiB4 shows non-specific binding across the *M. tuberculosis* genome with a preference for GC-rich sequences [92]. This makes WhiB4 the first redox dependent nucleoid associating protein (NAP) found in bacteria. WhiB3 directly regulates various genes involved in lipid/ polyketide biosynthesis, including pks2 (SL-1 production) and pks3 (PAT/DAT production) [93]. EMSA experiments show direct binding of WhiB3 to promoter regions of *pks2* and *pks3*. Although [4Fe-4S] WhiB3 exhibits weak DNA binding activity, apo-WhiB3 exhibits strong binding affinity, specifically upon oxidation of apo-WhiB3 cysteine thiols [93]. Reduction of thiols abolishes DNA binding completely, thus providing a thiol-based redox controlled switch mechanism for WhiB3 transcription regulation [93]. Interestingly, EMSA analysis of the WhiB orthologue in *Corynebacterium glutamicum*, WhcD, showed apo-WhcD has no DNA binding activity [94]. *In vivo* studies of *Streptomyces* WhiB have been possible since the introduction of the new model organism *S. venezuelae* by using ChIP-seq. ChIP-seq experiments suggest that WhiB interacts with DNA in concert with the non-Wbl regulatory protein WhiA to the promoter regions of ~250 transcriptional

units, including those involved in aerial growth arrest such as *filP*, and developmental cell division, such as *ftsZ, ftsW* and *ftsK* [16]. Interestingly, although many *M. tuberculosis* apo-Wbl proteins bind DNA *in vitro*, the importance of the conserved cysteines, and in turn the [4Fe-4S] cluster was clearly established in *S. coelicolor* WhiB, as substitutions of cysteine residues rendered WhiB unable to bind target promoters *in vivo* [16].

These studies demonstrate that individual Wbl proteins have adapted to utilise the [4Fe-4S] cluster in a range of ways as the presence/ absence and oxidation states of the clusters and proteins are utilised to control DNA binding. However, no direct binding of Wbl proteins to DNA has been observed yet *in vitro* for *Streptomyces* Wbl proteins.

1.3.3. Wbl proteins function with protein partners

The ability of Wbl proteins to interact with σ factors has been well established in mycobacteria. Apart from WhiB5, all 6 remaining *M. tuberculosis* Wbl proteins have been shown to be able to interact with the primary σ factor, also known as the "housekeeping" σ factor, σ^A [95, 96]. In particular, WhiB1, WhiB3 and WhiB7 have been shown to require σ^A interaction in order to function as transcriptional regulators [90, 97, 98]. As mentioned, a number of Wbl proteins directly interact with DNA in its apo-form. Thus it is interesting that the interaction between *M. tuberculosis* Wbl proteins and σ^A was established to be dependent upon the Wbl [4Fe-4S] cluster, as neither apo- nor NO treated- WhiB1 was able to interact with σ^A [89]. The Wbl- σ^A interaction occurs via region 4 of σ^A, located within the C-terminus [89, 90]. Region 4 is involved in recognition of the core -35 element of σ^{70} dependent promoters and is a well-established target of transcriptional regulators. In addition, located on the linear plasmid of *S. coelicolor, wblP* encodes an unusually large Wbl protein in which the N-terminus has conserved Wbl features, whilst the C-terminus encodes a σ-like domain [31].

A putative interaction specific to *Streptomyces* WhiB is with WhiA. As mentioned, both *whiB* and *whiA* belong to the *whi* family of developmental genes involved in sporulation. Initial observations in *S. coelicolor* showed mutations of the two genes resulted in an

identical mutant phenotype, suggesting that the two proteins may function in the same biochemical pathway. In line with this, ChIP-seq of *S.venezuelae* WhiB and WhiA proteins revealed identical regulons, both consisting of the same ~250 transcription units, many of which are involved in cell division [15, 16]. Furthermore, recent work in *C. glutamicum* showed that the WhiB orthologue WhcD directly interacts with WhiA in its apo-form [94].

Lastly, the WhiB4 orthologues in *C. glutamicum* and *S. coelicolor*, WhcA and WblA respectively, were shown to interact with a previously uncharacterised protein named SpiA (**s**tress **p**rotein **i**nteracting with Whc**A**). The interaction was identified in a two-hybrid system and confirmed with *in vitro* pull-down experiments [34, 99]. The WhcA/WblA -SpiA interaction may play a role in response to oxidative stress as the complex was lost in the presence of oxidants such as diamide, and deletion of SpiA increased transcriptional levels of oxidative stress response genes [34]. This suggests that SpiA may negatively regulate WblA during an oxidative stress response.

1.3.4. Wbl proteins are primarily NO sensors

1.3.4.1. NO signalling and NO induced stress in bacteria

Nitric oxide (NO) is a water-soluble free radical reactive gas which can freely diffuse across biological membranes. In mammals, low concentrations of NO (nanomolar) play a pivotal role as a signalling molecule in many physiological and pathological processes. These include blood pressure regulation, hormone release, nerve transmission and immune response [100]. Equally, NO plays an important role in plant physiological functions, ranging from development to defence responses [100]. Mammalian NO synthase (NOS) are highly regulated enzymes that produce NO by the catalysis of O_2^- and NADPH-dependent oxidation of a guanidino nitrogen of L-arginine. Bacterial NOS (bNOS) homologues have also been identified, including in the *Streptomyces* genus [101, 102]. Notably the model organism *S. coelicolor* genome does not encode an NOS [30], however, *S. coelicolor* has three nitrate reductase (Nar) enzyme homologs (Nar1, Nar2 and Nar3), and thus it is likely that a major source of endogenous NO originates from

the reduction of nitrate (NO_3^-) to nitrite (NO_2^-), which is a precursor of NO [103]. NO-mediated signal transduction in some cases occurs via S-nitrosylation: the oxidative addition of an NO group to a cysteine thiolate group. This process has been characterised in both eukaryotes and bacteria alike [104, 105].

Aside from the production of signalling NO from bNOS, bacteria are exposed to NO from other sources. Denitrifying bacteria are a crucial part of the nitrogen cycle in which they utilise an anaerobic respiratory pathway called denitrification, a fundamental process in which bacteria and some fungi use nitrogen oxides instead of oxygen as terminal electron acceptors. This process involves several redox proteins [106]. NO is an intermediate of this process, produced following the reduction of nitrite by nitrite reductase enzymes (Figure 1.6). Although NO is subsequently reduced to nitrous oxide by NO reductases, it can also freely diffuse out into the soil environment, and may contribute as a source of NO for soil dwelling bacteria [107].

High NO concentrations (micromolar) exert toxic effects within the cell as it can react with cellular components directly or can be converted to other RNS in the presence of oxygen or superoxide radicals. NO and RNS can damage proteins that contain Fe-S clusters, iron, and thiols, as well as the nitrosylation of amino acids and cause oxidative DNA damage [108-110]. NO toxicity is also exploited by host immune systems; bacterial pathogens must therefore be able to counter the toxic effects of NO at high concentrations in order to invade, survive and proliferate inside their hosts [111] .

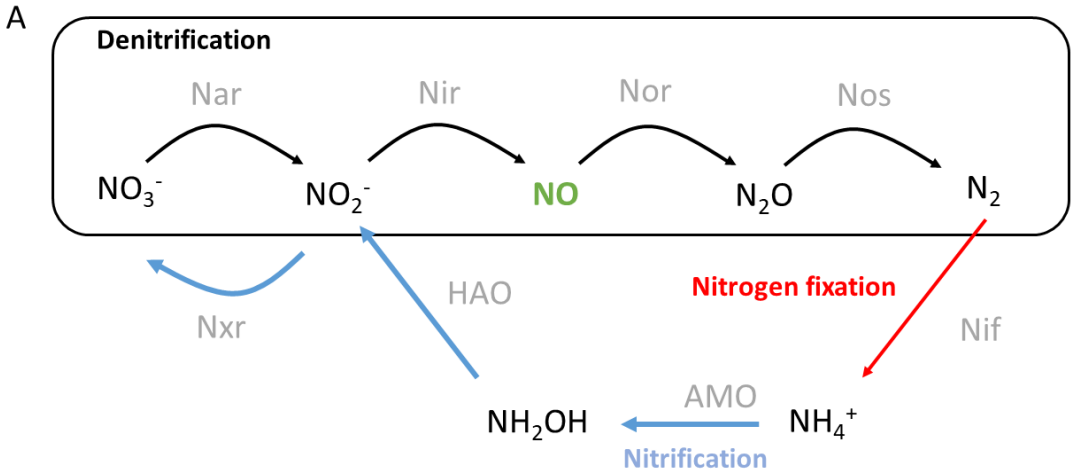

Figure 1.6 The microbial nitrogen cycle.

Pathways include nitrogen fixation (red), in which nitrogenases (Nif) catalyse the reduction of inert N_2 to ammonium (NH_4^+). In the nitrification pathway (blue), ammonia is oxidised to hydroxylamine (NH_2OH), nitrite (NO_2^-) and nitrate (NO_3^-) by ammonia- and nitrite- oxidising bacteria, and ammonium oxidising archea (AMO, HAO and NxR). The denitrification pathway (black) describes the process in which nitrate undergoes reduction, via nitrite, nitric oxide (NO) and nitrous oxide (N_2O), ultimately to form nitrogen gas. The enzymes responsible are: nitrate reductase (Nar), nitrite reductase (Nir), nitric oxide reductase (Nor) and nitrous oxide reductase (Nos).

To maintain strict control of the intracellular NO levels and respond to NO produced from both endogenous and exogenous sources, bacteria have evolved NO sensing transcriptional regulators that function via different mechanisms. *E. coli* NorR functions via a non-heme mononuclear iron centre to regulate expression of the *norVW* genes, which encode flavorubredoxin and its associated redox partner [112]. *M. tuberculosis* DosS and DosR are a two component system in which the heme-containing DosS undergoes autophosphorylation and transfers phosphate to DNA binding protein DosR to control entry into latent dormant state. Fe-S cluster regulators FNR and NsrR also have important roles in NO homeostasis; their transcriptional regulatory mechanism was previously described in section 1.2.1.

1.3.4.2. Nitrosylation of Wbl proteins

Although the functions of Wbl proteins have remained elusive for many years since their discovery, it is becoming clear that the reaction of Wbl proteins with NO plays a crucial part in their signalling process. This is supported by observation that nitrosylation directly affects the ability of WhiB1 to its bind target promoters [91]. Furthermore, biochemical characterisation has provided insights into the Wbl cluster nitrosylation and contributes to unveiling a common Fe-S cluster nitrosylation mechanism.

Reactions of Fe-S clusters with NO can result in iron-nitrosyl complexes. The simplest of these species are mono nitrosyl iron complexes (MNIC) and dinitrosyl iron complexes (DNIC) [113]. Some more complex iron nitrosyl complexes have also been characterised, including the multi-iron Roussin's red ester (RRE) and the Roussin's black salt (Figure 1.7). Previous studies of Fe-S cluster proteins including the NO sensor NsrR from *S. coelicolor*, and Wbl proteins *S. coelicolor* WhiD and *M. tuberculosis* WhiB1 revealed a slow reaction with O_2 (near O_2 insensitive in the case of WhiB1), but a very rapid reaction with 8-10 NO per cluster in a complex multi-phasic reaction [114-116] . Similarly, the primary O_2 sensor FNR also showed a rapid reaction with NO *in vitro* [80]. These Fe-S proteins react with NO to produce protein-bound iron-nitrosyl species. EPR studies of NsrR, FNR and Wbl proteins upon the addition of NO revealed that the reaction results in the formation of paramagnetic DNIC species detected by means of its distinctive S=½ EPR signal, at g = 2.03 [78, 116, 117]. However, this only accounted for a minor amount of total species formed (<16% for *Sc*WhiD and *Sc*NsrR) [118]. Studies of NsrR and WhiD using nuclear resonance vibrational spectroscopy (NRVS); an iron-specific vibrational technique revealed that the products are mostly a mixture of varying ratios of EPR silent species that resemble well known inorganic complexes RRE and RBS, along with minor amounts of DNIC species [118]. The primary species was proposed to be a novel black salt-like species in which one or more sulfides is substituted by a Cys thiolate to generate a species similar to Roussins' black ester [118]. Non-denaturing ESI-mass spectroscopy was also applied to studying iron-nitrosyl species and confirmed the precise nature of the RRE-type species formed upon nitrosylation of NsrR as $[Fe_2(NO)_4]$ and $[[Fe_2(NO)_4](S)]$ [119].

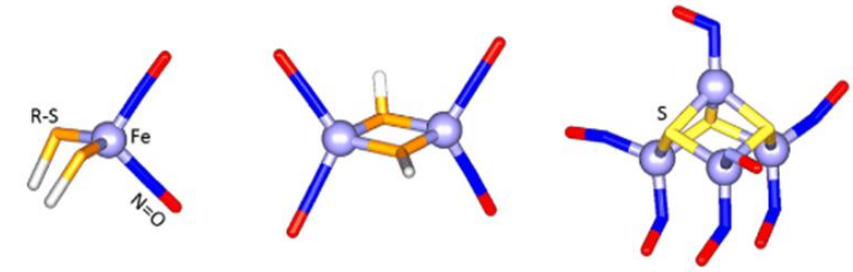

$[Fe(NO)_2](RS)_2$
DNIC
S=1/2

$[Fe_2(NO)_4](RS)_2$
RRE
S=0

$[Fe_4S_3(NO)_7]$
RBS
S=0

Figure 1.7 The major iron-nitrosyl species.

Structures of (mono- nuclear iron) dinitrosyl iron complex (DNIC), Roussin's red ester (RRE) and Roussin's black salt (RBS). Iron, sulfide, thiol, and NO are indicated. Spin states are also quoted for each iron-nitrosyl species.

1.4. Aims of project

Evidence obtained in recent years undoubtably points to Wbl proteins functioning as transcriptional regulators that play crucial roles in diverse aspects of Actinobacterial biology. The interaction between Wbl proteins and partner proteins such as σ factors have been characterised in mycobacteria, but its importance has yet to be elucidated in *Streptomyces*. Furthermore, although the nature of co-regulation between WhiA and WhiB have been well characterised, there still lacks evidence of direct interaction between the two proteins in *Streptomyces*. Recent works suggest a general regulatory mechanism for Wbl proteins could rely on their high sensitivity to NO, and the nature of the [4Fe-4S] cluster is crucial for Wbl proteins to act as transcriptional regulators. The work described in this thesis focusses on understanding the protein-protein interactions of the *S. venezuelae* developmental Wbl proteins WhiB and WhiD. Furthermore, this thesis explores the implications of NO exposure on both Wbl proteins and interacting complexes. Experiments employ a range of biochemical approaches, in particular characterisation of the nature of the cluster and exploration of protein-protein interactions using non-denaturing ESI-mass spectroscopy (MS), which detects intact proteins in their folded states as non-covalent interactions (including protein-metallocofactor) are preserved upon ionisation.

1.5. References

1. Muto, A. and S. Osawa, *The guanine and cytosine content of genomic DNA and bacterial evolution.* Proc Natl Acad Sci U S A, 1987. **84**(1): p. 166-9.
2. Procopio, R.E., et al., *Antibiotics produced by* Streptomyces*.* Braz J Infect Dis, 2012. **16**(5): p. 466-71.
3. Bush, M.J., et al., *c-di-GMP signalling and the regulation of developmental transitions in streptomycetes.* Nat Rev Microbiol, 2015. **13**(12): p. 749-60.
4. Merrick, M.J., *A morphological and genetic mapping study of bald colony mutants of* Streptomyces coelicolor*.* J Gen Microbiol, 1976. **96**(2): p. 299-315.
5. Chater, K.F., *A morphological and genetic mapping study of white colony mutants of* Streptomyces coelicolor*.* J Gen Microbiol, 1972. **72**(1): p. 9-28.
6. Vujaklija, D., et al., *Identification of an A-factor-dependent promoter in the streptomycin biosynthetic gene cluster of* Streptomyces griseus*.* Mol Gen Genet, 1991. **229**(1): p. 119-28.
7. Wolanski, M., et al., *The level of AdpA directly affects expression of developmental genes in* Streptomyces coelicolor. J Bacteriol, 2011. **193**(22): p. 6358-65.
8. Guyet, A., et al., *Identified members of the* Streptomyces lividans *AdpA regulon involved in differentiation and secondary metabolism.* BMC Microbiol, 2014. **14**: p. 81.
9. Elliot, M.A., et al., *BldD is a direct regulator of key developmental genes in* Streptomyces coelicolor *A3(2).* Mol Microbiol, 2001. **40**(1): p. 257-69.
10. Tschowri, N., et al., *Tetrameric c-di-GMP mediates effective transcription factor dimerization to control* Streptomyces *development.* Cell, 2014. **158**(5): p. 1136-1147.
11. den Hengst, C.D., et al., *Genes essential for morphological development and antibiotic production in* Streptomyces coelicolor *are targets of BldD during vegetative growth.* Mol Microbiol, 2010. **78**(2): p. 361-79.
12. Ryding, N.J., et al., *New sporulation loci in* Streptomyces coelicolor *A3(2).* J Bacteriol, 1999. **181**(17): p. 5419-25.
13. Soliveri, J.A., et al., *Multiple paralogous genes related to the* Streptomyces coelicolor *developmental regulatory gene* whiB *are present in* Streptomyces *and other actinomycetes.* Microbiology, 2000. **146 (Pt 2)**: p. 333-343.
14. Ainsa, J.A., et al., *WhiA, a protein of unknown function conserved among gram-positive bacteria, is essential for sporulation in* Streptomyces coelicolor *A3(2).* J Bacteriol, 2000. **182**(19): p. 5470-8.
15. Bush, M.J., et al., *Genes required for aerial growth, cell division, and chromosome segregation are targets of WhiA before sporulation in* Streptomyces venezuelae*.* mBio, 2013. **4**(5): p. e00684-13.
16. Bush, M.J., et al., *Genome-wide chromatin immunoprecipitation sequencing analysis shows that WhiB is a transcription factor that cocontrols its regulon with WhiA to initiate developmental cell division in* Streptomyces*.* mBio, 2016. **7**(2): p. e00523-16.
17. Bibb, M.J., V. Molle, and M.J. Buttner, *sigma(BldN), an extracytoplasmic function RNA polymerase sigma factor required for aerial mycelium formation in* Streptomyces coelicolor *A3(2).* J Bacteriol, 2000. **182**(16): p. 4606-16.
18. Al-Bassam, M.M., et al., *Response regulator heterodimer formation controls a key stage in* Streptomyces *development.* PLoS Genet, 2014. **10**(8): p. e1004554.
19. Bush, M.J., et al., *Multi-layered inhibition of* Streptomyces *development: BldO is a dedicated repressor of* whiB*.* Mol Microbiol, 2017. **104**(5): p. 700-711.

20. Ryding, N.J., et al., *A developmentally regulated gene encoding a repressor-like protein is essential for sporulation in* Streptomyces coelicolor *A3(2).* Mol Microbiol, 1998. **29**(1): p. 343-57.
21. Gallagher, K.A., et al., *c-di-GMP arms an anti-sigma to control progression of multicellular differentiation in* Streptomyces*.* Mol Cell, 2020. **77**(3): p. 586-599 e6.
22. Jakimowicz, P., et al., *Evidence that the* Streptomyces *developmental protein WhiD, a member of the WhiB family, binds a [4Fe-4S] cluster.* J Biol Chem, 2005. **280**(9): p. 8309-15.
23. Bush, M.J., *The actinobacterial WhiB-like (Wbl) family of transcription factors.* Mol Microbiol, 2018. **110**(5): p. 663-676.
24. Lee, J.Y., et al., Corynebacterium glutamicum whcB*, a stationary phase-specific regulatory gene.* FEMS Microbiol Lett, 2012. **327**(2): p. 103-9.
25. Morris, R.P., et al., *Ancestral antibiotic resistance in* Mycobacterium tuberculosis*.* Proc Natl Acad Sci U S A, 2005. **102**(34): p. 12200-5.
26. Burian, J., et al., *The mycobacterial transcriptional regulator* whiB7 *gene links redox homeostasis and intrinsic antibiotic resistance.* J Biol Chem, 2012. **287**(1): p. 299-310.
27. Chawla, M., et al., *Mycobacterium tuberculosis WhiB4 regulates oxidative stress response to modulate survival and dissemination in vivo.* Mol Microbiol, 2012. **85**(6): p. 1148-65.
28. Kim, T.H., et al., *The* whcE *gene of Corynebacterium glutamicum is important for survival following heat and oxidative stress.* Biochem Biophys Res Commun, 2005. **337**(3): p. 757-64.
29. Davis, N.K. and K.F. Chater, *The* Streptomyces coelicolor whiB *gene encodes a small transcription factor-like protein dispensable for growth but essential for sporulation.* Mol Gen Genet, 1992. **232**(3): p. 351-8.
30. Bentley, S.D., et al., *Complete genome sequence of the model actinomycete* Streptomyces coelicolor *A3(2).* Nature, 2002. **417**(6885): p. 141-7.
31. Bentley, S.D., et al., *SCP1, a 356,023 bp linear plasmid adapted to the ecology and developmental biology of its host,* Streptomyces coelicolor *A3(2).* Mol Microbiol, 2004. **51**(6): p. 1615-28.
32. Kang, S.H., et al., *Interspecies DNA microarray analysis identifies WblA as a pleiotropic down-regulator of antibiotic biosynthesis in* Streptomyces*.* J Bacteriol, 2007. **189**(11): p. 4315-9.
33. Kim, J.S., et al., *Negative role of wblA in response to oxidative stress in* Streptomyces *coelicolor.* J Microbiol Biotechnol, 2012. **22**(6): p. 736-41.
34. Kim, J.S., et al., *A WblA-binding protein, SpiA, involved in* Streptomyces *oxidative stress response.* J Microbiol Biotechnol, 2013. **23**(10): p. 1365-71.
35. Fowler-Goldsworthy, K., et al., *The actinobacteria-specific gene* wblA *controls major developmental transitions in* Streptomyces coelicolor *A3(2).* Microbiology, 2011. **157**(Pt 5): p. 1312-1328.
36. Yoo, J.S., et al., *Induction of a stable sigma factor SigR by translation-inhibiting antibiotics confers resistance to antibiotics.* Sci Rep, 2016. **6**: p. 28628.
37. Molle, V., et al., *WhiD and WhiB, homologous proteins required for different stages of sporulation in* Streptomyces coelicolor *A3(2).* J Bacteriol, 2000. **182**(5): p. 1286-95.
38. Glazebrook, M.A., et al., *Sporulation of* Streptomyces venezuelae *in submerged cultures.* J Gen Microbiol, 1990. **136**(3): p. 581-8.
39. Flardh, K. and M.J. Buttner, Streptomyces *morphogenetics: dissecting differentiation in a filamentous bacterium.* Nat Rev Microbiol, 2009. **7**(1): p. 36-49.
40. Pullan, S.T., et al., *Genome-wide analysis of the role of GlnR in* Streptomyces venezuelae *provides new insights into global nitrogen regulation in actinomycetes.* BMC Genomics, 2011. **12**: p. 175.

41. Munnoch, J.T., et al., *Characterization of a putative NsrR homologue in* Streptomyces venezuelae *reveals a new member of the Rrf2 superfamily.* Sci Rep, 2016. **6**: p. 31597.
42. Ishihama, A., *Prokaryotic genome regulation: multifactor promoters, multitarget regulators and hierarchic networks.* FEMS Microbiol Rev, 2010. **34**(5): p. 628-45.
43. Sun, D., et al., *Connecting metabolic pathways: Sigma Factors in* Streptomyces *spp.* Front Microbiol, 2017. **8**: p. 2546.
44. Buttner, M.J. and C.G. Lewis, *Construction and characterization of* Streptomyces coelicolor *A3(2) mutants that are multiply deficient in the nonessential hrd-encoded RNA polymerase sigma factors.* J Bacteriol, 1992. **174**(15): p. 5165-7.
45. Tanaka, K., T. Shiina, and H. Takahashi, *Multiple principal sigma factor homologs in eubacteria: identification of the "rpoD box".* Science, 1988. **242**(4881): p. 1040-2.
46. Johnson, D.C., et al., *Structure, function, and formation of biological iron-sulfur clusters.* Annu Rev Biochem, 2005. **74**: p. 247-81.
47. Rouault, T.A., *Biogenesis of iron-sulfur clusters in mammalian cells: new insights and relevance to human disease.* Dis Model Mech, 2012. **5**(2): p. 155-64.
48. Braymer, J.J. and R. Lill, *Iron-sulfur cluster biogenesis and trafficking in mitochondria.* J Biol Chem, 2017. **292**(31): p. 12754-12763.
49. Beinert, H., et al., *Iron-sulfur stoichiometry and structure of iron-sulfur clusters in three-iron proteins: evidence for [3Fe-4S] clusters.* Proc Natl Acad Sci U S A, 1983. **80**(2): p. 393-6.
50. Crack, J., J. Green, and A.J. Thomson, *Mechanism of oxygen sensing by the bacterial transcription factor fumarate-nitrate reduction (FNR).* J Biol Chem, 2004. **279**(10): p. 9278-86.
51. Fedor, J.G., R.A. Rothery, and J.H. Weiner, *A new paradigm for electron transfer through Escherichia coli nitrate reductase A.* Biochemistry, 2014. **53**(28): p. 4549-56.
52. Volbeda, A., et al., *Crystal structure of the nickel-iron hydrogenase from* Desulfovibrio gigas*.* Nature, 1995. **373**(6515): p. 580-7.
53. Anemuller, S., et al., *EPR characterization of an archaeal succinate dehydrogenase in the membrane-bound state.* Eur J Biochem, 1995. **232**(2): p. 563-8.
54. Beinert, H., R.H. Holm, and E. Munck, *Iron-sulfur clusters: nature's modular, multipurpose structures.* Science, 1997. **277**(5326): p. 653-9.
55. McGlynn, S.E., et al., *Classifying the metal dependence of uncharacterized nitrogenases.* Front Microbiol, 2012. **3**: p. 419.
56. Peters, J.W., et al., *Redox-dependent structural changes in the nitrogenase P-cluster.* Biochemistry, 1997. **36**(6): p. 1181-7.
57. Winkler, M., J. Esselborn, and T. Happe, *Molecular basis of [FeFe]-hydrogenase function: an insight into the complex interplay between protein and catalytic cofactor.* Biochim Biophys Acta, 2013. **1827**(8-9): p. 974-85.
58. Sticht, H. and P. Rosch, *The structure of iron-sulfur proteins.* Prog Biophys Mol Biol, 1998. **70**(2): p. 95-136.
59. Mulder, D.W., et al., *Insights into [FeFe]-hydrogenase structure, mechanism, and maturation.* Structure, 2011. **19**(8): p. 1038-52.
60. Beinert, H., M.C. Kennedy, and C.D. Stout, *Aconitase as Iron-Sulfur Protein, Enzyme, and Iron-Regulatory Protein.* Chem Rev, 1996. **96**(7): p. 2335-2374.
61. Thayer, M.M., et al., *Novel DNA binding motifs in the DNA repair enzyme endonuclease III crystal structure.* EMBO J, 1995. **14**(16): p. 4108-20.
62. Nunez, N.N., et al., *Fe-S clusters and MutY base excision repair glycosylases: purification, kinetics, and DNA affinity measurements.* Methods Enzymol, 2018. **599**: p. 21-68.
63. Fugate, C.J. and J.T. Jarrett, *Biotin synthase: insights into radical-mediated carbon-sulfur bond formation.* Biochim Biophys Acta, 2012. **1824**(11): p. 1213-22.

64. Begley, T.P., et al., *The enzymology of sulfur activation during thiamin and biotin biosynthesis.* Curr Opin Chem Biol, 1999. **3**(5): p. 623-9.
65. Crack, J.C., et al., *Iron-sulfur cluster sensor-regulators.* Curr Opin Chem Biol, 2012. **16**(1-2): p. 35-44.
66. Crack, J.C. and N.E. Le Brun, *Redox-sensing iron-sulfur cluster regulators.* Antioxid Redox Signal, 2018. **29**(18): p. 1809-1829.
67. Mettert, E.L. and P.J. Kiley, *Fe-S proteins that regulate gene expression.* Biochim Biophys Acta, 2015. **1853**(6): p. 1284-93.
68. Green, J., C. Scott, and J.R. Guest, *Functional versatility in the CRP-FNR superfamily of transcription factors: FNR and FLP.* Adv Microb Physiol, 2001. **44**: p. 1-34.
69. Jervis, A.J., et al., *The O_2 sensitivity of the transcription factor FNR is controlled by Ser24 modulating the kinetics of [4Fe-4S] to [2Fe-2S] conversion.* Proc Natl Acad Sci U S A, 2009. **106**(12): p. 4659-64.
70. Kiley, P.J. and H. Beinert, *Oxygen sensing by the global regulator, FNR: the role of the iron-sulfur cluster.* FEMS Microbiol Rev, 1998. **22**(5): p. 341-52.
71. Scott, C., et al., *DNA target sequence and FNR-dependent gene expression.* FEBS Lett, 2003. **541**(1-3): p. 97-101.
72. Lazazzera, B.A., et al., *DNA binding and dimerization of the Fe-S-containing FNR protein from* Escherichia coli *are regulated by oxygen.* J Biol Chem, 1996. **271**(5): p. 2762-8.
73. Constantinidou, C., et al., *A reassessment of the FNR regulon and transcriptomic analysis of the effects of nitrate, nitrite, NarXL, and NarQP as* Escherichia coli *K12 adapts from aerobic to anaerobic growth.* J Biol Chem, 2006. **281**(8): p. 4802-15.
74. Kang, Y., et al., *Genome-wide expression analysis indicates that FNR of* Escherichia coli *K-12 regulates a large number of genes of unknown function.* J Bacteriol, 2005. **187**(3): p. 1135-60.
75. Sutton, V.R., et al., *Kinetic analysis of the oxidative conversion of the $[4Fe\text{-}4S]^{2+}$ cluster of FNR to a $[2Fe\text{-}2S]^{2+}$ Cluster.* J Bacteriol, 2004. **186**(23): p. 8018-25.
76. Crack, J.C., et al., *Influence of the environment on the $[4Fe\text{-}4S]^{2+}$ to $[2Fe\text{-}2S]^{2+}$ cluster switch in the transcriptional regulator FNR.* J Am Chem Soc, 2008. **130**(5): p. 1749-58.
77. Crack, J.C., A.J. Thomson, and N.E. Le Brun, *Mass spectrometric identification of intermediates in the O2-driven [4Fe-4S] to [2Fe-2S] cluster conversion in FNR.* Proc Natl Acad Sci U S A, 2017. **114**(16): p. E3215-E3223.
78. Cruz-Ramos, H., et al., *NO sensing by FNR: regulation of the* Escherichia coli *NO-detoxifying flavohaemoglobin, Hmp.* EMBO J, 2002. **21**(13): p. 3235-44.
79. Pullan, S.T., et al., *Nitric oxide in chemostat-cultured* Escherichia coli *is sensed by Fnr and other global regulators: unaltered methionine biosynthesis indicates lack of S nitrosation.* J Bacteriol, 2007. **189**(5): p. 1845-55.
80. Crack, J.C., et al., *Mechanism of $[4Fe\text{-}4S](Cys)_4$ cluster nitrosylation is conserved among NO-responsive regulators.* J Biol Chem, 2013. **288**(16): p. 11492-502.
81. Tucker, N.P., et al., *There's NO stopping NsrR, a global regulator of the bacterial NO stress response.* Trends Microbiol, 2010. **18**(4): p. 149-56.
82. Partridge, J.D., et al., *NsrR targets in the* Escherichia coli *genome: new insights into DNA sequence requirements for binding and a role for NsrR in the regulation of motility.* Mol Microbiol, 2009. **73**(4): p. 680-94.
83. Volbeda, A., et al., *Crystal structures of the NO sensor NsrR reveal how its iron-sulfur cluster modulates DNA binding.* Nat Commun, 2017. **8**: p. 15052.
84. Crack, J.C., et al., *NsrR from* Streptomyces coelicolor *is a nitric oxide-sensing [4Fe-4S] cluster protein with a specialized regulatory function.* J Biol Chem, 2015. **290**(20): p. 12689-704.
85. Todd, J.D., et al., *RirA, an iron-responsive regulator in the symbiotic bacterium* Rhizobium leguminosarum. Microbiology, 2002. **148**(Pt 12): p. 4059-4071.

86. Rudolph, G., H. Hennecke, and H.M. Fischer, *Beyond the Fur paradigm: iron-controlled gene expression in rhizobia.* FEMS Microbiol Rev, 2006. **30**(4): p. 631-48.
87. Yeoman, K.H., et al., *Evidence that the* Rhizobium *regulatory protein RirA binds to cis-acting iron-responsive operators (IROs) at promoters of some Fe-regulated genes.* Microbiology, 2004. **150**(Pt 12): p. 4065-74.
88. Pellicer Martinez, M.T., et al., *Sensing iron availability via the fragile [4Fe-4S] cluster of the bacterial transcriptional repressor RirA.* Chem Sci, 2017. **8**(12): p. 8451-8463.
89. Kudhair, B.K., et al., *Structure of a Wbl protein and implications for NO sensing by* M. tuberculosis*.* Nat Commun, 2017. **8**(1): p. 2280.
90. Wan, T., et al., *Structural basis of non-canonical transcriptional regulation by the sigmaA-bound iron-sulfur protein WhiB1 in* M. tuberculosis*.* Nucleic Acids Res, 2020. **48**(2): p. 501-516.
91. Stapleton, M.R., et al., Mycobacterium tuberculosis *WhiB1 represses transcription of the essential chaperonin GroEL2.* Tuberculosis (Edinb), 2012. **92**(4): p. 328-32.
92. Chawla, M., et al., *Redox-dependent condensation of the mycobacterial nucleoid by WhiB4.* Redox Biol, 2018. **19**: p. 116-133.
93. Singh, A., et al., Mycobacterium tuberculosis *WhiB3 maintains redox homeostasis by regulating virulence lipid anabolism to modulate macrophage response.* PLoS Pathog, 2009. **5**(8): p. e1000545.
94. Lee, D.S., et al., Corynebacterium glutamicum *WhcD interacts with WhiA to exert a regulatory effect on cell division genes.* Antonie Van Leeuwenhoek, 2018. **111**(5): p. 641-648.
95. Casonato, S., et al., *WhiB5, a transcriptional regulator that contributes to* Mycobacterium tuberculosis *virulence and reactivation.* Infect Immun, 2012. **80**(9): p. 3132-44.
96. Feng, L., et al., *Genome-wide characterization of monomeric transcriptional regulators in* Mycobacterium tuberculosis*.* Microbiology, 2016. **162**(5): p. 889-897.
97. Burian, J., et al., *The mycobacterial antibiotic resistance determinant WhiB7 acts as a transcriptional activator by binding the primary sigma factor SigA (RpoV).* Nucleic Acids Res, 2013. **41**(22): p. 10062-76.
98. Steyn, A.J., et al., Mycobacterium tuberculosis *WhiB3 interacts with RpoV to affect host survival but is dispensable for in vivo growth.* Proc Natl Acad Sci U S A, 2002. **99**(5): p. 3147-52.
99. Park, J.S., et al., *Identification of SpiA that interacts with* Corynebacterium glutamicum *WhcA using a two-hybrid system.* FEMS Microbiol Lett, 2011. **322**(1): p. 8-14.
100. Wendehenne, D., et al., *Nitric oxide: comparative synthesis and signaling in animal and plant cells.* Trends Plant Sci, 2001. **6**(4): p. 177-83.
101. van Sorge, N.M., et al., *Methicillin-resistant* Staphylococcus aureus *bacterial nitric-oxide synthase affects antibiotic sensitivity and skin abscess development.* J Biol Chem, 2013. **288**(9): p. 6417-26.
102. Kers, J.A., et al., *Nitration of a peptide phytotoxin by bacterial nitric oxide synthase.* Nature, 2004. **429**(6987): p. 79-82.
103. Sasaki, Y., et al., *Nitrogen oxide cycle regulates nitric oxide levels and bacterial cell signaling.* Sci Rep, 2016. **6**: p. 22038.
104. Seth, D., et al., *Endogenous protein S-Nitrosylation in E. coli: regulation by OxyR.* Science, 2012. **336**(6080): p. 470-3.
105. Hess, D.T. and J.S. Stamler, *Regulation by S-nitrosylation of protein post-translational modification.* J Biol Chem, 2012. **287**(7): p. 4411-8.
106. Spiro, S., *Regulators of bacterial responses to nitric oxide.* FEMS Microbiol Rev, 2007. **31**(2): p. 193-211.

107. Goretski, J. and T.C. Hollocher, *Trapping of nitric oxide produced during denitrification by extracellular hemoglobin.* J Biol Chem, 1988. **263**(5): p. 2316-23.
108. Wink, D.A. and J.B. Mitchell, *Chemical biology of nitric oxide: Insights into regulatory, cytotoxic, and cytoprotective mechanisms of nitric oxide.* Free Radic Biol Med, 1998. **25**(4-5): p. 434-56.
109. Cooper, C.E., *Nitric oxide and iron proteins.* Biochim Biophys Acta, 1999. **1411**(2-3): p. 290-309.
110. Phoa, N. and B. Epe, *Influence of nitric oxide on the generation and repair of oxidative DNA damage in mammalian cells.* Carcinogenesis, 2002. **23**(3): p. 469-75.
111. Williams, D.E. and E.M. Boon, *Towards Understanding the Molecular Basis of Nitric Oxide-Regulated Group Behaviors in Pathogenic Bacteria.* J Innate Immun, 2019. **11**(3): p. 205-215.
112. Tucker, N.P., et al., *Mechanism of transcriptional regulation by the* Escherichia coli *nitric oxide sensor NorR.* Biochem Soc Trans, 2006. **34**(Pt 1): p. 191-4.
113. Butler, A.R. and I.L. Megson, *Non-heme iron nitrosyls in biology.* Chem Rev, 2002. **102**(4): p. 1155-66.
114. Smith, L.J., et al., Mycobacterium tuberculosis *WhiB1 is an essential DNA-binding protein with a nitric oxide-sensitive iron-sulfur cluster.* Biochem J, 2010. **432**(3): p. 417-27.
115. Crack, J.C., et al., *Differentiated, promoter-specific response of [4Fe-4S] NsrR DNA binding to reaction with nitric oxide.* J Biol Chem, 2016. **291**(16): p. 8663-72.
116. Crack, J.C., et al., *Mechanistic insight into the nitrosylation of the [4Fe-4S] cluster of WhiB-like proteins.* J Am Chem Soc, 2011. **133**(4): p. 1112-21.
117. Tucker, N.P., et al., *The transcriptional repressor protein NsrR senses nitric oxide directly via a [2Fe-2S] cluster.* PLoS One, 2008. **3**(11): p. e3623.
118. Serrano, P.N., et al., *Nitrosylation of nitric-oxide-sensing regulatory proteins containing [4Fe-4S] clusters gives rise to multiple iron-nitrosyl complexes.* Angew Chem Int Ed Engl, 2016. **55**(47): p. 14575-14579.
119. Crack, J.C. and N.E. Le Brun, *Mass spectrometric identification of [4Fe-4S](NO)x intermediates of nitric oxide sensing by regulatory iron-sulfur cluster proteins.* Chemistry, 2019. **25**(14): p. 3675-3684.

Chapter 2. Methods

2.1. Strains, growth conditions and genetic methods

Table 2.1 Plasmids used in this work.

PLASMIDS	DESCRIPTION	ANTIBIOTIC RESISTANCE	REFERENCE
pET28a	Expression vector designed to permit addition of an N-terminal hexahistidine affinity tag to a target protein	Kanamycin	Novagen
pET15b	Expression vector designed to permit addition of an N-terminal hexahistidine affinity tag to a target protein	Ampicillin	Novagen
pETDuet-1	Expression vector designed for co-expression of two target genes	Ampicillin	Novagen
pET11a	*E. coli* Expression vector	Ampicillin	Novagen
pMSW1	*S. venezuelae whiD* cloned into pET28a	Kanamycin	This work
pMSW2	*S. venezuelae hrdB* (encoding domain 4) cloned into pET15b	Ampicillin	This work
pMSW3	*S. venezuelae hrdD* (encoding domain 4) cloned into pET15b	Ampicillin	This work
pMSW4	*S. venezuelae whiB* cloned into pET28a	Kanamycin	★
pMSW5	*S. venezuelae whiB* and *whiA* cloned into pETDuet-1 in multiple cloning sites 1 and 2 respectively, to encode N-terminally His_{6}-tagged WhiB and non-tagged WhiA.	Ampicillin	This work
pMSW6	*S.venezuelae whiA* cloned into pET15b	Ampicillin	★
pMSW7	*S. venezuelae whiD* (res1-118) cloned into pET28a	Kanamycin	This work
pMSW8	*S. venezuelae whiD* (res1-123) cloned into pET28a	Kanamycin	This work
pMSW9	*R. leguminosarum rirA* (N8C mutant) cloned into pET11a	Ampicillin	This work [1]
pMSW10	*R. leguminosarum rirA* (N8D mutant) cloned into pET11a	Ampicillin	This work [1]
pIJ10648	*S. venezuelae WhiA* cloned into pSKB2	Kanamycin	★
pGS2252	Encoding I151A GST–FNR	Ampicillin	[2]

★ These plasmids were kindly provided by Dr Matt Bush (John Innes Centre, Norwich).

2.1.1. Plasmid storage, DNA isolation and transformations

E. coli JM109 was used as the plasmid storage strain, from which plasmid DNA was isolated from 5 mL overnight cultures of using a plasmid mini-prep kit (Qiagen).

E.coli BL21 (DE3) was used as the expression host and competent cells were prepared using the calcium chloride method, which encourages bacterial cells to take up DNA from the surrounding environment [3]. Prepared competent cells were aliquoted as 200 µL stocks and stored at -80 °C until required. Transformation was performed using the heat shock method. ~100 ng of plasmid DNA was added to 200 µL of competent cells, mixed gently and incubated on ice for 50 minutes, heat shocked at 42 °C for 2 minutes and then returned to ice for 5 minutes. Afterwards, 700 µL of 37 °C LB medium was added, and the samples incubated at 37 °C for 1 hour. After this, the cells were pelleted by centrifugation at 10,000 x g for 1 minute and 700 µL of the supernatant removed. The pellet was resuspended in the remaining supernatant and plated out on LB agar containing the appropriate antibiotic (Table 2.1). Plates were incubated overnight at 37 °C.

2.1.2 Media preparation

2.1.2.1 LB media

For LB medium and agar, ingredients from Table 2.2 were made up with distilled water and autoclaved to sterilise. Prior to use, LB agar was re-heated until molten and allowed to cool to ~50 °C before adding the appropriate antibiotic. It was then poured into petri-dishes (30 mL) and allowed to set. Plates were stored at 4 °C until required or discarded after one month.

Table 2.2 LB media/ agar components

LB media	
Tryptone	10 g/L
Yeast extract	5 g/L
NaCl	10 g/L
LB agar	2.5 g micro agar per 200 mL LB medium

2.1.2.2. Minimal medium

M9 salts were prepared as per Table 2.3 in distilled water. M9 salts mixture was then passed through 100 g of Chelex-100 resin (Bio-Rad) in a Whatman Klair-flex 0.2 µm filtration device, pre-rinsed with distilled water to remove polyvalent metal ions from the solution. M9 salts were then autoclaved (121 °C for 20 minutes), allowed to cool and then combined with the following, to final concentrations of; 0.2 % (w/v) glucose, 0.2 % (w/v) casein hydrolysate, 6 µM thiamine HCl, 1 mM $MgCl_2 \cdot 6H_2O$, 100 mM $CaCl_2 \cdot 2H_2O$, made up in Chelex-100 treated water and filter sterilized.

Table 2.3 M9 salts

Reagent	**Amount per litre**
$Na_2HPO_4 \cdot 7H_2O$	12.8 g
KH_2PO_4	3 g
NH_4Cl	1 g
NaCl	0.5 g

2.2. Protein overexpression and purification

Table 2.4 Buffers used in protein purification and their composition

Buffer Name	Composition	pH
Buffer A	50 mM Tris, 300 mM NaCl, 25 mM imidazole	7.5
Buffer B	50 mM Tris, 300 mM NaCl, 500 mM imidazole	7.5
Buffer C	50 mM Tris, 300 mM NaCl	7.5
Buffer D	50 mM Tris, 25 mM NaCl	7.5
Buffer E	50 mM Tris, 1 M NaCl	7.5
Buffer F	25 mM HEPES, 2.5 mM $CaCl_2$, 100 mM $NaNO_3$	7.5
Buffer G	25 mM HEPES, 2.5 mM $CaCl_2$, 100 mM $NaNO_3$, 1 M NaCl	7.5
Buffer H	25 mM HEPES, 2.5 mM $CaCl_2$, 50 mM NaCl	7.5
Buffer I	25 mM HEPES, 2.5 mM $CaCl_2$, 50 mM NaCl, 750 mM KCl	7.5

2.2.1. Overexpression and purification of *Sv*Wbl proteins

S. venezuelae WhiB overexpression vector (pMSW4) was kindly provided by Dr Matt Bush (John Innes Centre, Norwich). Correspondingly, an *S. venezuelae* WhiD (*Sv*WhiD) overexpression vector (pMSW1) was synthesised by ligating codon-optimised *whiD* into pET28a using *Nde*I and *Hin*dIII sites (Genscript). Both these expression vectors were generated to give an N-terminally His_6-tagged protein. Vectors were stored and subsequently used to transform *E. coli* BL21 (λDE3) according to section 2.1.1. *Sv*Wbl proteins were overproduced in *E. coli* cultures grown aerobically in 5 L (8 x 625mL in 2 L flasks) of LB medium containing 50 µg/mL kanamycin. The cultures were grown at 37 °C, with shaking at 200 rpm until OD_{600} reached 0.6-0.8, at which point flasks were placed on ice for 18 minutes. Protein expression was induced with 0.3 mM IPTG and cultures incubated for 50 minutes at 30 °C, with shaking at 105 rpm. Cultures were then supplemented with ammonium ferric citrate and L-methionine to give a final concentration of 200 µM and 25 µM, respectively, to promote Fe-S cluster incorporation, and incubated at 30 °C, 105 rpm for a further 4 hours. Cells were harvested by centrifugation at 10,000 x g, 4 °C for 20 minutes. Harvested cells from 5 L cultures were then washed with 50 mL buffer A (50 mM Tris, 300 mM NaCl, 25 mM imidazole, pH 7.5), pelleted at 10,000 x g at 4 °C for 10 minutes and stored at -80 °C until required.

Unless stated, all purification steps were performed in an anaerobic cabinet (O_2 < 5 ppm). Cell pellets were resuspended in buffer A with the addition of lysozyme (300 µg/mL) and PMSF (300 µg/mL). Resuspended cells were removed from the anaerobic cabinet and lysed by sonication on ice under N_2, twice for 8 minutes 20 sec, 0.2 sec bursts, 50% power and immediately returned to the anaerobic cabinet. Lysed cells were centrifuged in air-tight centrifuge tubes outside of the anaerobic cabinet at 40,000 × g for 45 minutes at 1 °C and returned into the anaerobic cabinet. The supernatant was loaded onto a HiTrap Ni-affinity column and washed with buffer A until $A_{280\ nm}$ was < 0.1. Bound proteins were eluted with buffer B (50 mM Tris, 300 mM NaCl, 500 mM imidazole, pH 7.5) from 0 to 100% (v/v) over a linear gradient of 10 mL. Fractions were kept at 4 °C until the protein purity was checked by SDS-PAGE. Fractions containing desired protein

were then pooled and immediately loaded onto a HiTrap desalting column equilibrated with imidazole-free buffer C (50 mM Tris, 300 mM NaCl pH 7.5) and stored in an anaerobic freezer until needed.

2.2.2. Overexpression and purification of region 4 of σ^{HrdB} and σ^{HrdD}

Codon-optimised genes for the expression of N-terminally $(His)_6$-tagged region 4 of *S. venezuelae* sigma factors σ^{HrdB} (σ^{HrdB}_4) and σ^{HrdD} (σ^{HrdD}_4) were synthesized and ligated into pET15b using *Nde*I and *Bam*HI sites, generating pMSW2 and pMSW3 (Genscript). Vectors were stored and introduced into *E. coli* BL21 (λDE3) according to section 2.1.1.

σ^{HrdB}_4 and σ^{HrdD}_4 were overproduced in transformed *E. coli* cells grown aerobically in 5 L (8 x 625 mL in 2L flasks) LB medium containing 100 µg/mL ampicillin. *E. coli* cells were grown at 37 °C, with shaking at 200 rpm until OD_{600} reached 0.6-0.8, at which point overproduction of proteins was induced by the addition of IPTG (0.5 mM final concentration). Cells were harvested by centrifugation at 10,000 x g, 4 °C for 20 minutes. Pellets from 5 L cultures were washed with 50 mL buffer A (50 mM Tris, 300 mM NaCl, 25 mM imidazole, pH 7.5), pelleted at 10,000 x g at 4 °C for 10 minutes and stored at -80 °C until required.

Cell pellets were resuspended in buffer A with the addition of lysozyme (300 µg/mL) and PMSF (300 µg/mL). Resuspended cells were lysed by sonication on ice, twice for 8 minutes 20 sec, 0.2 sec bursts, 50% power and lysates pelleted by centrifugation at 40,000 × g for 45 minutes at 1 °C. The supernatant was loaded onto a HiTrap Ni-affinity column and washed with buffer A until $A_{280\ nm}$ was < 0.1. Bound proteins were eluted with buffer B (50 mM Tris, 300 mM NaCl, 500 mM imidazole, pH 7.5) from 0 to 100% (v/v) over a linear gradient of 10 mL. The protein purity of fractions was checked by SDS-PAGE. Fractions containing desired protein were then pooled and desalted using a HiTrap desalting column into imidazole-free buffer C (50 mM Tris, 300 mM NaCl, pH 7.5) and stored in an anaerobic freezer until needed.

2.2.3. Overexpression and purification of WhiA

Plasmids containing codon-optimised genes for the expression of N-terminally $(His)_6$-tagged *Sv*WhiA (pMSW6) and *Sc*WhiA (pIJ10648) were kindly provided by Dr Matt Bush (John Innes Centre, Norwich). These vectors were stored and introduced into *E. coli* BL21 (λDE3) as described in section 2.1.1. *Sv*WhiA and *Sc*WhiA were overproduced in 5 L (8x 625 mL in 2 L flasks) aerobically grown *E. coli* BL21 (DE3) cultures in LB containing 100 µg/mL ampicillin and 50 µg/mL kanamycin, respectively. Cultures were grown at 37 °C, 200 rpm until OD_{600} reached 0.6-0.8, at which point overexpression of proteins was induced by the addition of 0.5 mM IPTG. Cultures were incubated further at 37 °C, 200 rpm for 4 hours. Cells were harvested by centrifugation at 10,000 x g, 4 °C for 20 minutes. Harvested cells from 5 L cultures were then washed with 50 mL buffer A (50 mM Tris, 300 mM NaCl, 25 mM imidazole, pH 7.5), pelleted at 10,000 x g at 4 °C for 10 minutes and stored at -80 °C until required.

Cell pellets were resuspended in buffer A (50 mM Tris, 300 mM NaCl, 25 mM imidazole, pH 7.5) with the addition of lysozyme (300 µg/mL) and PMSF (300 µg/mL). Resuspended cells were lysed by sonication on ice, twice for 8 minutes 20 s, 0.2 s bursts, 50% power and pelleted by centrifugation at 40,000 × g for 45 minutes at 1 °C. The supernatant was loaded onto a HiTrap Ni-affinity column, washed with buffer A until $A_{280\ nm}$ was < 0.1. Bound proteins were eluted with buffer B (50 mM Tris, 300 mM NaCl, 500 mM imidazole, pH 7.5) from 0 to 100% (v/v) over a linear gradient of 10 mL. Fractions were kept on ice as while the purity of the fractions was checked by SDS-PAGE. Fractions containing desired protein were then pooled and diluted 10-fold into buffer D (50 mM Tris, 25 mM NaCl pH 7.5) to decrease salt content. Sample was centrifuged at 10,000 x g, 4 °C for 8 minutes to remove any precipitate. The cleared supernatant was loaded onto 1 mL HiTrap Heparin HP affinity column, pre-equilibrated with 5 CV of buffer D. Non-specifically bound proteins were washed from the column with buffer C until $A_{280\ nm}$ was <0.1. WhiA was eluted with a gradient of 0-100% (v/v) of elution buffer E (50 mM Tris, 1 M NaCl, pH 7.5) over 10 mL. The purity of protein containing fractions was then checked by SDS-PAGE prior to pooling.

2.2.4. Overexpression and purification of I151A FNR

Aerobic cultures of *E. coli* BL21 (DE3) containing pGS2252 (encoding I151A GST-FNR) were grown and protein isolated as previously described [2], except that aerobic conditions were employed in order to generate the cluster-free form of I151A GST-FNR. I151A FNR was cleaved from the fusion protein using thrombin as previously described [4]. Protein content was analysed using SDS-PAGE gel electrophoresis. Apo-FNR preparations are frequently contaminated with DNA. Therefore, the I151A FNR sample was loaded onto a heparin column, pre-equilibrated with buffer F (25 mM HEPES, 2.5 mM $CaCl_2$, 100 mM $NaNO_3$, pH 7.5). The column was washed with buffer F until $A_{280\ nm}$ was <0.1, and DNA-free I151A FNR eluted from the column with buffer G (25 mM HEPES, 2.5 mM $CaCl_2$, 100 mM $NaNO_3$, 1 M NaCl, pH 7.5).

2.2.5. Overexpression and purification of RirA and RirA variants

R. leguminosarum RirA and were overproduced in *E. coli* and purified exactly as previously described [1]. Codon-optimised genes for the expression of N8C RirA and N8D RirA variants were synthesized (Genscript) and ligated into pET11a using *Nde*I and *Bam*HI sites, generating pMSW9 and pMSW10, respectively (Genscript). RirA variants were overproduced and purified exactly as wild type *R. leguminosarum* RirA.

2.3. Iron sulfur cluster protein methods

2.3.1. Fe-S cluster reconstitution

Fe-S cluster loading can be greatly improved by Fe-S cluster reconstitution. This can be achieved either by a classic chemical reconstitution using iron and sulfide salts, or by means of a semi-enzymatic NifS-catalysed reconstitution [5]. NifS is a cysteine desulfurase which catalyses the conversion of L-cysteine to L-alanine via the formation of a protein-bound cysteine persulfide (formed on a conserved cysteine within the enzyme). DTT is added to the reaction to mediate the reductive release of sulfide from

the persulfide. This system allows for a slow release of sulfide as a reconstitution substrate. An iron source is also required, such as ferrous ammonium sulfate. RirA was reconstituted to full cluster loading. Stock solutions of 20 mM L-cysteine, 124 mM DTT and 20 mM $(NH_4)_2Fe(II)(SO_4)_2$ were prepared in buffer H (25 mM HEPES, 2.5 mM $CaCl_2$, 50 mM NaCl, pH 7.5), under anaerobic conditions. Aliquots of the stock solutions were added to as isolated RirA (~200 µM) to give final concentrations of 1 mM L-cysteine, 2.5 mM DTT and 7-fold excess of Fe^{2+} ions per protein. The reconstitution reaction was initiated by introducing *Azotobacter vinelandii* NifS (prepared by Dr J. Crack, School of Chemistry, University of East Anglia, as described [6]) to a final concentration of 225 nM NifS and incubated at room temperature, with stirring until a deep brown colour developed. Once Fe-S cluster incorporation was complete (no further colour change observed by eye), the reconstitution mixture was passed through a 0.2 µm syringe filter. Excess low molecular mass contaminants were then removed by applying the reconstitution reaction mixture to a 1 mL HiTrap heparin column (GE Healthcare) and eluting with buffer I (25 mM HEPES, 2.5 mM $CaCl_2$, 50 mM NaCl, 750 mM KCl, pH 7.5).

2.3.2. ^{34}S isotope labelling.

^{34}S labelling facilitates many techniques including non-denaturing mass spectrometry where It is used to unambiguously identify Fe-S cluster species, as well as assign conversion and degradation products. This is observed as a +2 Da average increase in mass per sulfide, because natural abundance sulfur is primarily ^{32}S.

^{34}S labelling of RirA required cluster-free (apo-) sample. RirA was purified as previously described, but under aerobic conditions [1]. Residual Fe-S cluster was removed by dialysis of 200 µM RirA in 10 mL was dialysed into buffer I, with the addition of 5 mM DTT at 4 °C overnight. RirA was then diluted 5-fold into buffer H, loaded onto a 5mL Heparin column and washed with 30 mL of 2mM TCEP and 30 mL buffer H. Apo-RirA was eluted with 0-100% (v/v) buffer I over 10 CV. Apo-RirA was reconstituted with ^{34}S as described in section 2.3.1, but in the presence of ^{34}S-L-cysteine, instead of natural abundance L-cysteine. ^{34}S-L-cysteine was synthesised by Dr J. Crack using a thermostable *Geobacillus stearothermophilus* CysK, and commercially available ^{34}S-sulfur [7].

2.3.3. NO reactivity experiments

For NO reactivity experiments, DEA-NONOate (Sigma Aldrich) and PROLI-NONOate (Cayman Chemicals) were used as NO donors.

For UV-Vis spectroscopy, PROLI-NONOate solutions were prepared in 50 mM NaOH and quantified by absorbance at 252 nm (ε = 8400 M^{-1} cm^{-1}). PROLI-NONOate was titrated into the sample and incubated for 5 minutes at ambient temperature prior to measurement, to allow for full NO release of 2 moles of NO per mole of NONOate ($t_{1/2}$ ~2 s). In the case of UV-visible absorbance stopped-flow experiments, PROLI-NONOate was prepared and quantified. The NONOate solution was then diluted to the desired concentration in buffer C and incubated at room temperature for 5 minutes to allow for full NO release from NONOate (t 1/2 ~2 s). NONOate solutions were used within 30 minutes post NO release.

For non-denaturing ESI-MS experiments, NO donor DEA-NONOate solutions were prepared immediately before use in 250 mM ammonium acetate buffer, pH 7.2 at 4 °C and quantified by absorbance at 250 nm (ε = 6500 M^{-1} cm^{-1}). The half-life of DEA-NONOate at 25 °C in 250 mM ammonium acetate buffer pH 7.2 was determined as $t_{1/2}$ ~7 minutes, yielding overall 1.5 NO molecules per NONOate. DEA- NONOate was added directly to WhiD/ WhiD: σ^{HrdB}_4 samples to give a specific ratio of NO to [4Fe-4S] cluster of 20 over the course of 50 minutes. Samples were infused into the mass spectrometer using a temperature controlled syringe holder set to 25 °C. Spectra were averaged over 2.5 minutes to obtain data at intervals of 1.1 NO per cluster.

2.3.4. Fe^{2+} competition binding assay using Mag-fura-2

The dissociation constant (K_d) of Fe^{2+} to [3Fe-4S] RirA was determined by competition titrations in the presence of Mag-fura-2. Mag-fura-2 is a divalent metal chelator which binds Fe^{2+} to form a 1:1 complex with a K_d of 2.05 µM. It has been used previously to probe protein Fe^{2+} -binding [8]. Metal-free mag-fura-2 has an absorbance maximum of 366 nm, which shifts to 323 nm upon metal binding. Mag-fura-2 was dissolved in ultra-

pure water to give a 2 mM stock and stored at -80 °C until needed. Optimization experiments showed that absorbance changes due to Fe^{2+} binding to mag-fura-2 occurred quickly, thus spectra were taken immediately following each addition. Changes in mag-fura-2 were monitored using a Jasco V500 spectrometer using a 1 cm pathlength anaerobic quartz cuvette.

2.4. Techniques for protein analysis

2.4.1. Sodium dodecyl sulfate polyacrylamide gel electrophoresis (SDS-PAGE)

SDS-PAGE is an analytical method for the separation of macromolecules using an electric field to estimate their relative molecular mass. SDS is an amphipathic surfactant which denatures proteins and dissociates protein complexes. SDS also imparts a negative charge on to proteins, resulting in a roughly uniform charge-to-mass ratio which allows proteins to be resolved by size as they migrate through the polyacrylamide gel via attraction to the positively charged electrode. SDS-PAGE gels were prepared composed of 14% (v/v) resolving and 5% (v/v) stacking layers. The compositions of these are summarised in Table 2.4.

Table 2.5 SDS PAGE gel components

Component	14% Resolving	5% Stacking (mL)
Acrylamide (30%)	3.5 mL	1.28 mL
1M Tris pH 8.8	2.8 mL	-
1M Tris pH 6.8	-	1.25 mL
H_2O	1 mL	7 mL
SDS (10% w/v)	75 µL	100 µL
APS (10% w/v)	50 µL	75 µL
TMED	25 µL	25 µL

20 µl gel samples were mixed with 20 µl loading dye (200 mM Tris, pH 8.8, 200 mM DTT, 4% (w/v) SDS, 20% (v/v) glycerol, 0.2% (w/v) bromophenol blue) and heated to 100 °C for 5 minutes before loading. Gels were run for 50 minutes at 200 V and stained with Coomassie brilliant blue stain (0.1% (w/v) Coomasse blue, 10% (v/v) acetic acid 40% (v/v) MeOH, 50% (v/v) water) for 30 minutes, and de-stained (10% (v/v) acetic acid, 20% (v/v) MeOH, 70% (v/v) water) overnight. Alternatively, gels were visualised using silver stain (ProteoSilver™, Sigma Aldrich), following manufacturer's instructions.

2.4.2. Protein determination assays

Total protein concentration was determined using the Bradford (Bio-Rad) or Rose Bengal assays, with bovine serum albumin (BSA) as calibration standard.

2.4.2.1. Bradford assay

The Bradford assay involves an acidified solution of Coomassie Brilliant Blue G-250 dye. In this form the dye is primarily protonated and is red in colour. Upon addition to a protein solution, the dye deprotonates and the blue anionic form of the dye binds tightly to the protein via electrostatic and hydrophobic interactions [9]. BSA was used as the protein standard and was made up to 1 mg/mL stock concentration and incremented from 0-100 µL in order to obtain a calibration curve. Stocks were diluted with the same buffer as the proteins to be tested due to the pH sensitivity of the assay. The protein of unknown concentration was diluted to a range of concentrations to a final volume of 100 µL. 5x strength Bio-Rad dye was diluted to working strength and 5 mL of solution was added to each tube, mixed and left on the benchtop for 5 minutes before measuring the absorbance average of 3 readings for each sample at 595 nm.

2.4.2.2. Rose Bengal

Rose Bengal is a pink stain used as an alternative in protein assays for Fe-S cluster proteins, as the Bradford assay often overestimates the protein concentration. Rose Bengal has an absorbance maximum centred around 560 nm, which is bleached upon

addition of acetic acid. The protein-dye complex is resistant to this bleaching effect and remains stable for a prolonged period (>3 hours) [10]. A stock solution of Rose Bengal was made up to 1 mg/mL in water. BSA was again used to make up the calibration using 0.25 mg/mL diluted to 0-200 µL to a final volume of 200 µL. The protein of unknown concentration was also diluted to a range of concentrations to a final volume of 200 µL. 1.5 mL of 10 mM potassium phosphate pH 6.0 was added to each. This was followed by 100 µL of 1 mg/mL Rose Bengal stock solution and 100 µL of 50% (v/v) acetic acid in water. The absorbance at 560 nm was then taken as an average of 3 readings.

2.4.3. Iron assay

Fe-S cluster loading was determined by reference to a standard curve generated from Fe^{3+} solutions prepared from a commercial iron standard solution (SpectrosoL) in the range of 0-200 µM iron. A range of dilutions of protein of unknown iron concentration were prepared and all samples diluted with water to a final volume of 100 µL. 100 µL of 21.7% (v/v) nitric acid was then added to each sample and digested at 95 ^{O}C for 30 minutes. Samples were cooled for 2 minutes at 4 ^{O}C before the following was added to each sample: 0.6 mL of 7.5% (w/v) ammonium acetate, 100 µL of 12.5% (v/v) ascorbic acid and 100 µL of 10 mM Ferene. Samples were mixed and incubated at room temperature for 30 minutes. The concentration of iron present in the unknown sample was calculated by comparison of the $A_{593\ nm}$ measurement to the standard curve. The concentration of Fe-S cluster was estimated by dividing the iron concentration by the expected number of iron atoms present in the cluster [11].

2.4.4. Elemental analysis using inductively coupled plasma mass spectrometry (ICP-MS)

In preparation for ICP-MS analysis, samples were diluted to 500 µL to give a concentration of 1-20 µM. The diluted samples were then treated with 200 µL Ultra-Pure Nitric Acid, 200 µL Ultra-Pure Hydrogen Peroxide and fully digested overnight at 37

^{O}C. 500 µL of protein sample was combined with 500 µL ^{103}Rh internal standard (SPEX Certiprep) and 4 mL ultra-pure milli-Q water. For each sample three measurements were averaged, and data reported in ppb. This was then adjusted to the internal ^{103}Rh standard detected, dilution factor and and converted to molarity. Operation and calibration of the ICP-MS instrument was performed by Dr Graham Chivers, University of East Anglia.

2.4.5. Analytical gel filtration

Gel filtration, also known as size exclusion chromatography, separates molecules by size as they pass through a porous matrix. For steric reasons, proteins of different sizes will have different degrees of access to the matrix (defined to separate a specific size range) and elute in order of decreasing size. Molecules larger than the upper size limit are excluded from the matrix and elute rapidly with in the void volume of the column. Molecules within the size range of the column having greater access to the pores within the gel matrix, thus smaller molecules elute later than larger molecules (Figure 2.1). The elution volume is also affected by the conformation/ shape of the protein (Stokes radius). Gel filtration was utilised for analytical separations using a Superdex 75 10/300 GL column, pre-calibrated in the appropriate buffer. Anaerobic conditions were used with buffers purged with N_2 and kept in an anaerobic glovebox overnight, and until needed. Analytical gel filtration samples were prepared to ~40 µM, with 500 µL injected. The flow rate was set to 0.5 mL/ minute. Mass of proteins was estimated by reference to a calibration curve generated using BSA (3 mg/mL, 66 kDa), bovine erythrocyte carbonic anhydrase (10 mg/mL, 29 kDa) and horse heart cytochrome c *(*2 mg/mL, 12.5 kDa). Elution fractions were then analysed by SDS-PAGE and visualised either by Coomassie brilliant blue stain or silver stain using standard protocols (ProteoSilver^{TM}, Sigma Aldrich).

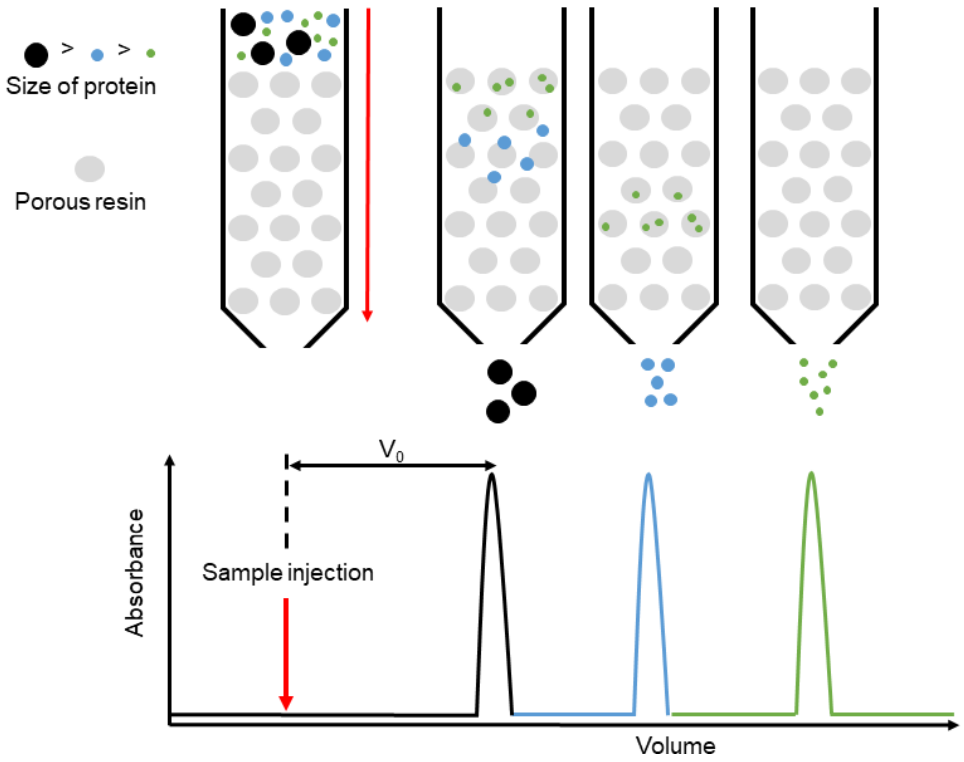

Figure 2.1 Analytical gel filtration.

Gel filtration columns are packed with porous resin made up of fine, uncharged beads, composed of polyacrylamide, agarose, or dextran polymers. The specific resin will have a pore size designed to separate proteins of a specific mass range according to size. In this work, a Superdex 75 10/300 GL column was used, an agarose-based resin with pore size designed to separate proteins between 3 – 75 kDa. Proteins larger than the size range of the gel filtration resin pass directly through and elute in the void volume (V_0). Within the size range, larger proteins are less able to access the pores of the resin and elute in lower volume than smaller proteins.

2.5. Spectroscopic techniques

2.5.1. UV-visible spectroscopy

UV-visible spectroscopy is a form of absorption spectroscopy. The region of wavelength covered by a regular UV-vis spectrophotometer is 200-1100 nm. This allows for the measurement of energy absorbed by a sample from the UV region (200-380 nm), visible region (380-750 nm) and the near infrared (>750 nm). Absorption spectroscopy can be used qualitatively to identify cluster species and oxidation states. Typically, Fe-S proteins display ligand-to-metal charge transfer bands from iron bound cysteines in the near UV and visible region, which results in a broad absorbance peak at 400 - 420 nm for [4Fe-4S] cluster proteins. [2Fe-2S] cluster proteins typically feature three bands in the 300-800 nm range. UV-Vis spectroscopy can also be used quantitatively to determine the concentration of protein or Fe-S cluster incorporation using the Beer-Lambert law which links absorbance (A) to the extinction coefficient (ε), the concentration of sample (c) and the pathlength of the sample (l) (Equation 2.1). The $A_{280\ nm}$ is often used to determine protein concentration as the aromatic side chains of tryptophan, tyrosine and phenylalanine absorb from 240-300 nm, due to excitation of electrons undergoing $\pi \rightarrow \pi^*$ transitions. In Fe-S cluster proteins, the cluster also significantly contributes to the 280 nm absorbance and would need to be accounted for. The yield of cluster incorporation for Fe-S cluster proteins can also be calculated using the absorbance measured at the absorbance maximum (~ 410 nm for [4Fe-4S] cluster proteins) and is typically ~4,000 $M^{-1}\,cm^{-1}$ per iron [12]. UV-visible absorbance measurements were made using a Jasco V550 spectrometer between 900 and 250 nm in a 1 cm pathlength quartz cuvette.

$$A = \epsilon . c . l \qquad \textbf{Equation.2.1}$$

Where A is absorbance, ε is molar extinction coefficient at the wavelength of absorbance ($M^{-1}\,cm^{-1}$), c is concentration of the absorbing species (M), and l is path length (cm).

2.5.2. CD spectroscopy

Circular dichroism is another form of optical absorption spectroscopy which can be applied to optically active chiral molecules. Within a CD spectrometer, monochromatic linearly polarised light is turned into left and right circularly polarized (LCP and RCP, respectively) light. The chiral molecule will preferentially absorb one type of circularly polarized light at a given wavelength, therefore depending on whether LCP or RCP light is absorbed to a greater extent, a positive or negative CD signal will result. CD data are measured as differential absorbance (ΔA) of left and right circularly polarized light (A_{LCP} and A_{RCP}, respectively) and expressed as:

$$\Delta A = A_{LCP} - A_{RCP} \qquad \textbf{Equation.2.2}$$

CD Data is commonly reported as ellipticity (θ), in millidegrees (mdeg). This is related to the absorbance by a factor of 32.98:

$$\theta = 32.98\,\Delta A \qquad \textbf{Equation.2.3}$$

As CD spectroscopy is an absorption technique based on Beer-Lambert's law, θ can be converted to molar absorptivity (Δε), which normalizes the circular dichroism spectra based on concentration and pathlength. Therefore:

$$\Delta A = (\varepsilon \mathrm{L} - \varepsilon \mathrm{R}) C l \qquad \textbf{Equation.2.4}$$

and

$$\Delta \varepsilon = \theta / (c \cdot l \cdot 3298) \qquad \textbf{Equation.2.5}$$

where c is the concentration (mol/L), l is the pathlength(cm), and ε_L and ε_R are the molar extinction coefficients for LCP and RCP light.

CD is most commonly used in the far UV region between 260 to 180 nm to study secondary protein structures. In the visible region, CD is a useful technique for studying

metallo-proteins, including Fe-S cluster proteins, as transition here reflect the cofactor to probe the ligand environment. Although difficult to predict the exact shape and intensity of an Fe-S cluster protein spectrum. Typically, [2Fe-2S] cluster proteins have more well-structured CD spectra in comparison to [4Fe-4S] cluster proteins [5]. The CD spectra reported here were measured with a Jasco J810 spectropolarimeter between 800 and 250 nm in a 1 cm pathlength quartz cuvette.

2.6. ESI-MS

Mass spectrometry is an analytical technique used to provide both qualitative and quantitative information on proteins. Generally, a mass spectrometer is composed of three basic components: an ion source, a mass analyser and a detector. Mass spectrometry experiments described were performed using a Bruker micrOTOF-QIII electrospray ionisation (ESI) time-of-flight (TOF) mass spectrometer (Bruker Daltonics). A schematic of the instrument is outlined in Figure 2.2.

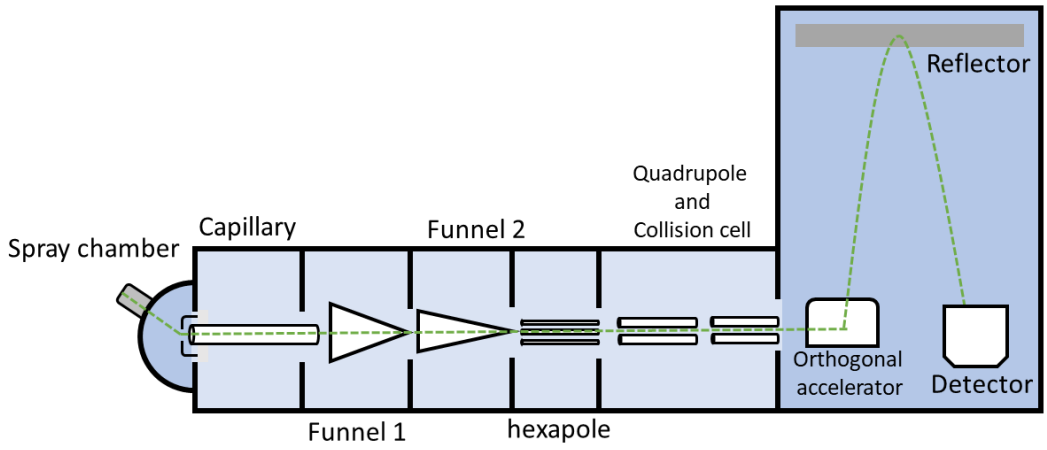

Figure 2.2 Schematic representation of Bruker microTOF-QIII ESI-TOF-MS

Components are labelled**.** Green line indicates path taken by analyte ions from introduction into the spray chamber, through the capillary, funnels, hexapole, mass analysers (quadrupole and TOF). Ions then pass to the detector, which generates the raw m/z spectrum.

In a typical mass spectroscopy experiment, the sample analyte solution is sprayed through a nebulizer needle (a narrow stainless steel / glass capillary). The capillary is held at high voltage, producing a potential difference between the spray needle and the sampling cone (the entrance to the spectrometer). The analyte solution is nebulised into an aerosol of highly charged droplets, due to the strong electric field. This mist of charged droplets further undergoes desolvation, in which the mobile phase solvent evaporates from the droplets. This is aided by the nebuliser gas (N_2). Heated drying gas which flows around the capillary and out from behind the spray shield, assisting solvent evaporation and preventing the entry of uncharged material into the spectrometer [13]. During desolvation, there comes a point at which surface tension no longer sustains the charge (the Rayleigh limit). This results in a coulombic fission event in which droplet "explodes" to form independently charged analyte ions. The subsequent gas-phase ions are drawn into the sampling cone. A potential difference of ~500 V between the spray shield and sampling cone draws ions in to the spectrometer [13]. The ESI process described is summarised in Figure 2.3. Since gas-phase ions are very reactive and short lived, analysis and detection in ESI-MS must be conducted under high vacuum. Therefore, once exited from the capillary, ions enter tandem ion funnels, a series of stacked ring electrodes with decreasing inner diameters. The ion funnels focus the beam of ions and transmit them to the low-pressure vacuum environment. Ions then enter the hexapole where pressure is lowered to 10^{-4} mbar and transported into the Q-q stage, which consists of a quadrupole and collision cell. The quadrupole stabilises and directs ions and can act as a mass filter to focus on a specific range of ion masses. The collision cell is utilised for fragmentation, where resulting daughter ions are separated in the second mass analyser. At the end of the collision cell is the TOF mass analyser. In the Bruker micrOTOF-QIII, this consists of an orthogonal accelerator and a reflector. The orthogonal acceleration unit undergoes pulses between a "fill" period, in which the region is filled with ions, and an "extract" mode, in which ions are accelerated in a vertical direction towards the reflector, which imposes an electric field that pushes the ions back down the flight tube. There are minute variations in the kinetic energy of ions as they are released due to the initial velocity and position of ions in the accelerator. As these ions approach the reflector, ions with more energy fly deeper into the reflector, and spend more time before reversing their direction of travel towards the detector,

thus correcting for variations in kinetic energy for ions of the same m/z and improving resolution. The determination of m/z is based upon the time it takes for ions to impact the detector.

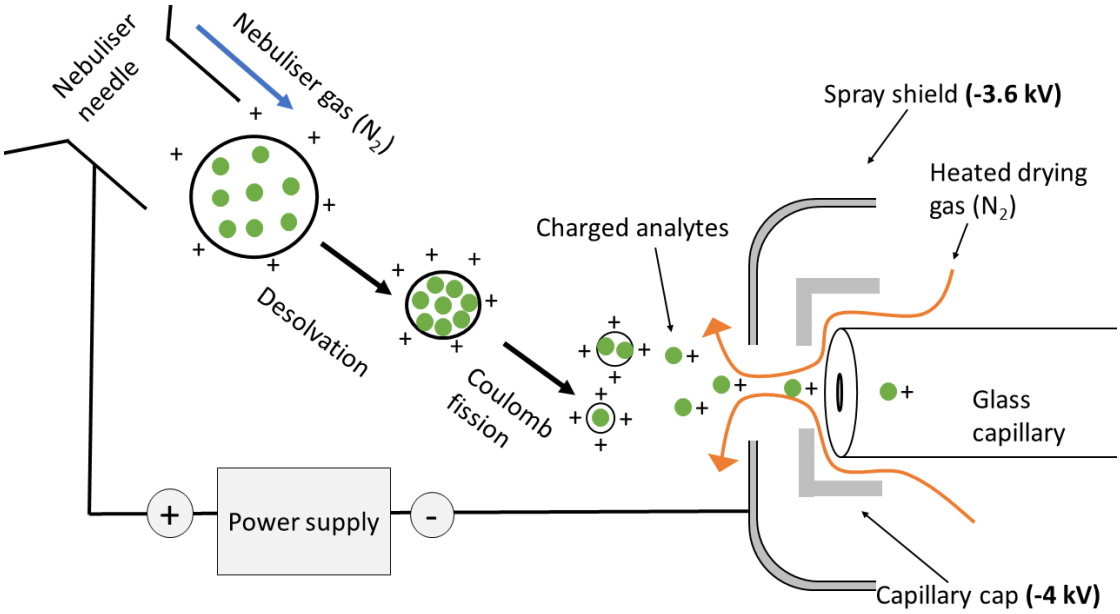

Figure 2.3 Electrospray ionisation occurs within the spray shield.

Analytes (green) are shown to exit the nebuliser needle, forming charged droplets which undergo desolvation and coulomb fission to form gas phase analyte ions. Analyte ions are then focused into the sampling cone and capillary, aided by the charge differential of the spray shield (-3.5 kV) and the capillary cap (-4 kV). Heated drying gas (orange) assists with the removal of uncharged material.

The resultant spectrum is a plot of relative intensity as a function of m/z, in which each analyte species will appear as an envelope of peaks resembling a Gaussian distribution. These peaks correspond to several sequential charge states. The raw m/z data is processed using the ESI Compass version 1.3 software automated Maximum Entropy deconvolution algorithm, and deconvoluted neutral mass spectra generated, which correspond to the mass of the protein. To aid the "deconvolution" process, a mass range is chosen appropriate for the protein analysed. Resultant exact masses (± 1 Da) are reported from peak centroids representing the isotope average neutral mass. Typically,

the deconvoluted spectrum is presented as percentage relative intensity (%), in which the most abundant species becomes 100% relative intensity and other species are normalised around this species.

Two methods of mass spectrometry experiments were carried out. LC-MS combines liquid chromatography with mass spectrometry, thus separating, and providing exact masses of proteins. LC-MS is a denaturing method, in which protein samples are unfolded in the acetonitrile/formic acid solvent. In contrast, and as the name suggests, non-denaturing ESI-MS (also known as native MS) allows for the study of proteins in their folded (or native) state. Thus, it is useful for studies of metalloproteins with intact cofactors, as well as protein complexes, as non-covalent interactions are preserved upon ionisation. Protein conformations can also be distinguished from charge state distributions.

2.6.1. Liquid chromatography mass spectrometry (LC-MS)

LC-MS was performed using an UltiMate 3000 HPLC system (Dionex). The ESI-TOF-MS was calibrated before use using ESI-L Low Concentration Tuning Mix (Agilent Technologies). Samples were typically made to 50 µL of ~50 µM protein, which was diluted with 450 µL LC-MS buffer (2% (v/v) acetonitrile, 0.1% (v/v) formic acid). 20 µL of each sample were injected onto a ProSwift reversed phase RP-1S column (4.6 x 50 mm; Dionex). Gradient elution was performed at a flow rate of 0.2 mL/minute using a linear gradient (15 minutes) of solvent A (0.1 % (v/v) formic acid) and solvent B (acetonitrile and 0.1% (v/v) formic acid) from 2 to 100% (v/v). The eluent was continuously infused into a Bruker micrOTOF-QIII mass spectrometer running Hystar (Bruker Daltonics), Mass spectra were acquired with the following parameters: dry gas flow 8 L min^{-1}, nebuliser gas pressure 0.8 bar, dry gas 240 ˚C, capillary voltage 4500 V, offset 500 V, collision RF 650 Vpp. Mass spectra from manually chosen elution volumes were averaged and deconvoluted over mass ranges appropriate for the sample analysed.

2.6.2. Non-denaturing mass spectrometry

As with LC-MS, The ESI-TOF-MS was calibrated before use using ESI-L Low Concentration Tuning Mix (Agilent Technologies). Non-denaturing ESI-MS samples were buffer exchanged into a volatile buffer (250 mM ammonium acetate, pH 7.2) inside an anaerobic cabinet using mini-PD10 (GE healthcare) desalting columns. Proteins or protein-DNA mixtures were infused directly into the ESI source of a Bruker micrOTOF-QIII mass spectrometer operating in positive ion mode at 0.3 mL/hour using a syringe pump. MS data were acquired typically around the m/z range of 1,000 – 3,500, continuously for 2-5 minutes using Bruker oTOF Control software. Unless stated overwise, non-denaturing ESI-MS parameters were as follows: dry gas flow of 4 L/minute, nebuliser gas pressure 0.8 Bar, dry gas 180 °C, capillary voltage 4500 V, offset 500 V, ion energy 5 eV, collision RF 650 Vpp, collision cell energy 10 eV. Mass spectra were averaged over time recorded, and deconvoluted over mass ranges appropriate for the sample analysed.

2.7. Reaction kinetics by stopped-flow UV-visible spectroscopy

Stopped-flow UV-visible spectroscopy is a rapid mixing technique used to study the kinetics of fast reactions in solution. The instrument is comprised of two sample syringes, which when a shot is fired, are pushed by a pneumatic driving ram and a specific volume of each sample is combined within an observation cell. Absorbance data acquisition is triggered as the sample begins to mix, allowing for a very short data acquisition deadtime (<2 ms). UV-visible stopped-flow experiments were performed with a Pro-Data upgraded Applied Photophysics Bio-Sequential DX.17 MV spectrophotometer, with a 1 cm path length cell. All stopped-flow experiments were carried out in anaerobic buffer using gastight syringes (Hamilton) at 25 °C. Prior to use, the stopped-flow system was flushed with ~50 mL of anaerobic buffer. Final traces are average of 10 individual traces. Fitting of kinetic data was performed using OriginPro8.

2.8. Protein-DNA interaction techniques

Electromobility shift assays (EMSA), also known as gel shift assays, were used to detect protein-DNA complexes. EMSA utilises a non-denaturing polyacrylamide gel and is based on the principle that the rate of migration of the complex is slower than the DNA alone. DNA probes corresponding to promoters in Table 2.5 were PCR-amplified using *S. venezuelae* genomic DNA and 5-Carboxyfluorescein (5-Fam) labelled primers (Eurofin). All probes and PCR steps were kindly performed by Dr Matt Bush (John Innes Centre, Norwich). EMSAs were carried out with varying concentrations of protein, and DNA probe in binding buffer (10 mM HEPES, 50 mM NaCl, 2.5% (w/v) sucrose, 2.5 mM $MgCl_2$, 1 mM DTT, pH 7.9) to a final volume of 20 µL. 1 µl of DNA probe is used to final concentration of 2-3 nM. The mixture was incubated on ice for 10 minutes, at which time, 2 µl of loading dye (50% glycerol (v/v), 50 mM Tris, 0.03% (w/v) bromophenol blue) was added and the reaction mixture immediately separated on a 7% (v/v) polyacrylamide gel in 0.5x TBE (89 mM Tris, 89 mM boric acid, 2 mM EDTA). Polyacrylamide gels were pre-run at 30 mA for 2 minutes prior to use. Gels were visualized (excitation, 488 nm; emission, 530 nm) on a molecular imager Typhoon FLA 9500 (GE healthcare) and processed using ImageJ (NIH).

Table 2.6 Promoter regions used in EMSA, primers used underlined.

Primers indicate the start and end of DNA probes used for EMSAs.

Promoter	Sequence
ftsW	ATCGAACTGGTCGAGGAGGTCCAGGGAGTCACGTACGTCGACGACTC CAAGGCCACCAACACCCACGCCGCGGAAGCCTCGTTGGCGGCCTACG ACCCGATCGTCTGGATCGCCGGCGGACTCGCCAAGGGC**GCGACCTTC** **GACGAACTG**GTGGAGAAGTCGGCGAAGCGCTTGCGCGGGGCCGTCCT GATCGGTGCCGACCGCGCCCTGATCCGCGAAGCCCTGGCGCGACACG CCCCGGAGGTACCGGTGGTGGACCTCGACCGGACCGACACTGGGGCG ATGTCCGAGGCGGTCCGCGAGGCGGCCCGGCTCGCCCGGGCGGGGGA CACGGTCCTGCTGGCCCCGGCCTG**CGCCTCGATGGACATGTTC**ACCA ACTACAACAAGCGGGGCGAGGCCTTCGCGGACGCGGTCCGCGCCCTC GCCGCCACCGGGGACGCCTGACCCGACCAGTGGGAGGGTCCGGCCGG ACCGGGCACGACCAGGAGGGGGCAGCGACC
filP	CTGGAGGTGCTGGTGCGCCGCCGCAAGGACATCAATGCGGAGATCTC CCGTGTCCAGGACGTGCTGGAGGCGTTGGAGTCTTTCGAGACCCCGG CTTCGGGTGC**CAAGTCCGCCGGTGCGGT**GGGCGCCAAGGCGGGCGCG TCAGCGGGGTCCACTCGTTCGGGTGGCAAGTCCCAGGACGGGTAGCC ACTCAAAAGGCTGGACATTCTCCAGATCAAACGGGCATACGCTCGAT GACACGCCGCTTCGGCCCCTAGGATTCCCTCTAACACCTCACCGGTC TCATTCGACAGGAAACCCATGAGCGACACATCCTCCCCCTTCGGCTT CGAGCTCGTGCGGCGCGGTTACGACCGCGGTCAGGTGGACGACCGCA TTA**CCAAGCTCGTGTCCGACC**GTGACAGTGCCCTGTCCCGCATCACC TCTCTGGAGAAGCGCATCGAGGAACTC

2.9. References

1. Pellicer Martinez, M.T., et al., *Sensing iron availability via the fragile [4Fe-4S] cluster of the bacterial transcriptional repressor RirA.* Chem Sci, 2017. **8**(12): p. 8451-8463.
2. Crack, J.C., et al., *Influence of association state and DNA binding on the $O_{(2)}$-reactivity of [4Fe-4S] fumarate and nitrate reduction (FNR) regulator.* Biochem J, 2014. **463**(1): p. 83-92.
3. Hanahan, D. and D. Glover, *DNA cloning: a practical approach.* DNA cloning: a practical approach, 1985. **1**: p. 109-135.
4. Crack, J.C., et al., *Reactions of nitric oxide and oxygen with the regulator of fumarate and nitrate reduction, a global transcriptional regulator, during anaerobic growth of Escherichia coli.* Methods Enzymol, 2008. **437**: p. 191-209.
5. Freibert, S.A., et al., *Biochemical reconstitution and spectroscopic analysis of iron-sulfur proteins.* Methods Enzymol, 2018. **599**: p. 197-226.
6. Zheng, L., et al., *Cysteine desulfurase activity indicates a role for NifS in metallocluster biosynthesis.* Proc Natl Acad Sci U S A, 1993. **90**(7): p. 2754-8.
7. Crack, J.C., M.Y.Y. Stewart, and N.E. Le Brun, *Generation of ^{34}S-substituted protein-bound [4Fe-4S] clusters using 34S-L-cysteine.* Biology Methods and Protocols, 2019. **4**(1).
8. Rodrigues, A.V., et al., *Iron loading site on the Fe-S cluster assembly scaffold protein is distinct from the active site.* Biometals, 2015. **28**(3): p. 567-76.
9. Bradford, M.M., *A rapid and sensitive method for the quantitation of microgram quantities of protein utilizing the principle of protein-dye binding.* Anal Biochem, 1976. **72**: p. 248-54.
10. Perez-Ruiz, T., et al., *Determination of proteins in serum by fluorescence quenching of rose bengal using the stopped-flow mixing technique.* Analyst, 2000. **125**(3): p. 507-10.
11. Crack, J.C., et al., *Techniques for the production, isolation, and analysis of iron-sulfur proteins.* Methods Mol Biol, 2014. **1122**: p. 33-48.
12. Sweeney, W.V. and J.C. Rabinowitz, *Proteins containing 4Fe-4S clusters: an overview.* Annu Rev Biochem, 1980. **49**: p. 139-61.
13. Banerjee, S. and S. Mazumdar, *Electrospray ionization mass spectrometry: a technique to access the information beyond the molecular weight of the analyte.* Int J Anal Chem, 2012. **2012**: p. 282574.

Chapter 3. Characterisation of *S. venezuelae* WhiB and WhiD

3.1. Introduction

WhiB and WhiD are *Streptomyces* Wbl proteins that have been identified as transcriptional regulators involved in *Streptomyces* development. Examples of both have previously been characterised to varying extents. *S. coelicolor* WhiB (*Sc*WhiB) was the first identified member of the Wbl family of proteins [1]. Recently, it was demonstrated that WhiB functions to coordinate the cessation of aerial hyphae growth and initiate sporulation septation in *Streptomyces* with another Whi regulator protein called WhiA. The interaction between these two proteins is covered in more detail in chapter 5. *S. venezuelae* WhiB (*Sv*WhiB) performs the same function: *S. venezuelae* w*hiB* mutants form long, extended aerial hyphae that fail to produce septa or to segregate chromosomes [2]. Similarly, WhiB homologues in mycobacteria, WhmD and WhiB2 in *M. smegmatis and M. tuberculosis* respectively and WhcD in *Corynebacterium glutamicum,* are all found to be involved in septation and cell division. *C. glutamicum* Δ*whcD* mutants displayed altered cell morphology with elongated filamentous rods with increased diameters [3]. Disruption of the *M. smegmatis whmD* gene leading to irreversible filamentous growth and unusual, at times non-existent, septation events [4]. Notably, the consequence of the loss of WhiB homologues is more severe in mycobacteria as the *whiB2* gene was shown to be essential [4, 5]. In contrast, a strain carrying a deletion of *Streptomyces* WhiB is viable during vegetative growth and only blocked in developmental sporulation septation, and *Corynebacterium whcD* mutant strains also only showed retarded growth compared to the wild type [2, 3, 6]. An interesting homologue of WhiB was found in the TM4 bacteriophage. WhiBTM4 is highly similar to *M. tuberculosis* WhiB2 and acts by competitively binding to the *whiB2* promoter in its apo-form [7]. Sequence alignments of WhiB homologues show extensive sequence similarities (Figure 3. 1). *Sv*WhiB shares 94% identity with *Sc*WhiB and 42-67% identity with *Mt*WhiB2, *Ms*WhmD and *Cg*WhcD. Variations occur primarily in WhiB homologues through N-terminal extensions, In the case of WhmD, this N-terminal extension was non-essential for activity [8].

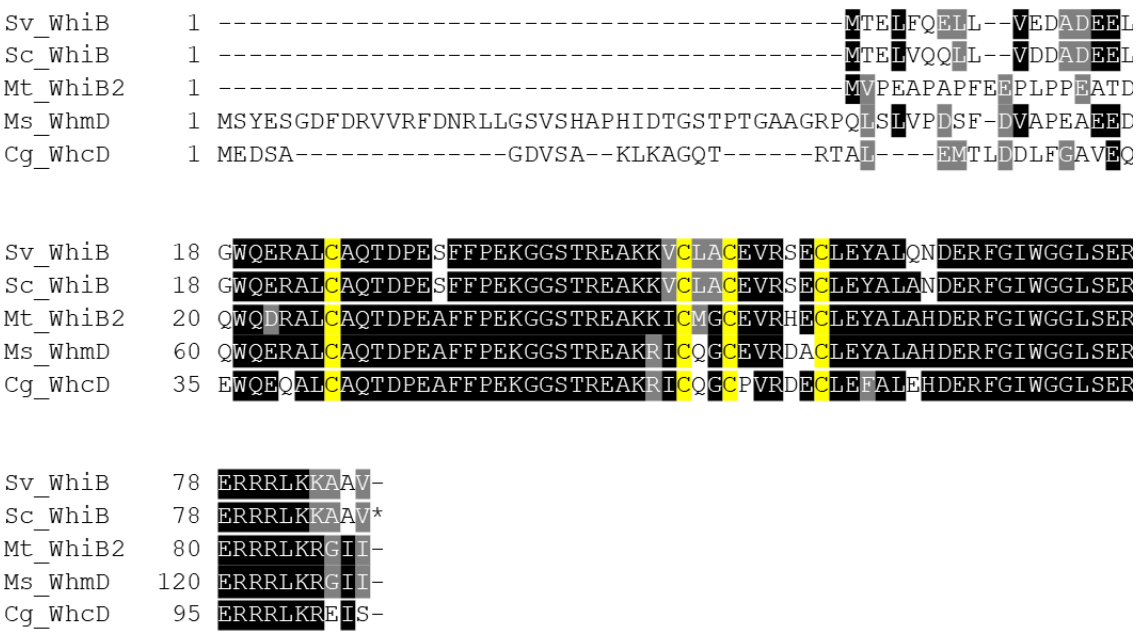

Figure 3.1 Sequence alignment of SvWhiB with frequently studied homologues.

Actinobacteria species included are *S. venezuelae* (Sv) *S. coelicolor* (Sc), *M. tuberculosis* (Mt), *M. smegmatis* (Ms) *C. glutamicum* (Cg). Conserved cysteines are highlighted in yellow.

WhiD is also required for the transition from vegetative to aerial growth in *Streptomyces*. *Sc*WhiD was the first Wbl protein to be shown to bind a [4Fe-4S] cluster [9]. In contrast to a *whiB* mutant which does not undergo septation, *whiD* mutants are able to form spores, but they are irregularly sized, sensitive to heat, prone to lysis and show variability in cell wall deposition [10]. The ability to form spores indicates that WhiD is involved in later stages of sporulation. Little else is known about the physiological functions of WhiD in *Streptomyces*.

In contrast, the *M. tuberculosis* WhiD homologue WhiB3 is one of the most widely studied of the 7 *M. tuberculosis* proteins and is shown to be heavily involved in modulating the host-pathogen interaction. WhiB3 is dispensable for *in vivo* growth, but is significantly upregulated in responses to the challenging low pH conditions encountered by *M. tuberculosis* during phagocytosis by macrophages in the lungs during early infection via the PhoPR regulatory system, and deletion of WhiB3 significantly compromises its survival at pH 4.5 [11-14]. WhiB3 is also upregulated in response to

hypoxia found during granuloma formation, and increased NO which is released by macrophages as part of the innate immune response [15]. In response to these infection stresses, WhiB3 facilitates metabolic switching to fatty acids as an energy source rather than carbohydrates during infection and latency. WhiB3 also regulates virulence lipid anabolism which functions as a reductant sink in order to maintain redox balance and long term persistence of *M. tuberculosis in vivo* [16, 17]. WhiB3 regulates the production of complex secretory polyketide lipids and proteins that modulate the host's immune response, thereby helping to regulate intraphagosomal pH, blocking phagosome maturation and facilitating granuloma formation [11, 12, 18].

Biochemical studies have demonstrated the sensitivity of Wbl proteins to O_2 and nitrosylation by nitric oxide (NO) [19-21]. In a recent study, a physiological link to the ability of *M. tuberculosis* to utilise WhiB3 in sensing and responding to ROS and RNS stress was provided, possibly explaining the ability of *M. tuberculosis* to counteract ROS and RNS despite lacking canonical primary regulators of oxidative and nitrosative stress such as OxyR, SoxR, NsrR or FNR [18].

WhiD homologues are well conserved within the Actinomycetes. Sequence alignments show high sequence similarity within the homologues (Figure 3.2). Strikingly, *Sv*WhiD and ScWhiD have 100% sequence identity from residues 1 – 95, but overall, 78% sequence identity due to a C-terminal extension in *Sv*WhiD. Although unusual, Blast analysis revealed that WhiD-like proteins exist with a comparable C-terminal extension in some other *Streptomyces* species. The significance of this will be explored in section 3.3.1.

Figure 3.2 Sequence alignment of SvWhiD with frequently studied homologues.

Actinobacteria species included are *S. venezuelae* (Sv), *S. coelicolor* (Sc), and *M. tuberculosis* (Mtb). Conserved cysteines are highlighted in yellow.

This chapter details the biochemical characterisation of *Sv*WhiB and *Sv*WhiD highlighting the similarities and differences between these proteins and Wbl proteins characterised previously from *S. coelicolor* and *M. tuberculosis*.

3.2. Expression and purification of *Sv*WhiB and *Sv*WhiD

Two different plasmids were used for the overexpression of *Sv*WhiB. *Sv*WhiB was initially over-produced by ligating codon-optimised *whiB* into pET28a using *Nde*I and *Hin*dIII sites, generating pMSW4 to encode an N-terminally His_6-tagged WhiB. This vector was introduced into in *E. coli* BL21 (DE3) and the *whiB* gene was overexpressed. WhiB was purified anaerobically as described in methods section 2.1. Elution from nickel- charged HisTRap Ni-IMAC column resulted in a light straw yellow coloured protein solution. However, WhiB had a poor cluster loading. Protein assays in conjunction with iron assays indicated a cluster load of ~15%. A pETDuet-1 vector, which permits the co-expression of two target genes and was used to attempt co-expression of the proteins *Sv*WhiB and *Sv*WhiA (pMSW5) to encode an N-terminal $(His)_6$-WhiB and un-tagged WhiA. Unfortunately, the co-expression was unsuccessful there as was no observed expression of *whiA* encoded in the second cloning site. However $(His)_6$-WhiB was produced much better with a higher cluster loading of ~50%. The reason for this enhanced expression is unclear but could be due to the composition of the N-terminal His-tag, which in the pET28a vector included a thrombin cleavage site. This is a larger tag than in the pETDuet-1 vector, which does not contain a thrombin cleavage site. The larger protein tag may hinder protein folding and destabilise the cluster. Thus, all further characterisation of WhiB utilised the pETDuet-1 vector-based construct. *Sv*WhiD was over-produced by ligating the codon-optimised *whiD* into pET28a using *Nde*I and *Hin*dIII sites, generating pMSW1 to encode an N-terminally His_6-tagged WhiD. This vector was then introduced in *E. coli* BL21 (DE3).

WhiD was purified anaerobically as described in methods section 2.1. Elution from a nickel- charged Hi-trap chelating column resulted in a dark brown coloured protein solution. Protein assay, in conjunction with iron assay, and ICP-MS confirmed that cluster load was typically ~90%. Protein purity was assessed by SDS-PAGE (Figure 3.3).

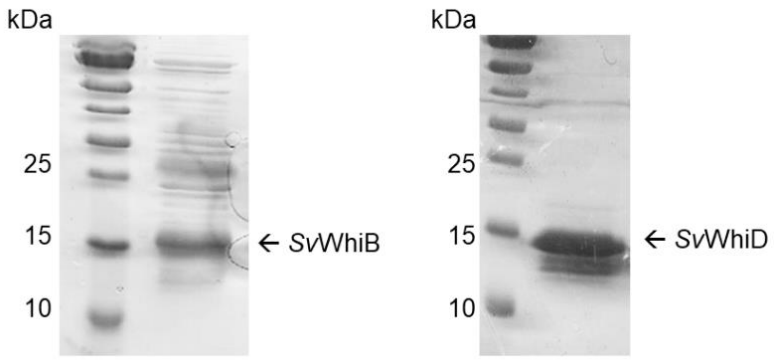

Figure 3.3 SDS-PAGE gels of as isolated *Sv*Wbl proteins.

Gels reveal typical SDS-PAGE gels after purification with Ni-charged Hi-trap chelating column. *Sv*WhiB and *Sv*WhiD are as indicated. The presence of the two protein bands located under *Sv*WhiD is explored in section 3.3.1.

3.3. Characterisation of as isolated *Sv*WhiB and *Sv*WhiD

UV-visible absorption spectroscopy revealed a band at 410 nm for both *Sv*WhiB and *Sv*WhiD, typical of a [4Fe-4S] cluster (Figure 3.4A and B). It is also possible to see the absorbance peak due to the aromatic amino acids in the protein at 280 nm. The extinction coefficient obtained from UV-visible absorption spectra at 410 nm can be used to determine concentration of [4Fe-4S]-bound protein and was determined as 18,180 and 17,500 M^{-1} cm^{-1} for WhiB and WhiD respectively. Circular dichroism (CD) spectroscopy was also used to provide information about the cluster environment (Figure 3.4C and D). Both spectra of WhiB and WhiD have distinct spectral features that are similar to those previously reported for *Sc*WhiD and *Mt*WhiB1, consistent with the presence of a [4Fe-4S] cluster in a similar protein environment [22, 23]

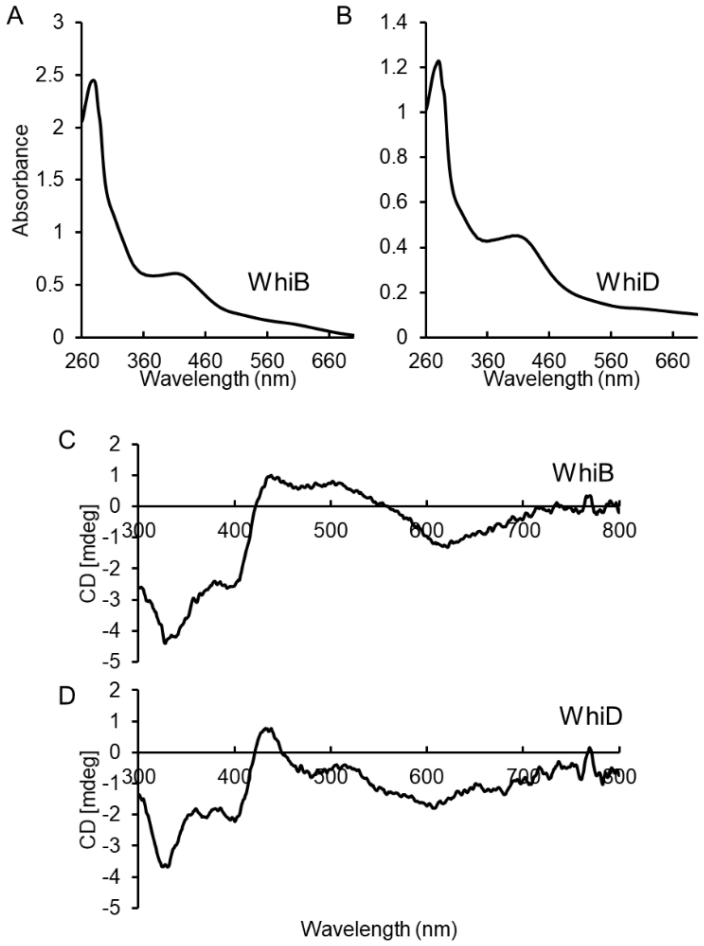

Figure 3.4 Spectroscopic characterisation of *Sv*Wbl proteins.

UV-visible absorbance spectra (A and B), and CD spectra (C and D) of *Sv*WhiB and *Sv*WhiD as indicated. Protein concentrations were 65 µM (51 % cluster load) and 29 µM (89% cluster load) for SvWhiD and SvWhiB respectively. Samples were in 50 mM Tris, 300 mM NaCl pH 7.2, 1 cm pathlength.

Liquid chromatography-mass spectrometry (LC-MS) can provide the exact mass data of proteins. The LC-MS spectrum of purified WhiD contained a major peak at 15,923 Da (predicted mass 15,924 Da) corresponding to cluster-free (apo) WhiD with an N-terminal methionine cleavage (Figure 3.5A). The LC-MS spectrum of purified WhiB shows the main peak at 11,263 Da (predicted mass 11,267 Da) corresponding apo-WhiB with an N-terminal methionine cleavage. The 4 Da difference between the predicted and observed mass corresponds to hydrogens lost due to disulfide bridging between the now available cysteines (Figure 3.5B).

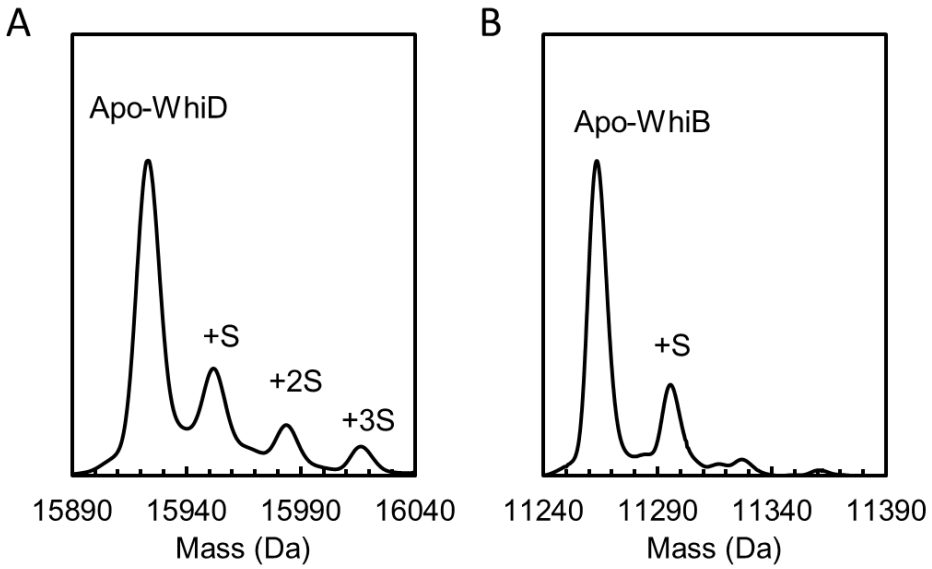

Figure 3.5 LC-MS characterisation of SvWbl proteins.

Deconvoluted LC-MS spectra of *Sv*Wbl proteins on an expanded mass scale. Apo-WhiD (A) and apo-WhiB (B) are observed, lacking their N-terminal Met residue. Sulphur adducts are indicated. WhiD (30 µM) and WhiB (15µM) were in an aqueous mixture of 2% acetonitrile, 0.1% (v/v) formic acid.

Non-denaturing ESI-MS (also referred to as native MS) confirmed the presence of the [4Fe-4S] cluster in both proteins. For WhiD, the range was set to 1500 – 2500 m/z to include a single charge packet consisting of charges +7, +8 and +9 (Figure 3.6A). The deconvoluted spectrum contained a major peak at 16,273 Da corresponded to [4Fe-4S] WhiD (predicted mass 16,273 Da) (Figure 3.6B). Adducts of +16, +38 and +61 are present in addition to [4Fe-4S] WhiD. Although these adducts are not identified for certain, the initial +16 adduct likely correspond to an oxygen adduct, and the +38 and +61 adducts are likely sodium adducts (Na and 2 Na, respectively) in addition to the oxygen adduct. Similarly, the range for WhiB was set to 1100 – 2500 m/z to include a single charge packet including charges +6, +7, +8 and +9 (Figure 3.7A). The deconvoluted spectrum contains a single major peak corresponding to [4Fe-4S] WhiB at 11,617 Da (predicted mass 11,617 Da) (Figure 3.7B). Again, adducts can be observed in addition to [4Fe-4S] WhiB at +23 and +38. The +23 adduct is likely corresponds to a single sodium. The +38 adduct likely corresponds to an oxygen in addition to the Na adduct. The origin of the sodium adducts could arise from incomplete buffer exchange from buffer containing high NaCl content into the volatile ammonium acetate buffer. The origin of the potential oxygen adducts was less clear but may be generated in aqueous samples in the ESI-source [24].

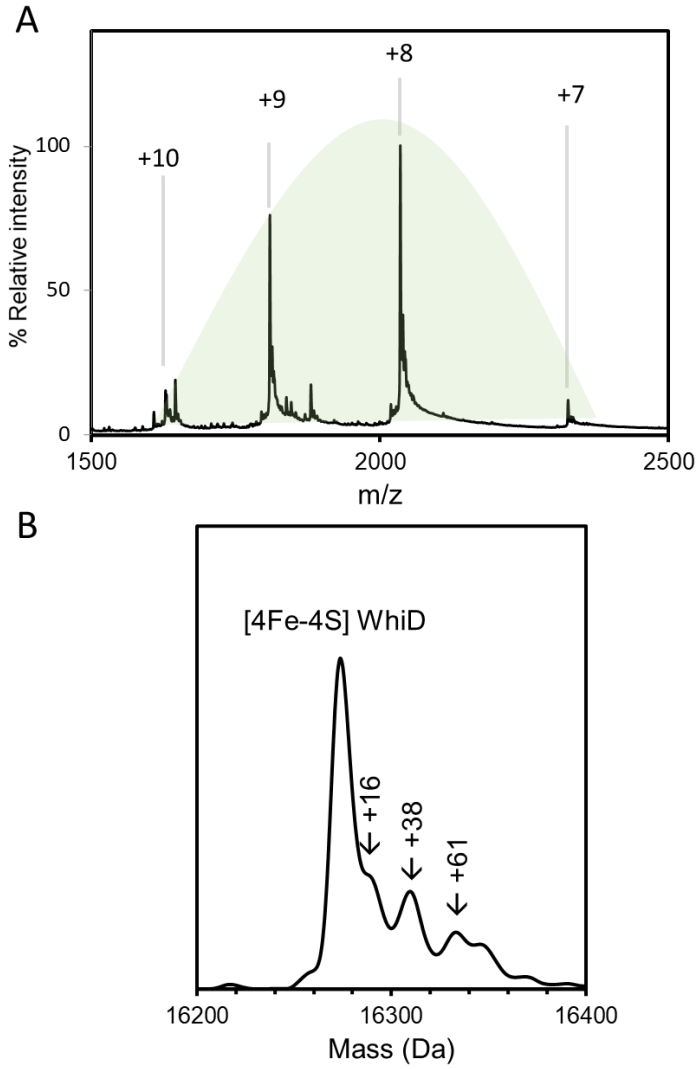

Figure 3.6 Non-denaturing mass spectrometry of *Sv*WhiD.

(A) m/z spectrum of WhiD under non-denaturing conditions shows bimodal charge state distribution. The major charge packet includes charges +7, +8 and +9 (green box). **(B)** Deconvoluted mass spectrum of WhiD showing the major species as [4Fe-4S] WhiD. Mass of adducts are indicated. WhiD (10 µM in cluster, 92% cluster load) was in 250 mM ammonium acetate, pH 7.2.

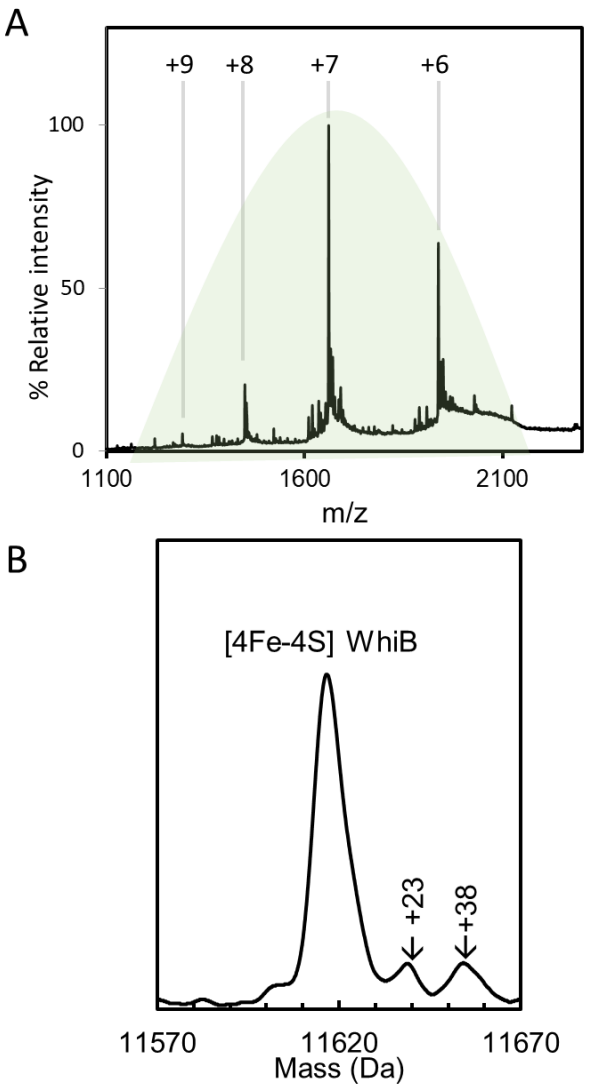

Figure 3.7 Non-denaturing mass spectrometry of *Sv*WhiB.

(A) m/z spectrum of WhiB under non-denaturing conditions. Charge states of ions are as indicated. **(B)** Deconvoluted mass spectrum of WhiB showing the major species as [4Fe-4S] WhiB. Mass of adducts are indicated. WhiB (15 µM in cluster, 64% cluster load) was in 250 mM ammonium acetate, pH 7.2.

3.3.1. Fragmentation of WhiD

SDS-PAGE analysis of as isolated *Sv*WhiD in Figure 3.3 presented three closely located, but distinct bands around the predicted mass of WhiD. This could be resultant from the truncation of *Sv*WhiD in two distinct places. LC-MS was used to identify these truncated species. Aside from the full length WhiD protein at 15,923 Da, two lower intensity peaks were also observed at 13,390 and 12,805 Da, resulting from cleavage of the 26 and 33 C-terminal residues, respectively, from the full-length protein (predicted masses 13,391 and 12,805 Da, respectively). From LC-MS and SDS-PAGE, the truncated forms were estimated to account for < 10% of the total protein (Figure 3.8A). The deconvoluted non-denaturing mass spectra of WhiD revealed in addition to the cluster bound full length protein, a peak at 13,154 Da, which corresponds to the [4Fe-4S]-bound form of WhiD lacking the 33 C-terminal residues (predicted mass 13,155 Da), indicating that these residues are not important for cluster binding (Figure 3.8B).

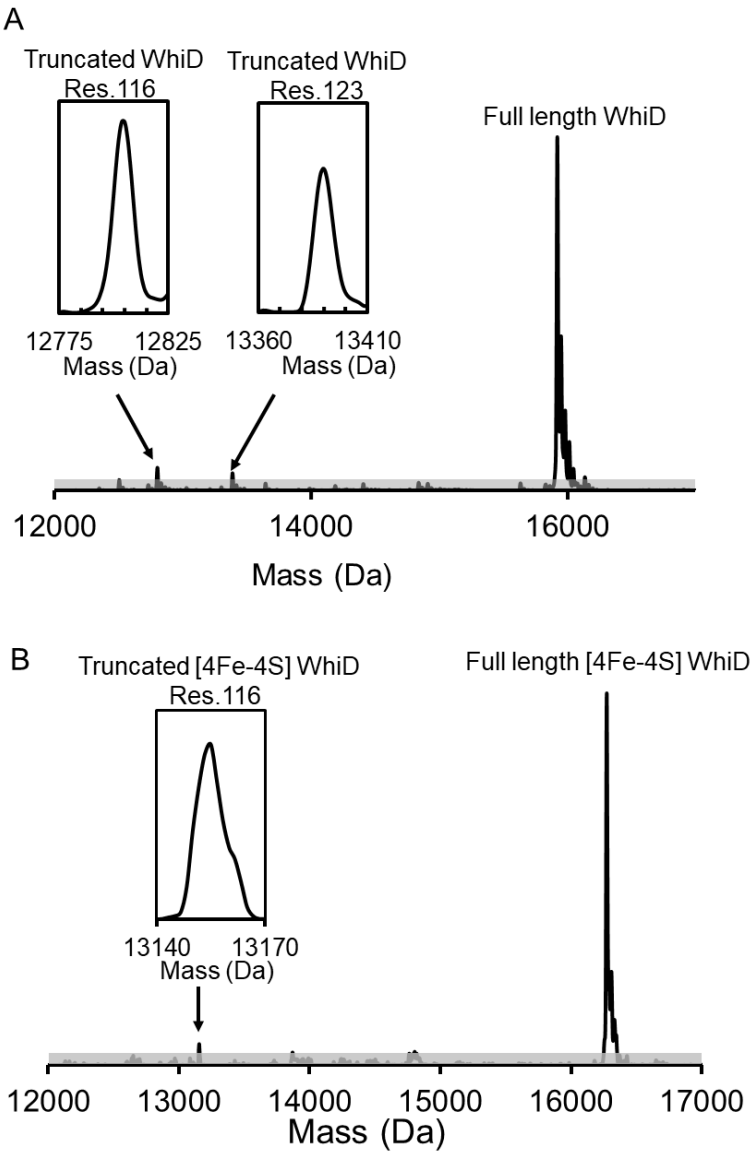

Figure 3.8 ESI-MS analysis of truncated *Sv*WhiD.

(A) Deconvoluted LC-MS of as isolated WhiD sample. The primary species is full length WhiD, minor amounts of the two truncated forms of WhiD resulting from cleavage of the 33 and 26 C-terminal residues can be also be seen. Insets show expanded mass spectra of the two truncated forms. As isolated WhiD (30 µM) was in an aqueous mixture of 2% acetonitrile, 0.1% (v/v) formic acid. **(B)** Deconvoluted non-denaturing ESI-MS of as isolated WhiD to show [4Fe-4S] WhiD as the primary species, with one of the minor species of truncated [4Fe-4S] WhiD, at residue 116. Inset shows expanded mass spectra of truncated form. As isolated WhiD (10 µM to cluster, 92% cluster loaded) was in 250 mM ammonium acetate, pH 7.2.

3.3.2. *Sv*WhiD exists as a monomer dimer equilibrium

The previously characterised Wbl proteins have all been found to be monomeric, including *Sc*WhiD and *Mt*WhiB1 [9, 25]. Equally, *Sv*WhiB was also found to elute from an analytical gel filtration (Superdex 75 10/300 GL) as a monomer at 14 kDa. SDS-PAGE confirms that WhiB was the only protein present in eluted fractions (Figure 3.9). In contrast, *Sv*WhiD exists in both monomeric and dimeric forms. WhiD as isolated was found to elute from an analytical gel filtration column as a broad peak with an elution volume indicative of a mass of ~27 kDa, midway between the masses of monomeric and dimeric forms. SDS-PAGE confirmed the presence of WhiD throughout the elution fractions (Figure 3.10A and B).

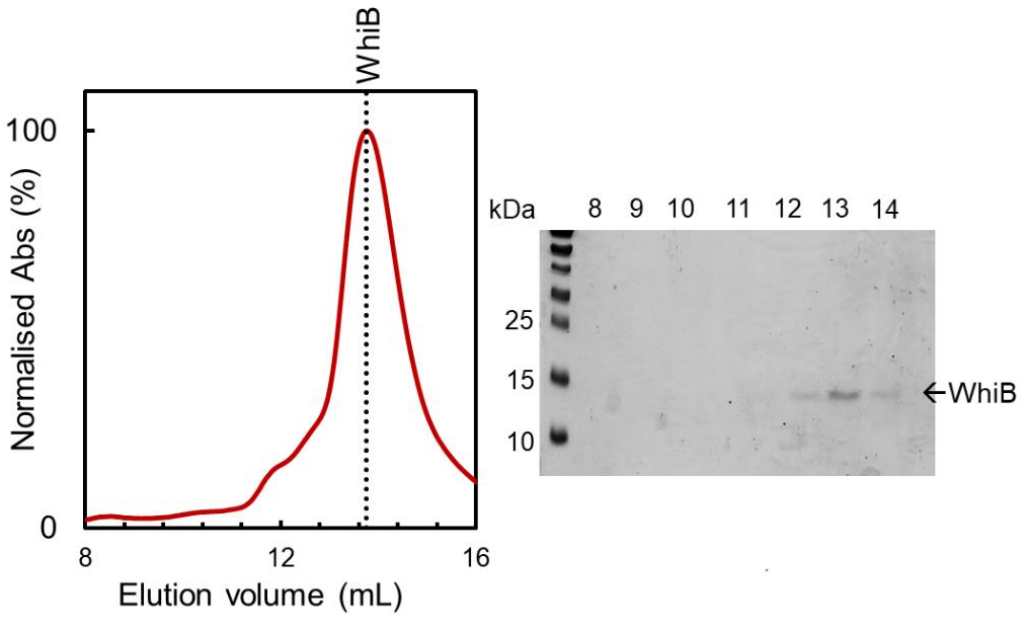

Figure 3.9 *Sv*WhiB exists in a monomeric form.

(A) Analytical gel filtration profile of *Sv*WhiB indicating that WhiB elutes at the mass corresponding to the monomeric protein. **(B)** SDS-PAGE analysis of fractions spanning elution volumes 8-14 mL. WhiB (46 µM to cluster, 53% cluster loaded) was in 50 mM Tris, 300 mM NaCl pH 7.2.

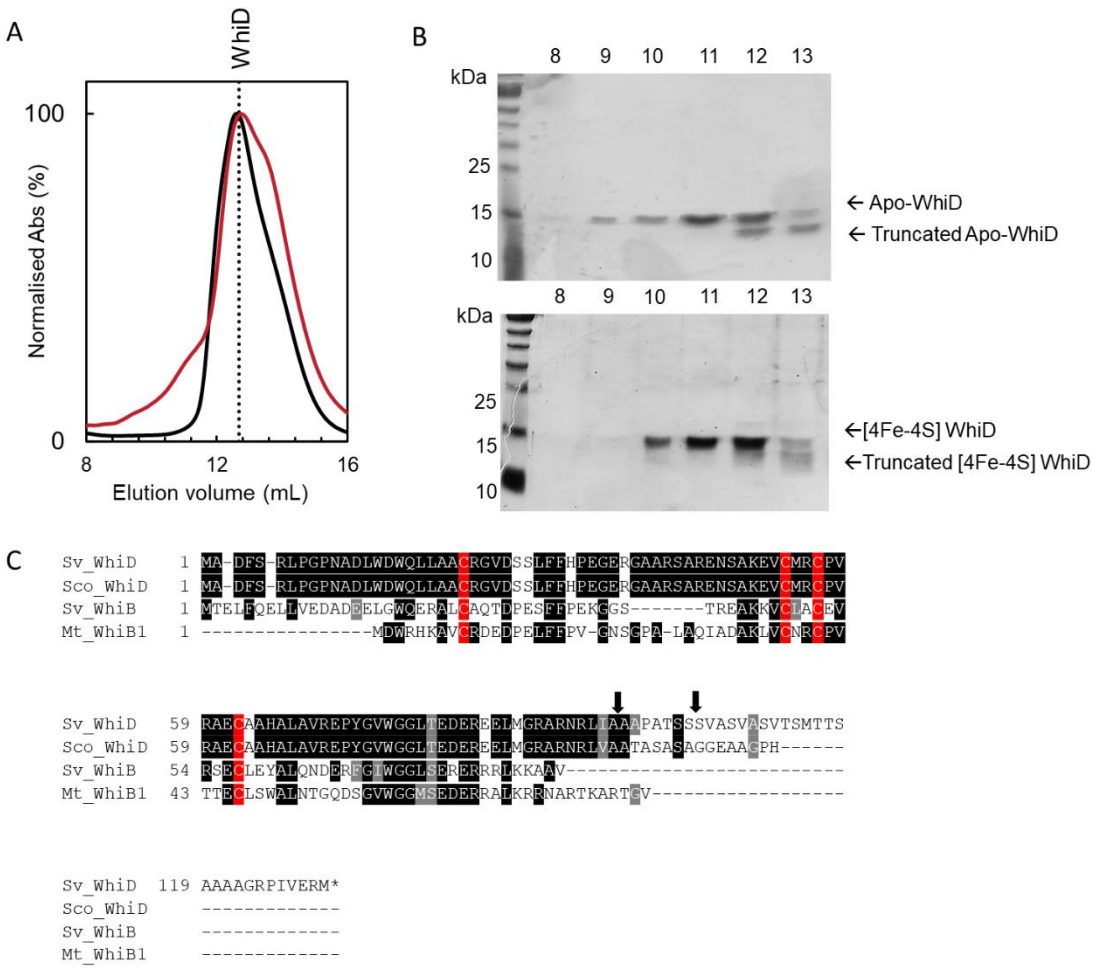

Figure 3.10 *Sv*WhiD exists in a monomer/dimer equilibrium.

(A) Analytical gel filtration profile of holo- WhiD (Black line) and apo-WhiD (red line). WhiD (45 µM) was in 50 mM Tris, 300 mM NaCl, pH 8.0. **(B)** SDS-PAGE analysis of gel filtration fractions spanning elution volumes 8-13 mL of apo- and holo-WhiD, respectively. **(C)** Sequence alignment of *Sv*WhiD with previously analysed monomeric Wbl proteins, to include *Sc*WhiD, *Sv*WhiB, and *Mt*WhiB1. Conserved cysteines are highlighted in red and truncation positions are indicated with arrows.

The necessity of the cluster for dimerization was also tested. Apo-WhiD was generated by the same method as holo-WhiD, except the purification was conducted under aerobic conditions. Purified *Sv*WhiD was left for an hour before use in order to destabilise any residual Fe-S cluster and confirmed by UV-visible absorbance spectroscopy as the 410 nm [4Fe-4S] peak was reduced to baseline. Apo-WhiD was also found to behave as a monomer-dimer mixture (Figure 3.10 A and B), but with some further higher mass species at lower elution volumes, which may arise from oxidation of Cys residues, resulting in disulphide bond cross-linking of WhiD monomers. Overall, this shows that the presence or absence of the cluster does not affect the association state of WhiD. It is possible that the ability to dimerise arises from the elongated C-terminus. A shoulder on the low mass side of the analytical gel filtration peak was also observed. SDS-PAGE revealed that the full-length protein was present across the full elution profile, while the truncated forms were only observed in the lower mass fractions, indicating that they exist as monomers (Figure 3.10B). *Sv*WhiD has a C-terminal extension of 18 residues compared to *Sc*WhiD, *Mt*WhiB1 and *Sv*WhiB. Therefore, the difference in the C-terminal and the ability to dimerise could be functionally important (Figure 3.10C). Non-denaturing ESI-MS also confirmed the presence of dimeric WhiD. ESI-MS parameters were tuned to optimise between 2100 and 3100 m/z. The isolation mass was increased to 2000 m/z, the transfer time was increased to 180 µs and the pre-pulse storage time was increased to 34 µs. This revealed 4 distinct m/z peaks corresponding to +12 to +15 charge states of a dimeric form of WhiD (Figure 3.11A) Deconvolution of the m/z spectrum revealed two main mass peaks of 16,273 Da and 32,550 Da, which corresponds to monomeric and homodimeric [4Fe-4S] WhiD, respectively (predicted masses 16,273 Da and 32,546 Da, respectively) (Figure 3.11B).

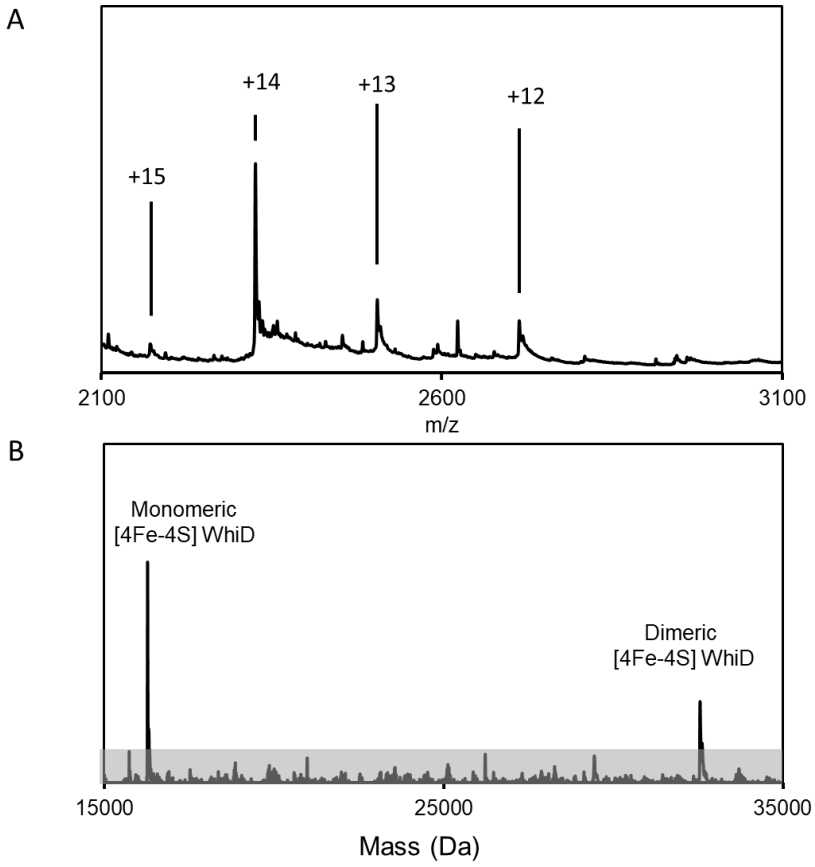

Figure 3.11 ESI-MS analysis of dimeric WhiD under non-denaturing conditions.

(A) m/z spectrum of WhiD shown from 2,100- 3,100. Charge states +12 to +15 correspond to dimeric WhiD. **(B)** Deconvoluted mass spectrum from 15 to 35 kDa to contain peaks corresponding to both monomer and dimer forms of WhiD. For non-denaturing ESI-MS experiments, WhiD (10µM) was in 250 µM ammonium acetate, pH 7.2.

3.3.3. The C-terminal extension of SvWhiD is crucial for protein dimerization

The importance of the C-terminal extension in *Sv*WhiD for dimerization was confirmed by generating a truncated form of WhiD which lacked 33 residues at the C-terminus. Truncated WhiD was found to elute from an analytical gel filtration column at a volume indicative of a monomer (Figure 3.12), and SDS-PAGE confirmed the presence of truncated WhiD across the elution profile. UV-visible absorbance and CD spectra revealed no significant differences between truncated and full-length *Sv*WhiD, indicating that the absence of the C-terminal extension does not affect the cluster environment. Non-denaturing ESI-MS revealed the presence of only monomeric truncated [4Fe-4S] WhiD, and no dimeric truncated [4Fe-4S] *Sv*WhiD, using parameters optimized to observe dimeric full-length *Sv*WhiD (Figure 3.13).

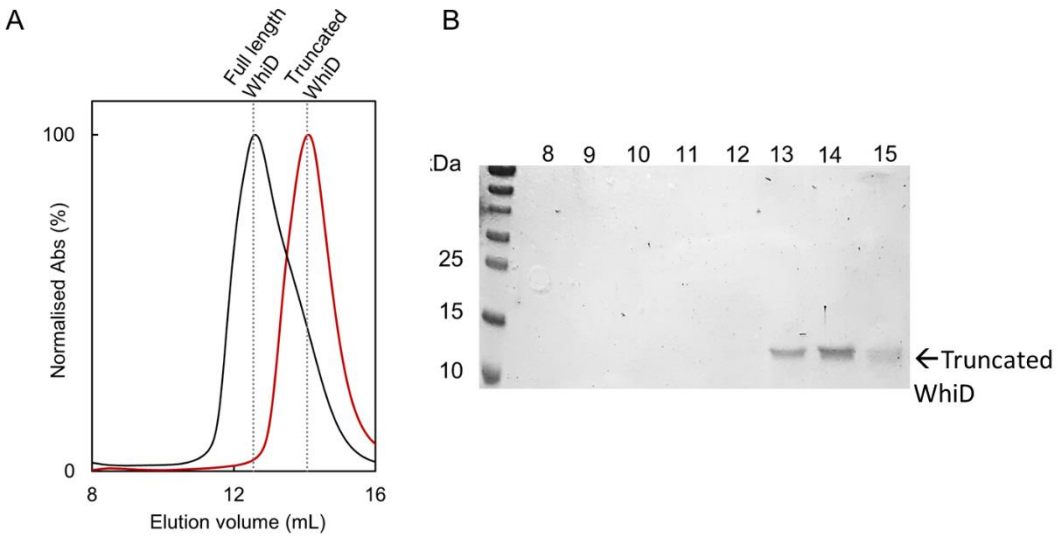

Figure 3.12 Gel filtration analysis of truncated *Sv*WhiD

(A) Gel filtration elution profiles ($A_{280\ nm}$) of truncated [4Fe-4S] WhiD (red line). The elution profile for full length [4Fe-4S] WhiD is shown for comparison (black line). **(B)** SDS-PAGE analysis of elution fractions for truncated *Sv*WhiD, spanning the elution volume 8-15 mL. Truncated *Sv*WhiD (32 µM) was in 50 mM Tris, 300 mM NaCl, pH 8.0.

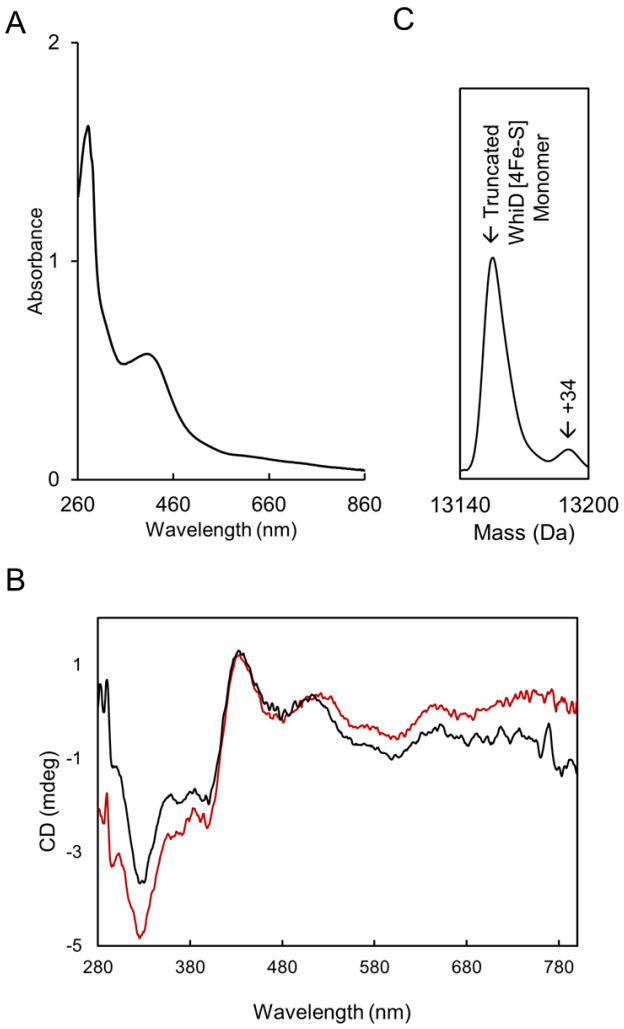

Figure 3.13 Spectroscopic characterisation and non-denaturing ESI-MS analysis of truncated *Sv*WhiD.

(A) UV-visible absorbance and **(B)** CD spectroscopic characterisation of truncated WhiD. In **(B)** spectra of truncated and full length WhiD are shown in black and red, respectively. **(C)** Deconvoluted non-denaturing ESI-MS. The spectrum features a major peak due to truncated [4Fe-4S] WhiD. A possible sulfur adduct is indicated. For spectroscopy experiments, truncated WhiD (32 µM) was in 50 mM Tris, 300 mM NaCl, pH 7.2. For non-denaturing ESI-MS, WhiD (15 µM) was in 250 mM ammonium acetate, pH 7.2.

3.4. Stability studies of *Sv*Wbl proteins

3.4.1. Both [4Fe-4S] clusters in *Sv*Wbl proteins are sensitive to O_2-mediated degradation

Exposure of WhiB [4Fe-4S] to 230 µM O_2 resulted in an immediate significant decrease in $A_{410\ nm}$ with the protein becoming destabilised after 40 minutes leading to precipitation and an increased absorbance scattering (Figure 3.14A and C). WhiD appears to be more tolerant of O_2. The spectra of [4Fe-4S] WhiD remained largely unchanged upon exposure to oxygen for ~20 minutes, after which time precipitation caused a drift in the baseline of the spectra (Figure 3.14B and D). Furthermore, aerobically purified WhiB resulted in a clear protein solution with no cluster. In contrast, WhiD retained some cluster load even after the ~2 hours aerobic exposure required for purification. After elution from the Hi-trap Ni-affinity column, aerobically purified WhiD results in light yellow coloured fractions which became colourless after 30 minutes to indicate the presence of apo-protein as indicated by the disappearance of the 410 nm absorbance band (Figure 3.15).

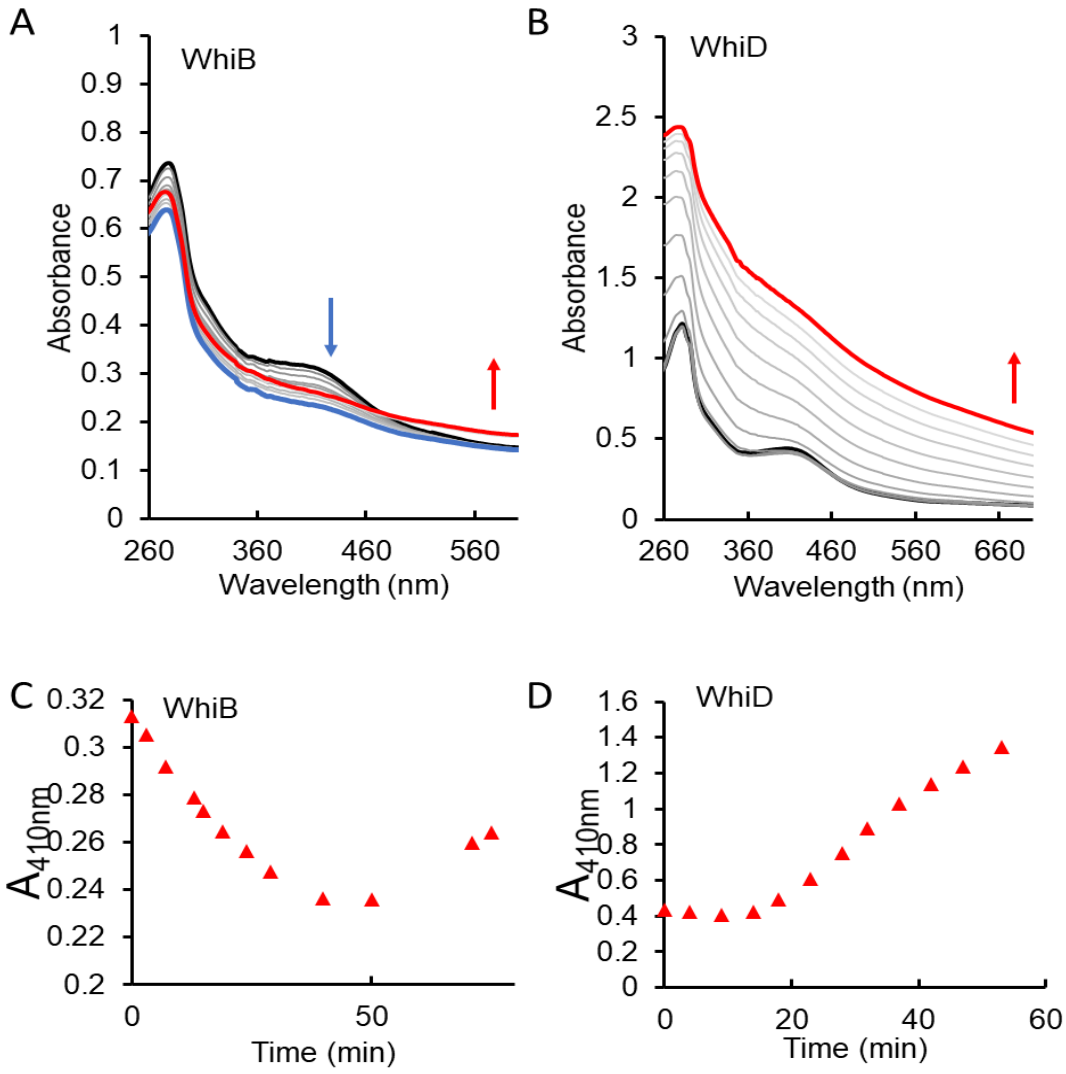

Figure 3.14 O_2 sensitivity of *Sv*Wbl proteins.

(A) UV-visible absorbance spectra of WhiB upon exposure to 230 µM O_2 over 60 minutes. Starting spectrum is in black, blue spectrum is after 40 minutes, red spectrum is the final spectra at 60 minutes, grey lines correspond to all intermediate spectra. **(B)** UV-visible absorbance spectra of WhiD upon exposure to 230 µM O_2 over 60 minutes. Black and red lines correspond to starting and final spectra respectively, grey lines correspond to intermediate spectra. **(C-D)** Kinetic plots of A_{410nm} over the course of 60 minutes of *Sv*WhiB and *Sv*WhiD respectively. Samples were prepared at ~25 µM [4Fe-4S] WhiB/WhiD, 50 mM Tris, 300 mM NaCl, pH 7.2. 1 cm Pathlength.

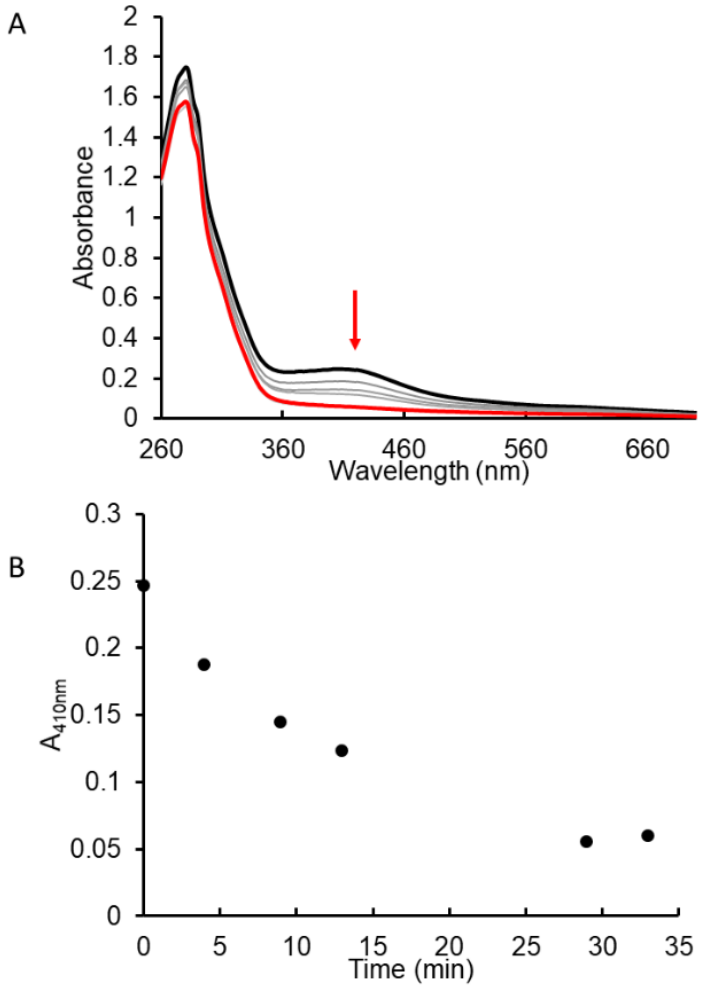

Figure 3.15 WhiD retains a [4Fe-4S] during aerobic purification which subsequently degrades to apo-WhiD.

(A) UV-visible absorbance spectra of *Sv*WhiD immediately post elution from a nickel-charged Hi-trap chelating column (black line) and after 30 minutes (red line). Intermediate spectra are shown in grey. **(B)** Time plot of $A_{410\ nm}$ over the course of 30 minutes. Sample was in elution buffer 50 mM Tris, 300 mM NaCl, 500 mM Imidazole, pH 7.2.

3.4.2. WhiD is sensitive to nitrosylation and NO mediated degradation

[4Fe-4S] WhiD was titrated with the NO-releasing agent PROLI-NONOate to give 0-20 NO per cluster in a stepwise titration and the reaction monitored by UV-visible absorbance spectroscopy. In response to the NO additions, a mild precipitation was observed causing absorbance scattering, suggesting that WhiD may be un-stable upon nitrosylation. Nevertheless, a peak was observed at 362 nm. By plotting the difference between the [4Fe-4S] peaks at 410 nm and 362 nm, the spectral changes upon the increase of NO can be tracked (Figure 3.16). Thus, WhiD was shown to undergo nitrosylation with 9-10 NO per cluster using absorbance spectroscopy.

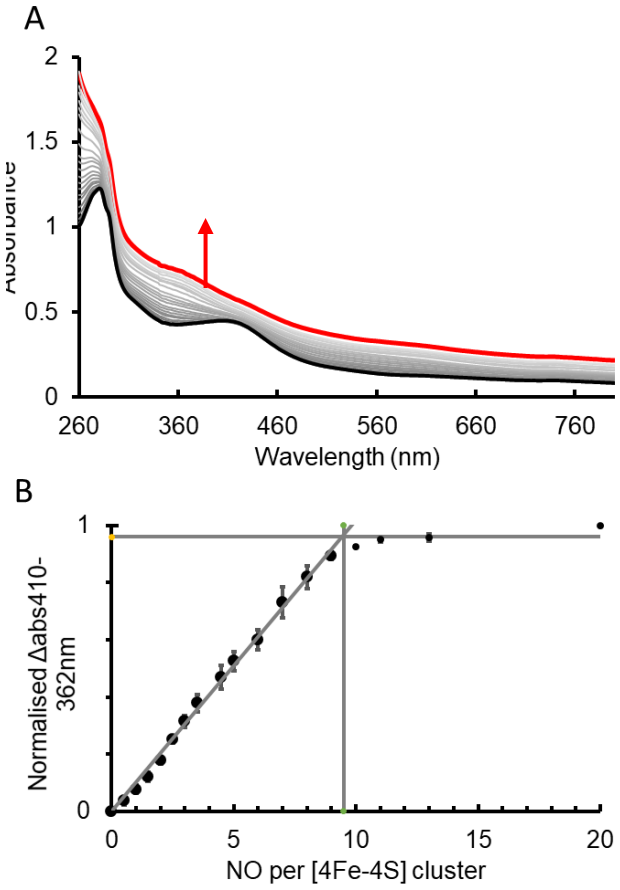

Figure 3.16 Reaction of *Sv*WhiD with NO by UV-visible absorbance spectroscopy.

(A) UV-visible absorbance titration of [4Fe-4S] WhiD with up to 20 NO per cluster. Black and red spectra correspond to the first and final spectra, respectively, with intervening spectra in grey. The arrow indicates the direction of change due to a combination of absorbance changes and scattering due to mild precipitation of the protein. **(B)** Plot of

normalised $\Delta A_{(410\ -362\ nm)}$ as a function of NO per cluster Phases are indicated by intersecting lines. The vertical line indicates the number of NO molecules required for full reaction. WhiD (21 µM) was in 50 mM Tris, 300 mM NaCl, pH 7.2.

Non-denaturing ESI-MS was used to further investigate the nitrosylation process. DEA-NONOate was used to release a known concentration of NO over time. The NONOate solution was added to WhiD and mass spectra recorded and averaged over 2.5-minute periods that each correspond to additions of 1.1 NO per cluster. The deconvoluted mass spectra of increasing NO per cluster showed the disappearance of the peak corresponding to [4Fe-4S] WhiD (at 16,273 Da, predicted mass 16,273 Da) and the increased abundance in peaks corresponding to apo-WhiD, with cysteine disulfide bridging (at 15,919 Da, predicted mass 15,920 Da), as well as 2 sulfur adducts (+32 and +64 Da) (Figure 3.17A). Mass spectra are normally generated as % relative abundance, however analysis of the nature and completion of the nitrosylation reaction via the % relative abundance is difficult. Here the % relative abundance shows [4Fe-4S] invariantly as the most abundant until ~6 NO per cluster, at which point the apo-form becomes the most abundant, which does not reflect the actual changes in abundance of each species. In order to better visualise abundance changes in the species, a plot of relative abundance of [4Fe-4S] WhiD was generated with raw ion counts for the [4Fe-4S] WhiD as a percentage of total ion count, to include [4Fe-4S]-bound, apo-form, and +S adducts. This was plotted against the number of NO per cluster (Figure 3.17B). The plot shows an immediate decrease in the abundance of [4Fe-4S] WhiD upon the increased addition of NO, and WhiD becomes fully nitrosylated upon ~10 NO per cluster. The non-linear nature of the plot indicates that the reaction is not fully concerted, in that NO reaction occurring at one cluster is not complete before a second cluster begins to react.

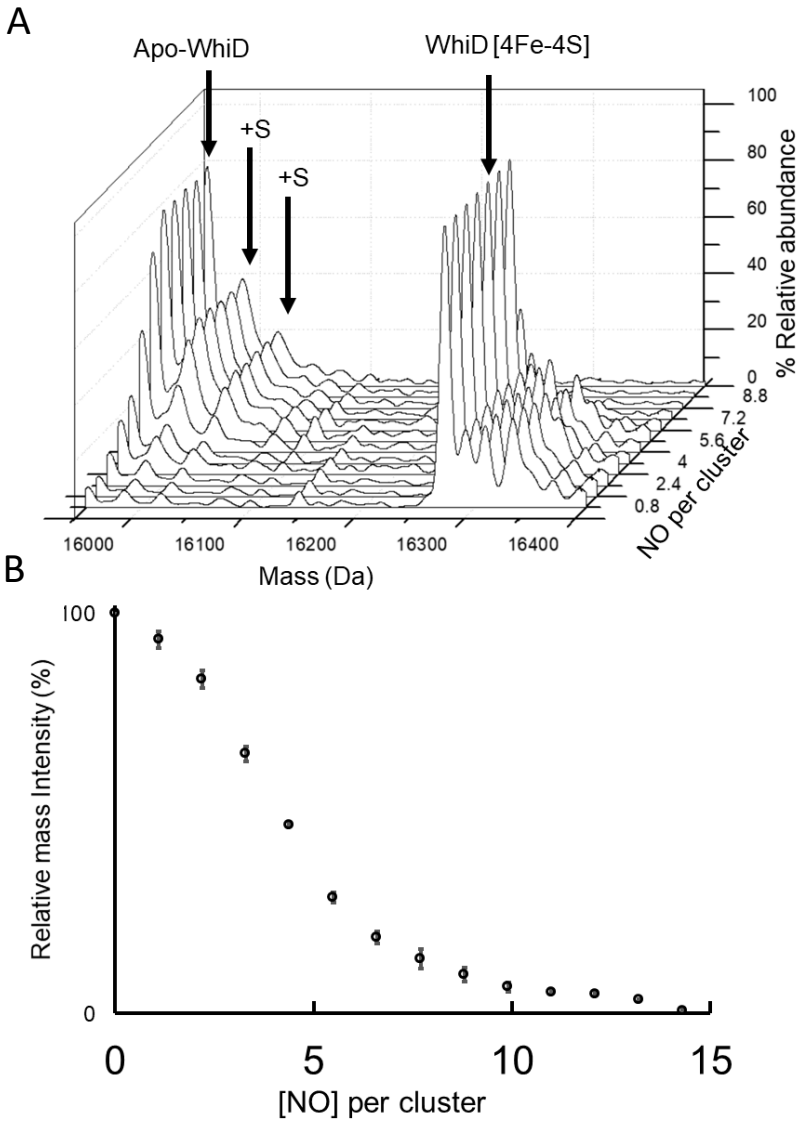

Figure 3.17 Reaction of *Sv*WhiD with NO by non-denaturing ESI-MS.

(A) Titration of holo-*Sv*WhiD with NO (up to 14 NO per cluster) monitored by non-denaturing ESI-MS. The 3D plot shows how the 2D spectrum changes with increasing NO as % relative abundance to the major species. **(B)** Plot of percentage relative mass intensity of [4Fe-4S] WhiD as a function of NO per cluster. The relative mass intensity is calculated using raw ion counts for the [4Fe-4S] WhiD as a percentage of total ion count, to include [4Fe-4S]-bound, apo-form, and +S adducts. Error bars represent standard errors from n = 2 experiments. WhiD (10µM in cluster) was in 250 mM ammonium acetate pH 7.2.

3.5. Kinetic characterisation of [4Fe-4S] WhiD with NO

Stopped-flow measurements revealed that the *Sv*WhiD behaves similarly upon exposure to NO to *Sc*WhiD and *Mt*WhiB1 [20]. For these Wbl proteins, four distinct kinetic steps were observed, which can be represented by a four-step reaction A→B→C→D→E. individual steps were detected by a combination of UV-visible and CD spectroscopy, in which steps A→B, B→C and D→E were detected at $A_{360\ nm}$.

It was not possible to obtain a full kinetic analysis of *Sv*WhiD, due to the instability of the protein upon reaction with NO causing scattering in the absorbance. However, this occurs only after ~500 ms, which allow measurement of the earlier 2 kinetic phases at 360 nm. The slower third phase was not resolved due to the drifting baseline (Figure 3.18A). The reaction of [4Fe-4S] WhiD with increasing excess NO, from 15 to 50 NO per cluster was followed. Data for the first two phases were fitted separately using single exponential fits (Figure 3.18B and C). Plots of the observed pseudo first-order rate constants (k_{obs}) against NO concentration were very similar to those reported previously for Wbl proteins. Plots of k_{obs} against NO concentration were linear for initial two phases, indicating first-order with respect to NO. The calculated second order rate constants determined from the slopes of these plots were 7.37 ± 0.18 $x10^5$ M^{-1} S^{-1} and 2.54 ± 0.001 $x10^4$ M^{-1} S^{-1} for phase 1 and 2 respectively.

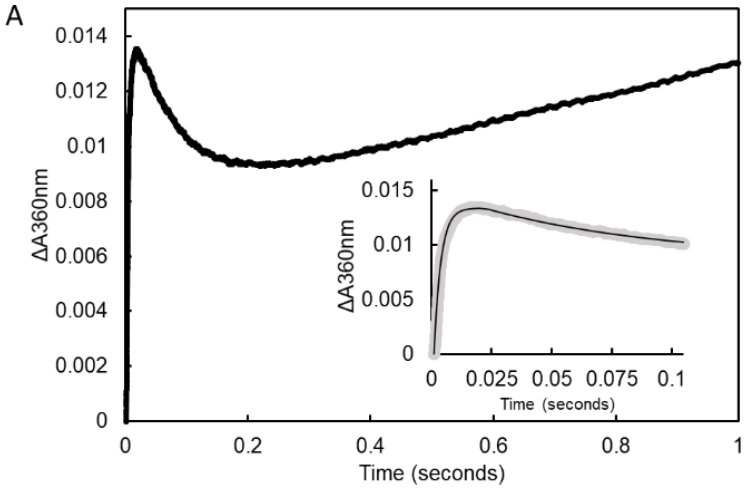
A
0.014
0.012
0.01
0.008
0.006
0.004
0.002
0
ΔA360nm
0
0.2
0.4
0.6
0.8
1
Time (seconds)
0.015
0.01
0.005
0
ΔA360nm
0
0.025
0.05
0.075
0.1
Time (seconds)

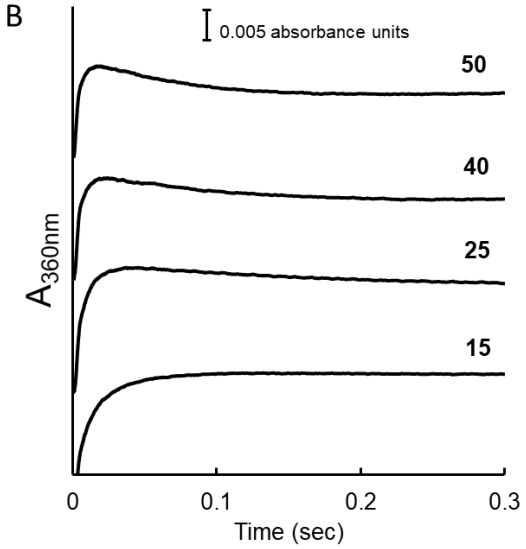
B
0.005 absorbance units
50
40
25
15
A360nm
0
0.1
0.2
0.3
Time (sec)

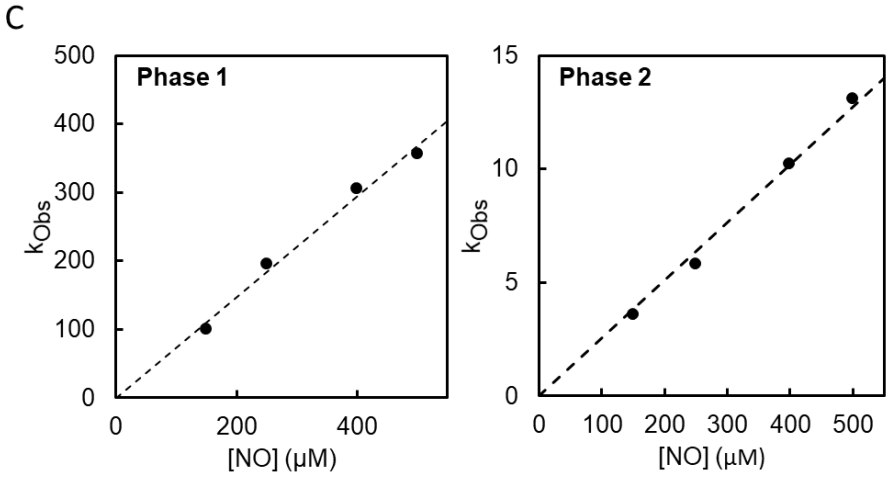
C
Phase 1
500
400
300
200
100
0
kObs
0
200
400
[NO] (μM)
Phase 2
15
10
5
0
kObs
0
100
200
300
400
500
[NO] (μM)

Figure 3.18 Stopped flow kinetics of [4Fe-4S] WhiD Nitrosylation.

(A) $A_{360\ nm}$ was recorded of [4Fe-4S] WhiD in the presence of 50-fold excess of NO (500 µM) over 1 second. Inset is a plot of the first 100 milli-seconds of the reaction. Data are in grey with a fit of the data for two single exponentials in black. **(B)** data at 360 nm for a range of excess NO additions to [4Fe-4S] WhiD, as indicated. **(C)** Plots of the observed (pseudo-first order) rate constants (k_{obs}) from fits of the kinetic data at $A_{360\ nm}$ for the two observed phases, over a range of NO concentrations. Phases both show a linear first order dependence, indicating that the rate-limiting step of these reactions involves NO. the second order rate constant was obtained directly from the gradient of the linear fit (broken line). Experiments were performed with 10 µM [4Fe-4S] WhiD in 50 mM Tris, 300 mM NaCl pH 7.2 a 25 °C.

3.6. Discussion

Wbl proteins have previously been characterised mechanistically as sensors of O_2 and NO where their [4Fe-4S] clusters function as the sensory unit. Sequence alignments of both *Sv*WhiB and *Sv*WhiD both reveal the signature conserved four cysteines that are indicative of a [4Fe-4S] cluster binding protein. Biophysical studies of anaerobically purified *Sv*WhiB and *Sv*WhiD revealed the presence of the [4Fe-4S] cluster for both proteins, as indicated by a peak at 410 nm in UV-Visible absorbance spectra. CD spectra have distinct spectral features that are similar to those previously reported for *Sc*WhiD and *Mt*WhiB1, consistent with the presence of a [4Fe-4S] cluster in a similar protein environment [22, 23]. The presence of a [4Fe-4S] cluster in each was demonstrated by non-denaturing mass spectrometry.

Whilst WhiB, in line with previous findings of Wbl proteins exists as a monomer, WhiD was unusually found to exist in a monomer dimer equilibrium. This monomer-monomer interaction is dependent on the C-terminal part of the protein. Notably, the extension is the only part of the protein sequence of *Sv*WhiD which differs from the previously characterised monomeric *Sc*WhiD protein. Indeed, the proteins are 100% identical for the first 95 residues. The physiological significance of dimerization remains unclear.

Wbl proteins bind [4Fe-4S] clusters with varying stability upon exposure to O_2. *M. tuberculosis* WhiB1 was found to be extremely O_2 stable, whilst *Sc*WhiD reacts slowly with O_2, with observable cluster remaining over the course of hours [23, 25]. Consistent with previous findings, *Sv*Wbl proteins also display varying sensitivity to O_2. It was immediately clear that the [4Fe-4S] *Sv*WhiB is fragile; aerobically purified WhiB was entirely in its apo-form, whilst aerobically purified WhiD retained some cluster, which was subsequently lost within 30 minutes. Furthermore, as isolated *Sv*WhiB began to degrade immediately upon exposure to O_2, whilst *Sv*WhiD under the same conditions remained largely stable for 20 minutes, with a proportion of cluster still present after 60 minutes.

Although Wbl proteins display sensitivity to O_2, their sensitivity to NO is far more distinctive. The reaction of *Sc*WhiD was previously shown to be 10^4-fold faster than that

observed with O_2 [20]. Furthermore, they react in a concerted manner with 8-10 NO per cluster, resulting in protein bound iron-nitrosyl species [21]. This ability to rapidly sense NO suggests that some Wbl proteins may function as NO sensors [19, 20, 22]. *Sv*WhiD is shown here to react with ~9NO per cluster. The addition of NO resulted in mild precipitation, which was not previously observed for *Sc*WhiD, suggesting that the nitrosylation intermediates/products of *Sv*WhiD may be less stable. Regardless, stopped flow kinetic studies revealed rate constants that are consistent with *Sc*WhiD and *Mt*WhiB1 for the first two steps of reaction (Table 3.1). Therefore, it is likely nitrosylation for all three Wbl proteins occurs via the same multi-phasic mechanism. The first phase, observed by an increase in the absorbance at 360 nm likely corresponds to the binding of one NO molecule to the cluster in the step A→B. This increases accessibility to further NO binding in step B→C, observed by a decrease in absorbance at 360 nm. Both steps are first order in NO, which suggests that either a single NO is involved in each step, or that NO binding to the different irons on the cluster occurs independently to give an overall first order dependence. Although further characterisation of reaction steps was not possible for *Sv*WhiD, previous experiments of *Sc*WhiD and *Mt*WhiB1 using absorbance (360 nm and 420 nm), and fluorescence (350 nm) concluded that further steps C→D → E are also first order in NO. Like step B→C, step C→D is also characterised by a net decrease in absorbance, which suggests that the iron-sulfide and/or iron-cysteine interactions which give rise to the cluster absorbance are disrupted during these steps [20]. The final step D→E leads to a majority of EPR-silent nitrosylated products. Recent application of NRVS to WhiD revealed the presence of iron nitrosyl species including minor amounts of DNIC, as well as species that resemble RRE and RBS, proposed to be a novel black salt species thus named a Roussins' black ester [21].

It was demonstrated that the model organism *S. coelicolor* encounters endogenously produced NO [26]. Although its genome does not encode for a nitric oxide synthase (NOS) enzyme, it can produce NO from organic nitrogen independent of NOS. NO regulation occurs via autoregulatory NO-dependent transcriptional systems; transcriptional factors NsrR and the DevS-DevR two component system regulate the expression of flavohemoglobin (NO dioxygenase) and nitrate reductase (Nar) respectively. The role of nitrite reductase (NIR) in removing NO_2^- by production of ammonium was also

demonstrated to be important in NO homeostasis [26-28]. Endogenous NO can promote metabolic and morphogenic changes, including antibiotic production and the development of aerial mycelium [26]. In M. *tuberculosis*, a physiological significance of the NO-sensitivity was recently established where WhiB3 acts directly as a redox sensor and contributes to adapting to ROS and RNS stress [18]. This redox sensing role for the *Mtb* homologue WhiB3 may indicate a similar regulatory function for *Sv*WhiD and *Sv*WhiB [29].

	Rate constant ($M^{-1} s^{-1}$)		
Phase	*Sv*WhiD	*Sc*WhiD	*Mt*WhiB1
1	(7.37± 0.18) x10^5	(6.50± 0.18) x10^5	(4.40± 0.44) x10^5
2	(2.54± 0.001) x10^4	(2.13± 0.12) x10^4	(1.38± 0.04) x10^4

Table 3.1 Kinetic rate constants for Wbl proteins.

Shown for the Initial 2 phases of the reaction of NO with [4Fe-4S] Wbl proteins: *S. Venezuelae* WhiD (*Sv*WhiD), *S. coelicolor* WhiD (*Sc*WhiD) and *M. tuberculosis* (*Mt*WhiB1).

3.7. References

1. Chater, K.F., *A morphological and genetic mapping study of white colony mutants of* Streptomyces coelicolor*.* J Gen Microbiol, 1972. **72**(1): p. 9-28.
2. Bush, M.J., et al., *Genome-wide chromatin immunoprecipitation sequencing analysis shows that WhiB Is a transcription factor that cocontrols its regulon with WhiA to initiate developmental cell division in* Streptomyces*.* mBio, 2016. **7**(2): p. e00523-16.
3. Lee, D.S., Y. Kim, and H.S. Lee, *The* whcD *gene of* Corynebacterium glutamicum *plays roles in cell division and envelope formation.* Microbiology, 2017. **163**(2): p. 131-143.
4. Gomez, J.E. and W.R. Bishai, whmD *is an essential mycobacterial gene required for proper septation and cell division.* Proc Natl Acad Sci U S A, 2000. **97**(15): p. 8554-9.
5. Raghunand, T.R. and W.R. Bishai, Mycobacterium smegmatis whmD *and its homologue Mycobacterium tuberculosis* whiB2 *are functionally equivalent.* Microbiology, 2006. **152**(Pt 9): p. 2735-47.
6. Flardh, K., K.C. Findlay, and K.F. Chater, *Association of early sporulation genes with suggested developmental decision points in* Streptomyces coelicolor *A3(2).* Microbiology, 1999. **145 (Pt 9)**: p. 2229-2243.
7. Rybniker, J., et al., *Insights into the function of the WhiB-like protein of mycobacteriophage TM4--a transcriptional inhibitor of WhiB2.* Mol Microbiol, 2010. **77**(3): p. 642-57.
8. Raghunand, T.R. and W.R. Bishai, *Mapping essential domains of* Mycobacterium smegmatis *WhmD: insights into WhiB structure and function.* J Bacteriol, 2006. **188**(19): p. 6966-76.
9. Jakimowicz, P., et al., *Evidence that the* Streptomyces *developmental protein WhiD, a member of the WhiB family, binds a [4Fe-4S] cluster.* J Biol Chem, 2005. **280**(9): p. 8309-15.
10. Molle, V., et al., *WhiD and WhiB, homologous proteins required for different stages of sporulation in* Streptomyces coelicolor *A3(2).* J Bacteriol, 2000. **182**(5): p. 1286-95.
11. Steyn, A.J., et al., Mycobacterium tuberculosis *WhiB3 interacts with RpoV to affect host survival but is dispensable for in vivo growth.* Proc Natl Acad Sci U S A, 2002. **99**(5): p. 3147-52.
12. Mehta, M., R.S. Rajmani, and A. Singh, Mycobacterium tuberculosis *WhiB3 Responds to Vacuolar pH-induced Changes in Mycothiol Redox Potential to Modulate Phagosomal Maturation and Virulence.* J Biol Chem, 2016. **291**(6): p. 2888-903.
13. Geiman, D.E., et al., *Differential gene expression in response to exposure to antimycobacterial agents and other stress conditions among seven* Mycobacterium tuberculosis whiB-*like genes.* Antimicrob Agents Chemother, 2006. **50**(8): p. 2836-41.
14. Feng, L., S. Chen, and Y. Hu, *PhoPR Positively Regulates* whiB3 *Expression in Response to Low pH in Pathogenic Mycobacteria.* J Bacteriol, 2018. **200**(8).
15. Larsson, C., et al., *Gene expression of* Mycobacterium tuberculosis *putative transcription factors* whiB1-7 *in redox environments.* PLoS One, 2012. **7**(7): p. e37516.
16. Singh, A., et al., Mycobacterium tuberculosis *WhiB3 maintains redox homeostasis by regulating virulence lipid anabolism to modulate macrophage response.* PLoS Pathog, 2009. **5**(8): p. e1000545.
17. Rodriguez, J.G., et al., *Global adaptation to a lipid environment triggers the dormancy-related phenotype of* Mycobacterium tuberculosis*.* mBio, 2014. **5**(3): p. e01125-14.
18. Mehta, M. and A. Singh, Mycobacterium tuberculosis *WhiB3 maintains redox homeostasis and survival in response to reactive oxygen and nitrogen species.* Free Radic Biol Med, 2019. **131**: p. 50-58.

19. Singh, A., et al., Mycobacterium tuberculosis *WhiB3 responds to O2 and nitric oxide via its [4Fe-4S] cluster and is essential for nutrient starvation survival.* Proc Natl Acad Sci U S A, 2007. **104**(28): p. 11562-7.
20. Crack, J.C., et al., *Mechanistic insight into the nitrosylation of the [4Fe-4S] cluster of WhiB-like proteins.* J Am Chem Soc, 2011. **133**(4): p. 1112-21.
21. Serrano, P.N., et al., *Nitrosylation of nitric-oxide-sensing regulatory proteins containing [4Fe-4S] clusters gives rise to multiple iron-nitrosyl complexes.* Angew Chem Int Ed Engl, 2016. **55**(47): p. 14575-14579.
22. Smith, L.J., et al., Mycobacterium tuberculosis *WhiB1 is an essential DNA-binding protein with a nitric oxide-sensitive iron-sulfur cluster.* Biochem J, 2010. **432**(3): p. 417-27.
23. Crack, J.C., et al., *Characterization of [4Fe-4S]-containing and cluster-free forms of* Streptomyces *WhiD.* Biochemistry, 2009. **48**(51): p. 12252-64.
24. Banerjee, S. and S. Mazumdar, *Electrospray ionization mass spectrometry: a technique to access the information beyond the molecular weight of the analyte.* Int J Anal Chem, 2012. **2012**: p. 282574.
25. Kudhair, B.K., et al., *Structure of a Wbl protein and implications for NO sensing by* M. tuberculosis*.* Nat Commun, 2017. **8**(1): p. 2280.
26. Sasaki, Y., et al., *Nitrogen oxide cycle regulates nitric oxide levels and bacterial cell signaling.* Sci Rep, 2016. **6**: p. 22038.
27. Crack, J.C., et al., *NsrR from* Streptomyces coelicolor *is a nitric oxide-sensing [4Fe-4S] cluster protein with a specialized regulatory function.* J Biol Chem, 2015. **290**(20): p. 12689-704.
28. Lee, J.M., et al., *O2- and NO-sensing mechanism through the DevSR two-component system in* Mycobacterium smegmatis*.* J Bacteriol, 2008. **190**(20): p. 6795-804.
29. Yukioka, Y., et al., *A role of nitrite reductase (NirBD) for NO homeostatic regulation in* Streptomyces coelicolor *A3(2).* FEMS Microbiol Lett, 2017. **364**(1).

Chapter 4. Interaction of the *S. venezuelae* Wbl proteins with the principal sigma factor σ^{HrdB}

4.1. Introduction

As described in section 1.3.3, σ factors are required for initiating transcription. The ability of Wbl proteins to interact with region 4 of σ factors has also been well established in mycobacteria. Apart from WhiB5, all 6 remaining *M. tuberculosis* Wbl proteins have been shown to be able to interact with the primary σ factor σ^A [1, 2]. WhiB1, WhiB3 and WhiB7 have been shown to require σ^A interaction in order to function as transcriptional regulators in a cluster dependant manner [3-5].

Mutagenesis studies determined the important residues required for interaction in WhiB3 and WhiB7 with σ^A to be the triplet of residues adjacent to the highly conserved G[V/I]WGG motif, located on a flexible loop region between helix 3 and 4. This triplet of residues (EPY and EPW in WhiB3 and WhiB7, respectively) is also conserved among homologues of each group of Wbl proteins. Furthermore, a mutation in an Arginine residue located in the C-terminus of region 4 (R515H) abolished the interaction of WhiB3 and WhiB7 with σ^A [3]. Although this mutation was viable *in vivo*, it results in decreased the virulence of *M. tuberculosis* [3]. The viability of the σ^A R515H mutation suggests that essential Wbl proteins, which include WhiB1 and WhiB2 may not interact with σ^A in the same manner as WhiB3 and WhiB7. Indeed, although WhiB1 also functions via its interaction with σ^A, the interaction does not depend upon the triplet motif, nor does the R515H mutation abolish the interaction [2]. The relatively low oxygen sensitivity of WhiB1 has allowed for structural information to be determined in recent years, shedding light on the nature of Wbl: σ^A interactions [6]. High resolution crystal structure of WhiB1 in complex with σ^A (domain 4) reveals an interesting binding mechanism between the two proteins [5]. The complex is driven by hydrophobic interactions/hydrogen bonding around the [4Fe-4S] cluster binding pocket, on which the complex is hinged (Figure 4.1A). The complex induces conformational changes in both WhiB1 and σ^A as the C-terminal helix 4 on WhiB1 moves by 120°, away from helix 2 and clamping onto the C-terminal of σ^A. C-terminal residues H516 and P517 insert into the [4Fe-4S] cluster binding pocket of WhiB1, and substitution of either residue by Ala

abolishes complex formation. Similarly, substitutions of F17A or F18A in WhiB1 also abolishes the interaction, whilst retaining coordination of the [4Fe-4S] cluster (Figure 4.1B) [5]. As the C-terminus is the putative DNA binding motif, the clamping of the C-terminal region of WhiB1 upon the association of the complex would account for the observation that only apo-WhiB1 is able to bind DNA *in vitro*.

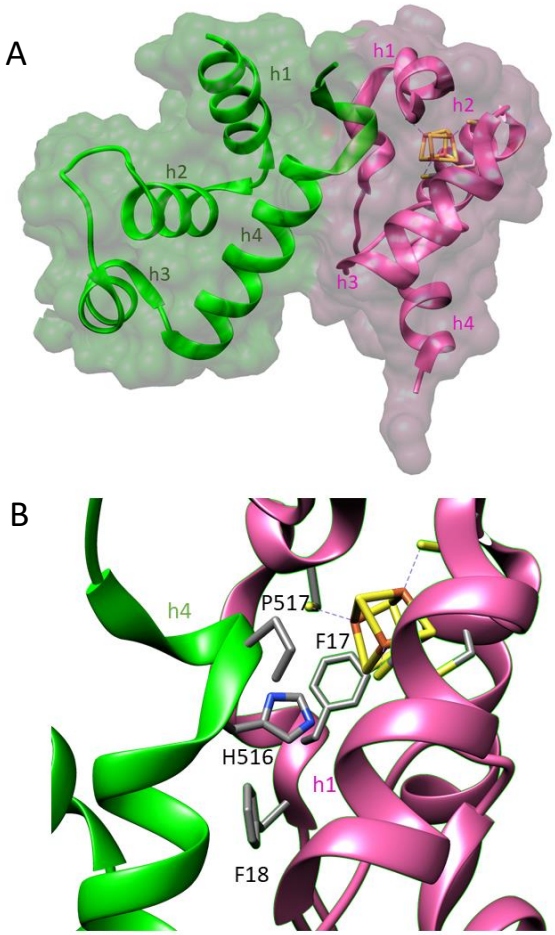

Figure 4.1 Structure of the *M. tuberculosis* WhiB1: σ^A complex.

(A) Cartoon and surface representation of the complex. WhiB1 is represented in pink and σ^A in green with labelled helices. The [4Fe-4S] cluster of WhiB1 is shown in ball-and-stick representation with Fe atoms coloured orange and yellow for S. **(B)** Close up of region of interaction, coordinating cysteines are depicted in ball-and-stick representation as well as crucial residues required for interaction highlighted in both WhiB1 (F17 and F18) and σ^A (H516 and P517). PDB ID : 6ONO.

Wbl proteins are sensitive to O_2 exposure and highly sensitive to NO, which ultimately results in the degradation of the cluster, as shown in chapter 3. Binding of the σ factor in *M. tuberculosis* WhiB1 results in shielding of the [4Fe-4S] cluster and increases the resistance of WhiB1 to O_2 [5]. Strikingly, the WhiB1: σ^A complex was reportedly stable under aerobic conditions for over 2 weeks [6]. Nevertheless, the complex does not protect the cluster from NO attack, which was still observed to rapidly react with NO and dissociate [6]. The retained sensitivity for NO highly suggests a role for WhiB1 as a NO sensing regulator.

The ability for *Streptomyces* Wbl proteins to interact with the primary σ factor σ^{HrdB} has yet to be explored. It is very likely some Wbl orthologues will function in conjunction with σ factors in a similar way to *M. tuberculosis* Wbl proteins. It is common to find genes encoding interacting proteins located in proximity and several *wbl* genes are located close to σ factors [7]. In this respect, it is interesting to note that, SCP1.161 (*wblP*) located on the SCP1 plasmid of *S. coelicolor* appears to encode a protein composed of an N-terminal Wbl domain fused to region 4 of an ECF σ factor at the C-terminal [8].

This chapter reports on biochemical studies of the interactions between *Sv*WhiB and *Sv*WhiD and the primary σ factors of *S. venezuelae,* σ^{HrdB}, and σ^{HrdD}. σ^{HrdD} is an alternative σ factor dispensable for growth, unlike σ^{HrdB}. Spectroscopic data such as UV-visible absorbance and CD spectroscopy were obtained to characterise changes in the cluster environment. Non-denaturing mass spectroscopy and analytical gel filtration were employed to characterise the formation and behaviour of protein complexes upon exposure to NO. Kinetic data is also presented to characterise the nitrosylation reaction of *S. venezuelae* WhiD: σ complex.

4.2. Overexpression and purification of *S. venezuelae* σ^{HrdB} and σ^{HrdD}

Truncated forms of *S. venezuelae* σ factor σ^{HrdB} and σ^{HrdD} , containing just region 4, were over-produced and purified as described in methods section 2.1 and will be referred to as σ^{HrdB}_4 and σ^{HrdD}_4 from now on, respectively. Following nickel affinity chromatography (HisTRap Ni-IMAC column), the purity of both proteins was confirmed with SDS-PAGE and exact mass provided by LC-MS as 11,464 Da and 11,528 Da, corresponding to the predicted masses of N terminally tagged $(His)_6$-σ^{HrdB}_4 and $(His)_6$-σ^{HrdD}_4 respectively, both with an N-terminal methionine cleavage (predicted masses 11,465 Da and 11,528 Da, respectively) (Figure 4.2).

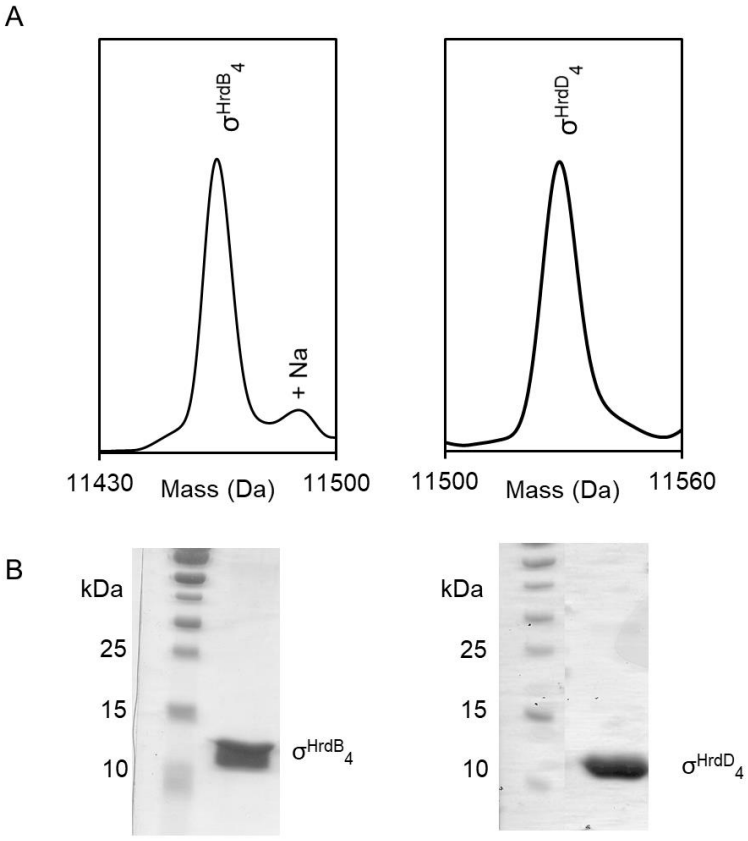

Figure 4.2 LC-MS and SDS-PAGE characterisation of purified *S. venezuelae* σ factors.

(A) Deconvoluted LC-MS spectrum of as isolated (His_6)-tagged σ^{HrdB}_4 and σ^{HrdD}_4, both lacking the N-terminal Met residue. Adducts are as labelled. σ factors (30 μM) were in aqueous mixtures of 2% (v/v) acetonitrile, 0.1% (v/v) formic acid. (**B**) SDS-PAGE analysis

of as isolated σ^{HrdB}_4 and σ^{HrdD}_4, reveals pure protein samples following purification by nickel- charged HisTRap Ni-IMAC column.

4.3. Characterising the interaction between *Sv*WhiB and *Sv*WhiD with σ^{HrdB}_4

4.3.1. WhiB and WhiD interact with σ^{HrdB}_4

Interaction between *Sv*WhiB and *Sv*WhiD with σ^{HrdB}_4 were observed using non-denaturing ESI-MS. A 2-fold excess of σ^{HrdB}_4 was added to [4Fe-4S] WhiB (50% cluster load). The resulting *m/z* spectrum was then deconvoluted over a 10-25 kDa range. Due to low cluster incorporation, the deconvoluted mass spectra showed a significant peak corresponding to apo-WhiB, with cysteine disulfide bridging, at 11,263 Da (predicted mass 11,263 Da). The σ^{HrdB}_4 mass peak was at 11,464 Da, holo-WhiB at 11,617 Da and the [4Fe-4S] WhiB: σ^{HrdB}_4 complex at 23,081 Da (predicted masses 11,464 Da, 11,617 Da and 23,081 Da, respectively) (Figure 4.3).

The interaction between σ^{HrdB}_4 and *Sv*WhiD was also observed. The deconvoluted spectra (range 10-30kDa) of a 2-fold excess mixture of σ^{HrdB}_4 to WhiD revealed the individual proteins (16,271 Da for holo-WhiD, predicted mass 16,273 Da, and 11,462 Da for σ^{HrdB}_4, predicted mass 11,464 Da) as well as a significant peak corresponding to the mass of a WhiD [4Fe-4S]: σ^{HrdB}_4 complex at 27,741 Da (predicted mass 27,737 Da). Apo-WhiD is not observed due to the high cluster load of [4Fe-4S] WhiD (Figure 4.4A and B). Two minor species could also be seen, at 13,154 Da and 24,619 Da, corresponding to the [4Fe-4S]- bound form of 33-residue truncated *Sv*WhiD alone and in complex with σ^{HrdB}_4 (predicted masses 13,155 Da and 24,619 Da, respectively). This indicates that the C-terminal part of WhiD is not important for interaction with the σ factor (Figure 4.4A). CD spectroscopy of a 2:1 WhiD : σ^{HrdB}_4 mixture showed that the spectra are largely identical, with the exception of a larger signal for WhiD/σ^{HrdB}_4 mixture in the near UV region (320-250 nm). This reflects the contribution of aromatic amino acid side chains

from the addition of σ^{HrdB}_4. The CD spectra comparison suggests that complex formation has no significant effect on the cluster environment (Figure 4.4C).

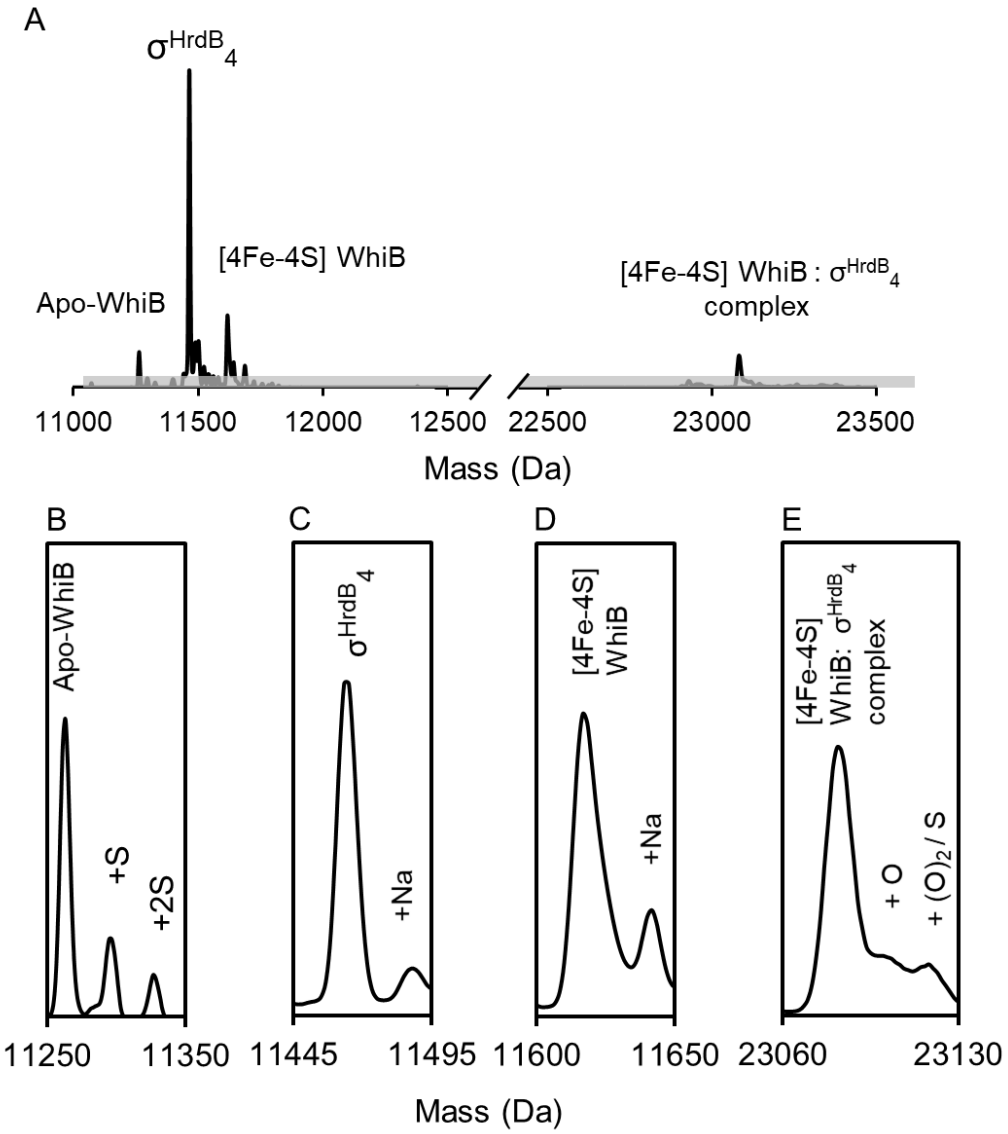

Figure 4.3 ESI-MS analysis demonstrates binding of cluster-bound *Sv*WhiB to σ^{HrdB}_4.

(A) Deconvoluted mass spectrum measured under non-denaturing conditions of a solution containing a 2:1 ratio of σ^{HrdB}_4 to [4Fe-4S] WhiB (50% cluster load). Mass spectra reveals apo-WhiD, [4Fe-4S] WhiB, $\sigma^{HrdB}4$ and a σ^{HrdB}_4 :[4Fe-4S] WhiB complex. **(B-E)** Spectra of four main species (apo-WhiB (B), σ^{HrdB}_4 (C), [4Fe-4S] WhiB (D) and σ^{HrdB}_4 : [4Fe-4S] WhiB complex (E)) plotted on an expanded mass scale, with oxygen/sulfur and sodium adducts indicated. [4Fe-4S] WhiB (7 µM) and σ^{HrdB}_4 (14 µM) were in 250 mM ammonium acetate, pH 7.2.

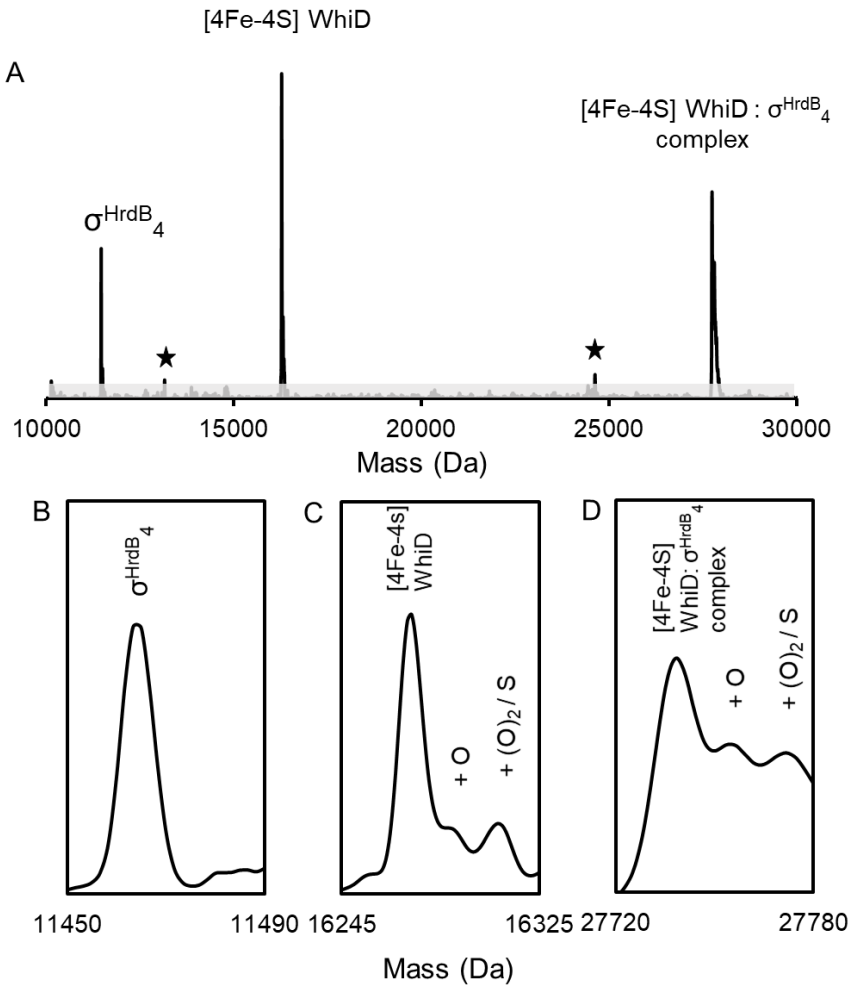
[4Fe-4S] WhiD
A
[4Fe-4S] WhiD : σ^HrdB_4 complex
σ^HrdB_4
10000
15000
20000
25000
30000
Mass (Da)
B
σ^HrdB_4
C
[4Fe-4s] WhiD
+ O
+ (O)2 / S
D
[4Fe-4S] WhiD: σ^HrdB_4 complex
+ O
+ (O)2 / S
11450
11490
16245
16325
27720
27780
Mass (Da)

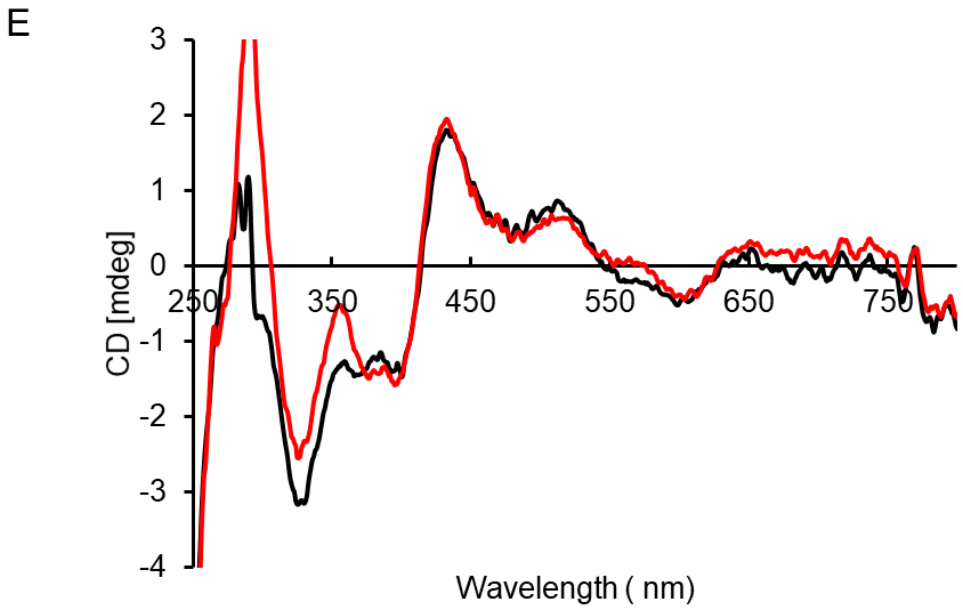
E
3
2
1
0
-1
-2
-3
-4
CD [mdeg]
250
350
450
550
650
750
Wavelength (nm)

Figure 4.4 ESI-MS analysis demonstrates binding of cluster-bound *Sv*WhiD to $\sigma^{HrdB}{}_4$.

(A) Deconvoluted mass spectrum measured under non-denaturing conditions of a solution containing a 2:1 ratio of $\sigma^{HrdB}{}_4$ to [4Fe-4S] WhiD containing $\sigma^{HrdB}{}_4$, [4Fe-4S] WhiD (90% cluster loaded), and a $\sigma^{HrdB}{}_4$: [4Fe-4S] WhiD complex. ★ indicate truncated forms of [4Fe-4S] WhiD alone and in complex with $\sigma^{HrdB}{}_4$. **(B-D)** show spectra of the three main species ($\sigma^{HrdB}{}_4$ (B), [4Fe-4S] WhiD (C), $\sigma^{HrdB}{}_4$: [4Fe-4S] WhiD complex (D)) plotted on an expanded mass scale, with oxygen/sulfur adducts indicated. [4Fe-4S] WhiD (5 µM) and $\sigma^{HrdB}{}_4$ (10 µM) were in 250 mM ammonium acetate, pH 7.2. **(E)** CD spectra of as isolated WhiD (red) and a 2:1 mixture of $\sigma^{HrdB}{}_4$: WhiD (black) demonstrating that the WhiD cluster environment is not significantly affected by binding to $\sigma^{HrdB}{}_4$. [4Fe-4S] WhiD (30 µM) and $\sigma^{HrdB}{}_4$ (60 µM) are in 50 mM Tris, 300 mM NaCl, pH 7.5.

4.3.2 The interaction of *Sv*WhiD is specific to the primary σ factor σ^{HrdB}_4

The specificity of the interaction between WhiD and σ^{HrdB}_4 was explored using analytical gel filtration. The lack of aromatic residues in σ^{HrdB}_4 results in a very low extinction coefficient at 280 nm. (ε= 2850 M^{-1} cm^{-1}), and so a 5-fold excess of σ^{HrdB}_4 was mixed with WhiD to allow detection of the protein through its $A_{280\ nm}$ during anaerobic gel filtration. Individually gel filtered proteins revealed σ^{HrdB}_4 as a monomer, and WhiD as a monomer/dimer equilibrium, as reported previously in section 3.3.2. The elution profile of the WhiD/ σ^{HrdB}_4 mixture contained peaks corresponding to the individual proteins, as seen from elution profiles of the individual proteins run down the column separately. Also present was a peak at a higher mass that was not observed in the elution profiles of the separate proteins corresponding to a mass of ~35 kDa. This mass was higher than predicted for a monomeric WhiD : σ^{HrdB}_4 complex, but too low to indicate a $(WhiD)_2$: σ^{HrdB}_4 complex. Thus, the WhiD monomer-dimer equilibrium described above remains a feature upon complex formation with σ^{HrdB}_4 (Figure 4.5A). SDS-PAGE analysis of the gel filtration elution fractions show individually ran σ^{HrdB}_4 was present solely in elution fractions 13-14 mL, but demonstrate that in the WhiD: σ^{HrdB}_4 mixture, σ^{HrdB}_4 becomes present across the high mass fractions along with WhiD confirming the peak at higher mass is indeed due to the a WhiD : σ^{HrdB}_4 complex (Figure 4.5B to D). SDS-PAGE also suggested the presence of a component of aggregated WhiD/ σ^{HrdB}_4 at ≥ 50 kDa. The specificity of complex formation for σ^{HrdB}_4 was tested by equivalent experiments with σ^{HrdD}_4. Because the extinction coefficient for σ^{HrdD}_4 is lower ($\varepsilon_{280\ nm}$ = 1490 M^{-1} cm^{-1}) than for σ^{HrdB}_4 *Sv*WhiD and σ^{HrdD}_4 were mixed in a 1:10 ratio to allow for detection of σ^{HrdD}_4 at $A_{280\ nm}$. Analysis by gel filtration and SDS-PAGE demonstrates no evidence of an interaction between the proteins. The elution profile of the WhiD/ σ^{HrdD}_4 mixture was a superposition of the profiles of the individual proteins with no higher mass complex, showing WhiD does not interact with σ^{HrdD}_4 (Figure 4.5E and F).

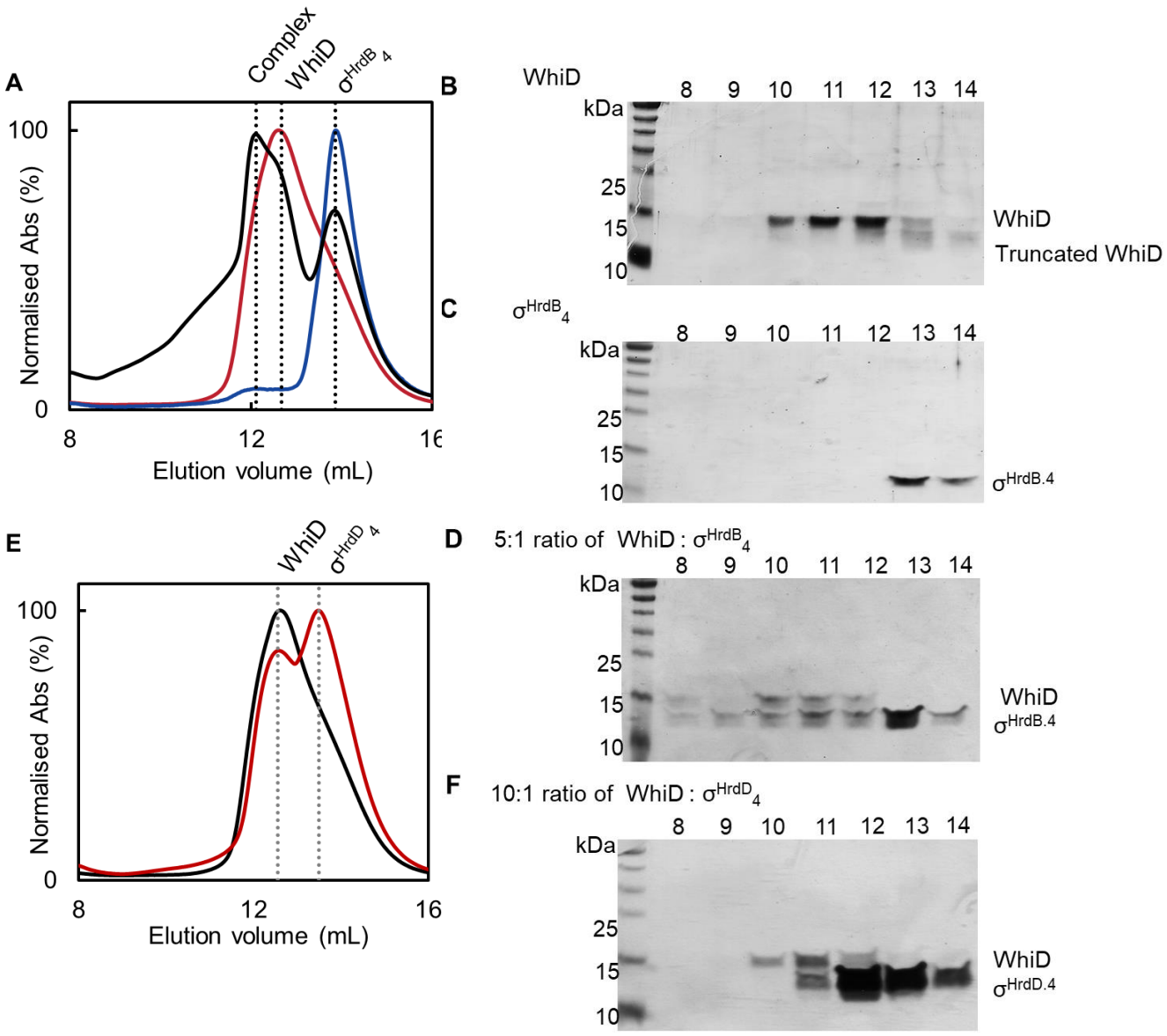

Figure 4.5 *Sv*WhiD binds specifically to domain 4 of the primary σ factor ($\sigma^{HrdB}{}_4$) but not to domain 4 of alternative σ factor ($\sigma^{HrdD}{}_4$).

(A) Gel filtration elution profiles ($A_{280\ nm}$) of WhiD (red line), $\sigma^{HrdB}{}_4$ (blue line) and a mixture of WhiD and $\sigma^{HrdB}{}_4$ in a 1:5 ratio (black line). **(B-D)** Fractions spanning the elution volume 8-14 mL were resolved by SDS PAGE and visualized by silver staining. *Sv*WhiD (B), $\sigma^{HrdB}{}_4$ (C) and WhiD : $\sigma^{HrdB}{}_4$ mixture (D). **(E)** Gel filtration elution profiles ($A_{280\ nm}$) of a mixture of WhiD and $\sigma^{HrdD}{}_4$ in a 1:10 ratio (red line), elution profile of WhiD alone is also shown for comparison (black line). **(F)** WhiD : $\sigma^{HrdD}{}_4$ mixture fractions spanning the elution volume 8-14 mL were resolved by SDS PAGE and visualised by silver staining. *Sv*WhiD (46 µM), $\sigma^{HrdB}{}_4$ (250 µM) and $\sigma^{HrdD}{}_4$ (500 µM) were in 50 mM Tris, 300 mM NaCl, pH 8.0.

4.3.3. Binding affinity of WhiD to σ^{HrdB}_4

Non-denaturing ESI-MS was used to measure the dissociation constant for the interaction between WhiD and σ^{HrdB}_4. In order to assist with quantification of the abundance of the complex, apo-I151A FNR was used as an internal protein standard. I151A FNR was chosen because its monomeric, with a mass of 29,123 Da (predicted mass 29,123 Da), close to that of the *Sv*WhiD- σ^{HrdB}_4 complex, 27,741 Da, allowing for an easier comparison in ion intensities. Multiple samples were prepared using individual proteins which were pre-exchanged into 250 mM ammonium acetate, pH 7.2. Samples were prepared with a constant concentration of WhiD at 3 µM, I151A FNR at 3 µM and with increasing concentrations of σ^{HrdB}_4 to give molar ratios of σ^{HrdB}_4 to WhiD between 0-7 excess σ^{HrdB}_4. Samples were incubated for 5 minutes before infusing into the mass spectrometer, as described in methods section 2.5. For each sample, data were collected over 2 minutes, averaged and deconvoluted over the 10-30 kDa range. (Figure 4.6A). As the concentration of I151A-FNR was kept constant, absolute ion counts for the WhiD : σ^{HrdB}_4 complex were compared to the combined absolute ion counts for FNR and complex. Data from multiple experiments (3 replicates) was then expressed as a function of free σ^{HrdB}_4 concentration and fitted using a simple binding isotherm, from which a K_d was calculated to be 7.4 (±1.4) × 10^{-7} M, indicating a relatively tight binding (Figure 4.6B).

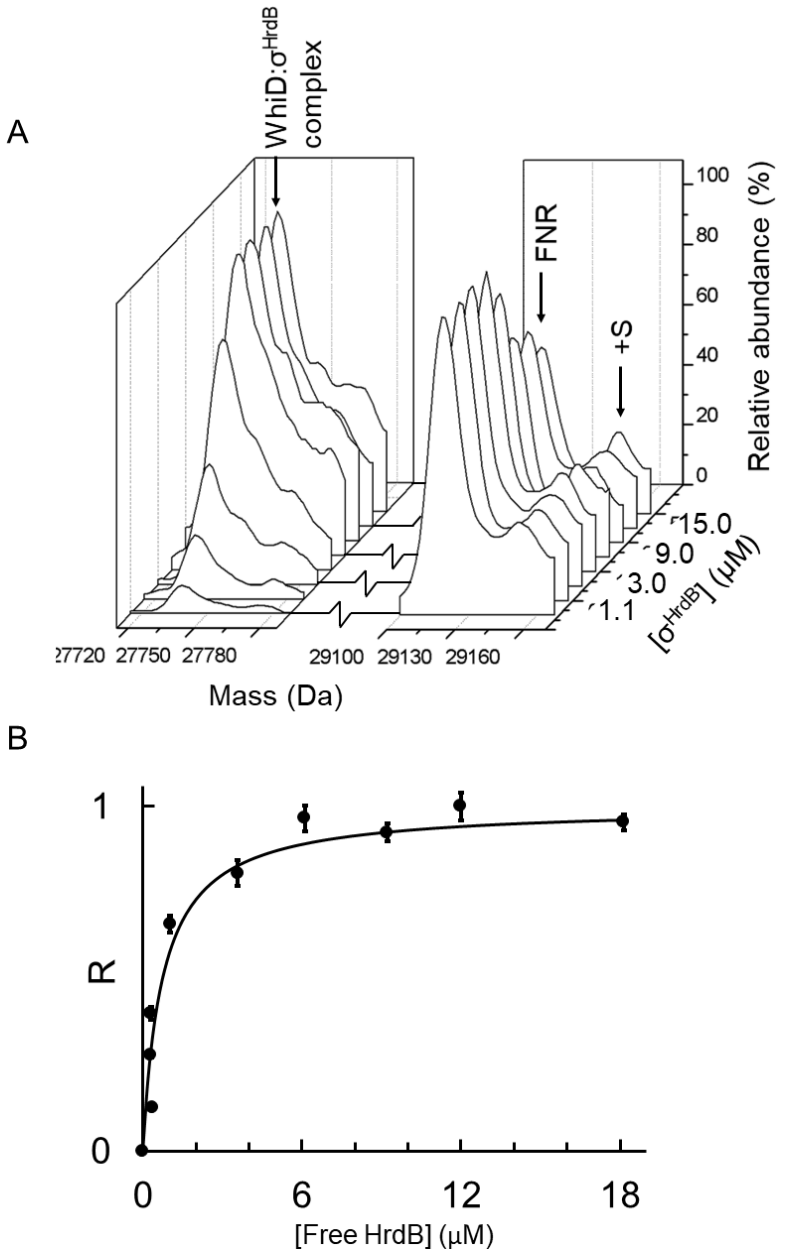

Figure 4.6 Determination of K_d for *Sv*WhiD-σ^{HrdB}_4 complex.

(A) Deconvoluted mass spectra under non-denaturing conditions of a solution containing *Sv*WhiD and increasing concentration of σ^{HrdB}_4, as indicated. An internal protein standard (FNR) was also present in the solution to enable quantification of the complex. (**B**) Plot of fractional saturation of *Sv*WhiD : σ^{HrdB}_4 complex formation as a function of the concentration of free σ^{HrdB}_4. Fractional saturation was determined from absolute ion counts due to the complex with reference to FNR ion counts. Error bars represent SE. Data were fitted using a simple binding equation from which the dissociation constant, K_d, was obtained directly. *Sv*WhiD (3 μM) and σ^{HrdB}_4 (0.75-21 μM) were in 250 mM ammonium acetate, pH 7.2.

4.4. O_2 and NO sensitivity of the Wbl : $\sigma^{HrdB}{}_4$ complex

4.4.1. $\sigma^{HrdB}{}_4$ protects WhiD and WhiB cluster from oxygen destabilisation

Exposure of [4Fe-4S] WhiB to oxygen in the absence and presence of $\sigma^{HrdB}{}_4$ revealed that $\sigma^{HrdB}{}_4$ at 1:1 mix substantially protected the [4Fe-4S] WhiB from oxidative degradation. In the absence of $\sigma^{HrdB}{}_4$, [4Fe-4S] WhiB exhibited a significant decrease in $A_{410\,nm}$ in the presence of oxygen, and signs of immediate destabilisation upon the addition of NO (see section 3.4.1). In the presence of $\sigma^{HrdB}{}_4$, a minor decrease in $A_{410\,nm}$ was observed, but the cluster absorbance remained largely stable for over 80 minutes in the presence of oxygen (Figure 4.7A and C). The same observation was seen for [4Fe-4S] WhiD in the presence of $\sigma^{HrdB}{}_4$, whereby in the absence of $\sigma^{HrdB}{}_4$, [4Fe-4S] WhiD remains largely unchanged for over 15 minutes, at which point precipitation caused scattering to the spectrum (Section 3.4.1) In the presence of $\sigma^{HrdB}{}_4$ a decrease in absorbance is still observed but the sample remains free of precipitation for over 60 minutes, suggesting that the presence of $\sigma^{HrdB}{}_4$ affects the oxidative degradation process of [4Fe-4S] WhiD and also to a degree protects the cluster from degradation (Figure 4.7B and D).

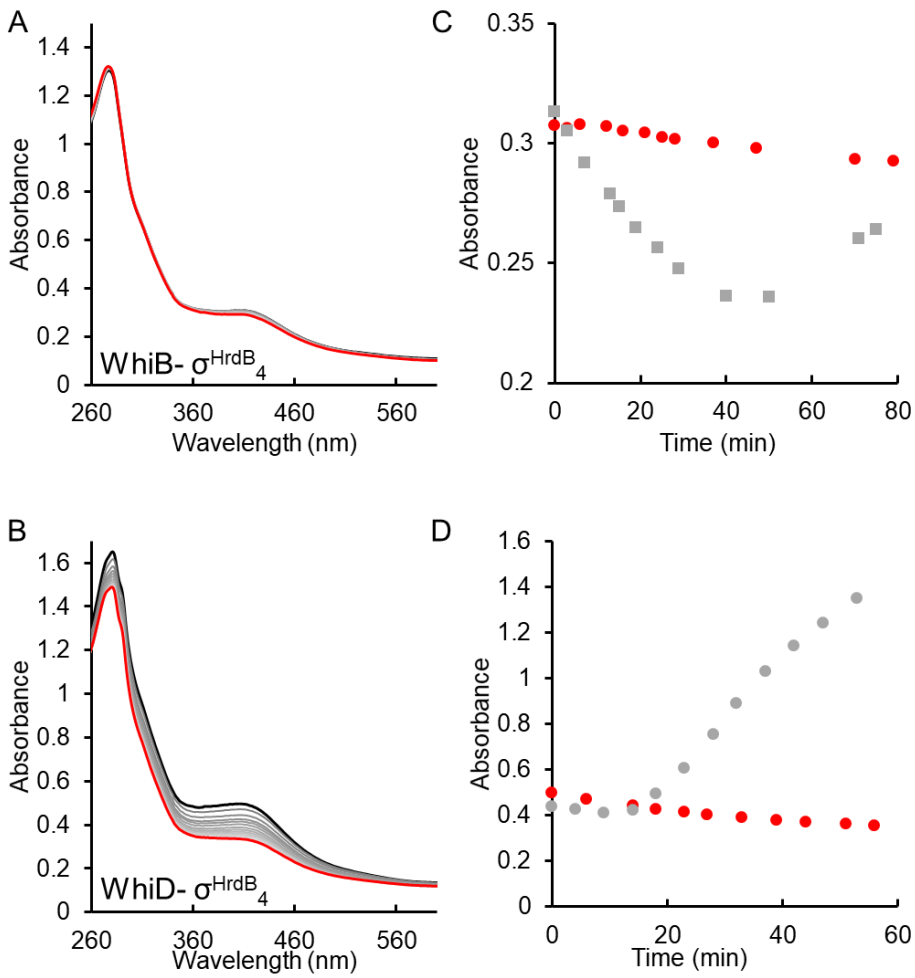

Figure 4.7 Sensitivity of *Sv*WhiB and *Sv*WhiD to O_2 is modulated by complex formation with σ^{HrdB}_4.

(A-B) spectra following the exposure to oxygen of [4Fe-4S] WhiB : σ^{HrdB}_4 (1:1 ratio) (A) and [4Fe-4S]WhiD : σ^{HrdB}_4 (1:2 ratio) (B). The starting spectra are in black, final spectra in red and intermediate spectra in grey. **(C-D)** Plot of $A_{410\,nm}$ as a function of time following exposure of [4Fe-4S]WhiB : σ^{HrdB}_4 (C) and [4Fe-4S]WhiD : σ^{HrdB}_4 (D) in red. Data following the exposure of [4Fe-4S] WhiB and [4Fe-4S] WhiD in the absence of σ^{HrdB}_4 are shown in grey for comparison. *Sv*WhiD (21 µM) and SvWhiB (25 µM) were in 50 mM Tris, 300 mM NaCl, pH 7.2 buffer.

4.4.2. Apo-*Sv*WhiD is unable to interact with σ^{HrdB}_4

Apo-WhiD was prepared with the same purification steps as normal, except aerobically. After purification, WhiD was incubated aerobically at room temperature for an hour before use to destabilise residual Fe-S cluster. Apo-WhiD was confirmed with UV-visible absorbance as $A_{410\ nm}$ cluster maximum reduced to baseline. Apo-WhiD was mixed with excess σ^{HrdB}_4 under the same conditions as [4Fe-4S] WhiD at a 1:5 ratio and analysed by gel filtration (Figure 4.8). Apo-WhiD was unable to form a complex with σ^{HrdB}_4, as evidenced by the absence of an elution peak corresponding to the higher massed WhiD: σ^{HrdB}_4 complex as judged by SDS-PAGE (Figure 4.8B). Although the ratio of WhiD and σ^{HrdB}_4 is still 1:5, there was a decrease in the UV absorbance of the peak corresponding to apo-WhiD. This is because of the loss of the [4Fe-4S] cluster, which contributes to $A_{280\ nm}$ intensity.

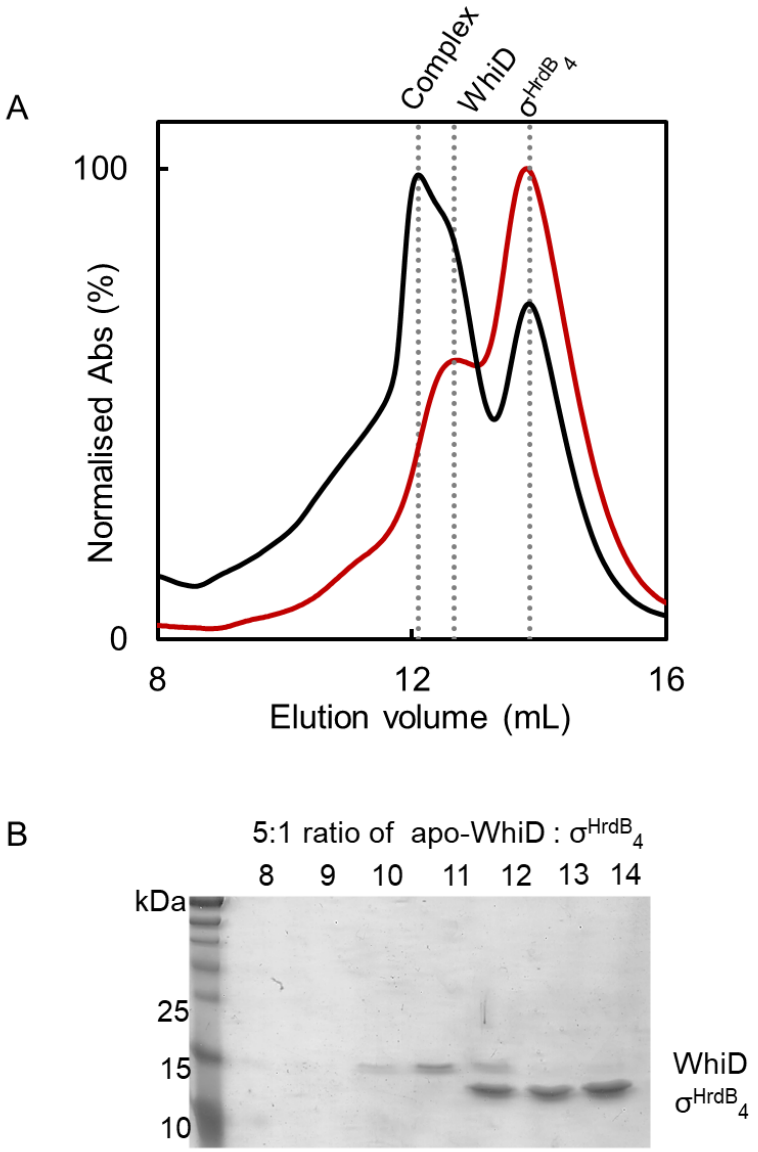

Figure 4.8 Apo-*Sv*WhiD does not bind to domain 4 of σ^{HrdB}_4.

(**A**) Gel filtration elution profiles ($A_{280\ nm}$) of a mixture of apo-WhiD and σ^{HrdB}_4 in a 1:5 ratio (red line). The elution profile of a mixture of cluster-containing WhiD and σ^{HrdB}_4 in a 1:5 ratio is shown for comparison (black line). (**B**) Fractions spanning the elution volume 8-14 mL were analysed by SDS-PAGE and silver stained. Apo-WhiD (48 µM) and σ^{HrdB}_4 (240 µM) were in 50 mM Tris, 300 mM NaCl pH 7.2.

4.4.3. Dissociation of the $\sigma^{HrdB}{}_4$: WhiD complex upon NO addition

The addition of 20 NO per cluster to WhiD : $\sigma^{HrdB}{}_4$ (5:1 excess of $\sigma^{HrdB}{}_4$) results in the nitrosylation of the [4Fe-4S] cluster as evidenced by the UV-Visible absorbance spectra. Analysis of the nitrosylated complex by analytical gel filtration revealed dissociation of the complex. This was particularly evident following SDS-PAGE of the elution fractions. Overall the behaviour of nitrosylated samples was reminiscent of the apo-WhiD : $\sigma^{HrdB}{}_4$ behaviour (Figure 4.9). Non-denaturing ESI-MS was also used to investigate the dissociation of WhiD : $\sigma^{HrdB}{}_4$ complex during the addition of NO. Individual proteins were desalted into 250 mM ammonium acetate, pH 7.2 and mixed at 1:1 ratio before infusing into the mass spectrometer with NO as described in the methods. Data were deconvoluted over the 10-30 kDa region and absolute ion count of the complex was taken as a percentage of total ion count of all components (to include [4Fe-4S] WhiD, apo-WhiD, $\sigma^{HrdB}{}_4$ and complex) (Figure 4.10). The plot of relative intensity as a function of NO shows the loss of the complex as NO was added and that dissociation of complex was complete at ~9 NO per cluster (Figure 4.10B). This is reminiscent of the plot observed for the loss of the [4Fe-4S] WhiD upon addition of NO, with the same non-linear plot, suggesting that the reaction is, again, not fully concerted. The data also demonstrates that the same reaction with NO is occurring in both scenarios and the loss of the cluster is linked to the dissociation of the complex.

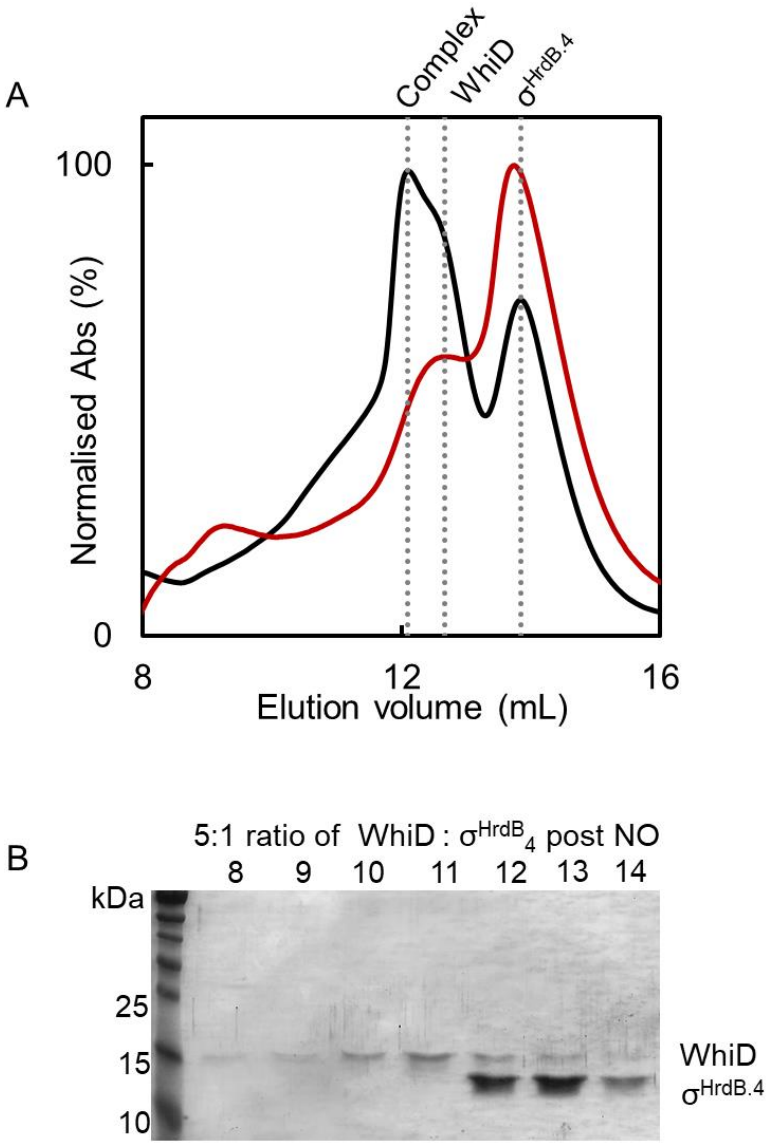

Figure 4.9 Reaction of the *Sv*WhiD-σ^{HrdB}_4 complex with NO results in dissociation.

(**A**) Gel filtration elution profiles ($A_{280\ nm}$) of a 5:1 mixture of σ^{HrdB}_4 : WhiD before (black line) and after (red line) reaction with 20 NO per cluster. (**B**) Fractions were resolved by SDS PAGE and visualized by silver staining. *Sv*WhiD (46 µM) and σ^{HrdB}_4 (250 µM) were in 50 mM Tris, 300 mM NaCl, pH 8.0

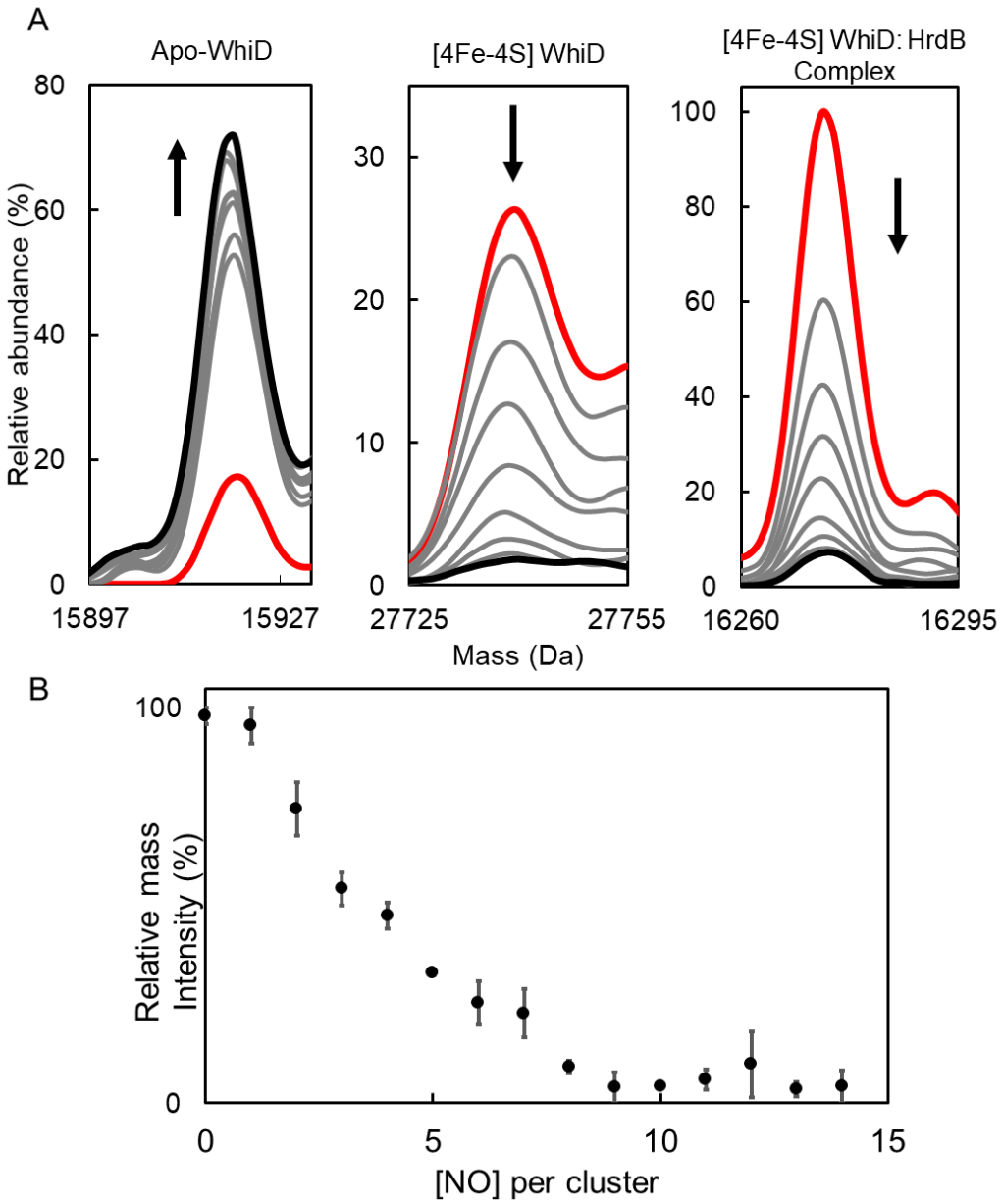

Figure 4.10 Non-denaturing mass spectrometric studies of reaction of *Sv*WhiD : σ^{HrdB}_4 complex with NO.

(**A**) Deconvoluted mass spectra showing the region corresponding to apo-WhiD, [4Fe-4S] WhiD and WhiD : σ^{HrdB}_4 complex, before (red spectrum) and during a titration with NO (grey spectra), up to 14 NO per cluster (black spectrum) followed under non-denaturing ESI-MS conditions. The arrows show the trend of the peak during the titration with NO. (**B**) Plot of percentage relative intensity of WhiD : σ^{HrdB}_4 complex as a function of NO per cluster. Error bars represent standard errors from n = 2 experiments. WhiD (10 µM cluster concentration) with σ^{HrdB}_4 (10 µM) in 1:1 ratio was in 250 mM ammonium acetate, pH 7.2.

4.5. Kinetic characterisation of WhiD : $\sigma^{HrdB}{}_4$ with NO

Although the interaction with $\sigma^{HrdB}{}_4$ is unable to protect [4Fe-4S] WhiD against NO mediated degradation, the rate and mechanism of the reaction may be affected. Stopped-flow kinetic measurements explore the initial stages of reaction. As described in section 3.5, [4Fe-4S] WhiD in undergoes nitrosylation in a similar mechanism to the previously characterised Wbl proteins in the presence of NO, showing a first order dependence to NO in the initial phases of the reaction.

Stopped-flow measurements were repeated for WhiD in the presence of 4-fold excess of $\sigma^{HrdB}{}_4$. Differences between the kinetic profiles in the presence and absence of $\sigma^{HrdB}{}_4$ were immediate. The first phase observed with [4Fe-4S] WhiD was split into two distinct consecutive phases, both of which occurring at a longer time period (Figure 4.11A). Furthermore, a stepwise increase from 10-50 NO per cluster demonstrate that the two initial phases in the [4Fe-4S] WhiD : $\sigma^{HrdB}{}_4$ complex were independent of NO (Figure 4.11B and C). Fitting of these phases independently allowed for the calculation of the k_{obs} to be 2.57 ± 0.13 x10^4 M^{-1} s^{-1} and 0.9 ± 0.07 x10^4 M^{-1} s^{-1} for the first and second phases respectively. Following the first two phases, a third phase that likely corresponds to the second phase of independent WhiD nitrosylation reaction and can be seen to be characterised by the same decrease in $A_{360\ nm}$ but due to the instability of the NO reaction, precipitation and scattering caused in the absorbance makes interpreting this data problematic.

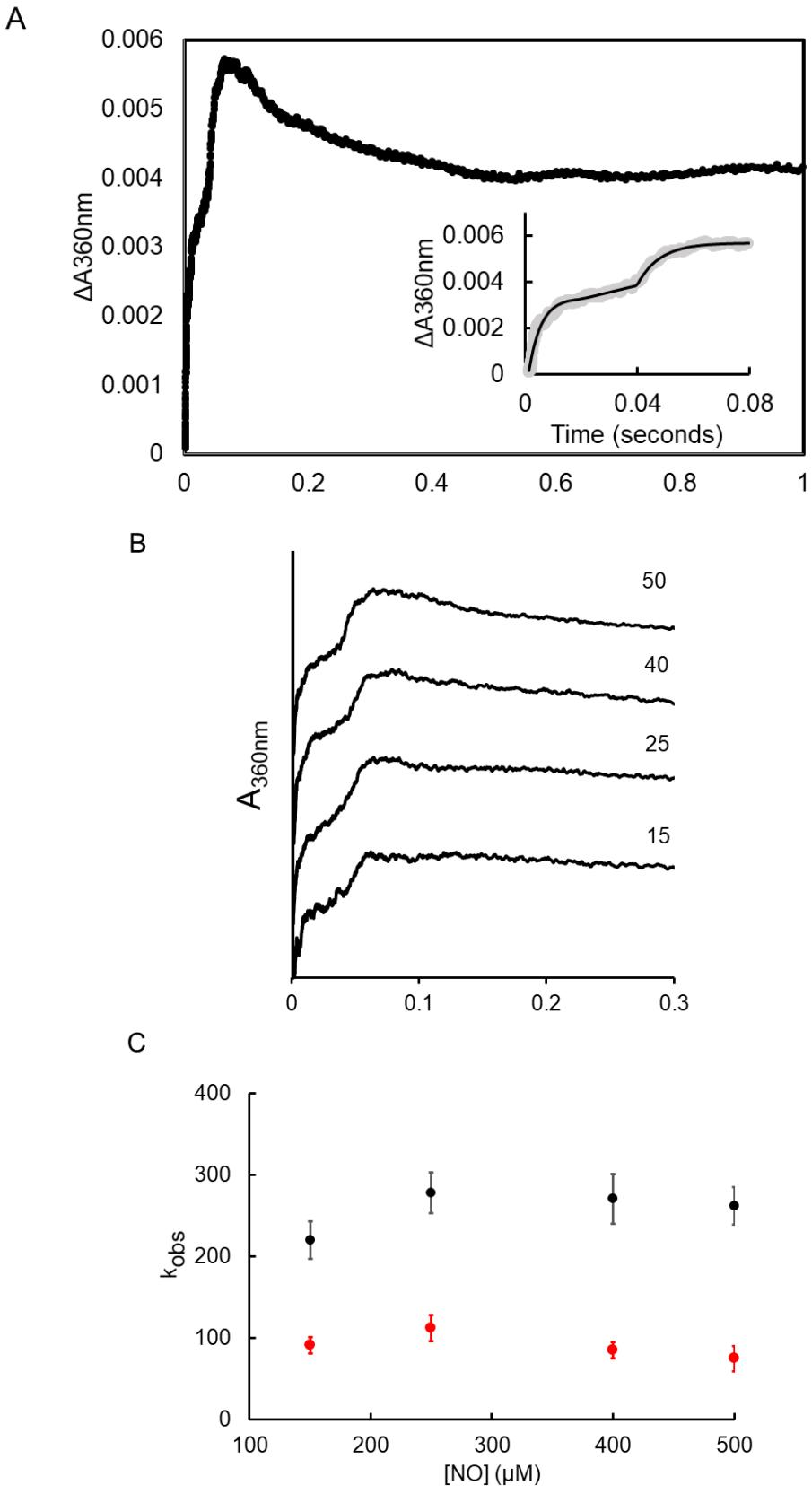
A
0.006
0.005
0.004
0.003
0.002
0.001
0
ΔA360nm
0
0.2
0.4
0.6
0.8
1
0.006
0.004
0.002
0
ΔA360nm
0
0.04
0.08
Time (seconds)
B
50
40
25
15
A360nm
0
0.1
0.2
0.3
C
400
300
200
100
0
kobs
100
200
300
400
500
[NO] (μM)

Figure 4.11 Stopped-flow kinetic studies of the nitrosylation of the [4Fe-4S] cluster of *Sv*WhiD : σ^{HrdB}_4 complex.

(**A**) Measurement of absorbance at 360 nm following addition of a 50-fold excess (over [4Fe-4S] cluster) of NO to WhiD in complex with σ^{HrdB}_4 (with σ^{HrdB}_4 in 4:1 excess). Inset shows the first 80 milli-seconds, in the reaction for WhiD-σ^{HrdB}_4. Solid lines show fits of the observed phases with exponential functions. **(B)** Shows data at 360 nm for a addition of 15-50 NO per cluster, as indicated. **(C)** Plots of observed rate constants for the first (black circles) and second (red circles) phases of $\Delta A_{360\ nm}$ following addition of varying concentrations of NO to WhiD-σ^{HrdB}_4. For both, a zero order dependence on NO was observed, indicating that the rate-limiting step of these reactions does not involve NO. Experiments were performed with WhiD (10 µM in [4Fe-4S]) in 50 mM Tris, 300 mM NaCl pH 7.2 at 25 °C. Data represents 4 technical replicates. Error bars represent SEM.

4.6. Discussion

Consistent with mycobacteria Wbl proteins, both *Sv*WhiB and *Sv*WhiD were able to interact with region 4 of the primary σ factor σ^{HrdB}. The interaction is specific as no interaction is observed between *Sv*WhiD and alternative σ factor σ^{HrdD}. The 1:1 complex between WhiD and σ^{HrdB}_4 is tight (K_d < 1 μM) and the interaction does not require the C-terminal extension found in *Sv*WhiD. The formation of the complex with σ^{HrdB}_4 is dependent upon the [4Fe-4S] cluster. Disruptions of the [4Fe-4S] cluster by both O_2 and NO abolishes the ability of WhiD to interact with σ^{HrdB}_4. This is unsurprising given the necessity for the hydrophobic residues located around the cluster binding pocket (specifically Trp3, Phe17, Trp60 and Phe18) reported for the interaction between *M. tuberculosis* WhiB1 and σ^A, highlighting the importance of the cluster environment, therefore absence and modification of the cluster environment would disrupt this interaction [5].

Although the Wbl : σ complexes analysed in this chapter significantly protects the [4Fe-4S] to O_2 mediated degradation for at least 60 minutes (consistent with the protective properties reported of the *M. tuberculosis* WhiB1: σ^A complex [6], exposure to O_2 ultimately results in cluster degradation and disassembly of the complex, with no observable cluster degradation intermediates by UV-absorbance spectroscopy or non-denaturing ESI-MS. The presence of σ^{HrdB}_4 also alters the nitrosylation reaction of [4Fe-4S] WhiD. The reaction of NO with the complex occurs via a multi-step process, reminiscent of the reaction of NO with WhiD alone, except the first phase (WhiD step 1) of the reaction becomes separated into two distinct steps in the presence σ^{HrdB}_4. These two initial steps are independent of NO which may suggest that rate is limited by a narrower access channel to the cluster in the complex, capable of allowing only one NO per reaction step. Alternatively, it may suggest that dissociation of σ factor, or a conformational change needs to occur prior to NO attack on the cluster. The distinct nature of the second step suggests that a second conformational change is dependent upon the completion of the first step. Therefore, the interaction between σ^{HrdB}_4 and WhiD appears to be protective in nature, likely to due to increased stability of the protein and/or limited accessibility of O_2 and NO to the cluster. The inaccessibility of O_2

was demonstrated in the WhiB1- σ^A structure which revealed the solvent inaccessible, buried nature of the [4Fe-4S] cluster [5, 6]. Nevertheless, O_2 mediated degradation does occur over time. Similarly, although a smaller molecule, the accessibility of NO to the cluster was also impaired in the complex, leading to a slower rate, independent of NO compared to the reaction of independent [4Fe-4S] WhiD cluster with NO.

To conclude, the novel observations that *Streptomyces* Wbl proteins also interact with σ factors, much like the mycobacterial Wbl proteins, suggests that Wbl : σ factor interaction could be an aspect of Wbl protein function that is conserved across Actinobacteria. Importantly, the protective effect of the Wbl : σ factor interaction upon oxidative cluster degradation results in an increased kinetic distinction in the sensitivity to O_2 and NO. This demonstrates that the WhiD : σ^{HrdB} complex is optimally arranged to distinguish between O_2 and NO and points to a likely mechanism by which environmental queues could be transduced to signal specific regulatory responses.

4.7. References

1. Casonato, S., et al., *WhiB5, a transcriptional regulator that contributes to* Mycobacterium tuberculosis *virulence and reactivation.* Infect Immun, 2012. **80**(9): p. 3132-44.
2. Feng, L., et al., *Genome-wide characterization of monomeric transcriptional regulators in* Mycobacterium tuberculosis*.* Microbiology, 2016. **162**(5): p. 889-897.
3. Burian, J., et al., *The mycobacterial antibiotic resistance determinant WhiB7 acts as a transcriptional activator by binding the primary sigma factor SigA (RpoV).* Nucleic Acids Res, 2013. **41**(22): p. 10062-76.
4. Steyn, A.J., et al., Mycobacterium tuberculosis *WhiB3 interacts with RpoV to affect host survival but is dispensable for in vivo growth.* Proc Natl Acad Sci U S A, 2002. **99**(5): p. 3147-52.
5. Wan, T., et al., *Structural basis of non-canonical transcriptional regulation by the sigmaA-bound iron-sulfur protein WhiB1 in* M. tuberculosis*.* Nucleic Acids Res, 2020. **48**(2): p. 501-516.
6. Kudhair, B.K., et al., *Structure of a Wbl protein and implications for NO sensing by* M*.* tuberculosis*.* Nat Commun, 2017. **8**(1): p. 2280.
7. Bush, M.J., *The actinobacterial WhiB-like (Wbl) family of transcription factors.* Mol Microbiol, 2018. **110**(5): p. 663-676.
8. Bentley, S.D., et al., *SCP1, a 356,023 bp linear plasmid adapted to the ecology and developmental biology of its host, Streptomyces coelicolor A3(2).* Mol Microbiol, 2004. **51**(6): p. 1615-28.

Chapter 5. Characterisation of *S. venzuelae* WhiA and its role in coregulating sporulation initiation with WhiB

5.1 Introduction

WhiA and WhiB are transcriptional regulators that play important roles in developmental cell division. Strikingly, initial mutagenesis studies showed that *S. coelicolor whiA* and *whiB* deletion strains exhibit identical phenotypes of abnormally long, tightly coiled aerial hyphae which lack septation and uncondensed DNA, resulting from uncontrolled growth [1-3]. This strongly suggests that WhiA and WhiB control the same regulatory checkpoint underlying differentiation. More recently, *in vivo* studies of *S. venezuelae* using ChIP-seq coupled with microarray transcriptional profiling reveal that the two transcriptional regulators have an overlapping regulon of ~250 transcriptional targets [4, 5]. Deletion of either *whiA* or *whiB* genes prevent the promoter binding ability of the remaining protein, suggesting WhiA and WhiB are functionally co-dependent. Together, WhiA and WhiB co-control the initial switch from aerial growth to sporulation by activating genes involved in septation , e.g. *ftsZ*, *ftsK* and *ftsW*, and repressing genes involved in aerial growth, e.g. *filP* [4, 5]. Moreover, mutations in any of the four conserved cysteines in WhiB also abolishes *in vivo* DNA-binding of both WhiA and WhiB, suggesting the [4Fe-4S] cluster of WhiB may be important for function [5]. Although the cooperativity has not been explored in mycobacteria, the *M. tuberculosis* genes encoding both the WhiB orthologue WhiB2, and WhiA are essential, therefore it is likely that the proteins function together in a similar manner [6, 7].

Bioinformatic analysis of the ChIP-seq data identified a short but conserved sequence (GACAC) present in WhiA and WhiB binding sites. However, this sequence is highly abundant, with ~15,000 copies in the *S. venezuelae* genome, which is mismatched with the limited ~250 transcriptional units bound by WhiA *in vivo* [4, 5]. Therefore, there must be yet un-identified specificity determinants in addition to the short GACAC sequence. Out of the two proteins, WhiB likely functions to regulate the binding of WhiA to specific target promoters. Recently, a direct interaction was observed between *C. glutamicum*

WhiB orthologue WhcD in its apo-form and WhiA. WhcD is also a transcriptional regulator which similarly targets genes involved in cell division [8, 9]. Although WhcD was unable to interact directly with DNA *in vitro*, it was shown to enhance the DNA-binding ability of WhiA [9]. The co-dependency of WhiA and WhiB from *S. venzeuelae* or *S. coelicolor,* has thus far, not been observed for *in vitro* DNA binding assays. In *S. coelicolor*, *whiA* is transcribed from two promoters, a constitutive promoter and a developmentally regulated promoter [10]. Corresponding work in *S. venezuelae* confirmed that *whiA* as is also transcribed throughout the *Streptomyces* lifecycle so that WhiA is similarly present in both vegetative growth and sporulation [4]. In contrast, w*hiB* transcription is developmentally induced. Therefore, at least in part, the role of WhiB may be to target WhiA to specific promoters and initiate sporulation [11]. A direct interaction between the *Sv*WhiA and *Sv*WhiB was anticipated based on the recent *C. glutamicum* WhcD observations.

WhiA is a member of the DUF199 family of proteins. Unlike the Wbl proteins, WhiA is not unique to actinobacteria and is found in many gram-positive bacteria, including many that do not sporulate [12]. This means that the collaborative nature of the WhiA and WhiB protein may be unique to actinomycetes. Furthermore, not all WhiA orthologues appear to act as transcriptional regulators; for example, the *Bacillus subtilis* WhiA orthologue, YvcL, appears to bind DNA to facilitate its localisation to the nucleoid [13]. The crystal structure was solved for *Thermatoga maritima* WhiA which revealed that WhiA is bipartite in nature [12]. The N-terminal region contains two LAGLIDADG motifs, reminiscent of a LAGLIDADG homing endonuclease (LHE), domestication of homing endonucleases to be employed by host organisms for alternative biological purpose has been frequently characterised [14]. The endonuclease-like region in *Tm*WhiA is noncatalytic as it lacks the residues required for DNA cleavage activity [15]. Tethered to the endonuclease-like region is a C-terminal conserved helix turned helix (HTH) region resembling the 4.2 region of bacterial σ^{70} (Figure 5.1A) [12]. In σ^{70}, this region is responsible for the targeted DNA binding to the -35 region of bacterial promoters [16]. Whilst both regions historically have DNA binding capabilities, the endonuclease domain displays an altered DNA-binding surface compared to active homing endonucleases, and the C-terminal HTH region was shown to be responsible for

binding DNA, notably the binding affinity of the HTH region is significantly lower than full length protein [12]. *Sv*WhiA and *Sc*WhiA share high sequence identity of 94%, and they share ~26% sequence identity with *Tm*WhiA (Figure 5.1B).

The WhiA and WhiB relationship in *Streptomyces* requires further study. One potential hinderance to characterising this relationship so far may be due to the fragility of the [4Fe-4S] cluster in WhiB, which makes *in vitro* biochemical studies difficult (see Chapter 3). This chapter highlights the characterisation of *S. venezuelae* and *S.coelicolor* WhiA as well as the mechanism of *Sv*WhiA and *Sv*WhiB as transcriptional regulators.

A

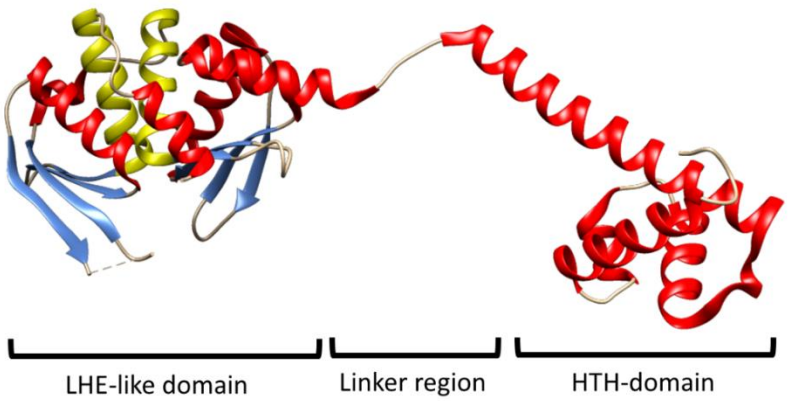

B

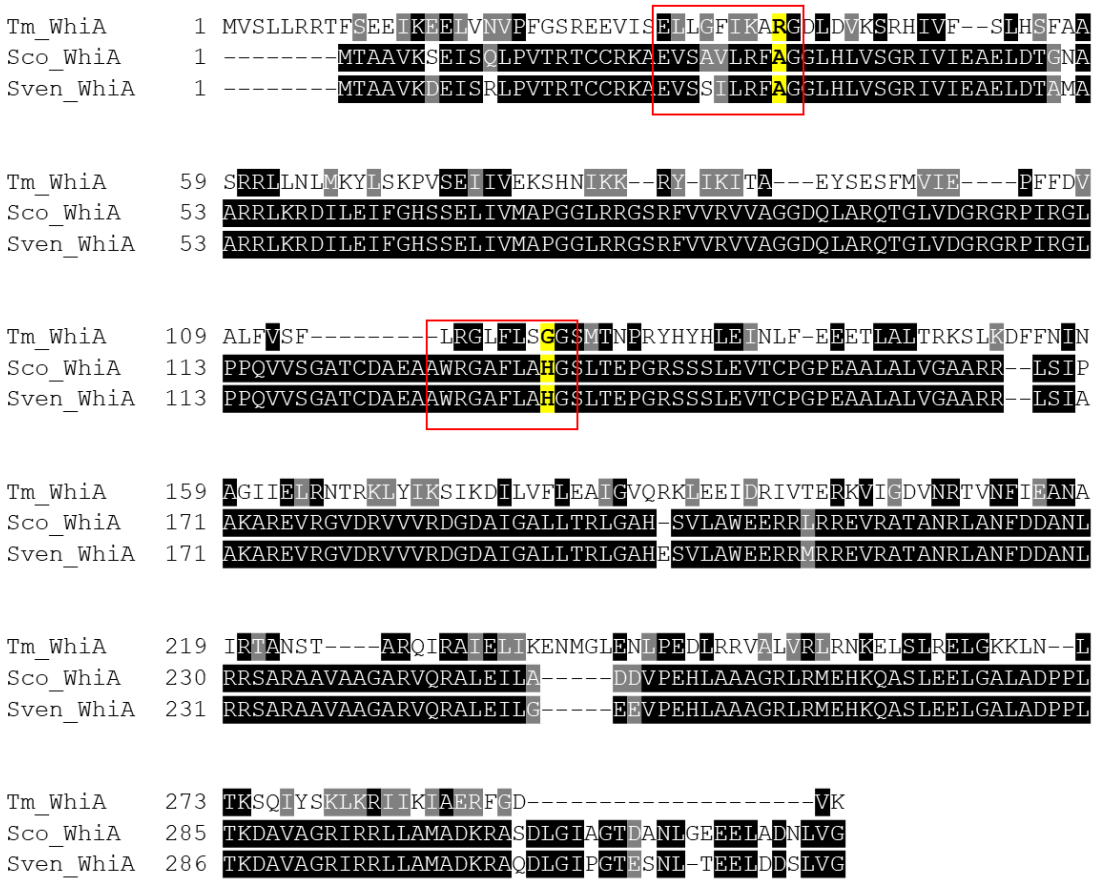

Figure 5.1 Sequence conservation and structure of WhiA.

(A) Structure of full length WhiA from *T.maritima*. LHE-like domain, linker region and helix turned helix (HTH)-domain are labelled. LADGLIDADG motif alpha helices are in yellow (α2 and α4). Remaining alpha helices are in red. Beta strands of the LHE domain are in blue. Disordered loop connecting β strands 3 and 4 is represented by dashes. **(B)** a multiple sequence alignment of WhiA from *T.maritima* (Tm), *S.coelicolor* (Sco) and *S.venezuelae* (Sven). Red boxes indicate the two LAGLIDADG motifs (LD_1 and LD_2), characteristic of conventional LAGLIDADG homing endonucleases (LHE). Yellow highlighted residues indicate location of the acidic residues required by LHEs to cleave DNA, which are not conserved and absent in WhiA orthologues.

5.2. Characterization of as isolated *Sv*WhiA

5.2.1. Purification of recombinant *Sv*WhiA

*Sv*WhiA was over-produced by ligating the codon-optimised *whiA* into pET15b using *Nde*I and *Xho*I sites, generating pMSW6 to encode an N-terminally His_6-tagged WhiA. This vector was then introduced in *E. coli* BL21 (DE3). WhiA was purified aerobically, as described in methods section 2.1. Elution from a nickel- charged Hi-trap chelating column resulted in a cloudy solution in fractions corresponding to the WhiA protein. SDS-PAGE confirmed that the precipitated material was WhiA. Subsequently, WhiA precipitation was minimised by keeping eluted fractions immediately on ice. Ni-affinity chromatography purification was followed by heparin affinity purification. This step simultaneously further removed contaminants, and imidazole from the buffer of WhiA. In the absence of imidazole, WhiA remained stable in solution. SDS-PAGE gel electrophoresis was used to check protein content of elution fractions (Figure 5.2A). Exact mass was confirmed with LC-MS as 37,138, corresponding to the mass of $(His)_6$ -WhiA, with an N-terminal methionine cleavage (predicted mass 37, 138 Da). An adduct of +178 Da excess mass corresponds to spontaneous α-N-6-Phosphogluconoylation of the N-terminal $(His)_6$-tag, during overexpression in *E. coli* (Figure 5.2B) [17].

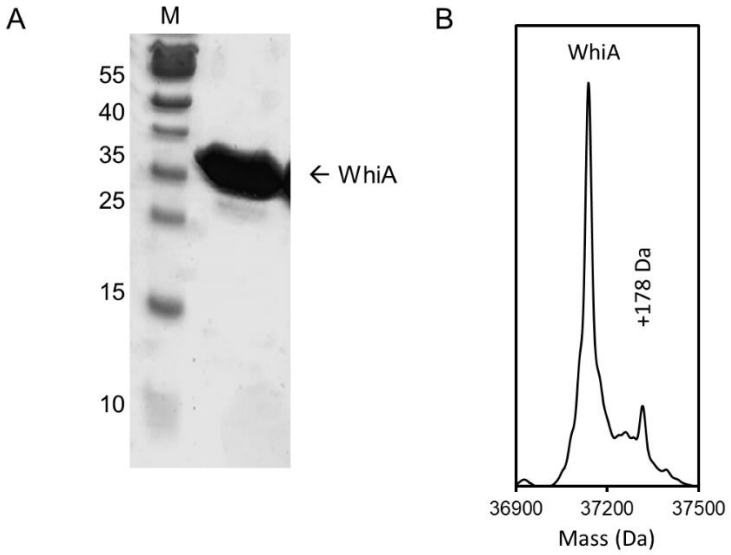

Figure 5.2 Characterisation of as isolated *Sv*WhiA.

(A) SDS-PAGE analysis of purified WhiA reveals largely pure protein sample following purification **(B)** Deconvoluted LC-MS spectrum reveals mass of (His_6)-WhiA, lacking the N-terminal Met residue. Adduct of +178 Da is labelled, representing spontaneous α-N-6-Phosphogluconoylation of the N-terminal $(His)_6$-Tag which occurs in overexpression in *E. coli*. For LC-MS experiments, WhiA (50 µM) was in aqueous mixtures of 2% (v/v) acetonitrile, 0.1% (v/v) formic acid.

5.2.2. Recombinant *Sv*WhiA is partially unfolded

Non-denaturing ESI-MS can be used to probe the conformation of proteins by looking at the charge state distributions. As described in section 2.6, a folded protein has fewer exposed sites for protonation and therefore the ions formed have fewer charges than the corresponding ions from unfolded/partially proteins. MS parameters were as described in section 2.6.1 and the spectrum was recorded from 1000 – 5000 m/z. The m/z spectrum of WhiA reveals two distinct charge packets; the first covering the 1000 – 2250 m/z and corresponds to WhiA with +16 to +32 charges and is indicative of partially folded or unfolded forms of WhiA. The second charge packet spans 2500 to 3500 m/z and corresponds to WhiA with +12 to +15 charges, consistent with the folded form of WhiA (Figure 5.3A).

The two distinct charge packets were individually deconvoluted. Unexpectedly, deconvolution of the +16 to +32 charge states revealed a small shoulder, likely corresponding to WhiA, but the majority of un-folded WhiA conditions exists in a +64 Da form, resulting in a dominant mass peak of 37,202 Da. This unexpected +64 Da additional mass observed in the deconvoluted non-denaturing ESI-MS spectra was not present in the LC-MS spectra, which indicates that the adduct was resultant of non-covalent interactions. In addition, mass adducts of +34 Da and +60 Da could also be seen (Figure 5.3B). Deconvolution of the +12 to +15 charge states again revealed a primary mass peak of 37,202 Da, corresponding to WhiA with a +64 Da mass addition. The presence of the +64 Da adduct in both the folded and misfolded forms of WhiA suggests that it is not responsible for the misfolding of WhiA. In the folded region of the WhiA m/z spectrum, the main mass peak of 37,202 Da is followed by four high intensity consecutive series of +60 Da mass adducts. These are unlikely to be 2x sulphur, or 4x oxygen adducts as no +32 or +16 adducts were observed. Instead these may correspond to acetate (+59 Da) adducts, acquired from the non-denaturing ESI-MS buffer (Figure 5.3C).

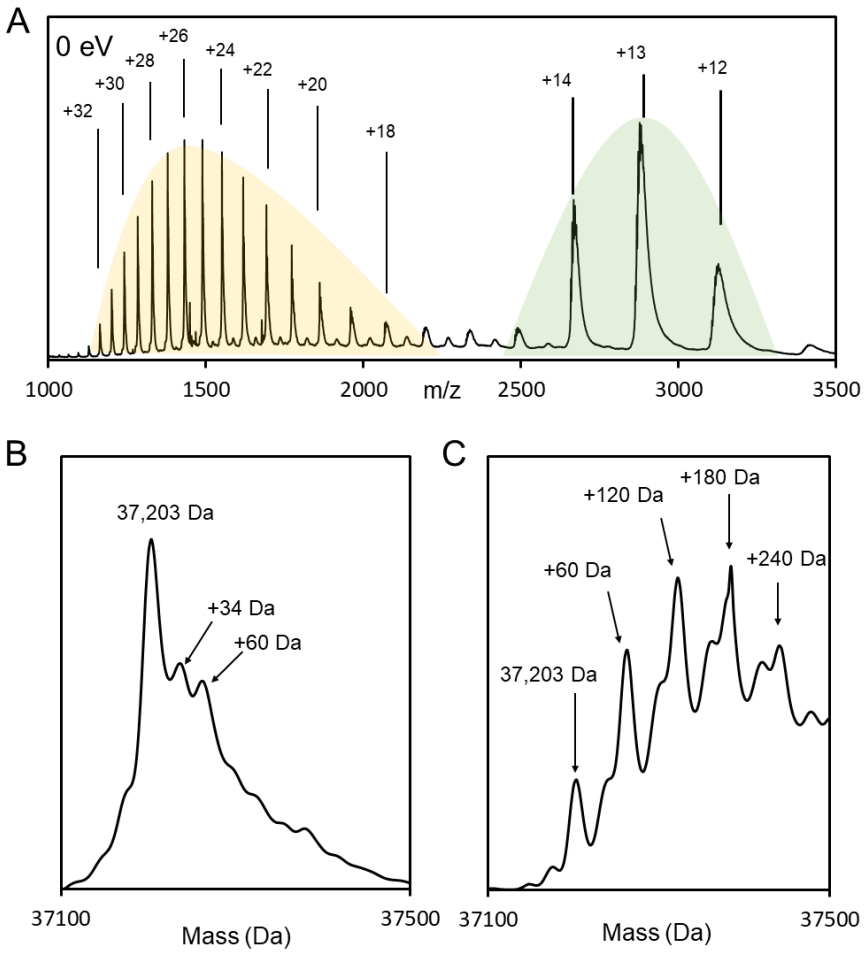

Figure 5.3 Non-denaturing mass spectrometry of *Sv*WhiA.

(A) m/z spectrum of WhiA is shown from 1,000- 3,500. Under non-denaturing conditions, the m/z of WhiA shows bimodal charge state distribution. Most of the charge distribution includes charges +16 to +32 (orange box). The large number of charges at lower m/z region suggests that a large proportion of protein is in an unfolded/ misfolded state. Charge states +12 to +15 make up a second distribution (green box). The low number of charges and high m/z is characteristic of a folded protein. **(B)** m/z corresponding to charges +16 to +32 was deconvoluted resulting in a mass spectrum of WhiA showing the mass major species as 37,203 Da, corresponding to the mass of WhiA, with N-terminal methionine cleavage, and an unexpected additional mass of +64. Additional mass adducts on top of the 37,203 Da mass is as indicated. **(C)** m/z corresponding to charges +12 to +15 was deconvoluted resulting in a mass spectrum of WhiA showing the same 37,201 Da, but with large adducts on top of this mass of +60 Da,

+120 Da, +180 Da and +240 Da. These consecutive + 60 Da adducts likely corresponding to acetate from the non-denaturing ESI-MS buffer. A small shoulder corresponding to the mass of apo-WhiA can again be seen. ★indicates a +24 mass adduct of apo-WhiA. For non-denaturing ESI-MS experiments, WhiA (10µM) was in 250 mM ammonium acetate, pH 7.2.

MS parameters were then optimised to isolate m/z region for the folded form of WhiA (Figure 5.4). This consisted of increasing transfer time to 200 µs, and pre-pulse storage time to 25 µs. Data was recorded from 2,200 - 3500 m/z. In order to probe the identity and stability of the non-covalently bonded +64 adduct on the mass of WhiA, IsCID (in-source collision induced dissociation) was applied. By increasing the IsCID voltage, a potential difference can be applied between funnel 1 and funnel 2 within the ESI-MS. Thus, incoming ions are accelerated towards funnel 2, increasing the likelihood of collision and potential fragmentation. By default, a value of 0 eV prevents unwanted collisions. Increasing this value (≤ 100 eV) can improve the passage of larger ions by promoting gentle de-clustering of ions without fragmentation. However, it is important that increasing the applied voltage does not damage the cluster or disrupt potential protein-protein interactions. In this case, the IsCID was applied at 75 eV. This resulted in the dissociation of the +60 Da acetate buffer contaminants. Nevertheless, the +64 adduct remained, indicating a strong non-covalent interaction, and/or it is shielded within the protein (Figure 5.4B).

The percentage of unfolded material in as isolated *Sv*WhiA was estimated with chemical unfolding experiments using 0 to 6M Guanidine-HCl (Figure 5.5). WhiA was isolated in buffer containing components which absorb in the far-UV region creating interference below 220 nm and 205 nm, respectively, e.g. Tris and NaCl. Thus, an initial spectrum of WhiA was collected using a phosphate buffer. This revealed negative bands at 222 nm and 208 nm and a positive band around 190 nm, characteristic of an α-helix rich protein. Subsequent denaturing steps were performed in the Tris-based buffer used for experimental characterisation, with the loss of secondary structure being followed at 222 nm. The data revealed a non-sigmoidal transition curve, which appeared to

associate with the latter part of a denaturation curve. The data fit well to a two-state unfolding model (ΔG_{unfold} of 4.4 ±0.3 kJ mol^{-1}), as previously performed for the characterisation of as isolated WhiD [18]. This suggested that, as isolated, WhiA samples contain ~15% unfolded protein in the absence of denaturant.

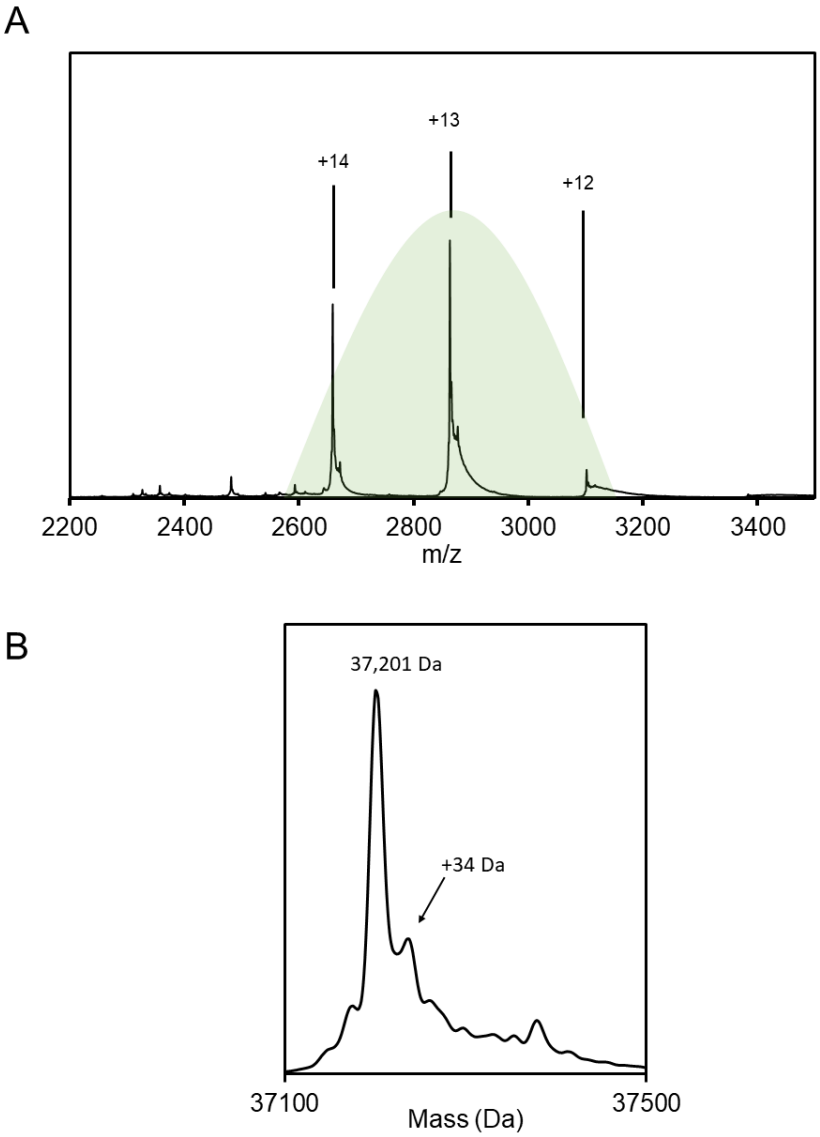

Figure 5.4 Non-denaturing mass spectrometry of *Sv*WhiA with 75 eV IsCID.

(A) m/z spectrum of WhiA is shown from 2,200- 3,500 with an applied 75 eV IsCID. Charge states +12 to +15 correspond to WhiA folded-state (green box). **(B)** m/z corresponding to charges +12 to +15 was deconvoluted resulting in a mass spectrum of WhiA showing a major mass peak at 37,201 Da, minor adduct of +34 is as indicated. WhiA (10 µM) was in 250 mM ammonium acetate, pH 7.2.

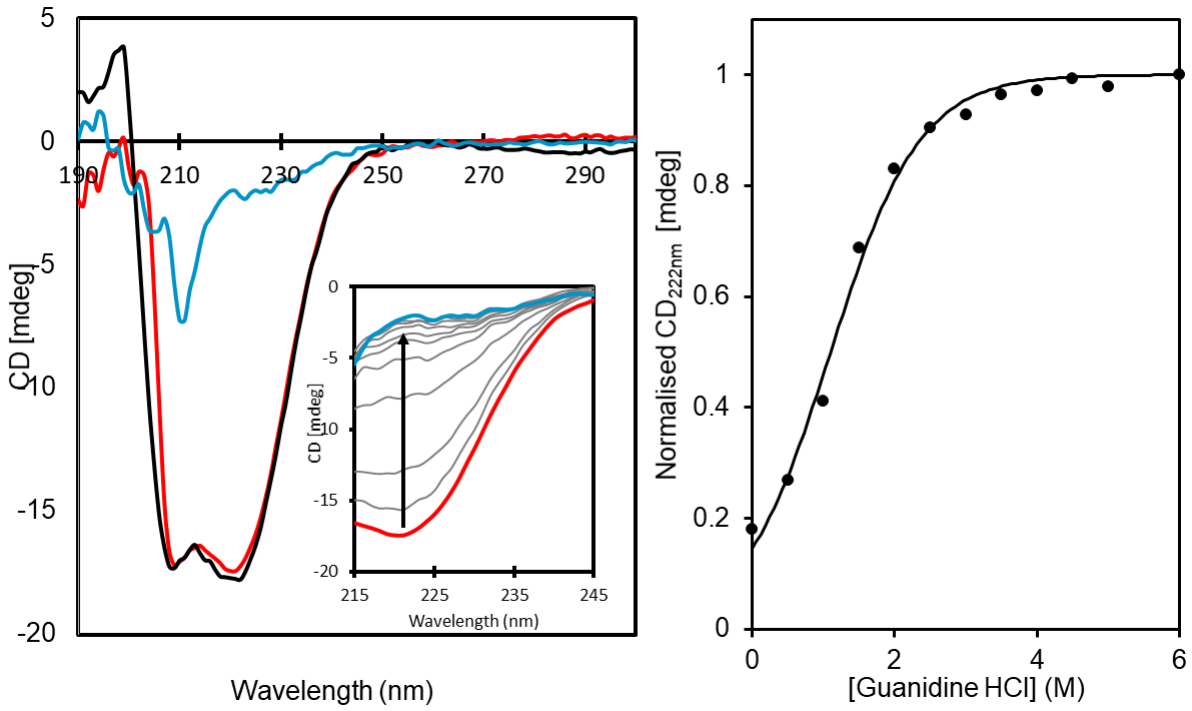

Figure 5.5 Chemical denaturation of as isolated *Sv*WhiA.

(A) Far-UV CD spectra of SvWhiA (6 µM) in 50 mM potassium phosphate, pH 8.0 (Black) and 50 mM Tris, 300 mM NaCl, pH 7.2 (all remaining spectra). Chemical denaturation was performed in increasing concentrations of guanidine-HCl. The Initial spectrum in 0 M guanidine-HCl is in red, and final spectrum is in blue. *Inset:* all intermediate spectra are shown in grey, with arrow following the change in CD in intensity at 222 nm. **(B)** The fraction of unfolded protein (as normalised intensity at 222 nm) is plotted as a function of guanidine-HCl concentration (0-6 M). *Sv*WhiA displayed a non-sigmoidal transition, which suggested that it was partly unfolded in the absence of denaturant. Assuming *Sv*WhiA was ~15% unfolded at zero denaturant, the data then fitted to a two-state unfolding model.

5.2.3. WhiA is a zinc-binding protein

ICP-MS was used to determine whether a metal cofactor was responsible for the +64 Da mass increase of WhiA. This revealed that 90% + of WhiA is bound to zinc. To test whether zinc binding is unique to *Sv*WhiA, an expression plasmid for the overexpression of *Sc*WhiA in *E. coli* was obtained (kindly provided by M. Bush, John Innes Center, Norwich). *Sc*WhiA was produced, purified and characterised by non-denaturing ESI-MS, which revealed the same +64 Da increase in mass when compared to the mass from LC-MS spectrum, suggesting zinc binding may be a common feature of *Streptomyces* WhiA (Figure 5.6).

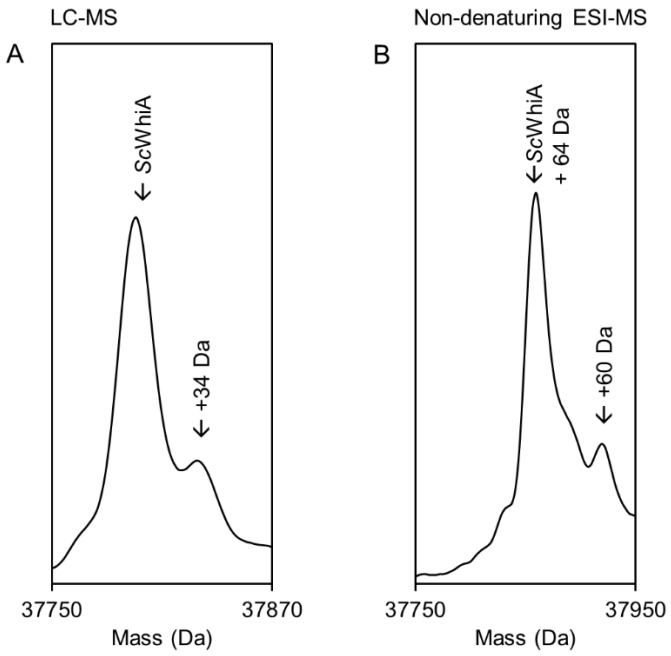

Figure 5.6 *S. coelicolor* WhiA coordinates zinc.

(A) Deconvoluted LC-MS spectrum of reveals mass of (his_6)-*Sc*WhiA, with N-terminal Met cleavage. **(B)** Deconvoluted non-denaturing ESI-MS spectrum reveals mass of *Sc*WhiA, with additional +64 Da corresponding to zinc binding. Mass adducts are labelled: + 34 Da and +60 Da adduct likely corresponds to chloride originating from buffer C and acetate contamination from ammonium acetate buffer, respectively. For LC-MS, *Sc*WhiA (50 µM) was in aqueous mixtures of 2% (v/v) acetonitrile, 0.1% (v/v) formic acid. For non-denaturing ESI-MS experiment, *Sc*WhiA (10 µM) was in 250 mM ammonium acetate, pH 7.2.

Zinc is an essential element for many proteins and can act functionally and/or structurally. However, structural studies of the *Tm*WhiA protein do not report any metal binding. Strikingly, *Tm*WhiA was described to have lost key residues required for metal binding and catalysis within the "LAGLIDADG" domains. Thus, the possibility of removing zinc from *Sv*WhiA was attempted using two chelators: EDTA (Ethylenediaminetetraacetic acid); a high affinity metal chelator and TPEN (N,N,N',N'-tetrakis (2-pyridinylmethyl)-1,2-ethanediamine; a chelator with affinity for many transition metals, but in particular high affinity for Zn^{2+} ($K_d = 2.6 \times 10^{-16}$ M). Both the addition of 10 mM EDTA or 1 mM TPEN to WhiA (80 µM), resulted in mild precipitation within an hour and near total protein precipitation overnight. This suggests that the absence of zinc destabilises WhiA and zinc may be important for the structural integrity of WhiA. This also provides an explanation for the instability of WhiA in imidazole rich buffers, observed during purification in section 5.2.1.

5.2.4. Location of zinc binding site

Several amino acids are known to coordinate zinc, such as Cys, His, Asp and Glu [19]. The sequence or predicted structure of *Sv*WhiA displays no obvious zinc binding sites. However, protein fragmentation points to the protein region responsible for zinc binding. Incubation of WhiA for 12 hours at room temperature leads to in spontaneous truncation of WhiA, shown in SDS-PAGE gel (Figure 5.7A). Furthermore, in addition to the N-terminal thrombin cleavage site for $(His)_6$-tag removal, a second predicted thrombin cleavage site exists within the WhiA protein which results in the cleavage of WhiA after residue 126. Thus, WhiA was incubated overnight at room temperature with an increasing amount of thrombin (GE healthcare) between 0 and 3 GE units per 100 µg protein. SDS-PAGE was used to confirm successful fragmentation of WhiA, with higher amounts of fragmentation being observed as the amount of thrombin was increased (Figure 5.7B).

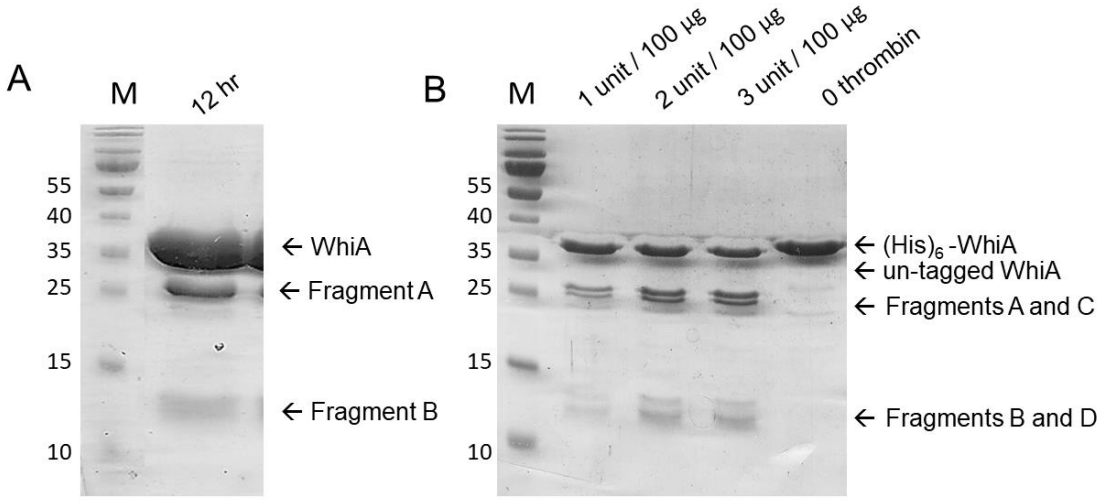

Figure 5.7 Fragmentation of *Sv*WhiA.

(A) SDS-PAGE showing spontaneous fragmentation of WhiA into two separate fragments (A and B). **(B)** SDS-PAGE of thrombin cleavage of WhiA. Incubation of WhiA with 1,2 and 3 GE units of thrombin / 100 µg WhiA results in cleavage of $(His)_6$-WhiA to un-tagged WhiA, and fragments C and D, and spontaneous fragmentation resulting in fragments A and B. For thrombin cleavage, 500 µg of WhiA was incubated with indicated amount of thrombin, overnight at room temperature.

LC-MS was used to identify the location of spontaneous fragmentation in WhiA. This revealed in masses of 9,705 Da, 10,019 Da and 10,176 Da, resulting from 3 closely located cleavage sites following residues 253, 254 and 258 (predicted masses 9,705 Da, 10,019 Da, and 10,176 Da, respectively). These fragments were labelled as fragments A1, A2 and A3, respectively. The corresponding fragments of masses 25,699 Da, 25,385 Da and 25,228 Da (predicted masses 25,699 Da, 25,385 Da, and 25,228 Da, respectively), were labelled as fragments B1, B2 and B3, respectively (Figure 5.8). LC-MS also confirms the thrombin cleavage, which results in the mass of 35,387 Da, corresponding to un-tagged WhiA (predicted mass 35,387 Da), as well additional the thrombin cleavage products of 11,820 Da and 23,585 Da (predicted mass 11,820 Da and 23,585 Da, respectively), labelled as fragment C and D, respectively (Figure 5.8). In order to identify which of the fragments bound zinc, non-denaturing ESI-MS experiments were

performed. Fragments A(1,2, and 3) and C exhibited identical masses during denaturing LC-MS and non-denaturing ESI-MS conditions. Fragment B (1,2 and 3) and D were observed to be ~64 Da heavier during non-denaturing ESI-MS (Figure 5.9). This indicates that the zinc binding site is located between residues 126 and 253 of *Sv*WhiA. Based on the homology model, this corresponds to the C-terminal LAGLIDADG motif of the endonuclease region, the linker region and first helix of the sigma factor region. Sequence alignments revealed considerable differences within this region between *Sv*WhiA and *Tm*WhiA. Furthermore, the region in *Sv*WhiA consists of numerous amino acid residues (2x His, 1x Cys, 5x Asp, and 9x Glu) with the potential for zinc coordination.

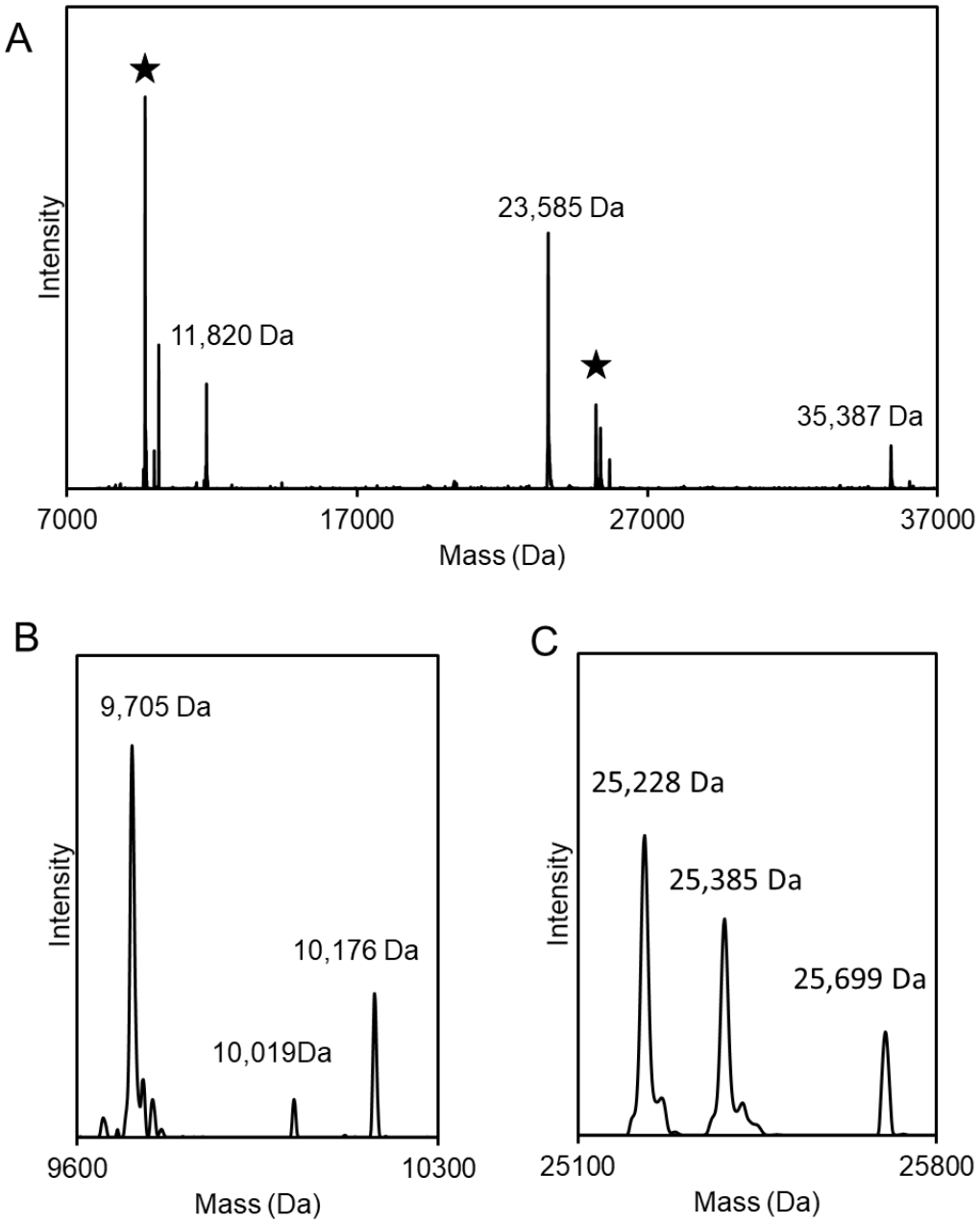
A
Intensity
23,585 Da
11,820 Da
35,387 Da
7000
17000
27000
37000
Mass (Da)
B
9,705 Da
Intensity
10,176 Da
10,019Da
9600
10300
Mass (Da)
C
25,228 Da
Intensity
25,385 Da
25,699 Da
25100
25800
Mass (Da)

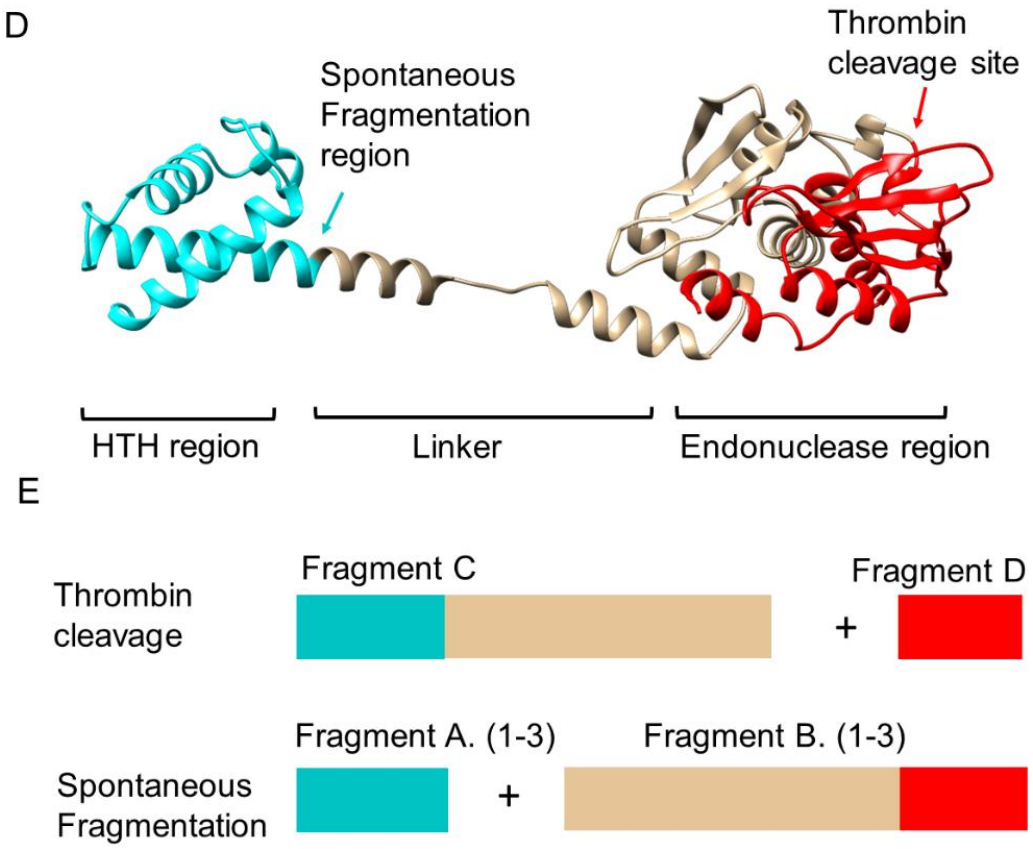

Figure 5.8 LC-MS of *Sv*WhiA fragmentation.

(A) Deconvoluted LC-MS of WhiA post overnight incubation with 2 units/ 100 µg thrombin (GE healthcare). Spectrum reveals un-tagged WhiA at 35,387 Da, as well the two predicted fragments of WhiA at predicted thrombin cleavage site at residues 126. ★indicates fragments corresponding to spontaneous fragmentation of WhiA. (B) and (C) show zoomed in view of regions previously indicated by ★ at 9,600 Da to 10,300 Da, and 25,100 Da to 25,800 Da, respectively. to show separate sites of fragmentation. **(D)** predicted structure of *Sv*WhiA, based previously solved crystal structure of *Tm*WhiA. Spontaneous fragmentation sites and thrombin cleavage sites are as indicated. HTH-domain, linker region and endonuclease region are also labelled. **(E)** Simplified representation of fragments as seen in LC-MS data to show fragments resulting from spontaneous fragmentation as A(1-3), to include the HTH-domain and B (1-3), to include the linker and endonuclease domain, and thrombin cleavage fragment products as C, to include C-terminal endonuclease domain, and D as N-terminal endonuclease domain, linker and HTH-domain.

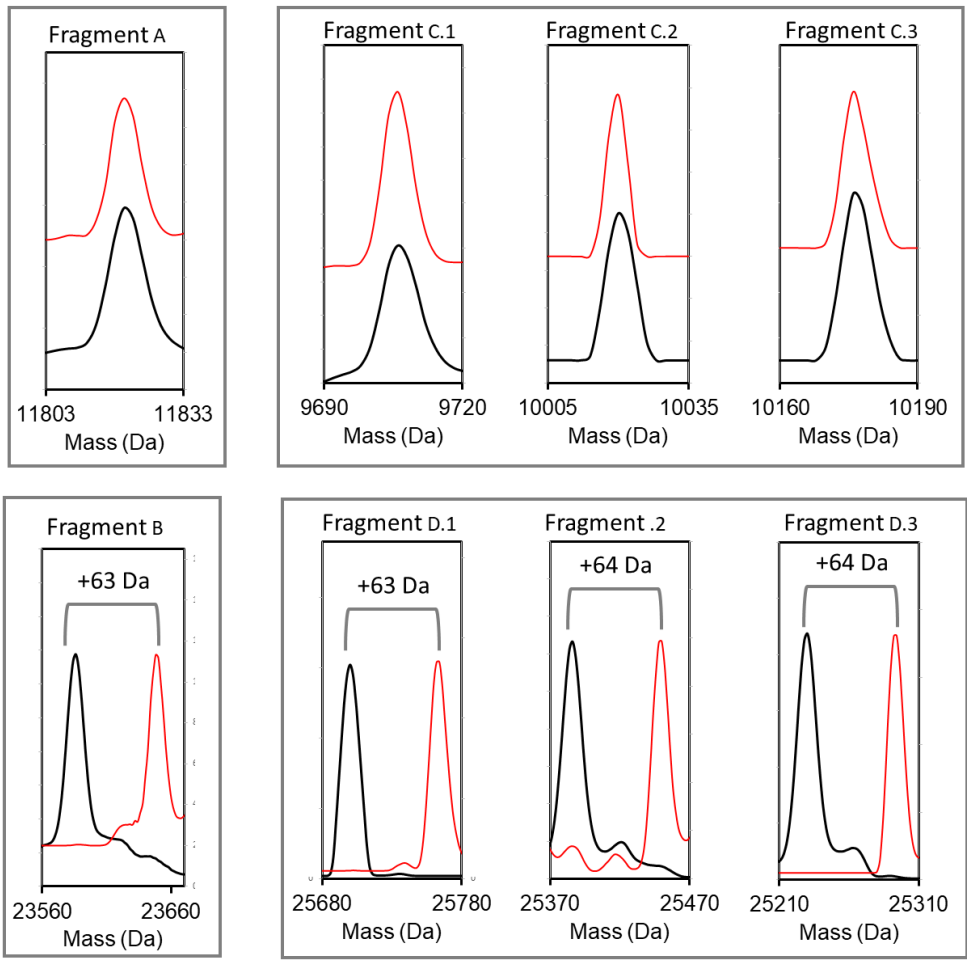

Figure 5.9 LC-MS and Non-denaturing ESI-MS of fragmented WhiA sample.

Fragments A(1-3), B(1-3), C and D are as indicated. LC-MS data, under denaturing conditions are shown in black. Non-denaturing ESI-MS data is shown in red. +63/ +64 Da, corresponding to zinc coordination are labelled. LC-MS experiments were in aqueous mixtures of 2% (v/v) acetonitrile, 0.1% (v/v) formic acid. Non-denaturing ESI-MS experiments were in 250 mM ammonium acetate, pH 7.2.

5.3. *S. venezuelae* WhiA and its DNA binding properties

5.3.1. WhiA binds to promoter regions of genes involved in sporulation initiation in its zinc bound form

Bush et al. identified the regulon of WhiA, which included several genes encoding key proteins required for initiating sporulation septation and the cell division machinery [4]. EMSAs were carried out to confirm the ability of *Sv*WhiA to bind upstream promoter regions of *ftsW* (P*ftsW*) and *filP* (P*filP*). EMSAs were performed as described in section 2.8. Increasing concentrations of WhiA were incubated with ~2 nM FAM-labelled P*filP* and P*ftsW*. Resultant EMSA gels revealed that *Sv*WhiA binds to both promoters with apparent low affinity, as the majority of DNA remains un-shifted (Figure 5.10).

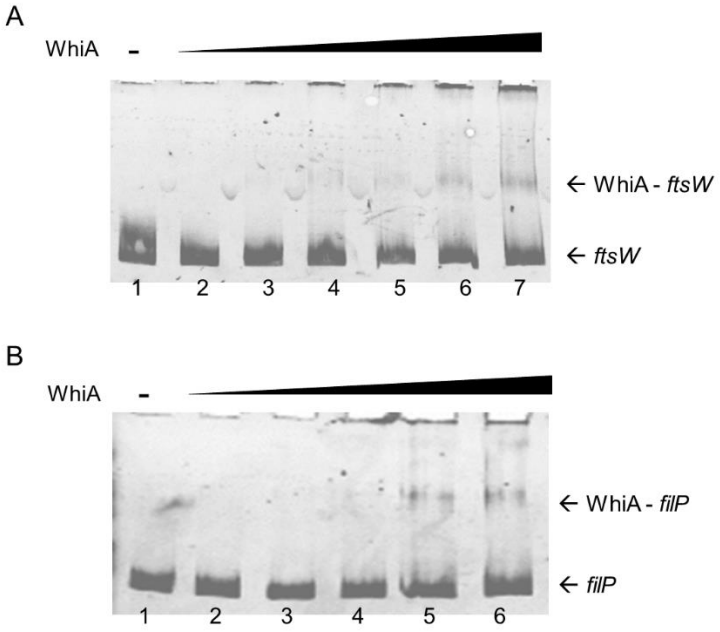

Figure 5.10 DNA binding activity of as isolated *Sv*WhiA.

(A) FAM-labelled P*ftsW* (2.7 nM) was incubated with increasing concentrations of WhiA. Lane 1 contains no protein, lanes 2-7 contain 11, 23, 35, 47, 56 and 70 nM WhiA, respectively. **(B)** FAM-labelled P*filP* (2.9 nM) was incubated with increasing concentrations of WhiA. Lane 1 contains no protein, lanes 2-6 contain 9, 19, 28, 37 and 47 nM WhiA, respectively. Separation of WhiA-DNA complexes from free DNA are as indicated.

As mentioned in section 5.2.3, 90% of as isolated WhiA associates with zinc. The low affinity of WhiA for DNA, as shown in the EMSA experiments, may be due to the presence of zinc hindering DNA binding. Therefore, non-denaturing ESI-MS was used to investigate the nature of the WhiA: P*ftsW* interaction. Instead of the 240 bp sequence used in the EMSA experiments, a smaller 21 bp double stranded fragment, P$ftsW_{21}$, was chosen to keep the mass of the resultant WhiA: P$ftsW_{21}$ complex within the operational limits of the ESI-MS. The chosen 21 bp sequence had previously been identified as a region of high affinity binding for WhiA to the *ftsW* promoter via DNase I footprinting experiments [4]. Non-denaturing ESI-MS parameters were tuned to optimise m/z corresponding to the folded form of WhiA between 2,400 and 4,000 m/z. Upon addition of 1:1 WhiA: P$ftsW_{21}$, 4 additional m/z peaks were observed (Figure 5.11A) indicative of the binding of WhiA to the P$ftsW_{21}$ oligo. Deconvolution of the m/z spectrum revealed a mass of 50,062 Da, which corresponds to a WhiA [Zn] : P$ftsW_{21}$ complex (predicted mass 50,061 Da)(Figure 5.11B). This demonstrated that the zinc associated form of *Sv*WhiA is capable of binding to the promoter region of *ftsW in vitro*.

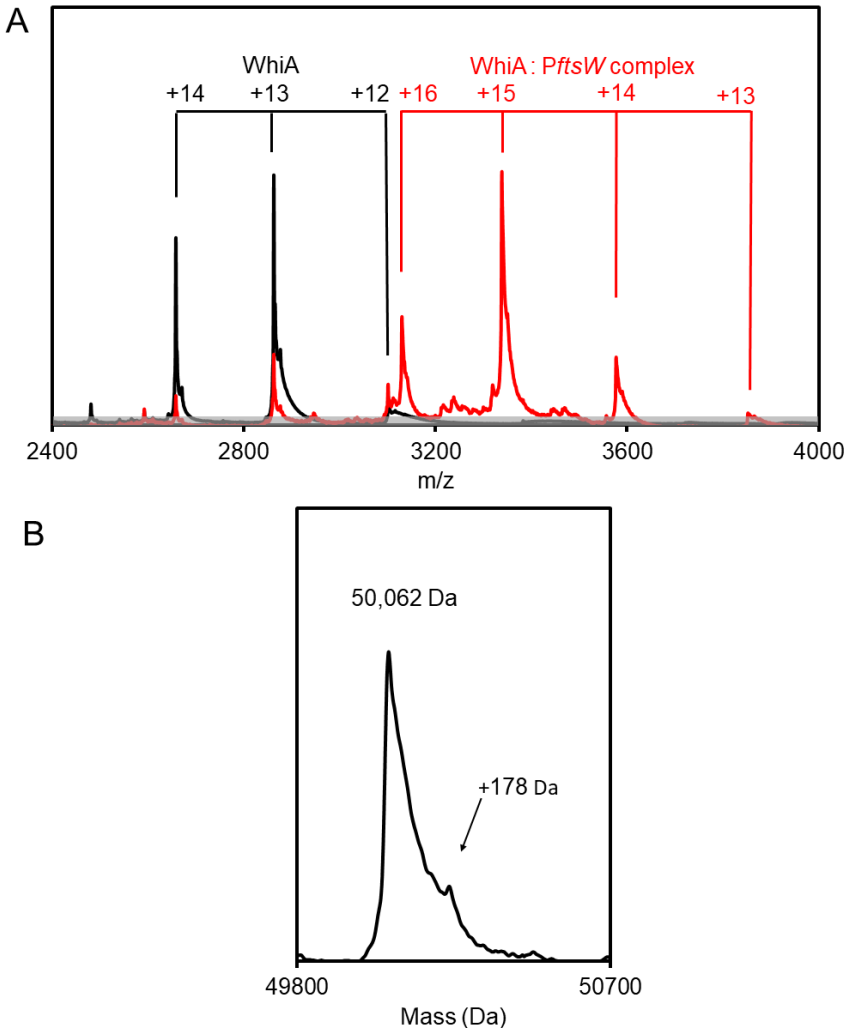

Figure 5.11 Non-denaturing mass spectrometry of the *Sv*WhiA: P*ftsW*$_{21}$ complex.

(A) Overlay of the m/z spectrum of WhiA independently, and in complex with P*ftsW*$_{21}$ is shown from 2,400- 4,500 m/z. Charge states +12 to +14 corresponding to WhiA folded-state are indicated in black. Charge states +13 to +16 corresponding to the WhiA: P*ftsW*$_{21}$ complex are indicated in red. **(B)** m/z peaks corresponding to the WhiA: P*ftsW*$_{21}$ complex was deconvoluted resulting in a major mass peak at 50,062 Da, minor adduct of +178 Da is as indicated. WhiA (10 µM) was in 250 mM ammonium acetate, pH 7.2.

5.3.2. WhiA binds specifically to GACAC containing DNA fragments

The GACAC sequence recognised by WhiA is highly abundant in the *S. venezuelae* genome, with ~15,000 copies. Upon closer inspection, it was realised that there were three GACAG sites located within the *ftsW* promoter region used for the EMSA experiments described in section 5.3.1. Five double stranded DNA oligonucleotides of 30 to 31 bp (P*ftsW*$_1$, P*ftsW*$_2$, P*ftsW*$_3$, P*ftsW*$_4$ and P*ftsW*$_5$) were chosen from the promoter region of *ftsW* to investigate the specificity of WhiA binding to DNA (Figure 5.12A). P*ftsW*$_1$ includes the WhiA-protected region identified by DNase I footprinting experiments [4]. P*ftsW*$_4$ and P*ftsW*$_5$ contain the additional GACAC sites within the *ftsW* promoter region. P*ftsW*$_2$ and P*ftsW*$_3$ are fragments of the *ftsW* promoter that do not contain a GACAC site.

Non-denaturing ESI-MS was performed for 1:1 ratio mixtures of WhiA : P*ftsW* fragments. Interestingly, the m/z spectra revealed that WhiA was able to form a complex with all GACAC containing fragments: P*ftsW*$_1$, P*ftsW*$_4$ and P*ftsW*$_5$, resulting in additional peaks corresponding to complex formation. No additional m/z peaks were observed for experiments with P*ftsW*$_2$ and P*ftsW*$_4$ (Figure 5.12B). Deconvolution of the m/z peaks corresponding to complex formation resulted in masses of 56,244 Da, 55,623 Da and 55,628 Da for P*ftsW*$_1$, P*ftsW*$_4$ and P*ftsW*$_5$, respectively (Figure 5.12C). In the case of P*ftsW*$_4$, this was identical to the theoretical mass of a WhiA [Zn] : P*ftsW*$_4$ complex. The theoretical mass of WhiA [Zn] : P*ftsW*$_1$ is 56,241 Da, and the theoretical mass of WhiA [Zn] : P*ftsW*$_5$ is 55,626 Da. The 2 Da mass difference in these complexes may be due to a combination of broad deconvoluted mass peaks, and the m/z peaks being close to the limit of the MS instrument. These experiments revealed that, *in vitro*, WhiA was able to bind all DNA fragments containing the GACAC motif. Thus, it is probable that, *in vitro*, WhiA is capable of binding weakly to DNA containing the GACAC motif. It is likely that the mechanism for WhiA to function as a sporulation specific transcriptional regulator, with the high specificity DNA binding observed in the *in vivo* ChIP-seq experiments may include other components in addition to the recognition of the GACAC motif by WhiA.

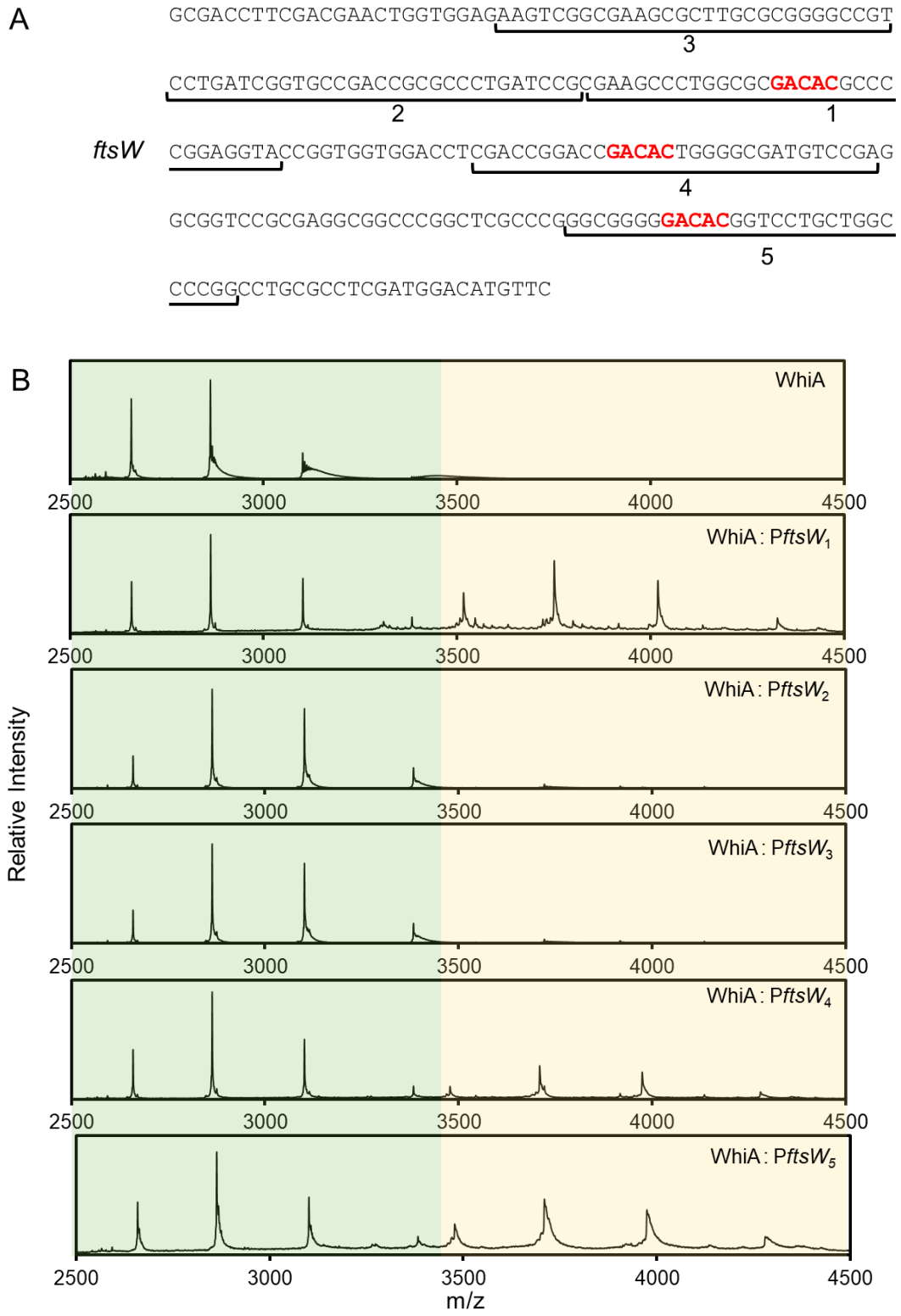
A
GCGACCTTCGACGAACTGGTGGAGAAGTCGGCGAAGCGCTTGCGCGGGGCCGT
3
CCTGATCGGTGCCGACCGCGCCCTGATCCGCGAAGCCCTGGCGCGACACGCCC
2
1
ftsW
CGGAGGTACCGGTGGTGGACCTCGACCGGACCGACACTGGGGCGATGTCCGAG
4
GCGGTCCGCGAGGCGGCCCGGCTCGCCCGGGCGGGGGACACGGTCCTGCTGGC
5
CCCGGCCTGCGCCTCGATGGACATGTTC
B
WhiA
WhiA : PftsW1
WhiA : PftsW2
WhiA : PftsW3
WhiA : PftsW4
WhiA : PftsW5
Relative Intensity
2500
3000
3500
4000
4500
m/z

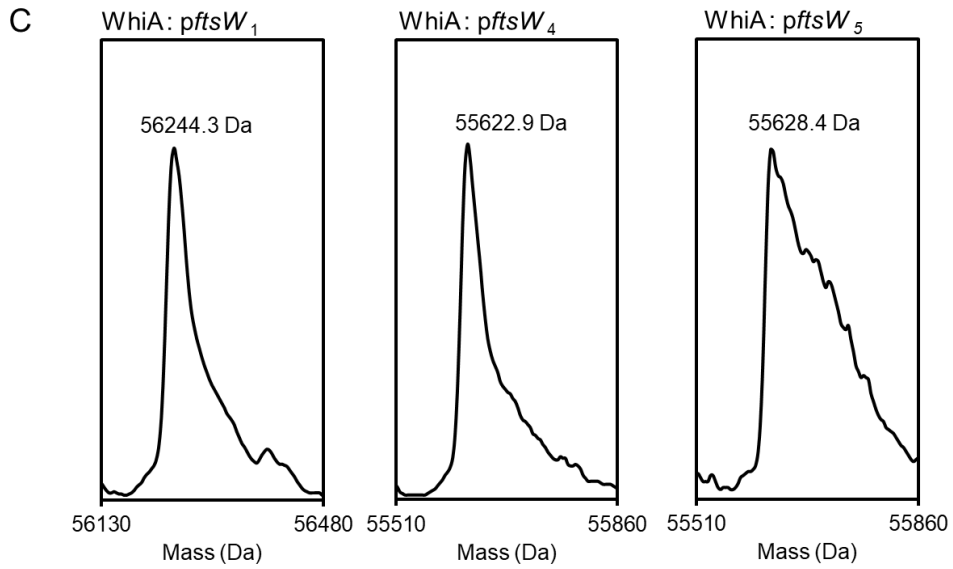

Figure 5.12 *Sv*WhiA binds specifically to DNA containing the GACAC motif.

(A) Sequence of the *ftsW* promoter region. DNA fragments are as indicated: (1) P*ftsW*$_1$, (2) P*ftsW*$_2$, (3) P*ftsW*$_3$, (4) P*ftsW*$_4$ and (5) P*ftsW*$_5$. GACAC motifs are indicated in red. **(B)** m/z spectra of WhiA independently, and in the presence of P*ftsW*$_{1\text{-}5}$, as indicated. Spectra are shown in the range m/z 2,500-4,500. Charge states corresponding to WhiA are highlighted in green. Charge states corresponding to a WhiA: P*ftsW* complex are highlighted in orange. **(C)** Deconvoluted mass spectra of the m/z corresponding to the WhiA: PftsW complexes. Exact masses are labelled. For non-denaturing ESI-MS experiment, WhiA (10 µM) was mixed with P*ftsW* fragments in a 1:1 ratio, in 250 mM ammonium acetate, pH 7.2.

5.4. *S. venezuelae* WhiB interacts directly with DNA

5.4.1. WhiB binds to promoter regions of genes for sporulation

Strikingly, the regulon of WhiB was found to be identical to WhiA. In order to further elucidate how these two proteins function together, the ability of WhiB to directly bind DNA was tested. EMSAs were performed using increasing concentrations of [4Fe-4S] WhiB (38% cluster loading) and incubated with ~2 nM FAM-labelled P*filP* and P*ftsW*. The EMSA observations confirm that WhiB can bind directly to both promoter regions of *ftsW* and *filP.* As observed for WhiA, a considerable amount of DNA remains un-shifted indicating WhiB binds weakly to DNA (Figure 5.13).

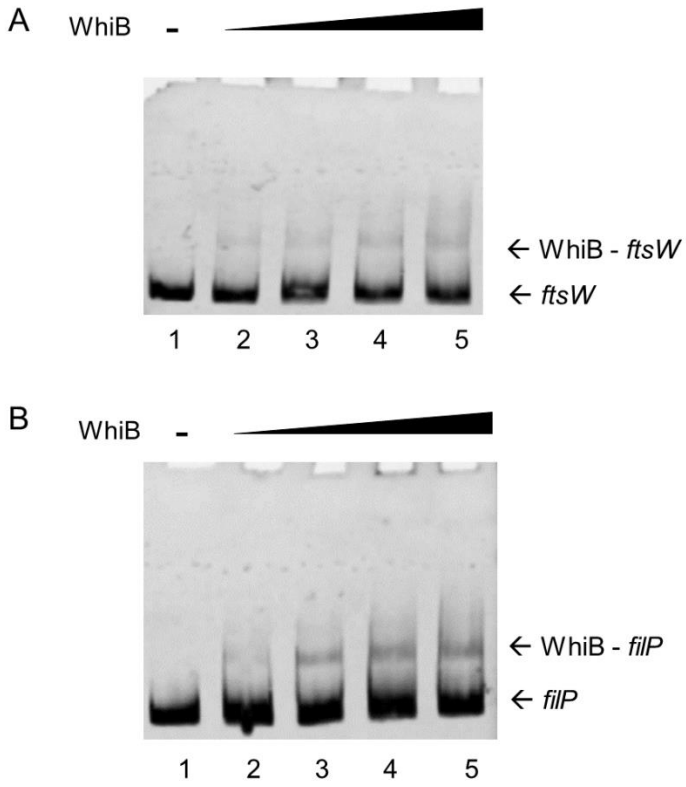

Figure 5.13 DNA binding activity of as isolated *Sv*WhiB.

(A) and **(B)** Fam-labelled P*ftsW* (2.7 nM) and P*filP* (2.9 nM), respectively were incubated with increasing concentrations of holo-WhiB (38% cluster loading). Lane 1: no protein, lanes 2-5 contain 90, 180, 270 and 360 nM WhiB (38 % cluster loading), respectively. Holo-WhiB was stored anaerobically until immediately before incubation with DNA. Separation of WhiB-DNA complexes from free DNA are as indicated.

The necessity of the [4Fe-4S] cluster for DNA binding was then tested. Apo-WhiB was generated by an aerobic overnight dialysis against 50 mM Tris, 300 mM NaCl, pH 7.2, with the addition of 5 mM EDTA. The generation of apo-WhiB was confirmed by UV-visible absorbance spectroscopy as the intensity of the 410 nm [4Fe-4S] peak was reduced to baseline. EMSA experiments were repeated with increasing concentrations of apo-WhiB, in the presence and absence of DTT and ~2 nM FAM-labelled P*filP* and P*ftsW*. This showed that apo-WhiB bound weakly to both promoter regions of *filP* and *ftsW,* specifically in the reduced state (Figure 5.14). Both P*ftsW* and P*filP* required a higher concentration of apo-WhiB to achieve DNA binding when compared to the corresponding EMSA experiments consisting of a mixture of holo- and apo-WhiB. This suggests that both apo-WhiB and [4Fe-4S] WhiB are capable of binding to the *ftsW* and *filP* promoter regions. The stability of WhiB and low cluster incorporation makes exploring the binding capabilities of [4Fe-4S] WhiB independently difficult.

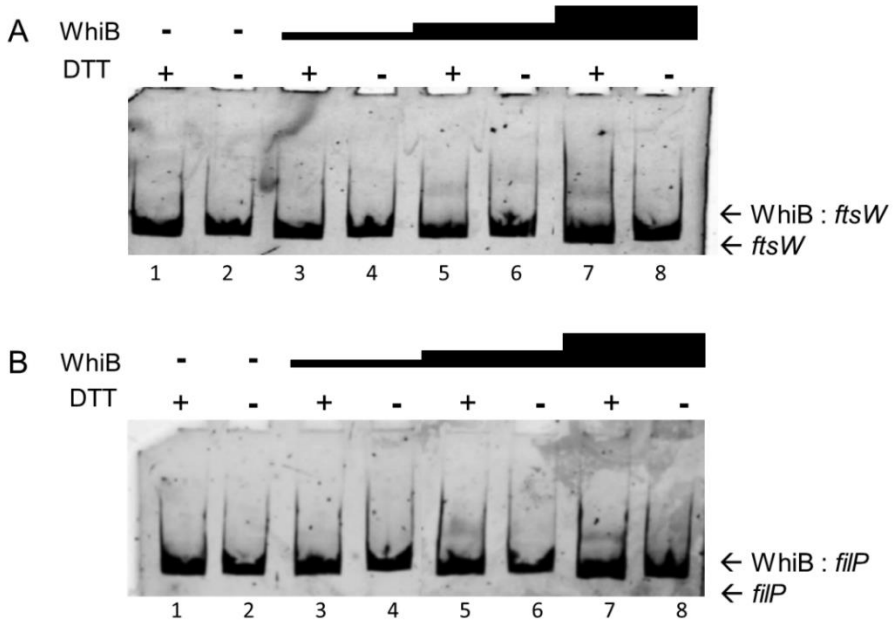

Figure 5.14 DNA binding activity of apo-WhiB.

FAM-labelled probes were incubated with increasing concentrations of apo-WhiB under aerobic conditions in the presence and absence of DTT (5 mM) as labelled. **(A)** Apo-WhiB was incubated with P*ftsW* (2.7 nM) Lanes 1-2: no protein, lanes 3-4, 5-6 and 7-8 contain 107, 214, 427 nM WhiB, respectively. **(B)** Apo-WhiB was incubated with P*filP* (2.9 nM) Lanes 1-2: no protein, lanes 3-4, 5-6 and 7-8 contain 107, 320, 427 nM WhiB, respectively. Separation of WhiB-DNA complexes from free DNA are as indicated.

The specific binding site for apo-WhiB was probed by dividing the length of the 240 bp DNA sequence used for EMSA experiments into 30bp fragments. DNA fragments were staggered by 15 bp, resulting in a total of 16 fragments. 2:1 apo-WhiB : P*ftsW* fragment mixtures were scanned using non-denaturing ESI-MS for additional m/z peaks due to apo-WhiB: P*ftsW* complex formation. Both apo-WhiB and P*ftsW* fragments were desalted into a volatile buffer under reducing conditions (250 mM ammonium acetate, 5 mM DTT, pH 7.2) before injection into the MS. No complex formation was observed for any P*ftsW* fragments. This may be due to the high ratio of WhiB: P*ftsW* required for binding in EMSA experiments, which could not be replicated within the MS experiment conditions.

5.4.2. σ^{HrdB}_4 competes with DNA for [4Fe-4S] WhiB

As described in section 4.3.2, [4Fe-4S] WhiB binds specifically to σ^{HrdB}. Thus, the significance of the σ^{HrdB}_4: WhiB interaction on DNA binding was tested. EMSA experiments were performed using 2.9 nM P*filP*, with [4Fe-4S] WhiB (42% cluster loading), and increasing concentrations of σ^{HrdB}_4, up to 5x molar ratio of σ^{HrdB}_4 to [4Fe-4S] WhiB (Figure 5.15A). Incubation of σ^{HrdB}_4 alone with P*filP* reveals no evidence of DNA binding. Increasing concentration of σ^{HrdB}_4 resulted in the fading of the WhiB: P*filP* band, as shown by densitometry (Figure 5.15B). There was no evidence of a supershifted band corresponding to WhiB: σ^{HrdB}_4 complex formation in conjunction with DNA binding. Thus, σ^{HrdB}_4 likely competes with P*filP* for the pool of [4Fe-4S] WhiB.

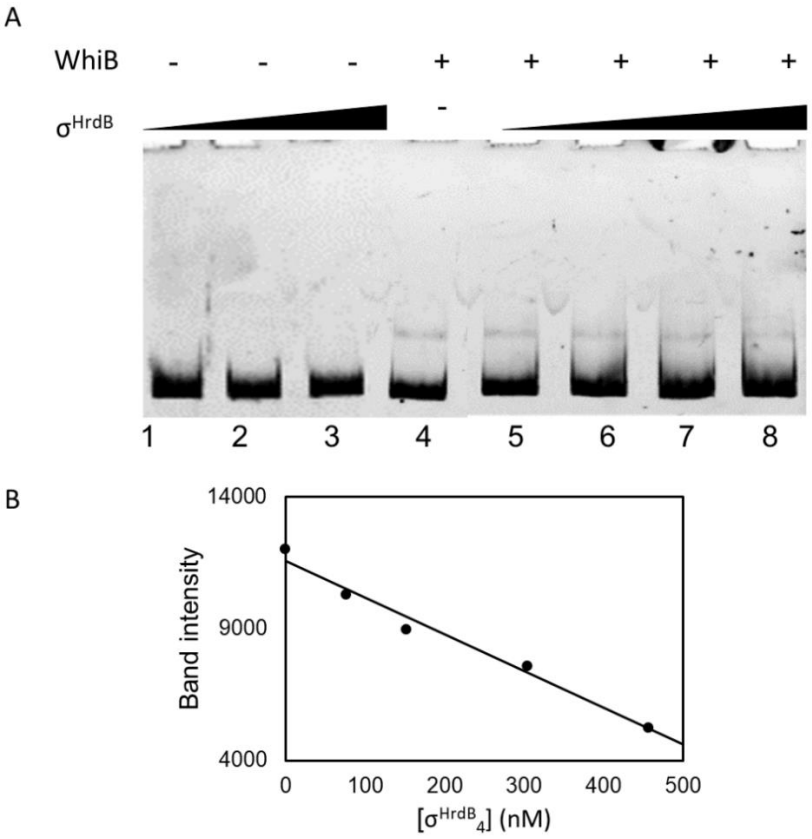

Figure 5.15 The presence of σ^{HrdB}_4 diminishes the DNA binding abilities of WhiB.

(A) FAM-labelled P*filP* (2.9 nM) varying concentrations of σ^{HrdB}_4 and holo-WhiB. Lanes 1-3 contain no holo-WhiB and increasing concentrations of σ^{HrdB}_4 at 152, 304 and 457 nM, respectively. Lanes 4-8 contain 90 nM holo-WhiB (50% cluster loading), with increasing concentrations of σ^{HrdB}_4 at 0, 76, 152, 304 and 457 nM respectively. Holo-WhiB was stored anaerobically until immediately before incubation with DNA. separation of WhiB-DNA complexes from free DNA are as indicated. **(B)** Densitometric analysis of correlation between DNA binding and increasing concentrations of σ^{HrdB}_4 by ImageJ.

5.5. *S. veneuzelae* WhiB stimulates DNA-binding activity of WhiA

The collaborative nature of WhiA and WhiB has been established by *in vivo* studies, with the loss of either protein abolishing the ability the remaining protein to interact with their DNA regulon. Thus, the DNA-binding ability of WhiA with P*ftsW* was tested in the presence of increasing concentrations of [4Fe-4S] WhiB (40% cluster loading). Interestingly, although the concentration of WhiB added was enough to promote WhiB

binding to P*ftsW*, only a single band shift was observed. The degree of shifting was the identical to the shift resultant from WhiA: P*ftsW* in the absence of WhiB (Figure 5.16). There was no additional band present that might corresponding to a WhiB : P*ftsW* complex or a supershifted complex of WhiA: WhiB: P*ftsW*. These observations suggest increasing amounts WhiB enhanced the binding properties of WhiA to P*ftsW*.

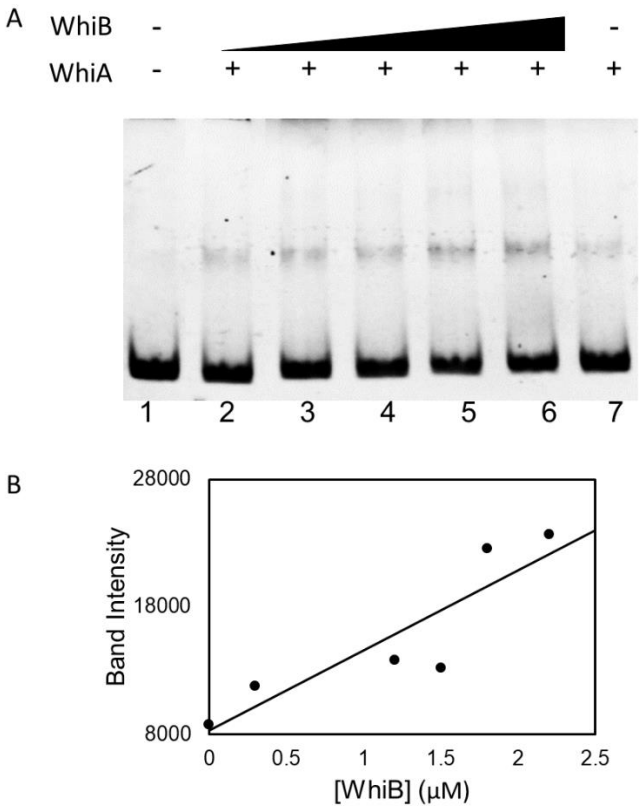

Figure 5.16 *Sv*WhiB stimulates binding of *Sv*WhiA to the *ftsW* promoter region.

(A) P*ftsW* (2.7 nM) was incubated with varying concentrations of WhiA and holo-WhiB. Lane 1 contains no protein. Lanes 2-6 contain 56 nM of WhiA with increasing concentrations of WhiB (34% cluster loading) at 0.3, 1.2, 1.5, 1.8 and 2.2 mM, respectively. Lane 7 contains 56 nM of WhiA with no WhiB. Holo-WhiB was stored anaerobically until immediately before incubation with DNA. Separation of WhiB-DNA complexes from free DNA are as indicated. **(B)** Densitometric analysis of correlation between WhiA: DNA binding and increasing concentrations of WhiB by ImageJ.

5.6. Discussion

Characterisation of *Sv*WhiA and *Sc*WhiA has revealed previously undetected metal binding capabilities. Although no metal binding was observed in the crystal structure obtained from *T. maritima*, it is not uncommon for transcriptional regulators to utilize a metal ion(s) during DNA binding. Indeed, non-denaturing ESI-MS revealed that zinc bound form of *S. venezuelae* WhiA was competent for DNA binding. Fragmentation experiments of *Sv*WhiA showed that the binding site is located within the linker region and C-terminal region of the endonuclease domain; a region with a high number of amino acid residues capable of zinc coordination. Although *Tm*WhiA was not reported to coordinate metal ion(s), *Tm*WhiA and *Sv*WhiA share low sequence similarity. The diverse nature of functions attributed to WhiA orthologues means it is likely that *Sv*WhiA and *Sc*WhiA belong to a specific subset of the WhiA family that has retained some metal binding capabilities typical of LAGLIDADG homing endonucleases [20]. Notably, attempts to remove the coordinated zinc from *Sv*WhiA to produce apo-protein were unsuccessful as SvWhiA was destabilised. Thus, the zinc may provide structural stability. Therefore, as *T. maritima* is a thermophile, *Tm*WhiA is likely to be more stable than those from mesophilic *S. venezuelae* and *S. coelicolor* and may not require the additional stabilisation provided by zinc binding.

EMSA experiments confirmed binding of *Sv*WhiA to promoter regions of both a gene encoding sporulation machinery (*ftsW*) and a gene encoding a protein involved in aerial growth (*filP*), in line with previous *in vivo* ChIP-seq and *in vitro* DNA footprinting studies [5]. Significantly, EMSAs revealed that *Sv*WhiB was also able to directly bind to the same promoter regions. Although the regulon of WhiB was reported to be identical to WhiA, direct interaction between WhiB and DNA was not observed previously [4]. Moreover, the WhiB orthologue in *C. glutamicum*, WhcD, showed no direct binding to the promoter region of *ftsZ* in corresponding EMSA studies [9]. Specifically, apo-WhiB was shown to have DNA binding capabilities only in its reduced form. Unfortunately, studies of the affinity of [4Fe-4S] WhiB for DNA were hampered due to the low cluster incorporation. However, binding was enhanced in the presence of both reduced apo- and holo- WhiB. Moreover, the addition of $\sigma^{HrdB}{}_4$, which interacts with [4Fe-4S] WhiB, competed with

P*filP* for [4Fe-4S] WhiB. Thus, it is possible that [4Fe-4S] WhiB also binds in addition to apo-WhiB. Alternatively, the protective nature of the [4Fe-4S] WhiB: $\sigma^{HrdB}{}_4$ which prevents the formation of apo-WhiB may diminish the pool of available apo-WhiB capable of binding to P*filP*.

The co-dependency of WhiB and WhiA to function as transcriptional regulators was clear from *in vivo* studies in *S. venezuelae*, where the absence of either WhiB or WhiA abolishes the regulatory capability of other protein to initiate sporulation. Furthermore, recent *in vitro* studies of *C. glutamicum* proteins showed direct interaction between the WhiB orthologue WhcD and WhiA [9]. EMSA studies with S*v*WhiA and *Sv*WhiB revealed that in the presence of both WhiA and WhiB, only WhiA: DNA binding was observed but the affinity was enhanced by the presence of WhiB. This assistive effect of WhiB was previously observed for *C. glutamicum* WhcD. Thus, these corresponding observations in *S. venzuelae* promote a common mechanism by which WhiA and WhiB collaboratively exert a regulatory function.

Interestingly, non-denaturing ESI-MS demonstrated the ability of WhiA to bind to three different GACAC sites just within the promoter region of *ftsW.* The capacity to bind such a common sequence motif, and the weak affinity of WhiA for the motif observed in *in vitro* EMSA experiments suggest that WhiA is capable of weak, transient interactions with GACAC sites throughout the *S. venezuelae* genome. As there are ~15,000 copies of the GACAC sequence within the *S. venzuelae* genome, of which only ~250 are identified as part of the WhiA regulon, if indeed WhiA binds untargeted to the GACAC sequence, it follows that direct binding of [4Fe-4S] and/or reduced apo-WhiB to DNA may be the key to targeting WhiA to specific promoter regions of genes involved in the initiation of sporulation [5]. This is in line with previous observations that WhiA expression remains consistent throughout both the vegetative and developmental stages in the *S. venezuelae* lifecycle, and initiation of sporulation septation is likely controlled, at least in part, by the developmentally induced WhiB [11]. An interesting observation from the EMSA studies exploring the cooperativity of WhiA and WhiB was the absence of direct WhiB binding to specific DNA targets. One possible interpretation of this may be that WhiB binds specifically to targeted promoter regions and induces a conformational change in the DNA backbone that could allow for a tighter and more specific interaction

between WhiA and the DNA, which then results in the subsequent dissociation of WhiB from the DNA.

5.7. References

1. Chater, K.F., *A morphological and genetic mapping study of white colony mutants of* Streptomyces coelicolor*.* J Gen Microbiol, 1972. **72**(1): p. 9-28.
2. Ainsa, J.A., et al., *WhiA, a protein of unknown function conserved among gram-positive bacteria, is essential for sporulation in* Streptomyces coelicolor *A3(2).* J Bacteriol, 2000. **182**(19): p. 5470-8.
3. Soliveri, J.A., et al., *Multiple paralogous genes related to the Streptomyces coelicolor developmental regulatory gene* whiB *are present in* Streptomyces *and other actinomycetes.* Microbiology, 2000. **146 (Pt 2)**: p. 333-343.
4. Bush, M.J., et al., *Genes required for aerial growth, cell division, and chromosome segregation are targets of WhiA before sporulation in* Streptomyces venezuelae*.* mBio, 2013. **4**(5): p. e00684-13.
5. Bush, M.J., et al., *Genome-wide chromatin immunoprecipitation sequencing analysis shows that WhiB Is a transcription factor that cocontrols its regulon with WhiA to initiate developmental cell division in* Streptomyces*.* mBio, 2016. **7**(2): p. e00523-16.
6. DeJesus, M.A., et al., *Comprehensive essentiality analysis of the* Mycobacterium tuberculosis *genome via saturating transposon mutagenesis.* mBio, 2017. **8**(1).
7. Bush, M.J., *The actinobacterial WhiB-like (Wbl) family of transcription factors.* Mol Microbiol, 2018. **110**(5): p. 663-676.
8. Lee, D.S., Y. Kim, and H.S. Lee, *The* whcD *gene of* Corynebacterium glutamicum *plays roles in cell division and envelope formation.* Microbiology, 2017. **163**(2): p. 131-143.
9. Lee, D.S., et al., Corynebacterium glutamicum *WhcD interacts with WhiA to exert a regulatory effect on cell division genes.* Antonie Van Leeuwenhoek, 2018. **111**(5): p. 641-648.
10. Kaiser, B.K. and B.L. Stoddard, *DNA recognition and transcriptional regulation by the WhiA sporulation factor.* Sci Rep, 2011. **1**: p. 156.
11. Bush, M.J., et al., *Multi-layered inhibition of Streptomyces development: BldO is a dedicated repressor of whiB.* Mol Microbiol, 2017. **104**(5): p. 700-711.
12. Kaiser, B.K., et al., *The structure of a bacterial DUF199/WhiA protein: domestication of an invasive endonuclease.* Structure, 2009. **17**(10): p. 1368-76.
13. Bohorquez, L.C., et al., *The Conserved DNA Binding Protein WhiA Influences Chromosome Segregation in* Bacillus subtilis*.* J Bacteriol, 2018. **200**(8).
14. Burt, A. and V. Koufopanou, *Homing endonuclease genes: the rise and fall and rise again of a selfish element.* Curr Opin Genet Dev, 2004. **14**(6): p. 609-15.
15. Knizewski, L. and K. Ginalski, *Bacterial DUF199/COG1481 proteins including sporulation regulator WhiA are distant homologs of LAGLIDADG homing endonucleases that retained only DNA binding.* Cell Cycle, 2007. **6**(13): p. 1666-70.
16. Paget, M.S. and J.D. Helmann, *The sigma70 family of sigma factors.* Genome Biol, 2003. **4**(1): p. 203.
17. Geoghegan, K.F., et al., *Spontaneous alpha-N-6-phosphogluconoylation of a "His tag" in Escherichia coli: the cause of extra mass of 258 or 178 Da in fusion proteins.* Anal Biochem, 1999. **267**(1): p. 169-84.
18. Crack, J.C., et al., *Characterization of [4Fe-4S]-containing and cluster-free forms of* Streptomyces *WhiD.* Biochemistry, 2009. **48**(51): p. 12252-64.
19. McCall, K.A., C. Huang, and C.A. Fierke, *Function and mechanism of zinc metalloenzymes.* J Nutr, 2000. **130**(5S Suppl): p. 1437S-46S.
20. Belfort, M. and R.P. Bonocora, *Homing endonucleases: from genetic anomalies to programmable genomic clippers.* Methods Mol Biol, 2014. **1123**: p. 1-26.

Chapter 6. Studies of the iron-sulfur cluster protein RirA, a global regulator of iron metabolism

6.1 Introduction

Iron is required for virtually all forms of life and is involved in many major biological processes, including photosynthesis, N_2 fixation, respiration, gene regulation and DNA biosynthesis [1]. It is an extremely versatile prosthetic component in iron containing metalloproteins, where it primarily functions catalytically, or as an electron carrier [1]. Under physiological conditions, iron exists primarily in one of two readily convertible redox states: ferrous (Fe^{2+}) and ferric (Fe^{3+}). In both forms, iron can also adopt high or low spin states depending upon its ligand environment [1]. The introduction of oxygen into the Earth's atmosphere has challenged organisms to acquire iron in the ferric (Fe^{3+}) state, which in an aqueous environment is extremely insoluble. Furthermore, and under aerobic conditions, ferrous iron can also be extremely toxic as it potentiates oxygen toxicity by promoting the production of damaging reactive oxygen species (via the Fenton reaction) [2]. Thus, effective iron uptake and iron homeostasis is crucial. The ferric uptake regulator (Fur) protein is a global iron regulator. It was initially identified in *E. coli*, but is found in many bacteria [3]. Fur functions by the directly binding Fe^{2+}; Fe^{2+}-bound Fur acts as a transcriptional regulator and binds to "Fur" box operator sequences within target promoters, thus repressing genes encoding proteins involved in the iron-uptake machinery [4]. The diphtheria toxin repressor (DtxR) represents another class of Fe-dependent regulators which can undertake Fur-like roles in some Gram-positive bacteria [5]. Although Fur and DtxR proteins have no sequence similarities, they have structural and mechanistic similarities [6].

RirA is an alternative global iron regulator, found in *Rhizobium* species and related α-proteobacteria. It represents a novel class of iron regulators as it shows no sequence similarity to previously characterised iron regulatory protein families. Instead, RirA is a member of the Rrf2 superfamily of transcriptional regulators, which include NsrR (a nitric oxide responsive regulator) and IscR (a regulator of FeS biogenesis) [7, 8]. Much

like NsrR and IscR, RirA is a homo-dimeric iron-sulfur (Fe-S) protein [9]. RirA senses iron in a different way than those previously characterised in Fur/DtxR iron sensing regulators. Therefore, there is much current interest in understanding the mechanism by which RirA acts as an iron sensor via its [4Fe-4S] cluster.

Previous studies using absorption and CD spectroscopy showed that, under iron limited conditions, [4Fe-4S] RirA undergoes cluster conversion to a [2Fe-2S] cluster form, which eventually degrades to apo-RirA upon prolonged exposure to low iron conditions [9]. EPR spectroscopy revealed that the conversion involves the formation of a transiently stable $[3Fe\text{-}4S]^{1+}$ [9]. However, spectroscopic approaches could not identify any other specific degradation cluster species, which are EPR silent and indistinguishable by UV-visible absorbance spectroscopy, and indeed other spectroscopic methods.

Recently, non-denaturing ESI-MS was employed to both identify the cluster conversion intermediates, and to elucidate the series of molecular events involved in the conversion of [4Fe-4S] RirA cluster in response to low iron, under aerobic and anaerobic conditions. This was possible due to the time resolved nature of non-denaturing ESI-MS experiments, which allowed for the kinetic analysis of the RirA cluster conversion intermediates. MS data was obtained by Dr Maria Teresa Pellicer Martinez (University of East Anglia, Norwich) and Dr Jason Crack (University of East Anglia, Norwich).

Although ESI-TOF-MS is a very sensitive experimental technique, capable of delivering exact masses to within 1 Da, it is possible to mis-assign mass peaks due to different species having the same mass. For example, a ^{32}S would have the same mass as an adduct with 2 x ^{16}O. Therefore, ^{34}S labelling was required for unambiguous assignment of cluster bound forms of RirA, obtained from the +2 Da shifts observed in ^{34}S-isotope substituted protein compared to natural (predominantly ^{32}S) protein [10]. This chapter describes supporting data for the identification of intermediates in the [4Fe-4S] RirA cluster degradation reaction, including UV-visible absorbance and ^{34}S substitution time-resolved non-denaturing ESI-MS experiments.

Kinetic analysis of the non-denaturing ESI-MS data for the RirA cluster conversion/degradation suggested an iron sensing mechanism of [4Fe-4S] RirA based on the cluster existing in an $[4Fe\text{-}4S]^{2+} \leftrightarrow [3Fe\text{–}4S]^{0} + Fe^{2+}$ equilibrium. Under iron replete

conditions, the $[4Fe\text{-}4S]^{2+}$ cluster form is favoured, whilst under iron depleted conditions, an unstable $[3Fe\text{-}4S]^{0}$ cluster is favoured, which subsequently undergoes cluster degradation, ultimately resulting in apo-RirA [11]. The $[3Fe\text{-}4S]^{0}$ intermediate was found through electron paramagnetic resonance (EPR) studies to be susceptible to oxidation in the presence of O_2, resulting in a $[3Fe\text{-}4S]^{1+}$ form that exhibited an enhanced rate of degradation. The susceptibility of the [3Fe-4S] intermediate to oxidation provides the molecular basis for O_2-sensing by RirA. This chapter also details thermodynamic studies of the dissociation of the first iron from the $[4Fe\text{-}4S]^{2+}$ cluster, which provide key information to support the labile iron sensing mechanism.

Finally, *R. leguminosarum* RirA features 3 Cys residues which are conserved amongst some of the larger Rrf2 family, including NsrR and IscR. Substitutions of these Cys residues have been shown to abolish the regulatory activity of RirA in *A. tumefaciens* [12].However, the identity, or indeed the existence, of a fourth ligand to the RirA cluster is unknown. In *E. coli* IscR, the [2Fe-2S] cluster is coordinated by three conserved Cys ligands, and a fourth, His ligand (His106). In *S. coelicolor* [4Fe–4S] NsrR, the fourth ligand is an Asp residue (Asp8), but neither of these residues are conserved in RirA [13, 14]. This chapter details mutagenesis studies that explore the coordination of the [4Fe-4S] RirA cluster.

6.2. Characterisation of [4Fe-4S] RirA degradation using non-denaturing ESI-MS

6.2.1. Time-dependent UV-visible absorbance spectroscopy of the RirA cluster conversion, under non-denaturing ESI-MS conditions

Kinetic data previously derived from UV-visible spectroscopy showed that [4Fe-4S] RirA undergoes cluster degradation under iron-depleted, anaerobic conditions over a period of several hours. In these experiments, ethylenediaminetetraacetic acid (EDTA) (Figure 4.1) was used to mimic low iron conditions by providing a thermodynamic sink for the iron. However, in equivalent experiments performed using non-denaturing ESI-MS, cluster degradation occurred within 30 minutes [9].The substantial difference in decay rates are likely due to the different buffer conditions between the two experiments;

Spectroscopic studies were performed with samples in 25 mM HEPES, 2.5 mM $CaCl_2$, 50 mM NaCl, 750 mM KCl, pH 7.5, whilst the non-denaturing ESI-MS was performed in 250 mM ammonium acetate, pH 7.5. Therefore, to confirm that spectroscopic and mass spectrometric experiments were reporting on the same process, cluster degradation under iron-depleted conditions was monitored using UV-visible absorbance, under the same conditions as those used for non-denaturing ESI-MS.

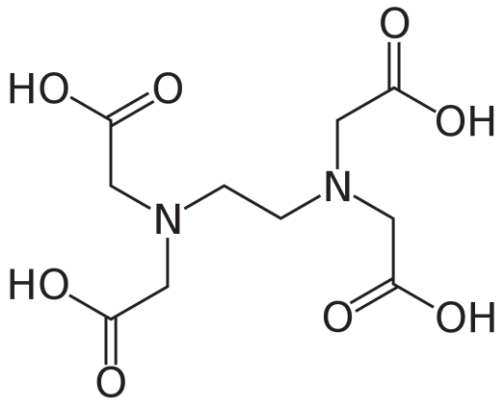

Figure 6.1 Structure of ethylenediaminetetraacetic acid.

[4Fe-4S] RirA was buffer exchanged into 250 mM ammonium acetate, pH 7.3. RirA cluster degradation was monitoring via $A_{382\ nm}$, over 30 minutes, at 37 °C. After 30 minutes, the spectra showed an overall decrease in absorbance intensity, with changes in spectral features at 330 nm and 382 nm that are characteristic of a [2Fe-4S] cluster (Figure 6.2A). Spectral changes at 382 nm were plotted against time, which showed that the cluster conversion was largely complete within 30 minutes (Figure 6.2B). The decay fitted well to a bi-exponential function consisting of an initial rapid phase, followed by a slower phase that corresponds to further decay of the cluster. Although the specific cluster conversion species in these spectroscopic studies could not be identified by absorbance data alone, the rate constant for the initial phase, k = 0.34 min^{-1}, agrees very well with the reported rate constant for the [4Fe-4S] to [3Fe-4S] conversion derived from the ESI-MS kinetic data (k = 0.30 min^{-1}) [11]. Equivalent measurements were performed under aerobic conditions. Spectral changes were again plotted against time. In contrast to anaerobic experiments, the decay fitted well to a single exponential function however the rate constant was k=0.34 min^{-1}, again in agreement with the rate constant for the [4Fe-4S] to [3Fe-4S] conversion under aerobic conditions, derived from ESI-MS kinetic data (k = 0.30 min^{-1}). Thus, these data confirm that UV-visible absorption spectroscopy likely reports upon the same process as the non-denaturing ESI-MS experiments. The previously observed difference in kinetics is most probably due to the different buffer conditions, with [4Fe-4S] RirA being significantly more labile in the ammonium acetate buffer.

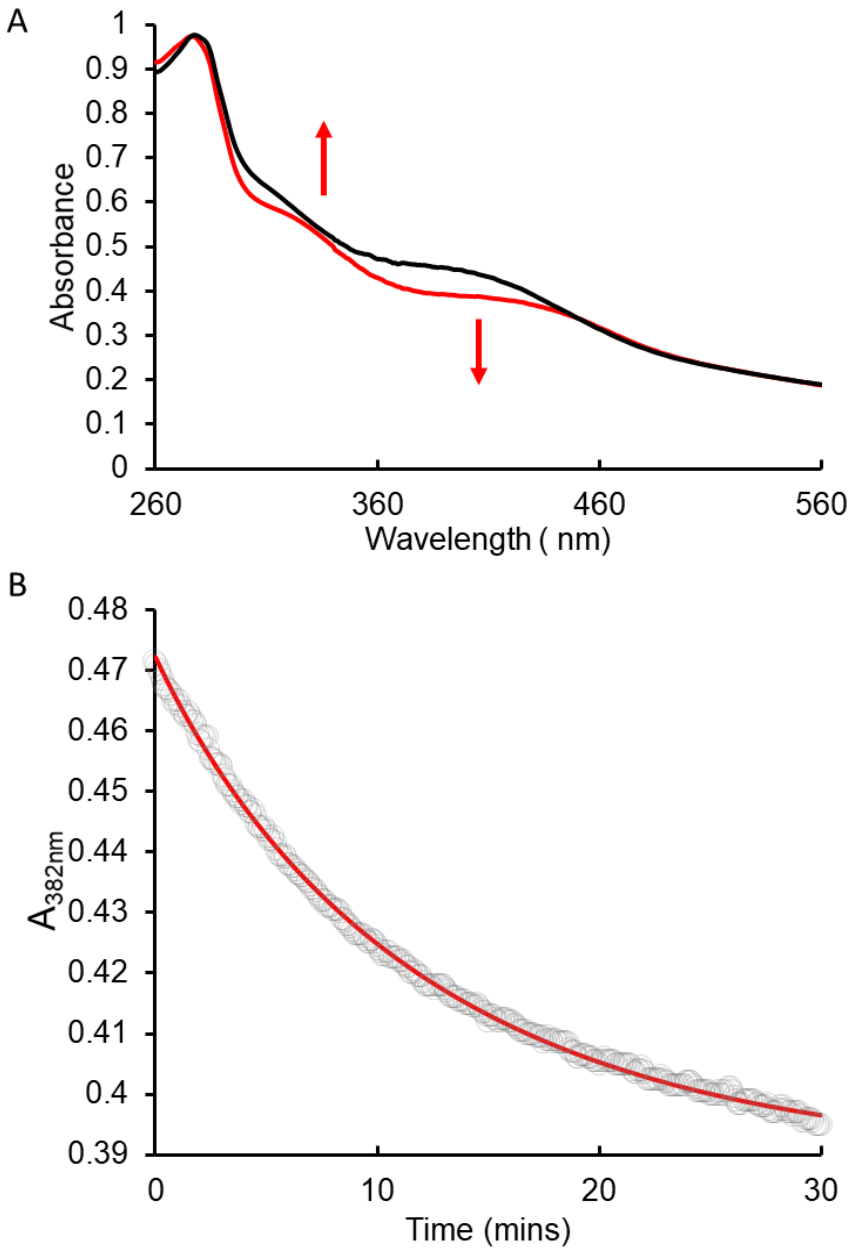

Figure 6.2 Degradation of [4Fe-4S] RirA under anaerobic, iron-depleted conditions.

(A) UV-visible absorbance spectra of [4Fe-4S] RirA (30 µM in cluster) before (black) and 30 minutes following addition of 250 µM EDTA. Arrows indicate direction of spectral changes at 330 nm and 382 nm. **(B)** Plot of $A_{382\ nm}$ versus time following addition of 250 µM EDTA in 250 mM ammonium acetate, pH 7.3, plot of at 37° C. The red line indicates a fit of the data generated using a double exponential function.

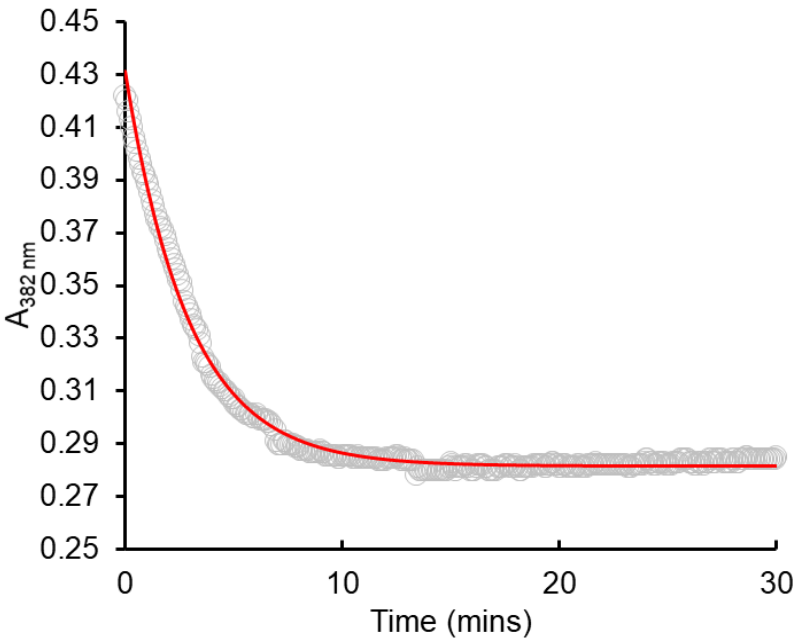

Figure 6.3 Degradation of [4Fe-4S] RirA under aerobic, iron-depleted conditions.

Plot of $A_{382\ nm}$ versus time following addition of 250 µM EDTA, 228 µM O_2 and to 500 µM glutathione (GSH) to RirA (32 µM) in 250 mM ammonium acetate, pH 7.3. For aerobic absorbance experiments GSH was added to the sample to help solubilise oxidised sulfur species that otherwise caused significant scattering of light. The red line indicates a fit of the data generated using a single exponential function.

6.2.2. Identification of degradation products using ^{34}S substitution

Although RirA is dimeric in solution, a significant amount of the protein monomerizes during the ionization step in non-denaturing ESI-MS conditions. This is commonly observed for other dimeric Fe-S proteins, such as NsrR and FNR [9, 15, 16]. Fortunately, monomerization allowed for the characterisation of RirA cluster degradation products, without the complications of working with a dimeric protein.

^{34}S labelling of cluster sulfides (but not coordinating Cys residues) was achieved using the techniques described in section 2.3.2. Time resolved ESI-MS under non-denaturing conditions was repeated with ^{34}S-substituted RirA, under low iron, anaerobic conditions. As previously, m/z data were averaged over 2 minutes and deconvoluted. Over a 30

minute time course, cluster-bound forms of RirA, including [4Fe-3S], [3Fe-4S], [3Fe-3S], [3Fe-2S], [3Fe-S], [2Fe-2S] and [2Fe-S], were observed to undergo an initial increase as the [4Fe-4S] mass peak decayed. These intermediate cluster species subsequently also decayed away, resulting in apo-RirA as the major species remaining.

The m/z data from 2-4 minutes were averaged and deconvoluted for both ^{34}S-substituted RirA and natural abundance (predominantly ^{32}S) form of [4Fe-4S] RirA for comparison. The latter data were provided by Dr Jason Crack. The natural abundance form of [4Fe-4S] RirA in the deconvoluted mass spectrum was at 17,792 Da. As expected, this shifted by + 8 Da to 17,800 Da in the ^{34}S-substituted [4Fe-4S] RirA spectrum. Equally, intermediate cluster species were shifted by + 2 Da per sulfide, which confirms the identification of each cluster form. The apo-RirA peak remained unshifted at 17,442 Da, as expected. Clear shifts of peaks in the spectra could be seen in overlays of ^{32}S and ^{34}S data (Figure 6.4A to H). As the apo-RirA intensity increases, some adducts arose attached to apo-RirA at +16, +32 and +64 Da. It was previously un-clear whether these are oxygen or sulfur adducts. The ^{34}S-substituted sample revealed that +16 and +32 Da adducts were not shifted, indicating these are due to one and two oxygen adducts, respectively. The +64 adduct was shifted by + 4 Da, indicating this adduct was due to two sulfurs, likely a result of the oxidation of cluster sulfides, which generates sulfane that can be incorporated into Cys-thiol side chains (Figure 6.4I). The observed masses for ^{32}S RirA and ^{34}S RirA mass shifts are summarised in Table 6.1.

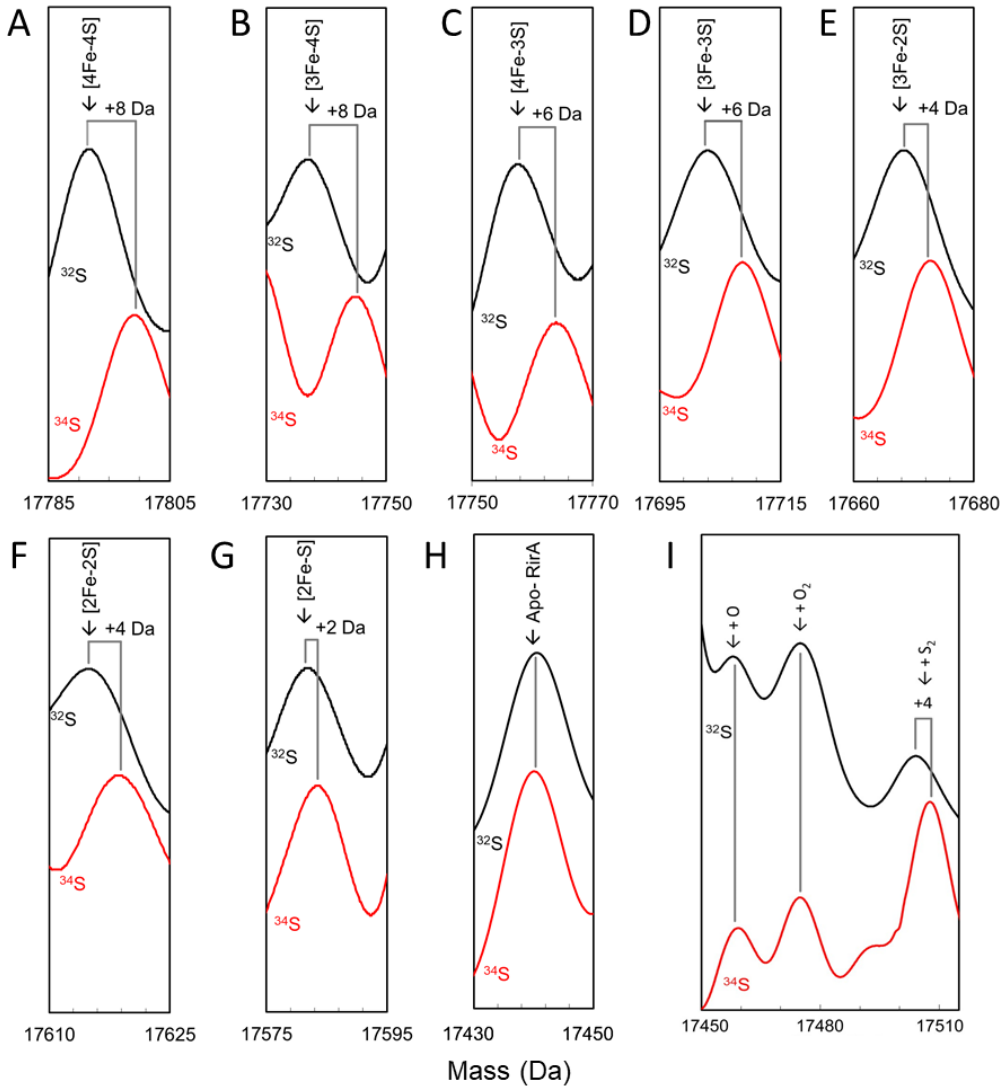

Figure 6.4 Mass shifts observed for the RirA [4Fe-4S] cluster, conversion intermediates and cluster products upon ^{34}S substitution of cluster sulfides.

Deconvoluted mass spectra of natural abundance sulfur (black) and equivalent ^{34}S-substituted (red) [4Fe-4S] RirA and cluster conversion intermediates. Spectra were recorded at 2 minutes following addition of EDTA for both experiments. (A-G) show mass peaks of RirA [4Fe-4S], [3Fe-4S], [4Fe-3S], [3Fe-3S], [3Fe-2S], [2Fe-2S], and [2Fe-S] clusters, respectively. Predicted mass shifts for the assigned species are indicated. (H) shows peaks for resultant apo-RirA, with no mass shift between the two samples observed. (I) assignment of apo-RirA adduct species are indicated. +16 and +32 Da adducts are not shifted, indicating these are most likely oxygen adducts. The +64 Da adduct is shifted by +4 Da, suggesting this is a double sulfur adduct.

Table 6.1 Observed masses for cluster bound species of monomeric RirA, and 34S isotope shifts.

RirA species	^{32}S RirA observed mass (Da)	^{34}S Isotope shift (Da)
[4Fe-4S]$^{2+}$	17,792	+8
[3Fe-4S]$^{1+}$	17,736	+8
[4Fe-3S]$^{4+}$	17,758	+6
[3Fe-3S]$^{3+}$	17,703	+6
[3Fe-2S]$^{5+}$	17,668	+4
[2Fe-2S]$^{2+}$	17,615	+4
[2Fe-S]$^{4+}$	17,582	+2
Apo-	17,441	0

6.3. Characterisation of labile Fe in [4Fe-4S] RirA

6.3.2. [4Fe-4S] RirA spontaneously breaks down to apo-RirA upon the removal of 1 iron per cluster

RirA is proposed to exist in an $[4Fe\text{-}4S]^{2+} \rightleftharpoons [3Fe\text{-}4S]^{\mathbf{0}} + Fe^{2+}$ equilibrium, which is key for iron-sensing. Under low iron conditions, the unstable $[3Fe\text{-}4S]^{0}$ RirA is favoured, which then undergoes spontaneous degradation to form apo-RirA. In order to confirm that the [3Fe-4S] intermediate is unstable and undergoes spontaneous degradation to form apo-RirA, sufficient EDTA was added to RirA to chelate only 1 Fe per cluster. The 1:1 RirA: EDTA sample was incubated at room temperature and spectra taken at standard time intervals. Over the course of 3 hours, the RirA spectra showed a decrease in the [4Fe-4S] peak at 382 nm, but a redshift of the 382 nm band, which is characteristic of the formation of [2Fe-2S] cluster, was not observed. Overnight incubation resulted in further loss of the 382 nm band to near baseline, representing largely apo-RirA (Figure 6.5). This suggested that, upon the loss of 1 Fe per cluster to form the [3Fe-4S] intermediate, the RirA cluster spontaneously undergoes further degradation leading to complete cluster loss.

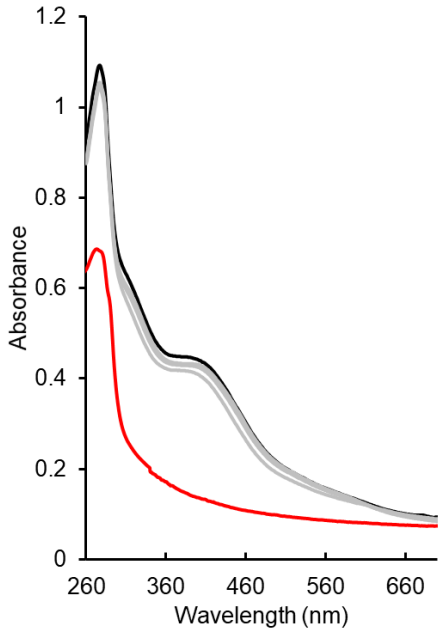

Figure 6.5 Spontaneous breakdown of [4Fe-4S] RirA upon removal of first iron.

UV-visible absorbance spectra of [4Fe-4S] RirA upon exposure to equimolar EDTA over 2 hours. Starting spectrum is in black, grey spectra are taken at ~20 minute intervals. Spectrum following overnight incubation with 1:1 EDTA: RirA is in red. [4Fe-4S] RirA sample (33 µM in cluster) was prepared in 25 mM HEPES, 50 mM NaCl, 750 mM KCl, pH 7.5, 1 cm pathlength anaerobic quartz cuvette.

6.3.3. K_d for the fourth iron binding to the cluster

To support the mechanism proposed for iron sensing in RirA, in which dissociation of the fourth iron constitutes the key sensing step, the K_d was determined for this labile iron. In order to do this, the dissociation of the labile iron must be kinetically separated from the remaining the cluster conversion. The iron chelator EDTA could not be used for these experiments because it binds Fe^{2+} tightly and is capable of chelating more than one (i.e. the first) iron per cluster. Furthermore, it does not form a coloured complex and so is not useful for simple competition binding experiments of the type envisaged here.

Mag-fura-2 is a divalent metal chelator that binds Fe^{2+} to form a 1:1 complex with a K_d of 2.05 µM and has been used previously to probe protein Fe^{2+}-binding [17]. A particularly useful feature of this chelator is that its absorbance spectrum exhibits a shift of its principal absorbance from 366 nm in the apo-form to 325 nm in the Fe^{2+}-bound form, providing a direct measure of the proportion of the chelator that is in the bound state. An Fe^{2+}-binding competition assay was set up using mag-fura-2 to determine the dissociation constant (K_d) for Fe^{2+} binding to [3Fe-4S] RirA. Mag-fura-2 was prepared according to section 2.3.4. Titrations of ~7 µM [4Fe-4S] RirA in 25 mM HEPES, 50 mM NaCl, 750 mM KCl, pH 7.5 with mag-fura-2 were carried out under anaerobic conditions at room temperature. The titration showed that, for each experiment, the concentration Fe^{2+}-magfura-2 formed at the end of the titration corresponded to ~1 iron per [4Fe-4S] cluster. This indicated that the first Fe^{2+} dissociation from [4Fe-4S] to [3Fe-4S] was an independent step as no further cluster degradation was observed within an hour of mixing the protein and chelator. However, overnight incubation of RirA with mag-fura-2 did lead to cluster breakdown and increased the coordination of Fe^{2+} to mag-fura-2. Thus, all titrations were completed within ~60 minutes to kinetically isolate the dissociation of the first Fe^{2+} from [4Fe-4S], from the resultant breakdown of the remaining cluster.

The UV-visible absorbance shift spectra of metal-bound mag-fura-2 and apo-mag-fura-2 overlaps with that of the RirA cluster, with the result that interpretation of the raw spectra is difficult. Furthermore, the absorbance changes due to the loss of a single Fe^{2+} further complicates interpretation. Fortunately, the absorbance profiles of apo- and

metal-bound mag-fura-2 overlap with an isosbestic point of 345 nm, which provided a means to correct for any underlying absorbance changes due to the RirA cluster conversion [17]. Firstly, the spectrum due to initial [4Fe-4S] cluster was subtracted from each subsequent spectrum. Then the data were normalised so that the resulting nest of spectra reported on the changing proportions of Fe^{2+}-bound and apo-mag-fura-2. Finally, spectra were corrected for any changes in the subtracted cluster spectrum using a scaling factor that preserved the isosbestic point. Spectra of mag-fura-2 in apo and Fe^{2+} forms (in the absence of RirA) were used to assist with this (Figure 6.6A). Changes due to the scaling factor were <0.07 AU, within the range expected for the absorbance change during cluster conversion. From this, the percentage of maximum Fe^{2+}-mag-fura-2 complex present (where 100% equated to the concentration of [4Fe-4S] RirA, i.e. one Fe^{2+} per cluster) was plotted as a function of free mag-fura-2. This resulted in a plot with a hyperbolic form, which was fitted with an equation describing a simple binding isotherm using Origin8 (OriginLabs) (Figure 6.6B). This yielded an apparent competition dissociation constant (n=3), from which the K_d for RirA was determined as 3.16 ± 0.12 µM, using the expression:

$$K_{d(MF2\ app)} = K_{d(MF2)}\left(1 + \frac{[RirA]}{K_{d(RirA)}}\right) \qquad \textbf{Equation 6.1}$$

Where $K_{d(MF2\ app)}$ is the determined apparent K_d from the competition binding assay, $K_{d(MF2)}$ is the K_d for mag-fura-2 binding to Fe^{2+}, (previously determined as K_d = 2.05 µM [17]) and $K_{d(RirA)}$ is the K_d for [3Fe-4S] binding to Fe^{2+} [18]. The resulting K_d and standard error was determined from three equivalent titration experiments.

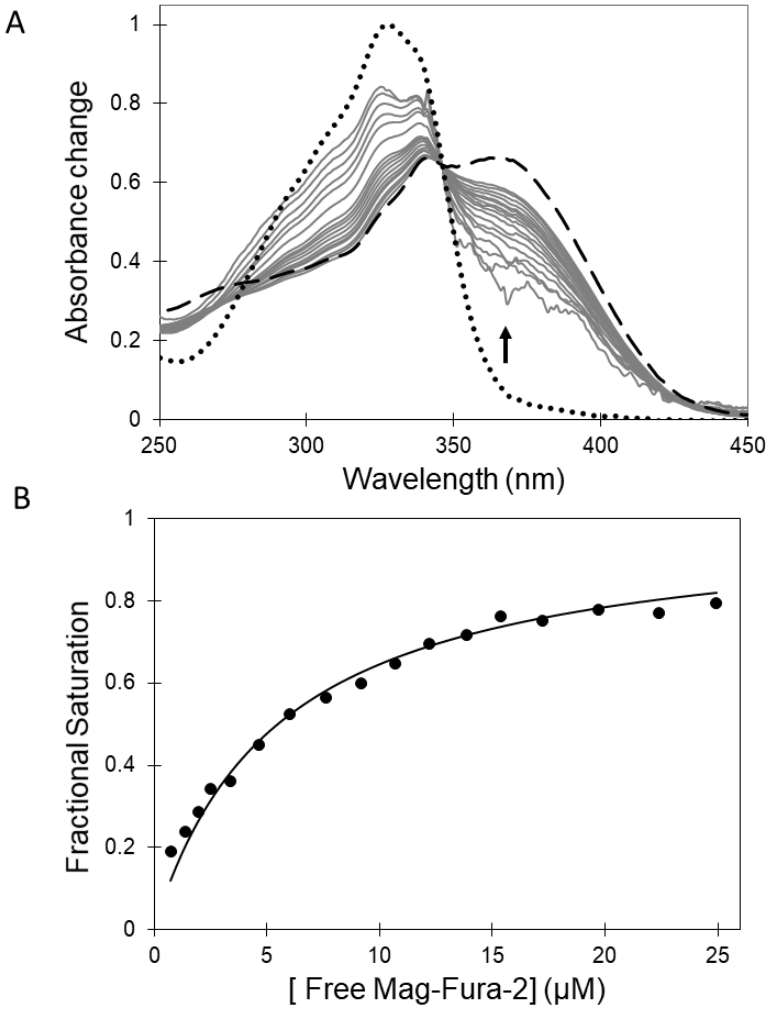

Figure 6.6 Determination of the binding affinity of the fourth iron of the RirA [4Fe-4S] cluster.

(**A**) Normalised UV-visible absorbance spectra showing the ratio of apo- and Fe^{2+}-bound mag-fura-2 upon addition of increasing concentrations of mag-fura-2 to [4Fe-4S] RirA (7 μM), in 25 mM HEPES, 50 mM NaCl, 750 mM KCl, pH 7.5. In addition to the titration spectra (solid grey lines), spectra of fully apo- (dashed line) and Fe^{2+}-bound (dotted line) forms of mag-fura-2 are shown. Arrow denote the direction of absorbance change upon increasing concentration of mag-fura-2. (**B**) Plot of extent of Fe^{2+}-mag-fura-2 complex formation (determined from data at 366 nm and expressed as fractional saturation, where one equals one Fe^{2+} per initial [4Fe-4S] cluster) as a function of concentration of free mag-fura-2. The data were fitted using a simple binding isotherm, giving an apparent K_d, which reflects the competition between mag-fura-2 and RirA for iron. From this, the K_d for binding of the fourth iron to the RirA cluster was determined as ~3 μM.

6.4. Characterising N8C and N8D RirA variants

6.4.1. N8D and N8C RirA variants have significantly different cluster environments

R. leguminosarum RirA features 3 Cys residues which are conserved amongst the larger Rrf2 family. The identity, or indeed the existence, of a fourth ligand is unknown. If a fourth protein ligand does not exist for RirA, it may be possible to engineer in an artificial ligand to stabilise the fragile RirA cluster. NsrR is a well characterised member of the Rrf2 family. Like RirA, NsrR homologues also coordinate a [4Fe-4S] cluster. In *S. coelicolor* NsrR, the fourth ligand to the [4Fe-4S] cluster is an Asp residue (from the other monomer of the NsrR dimer). The corresponding residue in RirA is an Asn residue. Due to sequence similarities between the two proteins, a plasmid encoding a N8D variant of RirA was generated to test the possibility of generating an NsrR-type coordination for the cluster. In addition, a second plasmid, encoding a N8C variant was also generated, in order to determine if a conventional all Cys ligand cluster coordination might be achievable.

CD spectroscopy of both variants in their as isolated forms revealed substantially different spectra when compared to the wild type RirA spectrum, indicating the cluster environment is different in the variants. In particular, the spectrum of the N8D variant now closely resembles the spectrum of NsrR (Figure 6.7A). Furthermore, wild type RirA has a wavelength maximum for the cluster at 382 nm, which is unusual for a [4Fe-4S] cluster, in that it is below 400 nm. Although the N8C variant had the same UV absorption profile as wild type RirA, the absorption spectrum for N8D RirA had a maximum cluster peak at 410 nm (Figure 6.7B). This is more conventional for a [4Fe-4S] cluster and closely resembles the broad absorbance band of NsrR, which has a reported maximum cluster peak at 406 nm [19].

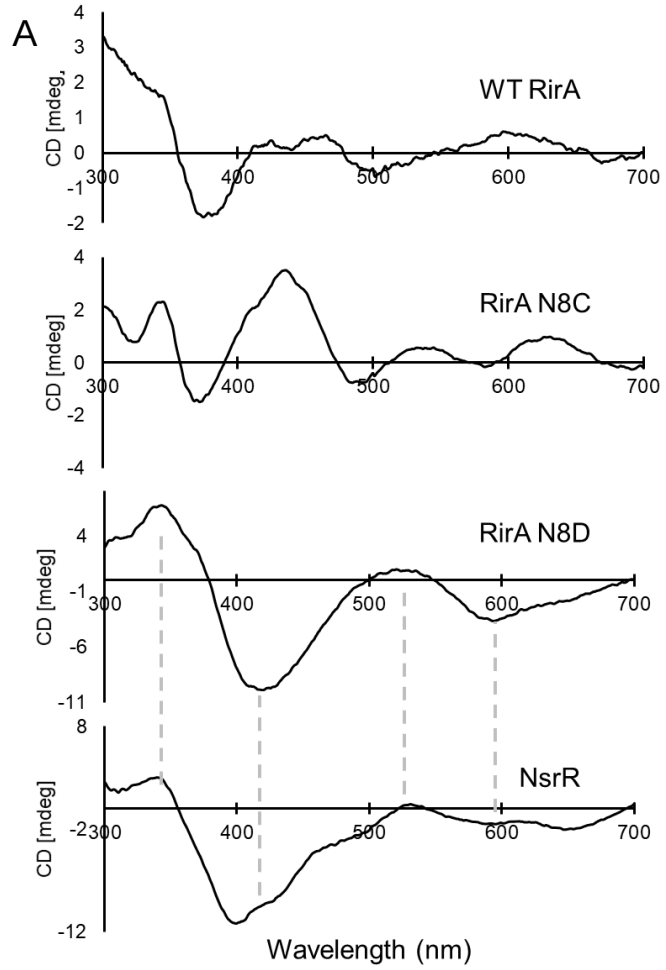
A
WT RirA
RirA N8C
RirA N8D
NsrR
CD [mdeg]
Wavelength (nm)

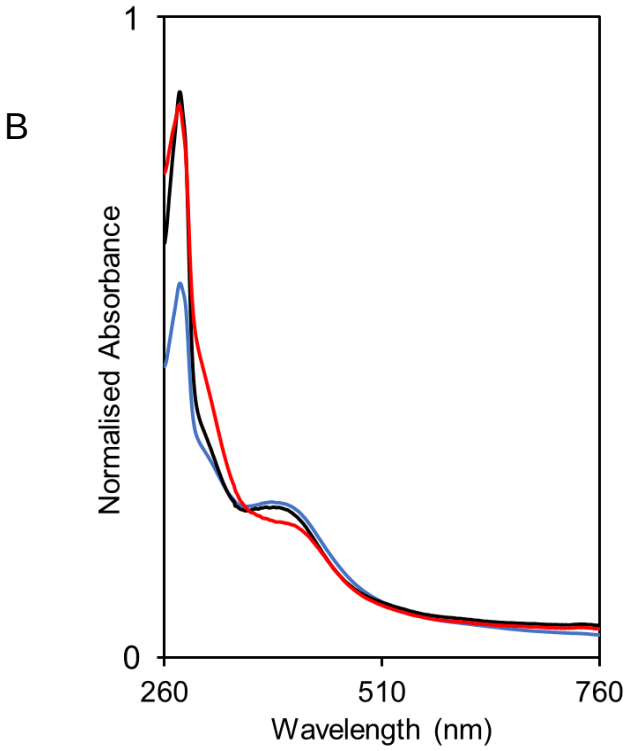
B
Normalised Absorbance
Wavelength (nm)

Figure 6.7 Spectroscopic characterisation of RirA variants.

(A) Circular dichroism (CD) spectra for wild type RirA, and variants N8D and N8C RirA, as labelled. NsrR (*S. coelicolor*) is also shown for comparison. Grey dotted line shows similar spectral characteristics between spectra **(B)** Normalised UV-visible spectra of wild type RirA (Black) and variant N8D RirA (Red) and N8C RirA (Blue). Samples were prepared in 25 mM HEPES, 50 mM NaCl, 750 mM KC, pH 7.5. Spectra were recorded using a 1 cm pathlength anaerobic quartz cuvette.

6.4.2. N8D substitution affects the stability of [4Fe-4S] RirA

Due to the striking similarities of the spectroscopic properties of N8D RirA variant with those of the previously characterised NsrR, experiments were performed to see whether there were changes in the cluster stability when compared to wild type RirA. Previous characterisation of as isolated wildtype RirA showed drastic changes in the CD spectra before and after cluster reconstitution [9]. Furthermore, the cluster was not stable under gel filtration conditions, as during gel filtration dissociated iron was separated from the protein bound cluster. The CD spectra before and after gel filtration revealed some differences, and the UV-visible spectrum revealed a decreased intensity of the 382 nm cluster peak [9]. Gel filtration also resulted in an increase in the $[3Fe\text{-}4S]^{1+}$ signal in the EPR spectrum to ~13% of total cluster concentration [9].

Similar characterisation experiments were performed for N8D. *In vivo* cluster incorporation of N8D RirA was also low, thus *in vitro* reconstitution was performed and was followed using UV-visible absorbance spectroscopy (Figure 6.8A), which indicated significant further incorporation, as for wild type RirA. However, CD spectroscopy revealed that the spectrum of N8D RirA variant retained the same spectral features before and after *in vitro* cluster reconstitution. This differs from wildtype RirA, where CD reveals differences between as isolated and reconstituted RirA [9]. Importantly, identical UV-visible absorbance and CD spectra were also observed before and after gel filtration of reconstituted N8D RirA in anaerobic conditions (Figure 6.8B to C). This indicates that no cluster loss/ conversions occurred during these manipulations.

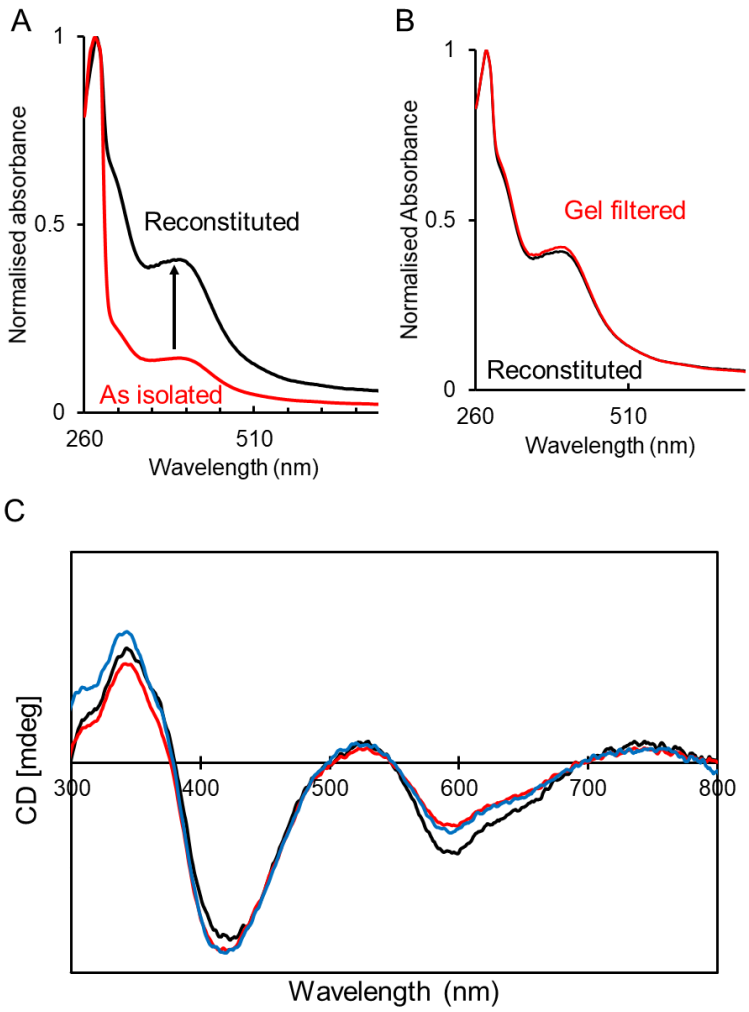

Figure 6.8 Spectroscopic characterisation of N8D RirA during purification and *in vitro* cluster reconstitution.

(A) Normalised UV-visible absorbance spectra for comparison between as isolated RirA (black) and reconstituted RirA (red). Arrow indicates increase of maximum peak at 410 nm corresponding to increase in [4Fe-4S] cluster. **(B)** Normalised UV-visible absorbance spectra for comparison between reconstituted RirA before (black) and after (red) gel filtration. **(C)** Normalised CD spectra of as isolated N8D RirA (black), reconstituted N8D RirA before (blue) and after (red) gel filtration. Spectra were recorded for as isolated N8D RirA, and reconstituted N8D RirA in 25 mM HEPES, 2.5 mM $CaCl_2$, 50 mM NaCl, 750 mM KCl, pH 7.5. Gel filtered N8D RirA samples were in 25 mM Hepes, 2.5 mM $CaCl_2$, 50 mM NaCl, 333 mM KCl, pH 7.5. The measurements were obtained using a 1 mm sealed anaerobic cuvette.

Non denaturing ESI-MS was performed for reconstituted N8D RirA under the same conditions as previously for wildtype RirA [9, 11]. For wildtype RirA, upon ionization the m/z spectrum contained peaks in two distinct regions, corresponding to monomeric (600– 1500 m/z), and dimeric (1800–3000 m/z) RirA [9]. In contrast, the electrospray ionization process does not monomerise N8D RirA to any significant extent and the peaks observed in the m/z spectrum corresponding only to the dimeric region (Figure 6.9A). In the deconvoluted mass spectrum of N8D RirA in the dimer region contains a major peak at 35,585 Da, corresponding to [4Fe-4S]/[4Fe-4S] cluster containing dimer (predicted mass 35,586 Da). Importantly, the [4Fe-4S]/[4Fe-4S] cluster species was the only form observed for N8D RirA. This differs from the deconvoluted spectra of the wildtype dimer region, which revealed distinct peaks on the lower mass side of the [4Fe-4S]/[4Fe-4S] RirA dimer, due to [3Fe– 4S]/[4Fe–4S], [3Fe–4S]/[3Fe–4S], and [3Fe–3S]/[3Fe–3S], [2Fe–2S]/[2Fe–2S] cluster breakdown products [9].

The N8D RirA dimer can be disturbed by the increasing the in-source collision-induced dissociation (isCID) from 0 to 100 eV. This resulted in the emergence of peaks corresponding to the monomer region (Figure 6.10A). At the same time, Increasing the isCID also resulted in cluster breakdown. The deconvolution of the monomer region revealed two significant peaks corresponding to [4Fe-4S] and apo- N8D RirA (Figure 6.10B). Again, although the apo-form was formed, there were no traces of the intermediate cluster breakdown species between [4Fe-4S] and apo- N8D RirA, such as the [4Fe–3S], [3Fe–4S], [3Fe–3S], [3Fe–2S], [2Fe–3S], [2Fe–2S] breakdown products as previously observed for wildtype RirA [9]. The lack of intermediate cluster breakdown products observed in these non-denaturing ESI-MS experiments suggests that the N8D substitution has altered the concerted breakdown nature of the cluster of the [4Fe-4S] cluster in wildtype RirA, likely by stabilising the theorised labile fourth iron.

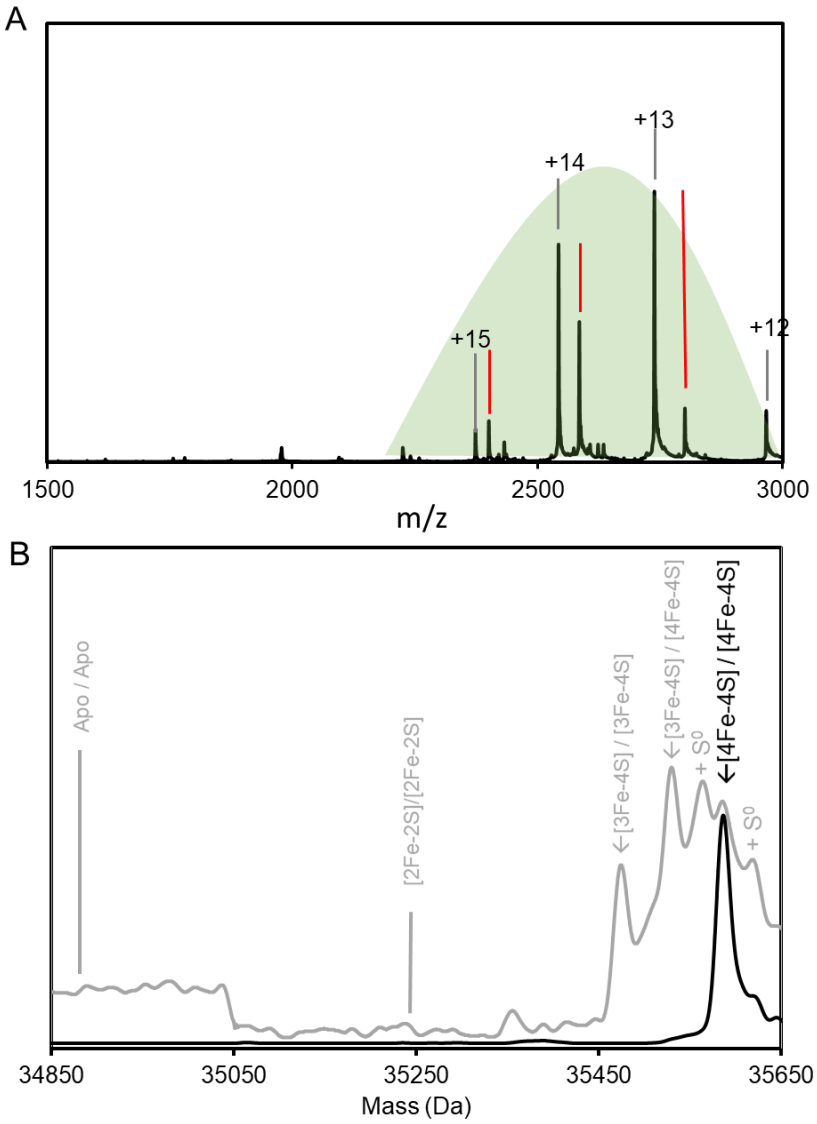

Figure 6.9 Non-denaturing ESI-MS characterisation of reconstituted N8D RirA.

(A) m/z spectrum of reconstituted N8D RirA under non-denaturing conditions shows charge states present in the dimer region (green box). Charge peaks correspond to two major species. The first corresponds to full length N8D RirA, to include charges +15, +14, +13 and +12 (black) and the second corresponds to a truncated version of N8D RirA (red). **(B)** Deconvoluted mass spectrum of dimeric N8D RirA showing the major species [4Fe-4S] / [4Fe-4S] dimeric N8D RirA with no observable cluster degradation species. The deconvoluted mass spectrum of dimeric wildtype RirA is also shown for comparison in grey [11] . Cluster species [3Fe-4S] / [4Fe-4S], [3Fe-4S] / [3Fe-4S] and sulfur adducts are as labelled. Positions of apo- and [2Fe-2S]/[2Fe-2S] species of N8D RirA are indicated. N8D RirA (28 µM in cluster, fully cluster load) was in 250 mM ammonium acetate, pH 7.32.

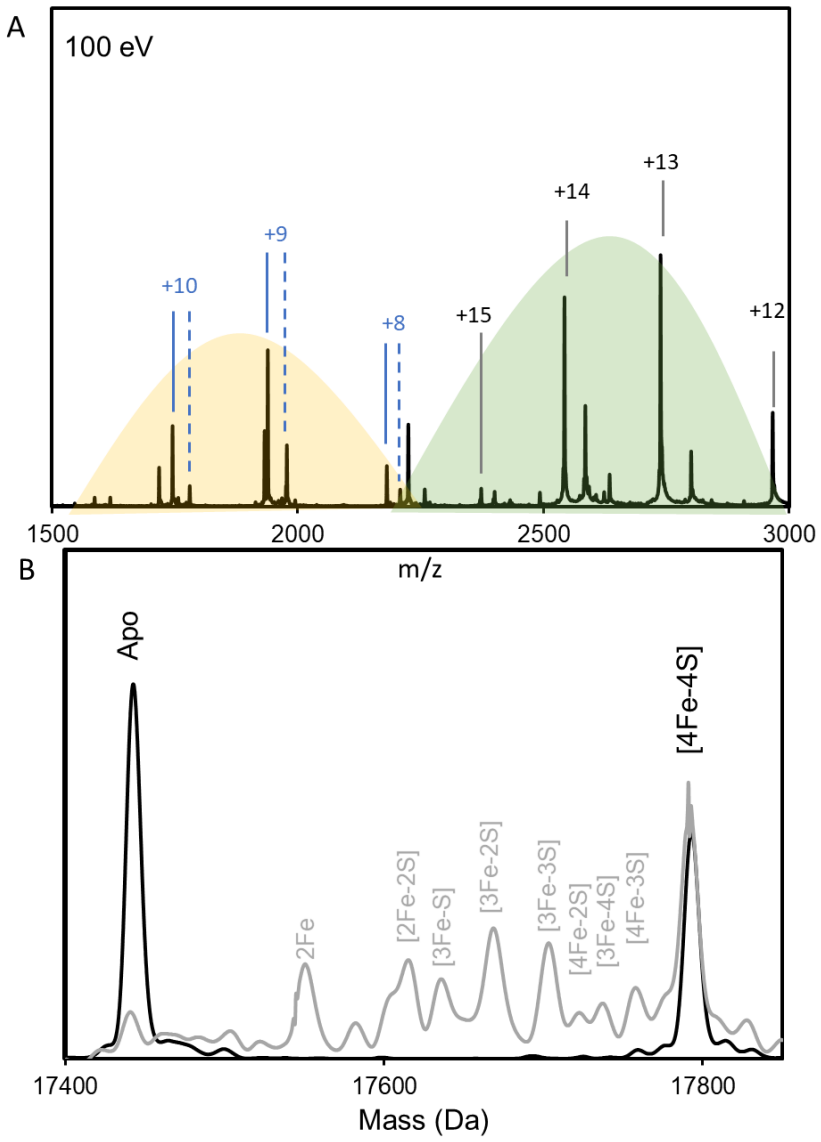

Figure 6.10 In-source collision-induced dissociation (IsCID) of N8D RirA results in protein monomerization and loss of cluster.

(A) m/z spectrum of N8D RirA upon 100 eV IsCID shows a bimodal charge state distribution with charge states corresponding to monomeric (yellow box) and dimeric (green box) N8D RirA. Monomeric charge states of +10, +9 and +8 are shown in blue. Peaks corresponding to apo- (solid line) and holo- (dashed line) charge states are also shown. Dimeric charge states +15, +14, +13 and +12 are shown in black. **(B)** Deconvoluted mass spectrum of the monomeric region of N8D RirA (from m/z 1500 to 2200) to show apo- and [4Fe-4S] N8D RirA, with no cluster degradation species in between. The deconvoluted mass spectrum of the monomeric region of wildtype RirA is shown in grey, with cluster degradation species labelled for comparison [9]. N8D RirA (28 µM in cluster, fully cluster load) was in 250 mM ammonium acetate, pH 7.32.

6.4.3. N8D substitution in RirA abolishes iron-sensing capabilities

The effect of low iron conditions mimicked by the presence of EDTA was followed using both UV-visible absorbance spectroscopy and non-denaturing ESI-MS.

For UV-visible absorbance spectroscopic experiments, both wild type RirA and the N8D RirA variant were exposed to 1 mM EDTA, under aerobic and anaerobic conditions, over time. In wild type RirA, spectral changes can be followed by the absorbance maximum peak shift from 382 nm to 425 nm. By plotting the difference between absorbance at these wavelengths ($A_{382\ nm} – A_{425\ nm}$), the cluster degradation could be followed (Figure 6.11). This showed that under anaerobic conditions, in response to low iron conditions, intensity due to the wild type RirA [4Fe-4S] cluster was lost gradually over several hours, with the formation of a relatively stable [2Fe–2S], within the timescale of the experiment. Fitting of absorbance data ($A_{382\ nm} – A_{425\ nm}$) gave a rate constant of ~0.009 min^{-1} (Figure 6.11B). The combined exposure to low iron and aerobic conditions resulted in a very similar reaction, except cluster conversion occurred significantly more rapidly, giving a rate constant 3-fold higher (~0.029 min^{-1}) than for the same reaction under anaerobic conditions (Figure 6.11D).

In contrast, in low iron, anaerobic conditions the UV-visible absorbance spectrum for N8D RirA remained largely unchanged in the 400 minutes of the experiment, indicating that the cluster has little or no sensitivity to low iron conditions mimicked by 1 mM EDTA. Furthermore, under aerobic conditions there was a linear decrease in the 410 nm absorbance, i.e. the main cluster absorbance did not undergo a red shift (in the peak maximum) that indicates conversion of the cluster to a [2Fe-2S] cluster (Figure 6.12). Thus, N8D RirA does not sense low iron and does not undergo conversion to stable a [2Fe-2S] cluster species, as observed in wild type RirA.

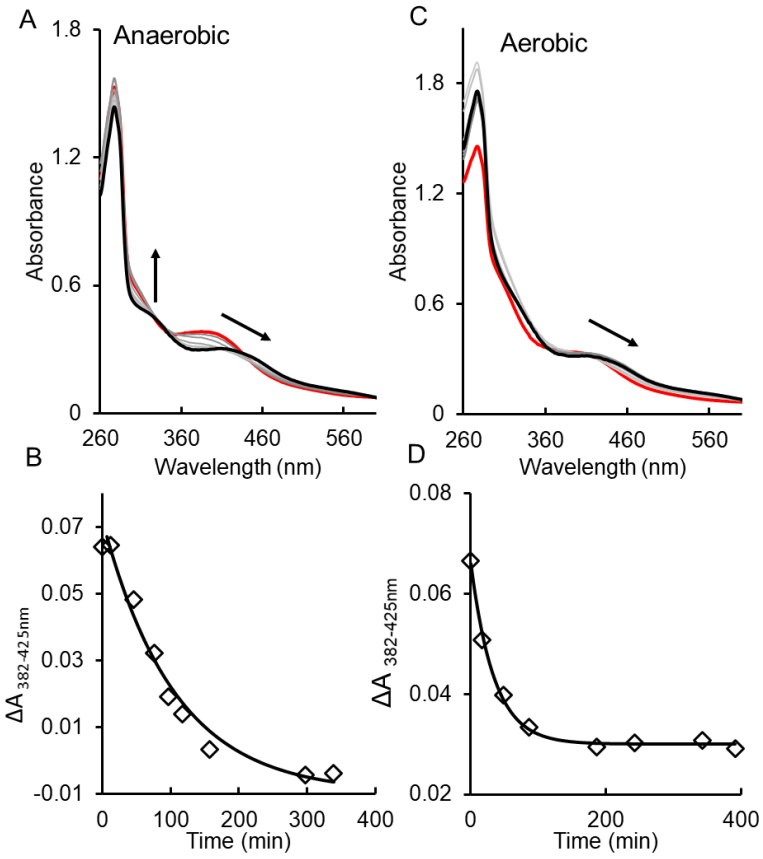

Figure 6.11 Time dependence of wild type RirA [4Fe-4S] to [2Fe-2S] conversion promoted by 1 mM EDTA.

(A) UV-visible absorbance spectra recorded of wild type RirA over several hours following the addition of 1 mM EDTA, under anaerobic conditions. Initial spectrum is in red, all intervening spectra are in grey, end point (after 350 minutes) is in black. Arrows indicate direction of absorbance change. RirA (29 µM) was in 25 mM HEPES, 2.5 mM $CaCl_2$ 50 mM NaCl, 750 mM KCl, pH 7.5. **(B)** Plot of absorbance obtained for anaerobic data: $A_{382\ nm} - A_{425\ nm}$ as a function of time, solid line represents a fit of a single exponential function to the data (k = 0.009 min^{-1}). **(C)** UV-visible absorbance spectra recorded of wild type RirA following addition of 1 mM EDTA in the presence of 230 µM O_2. Initial spectrum is in red, all intervening spectra are in grey, end point (after 400 minutes) is in black. Arrows indicate direction of absorbance change. RirA (28 µM in cluster) was in 25 mM Hepes, 2.5 mM $CaCl_2$ 50 mM NaCl, 750 mM KCl, pH 7.5. **(D)** Plot of absorbance obtained from aerobic data: $A_{382\ nm} - A_{425\ nm}$ as a function of time. The solid line represents a fit to the data (k = 0.029 min^{-1}), as in (B). The measurements were obtained using a 1 cm pathlength sealed anaerobic quartz cuvette.

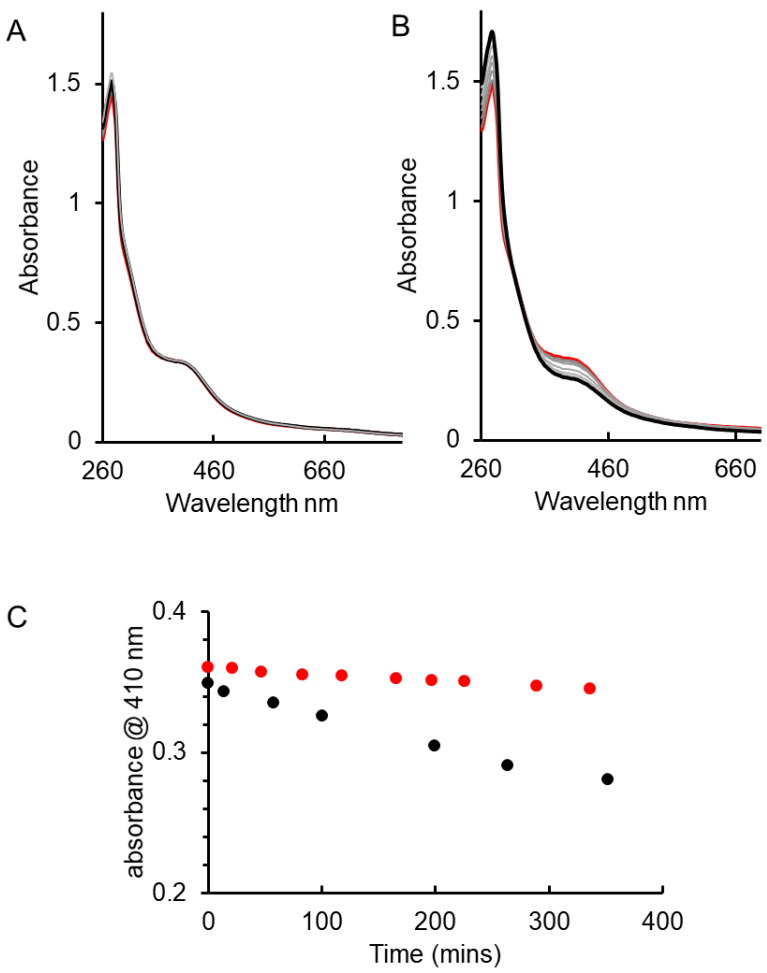

Figure 6.12 Effect of 1 mM EDTA on N8D RirA [4Fe-4S] cluster over time.

(A-B) UV-visible absorbance spectra recorded of N8D RirA over several hours following the addition of 1 mM EDTA, under anaerobic (A) and anaerobic (B) conditions. Initial spectra are in red, all intervening spectra are in grey, end point (after ~400 minutes) are in black. **(C)** Plot of absorbance change obtained from anaerobic (red) an aerobic (black) experiments: $A_{410\ nm}$ was plotted as a function of time. For both experiments, N8D RirA (29 µM in cluster) was in 25 mM HEPES, 2.5 mM $CaCl_2$ 50 mM NaCl, 750 mM KCl, pH 7.5. Measurements were obtained using a 1 cm pathlength sealed anaerobic quartz cuvette.

Non-denaturing ESI-MS experiments were also performed exactly as for wildtype previously [11]. N8D RirA was exposed to EDTA under both aerobic and anaerobic conditions. Both in the presence, and absence of oxygen, the initial deconvoluted spectrum reveals the major peak as [4Fe-4S]/[4Fe-4S] N8D RirA, with the addition of two EDTA adducts (Figure 6.13). 30 minutes after the exposure to EDTA, N8D RirA remains unchanged as a [4Fe-4S]/[4Fe-4S] dimer with no monomerization, or cluster breakdown, supporting the UV-visible absorbance data, that N8D RirA does not sense low iron and does not undergo any cluster conversion as observed in wild type RirA (Figure 6.13 B to C).

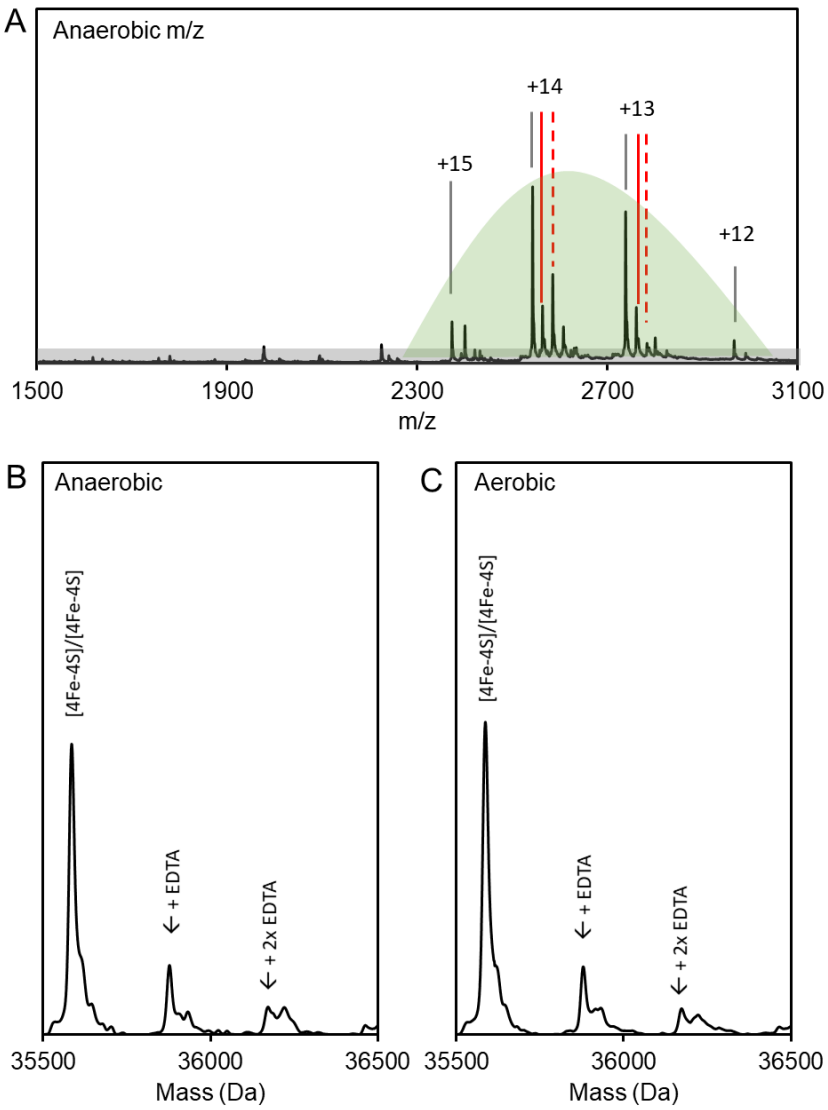

Figure 6.13 Spectra of N8D RirA after exposure to EDTA for 30 minutes.

(A) Final m/z spectrum of N8D RirA after exposure to EDTA for 30 minutes shows charge states present in the dimer region (green box). Peaks corresponding to [4Fe-4S]/[4Fe-4S] dimeric N8D RirA are shown in black, to include charge states of +15, +14, 13 and +12. Peaks due to to EDTA adducts can be most prominently seen on charge states +14 and +13 and are indicated in red, to correspond with 1 (solid line) and 2 (dashed line) EDTA adducts. **(B-C)** Deconvoluted final mass spectrum of N8D RirA 30 minutes after exposure to EDTA in the absence of oxygen **(B)** and the presence of 230 µM O_2 **(C).** In both cases, spectra show mass peaks corresponding primarily to [4Fe-4S]/[4Fe-4S] dimeric N8D RirA, with EDTA adducts as indicated. N8D RirA (28 µM in cluster, fully cluster load) was exposed to 250 µM EDTA at 37 °C in 250 mM ammonium acetate, pH 7.32.

6.5. Discussion

RirA senses and responds to levels of intracellular iron via a novel mechanism. Previously, a range of biophysical approaches were used to demonstrate that RirA contains a [4Fe-4S] cluster, and DNA binding experiments confirmed that [4Fe-4S] RirA binds RirA-regulated DNA sequences with the function of repressing genes involved in iron uptake. However, under low iron conditions, RirA undergoes cluster conversion via a semi-stable [2Fe-2S] form, which exhibits lower affinity for DNA binding. [2Fe-2S] RirA eventually degrades to apo-RirA under prolonged low iron conditions, which has no DNA binding abilities [9]. Recently, non-denaturing ESI-MS was used to study the cluster disassembly reaction in response to low iron and provided high resolution information about the cluster conversion intermediates. These experiments demonstrated that, as the [4Fe-4S] decayed away, numerous peaks corresponding to protein-bound cluster species were observed to increase in intensity. These included [4Fe-3S], [3Fe-4S], [3Fe-3S], [3Fe-2S], [3Fe-S], [2Fe-2S] and [2Fe-S] forms, which subsequently decayed away as apo-RirA became the highest abundance species. Interestingly, the [3Fe-3S] cluster is a novel intermediate previously only observed by mass spectrometry during the O_2-dependent cluster conversion reaction of [4Fe-4S] FNR to [2Fe-2S] FNR [15].

To further the identification of cluster species, analysis of the mass spectrometric kinetic data led to a reaction scheme modelling the formation and decay of the cluster intermediate species. This proposed reaction is detailed in full in Pellicer Martinez et al, 2019 [11]. This chapter detailed the generation of ^{34}S-substituted protein bound [4Fe-4S] RirA via *in vitro* cluster reconstitution, using ^{34}S-L-cysteine (generated by Dr J, Crack, UEA) [10]. This assisted with unambiguous assignment of cluster species. The ^{34}S-substituted RirA-bound [4Fe-4S] cluster was analysed using non-denaturing ESI-MS. When compared with the deconvoluted mass spectra of natural abundance (primarily ^{32}S) sulfur containing [4Fe-4S] RirA, it allowed for the confirmation of cluster species, which were shifted by +2 Da for each sulfide.

The proposed mechanism involves a complex series of degradation species. Importantly, cluster decay is initiated by the loss of a single iron, which results in a [3Fe-4S] unstable intermediate. The dissociation of the initial iron occurs at a similar rate under both

aerobic and anaerobic conditions, suggesting that, although RirA has both iron and O_2 sensing capabilities, primarily it is an iron sensor [11]. For RirA to act as an effective sensor of iron levels, the dissociation constant of the fourth labile iron must be in the range of the free iron concentration within the cytoplasm. This concentration is unknown for *R. leguminosarum*, but available cytoplasmic iron has been characterised in *E. coli* as ~10 μM [20]. Using mag-fura-2 in competition binding experiments, the K_d for the $[4Fe\text{-}4S]^{2+} \rightleftharpoons [3Fe\text{-}4S]^{0} + Fe^{2+}$ equilibrium was determined as ~3 μM, which is in the expected range and thus fits well with iron sensing capabilities. Furthermore, this is comparable to the binding affinity of the more widespread global iron regulator Fur, which in *E. coli* was reported to bind Fe^{2+} with a K_d of ~10 μM [20]. Spontaneous loss of cluster following the removal of the first Fe^{2+} from [4Fe-4S] RirA was also confirmed, as the addition of enough EDTA to chelate only the first iron per cluster resulted in an unstable [3Fe-4S] RirA that was observed to undergo complete cluster loss overnight to form primarily apo-RirA.

So far, a fourth ligand of for the [4Fe-4S] cluster in RirA has not been identified. It is clear that the lability of the fourth iron of the RirA [4Fe-4S] cluster is crucial for its function as an iron sensor. Furthermore, the lability of the fourth iron under low iron conditions is not a feature shared by most [4Fe-4S] cluster proteins. Thus, one possibility is that the cluster is bound to RirA by only three amino acid side chains (the three conserved Cys residues), with the fourth labile iron coordinated by a transient ligand such as water or hydroxide. Based on this hypothesis, attempts were made to introduce a fourth amino acid ligand which could stabilise the cluster. Based on the high sequence similarities between RirA and the previously structurally characterised NsrR, in which the fourth ligand is an Asp residue (Asp8), N8C and N8D RirA variants were generated. Spectroscopic characterisation of the RirA variants showed that the N8D RirA variant displayed UV-visible absorbance properties that are characteristic of a more conventional [4Fe-4S] cluster. Strikingly, N8D RirA also exhibited a CD spectrum very similar to that of NsrR.

Furthermore, in contrast to wild type RirA, which undergoes conversion from [4Fe-4S] RirA to [2Fe-2S] RirA over the course of >6 hours upon exposure to low iron/anaerobic

conditions, the N8D RirA variant was found to have lost its iron sensing ability in that it remained stable under these same conditions. Under aerobic conditions, N8D RirA was observed to undergo cluster degradation in the UV-visible absorption spectroscopy experiments, but this was distinct from that observed for wild type RirA, in that the process is very slow and no evidence for a [2Fe-2S] cluster intermediate was observed. Equally, under non-denaturing ESI-MS conditions no cluster breakdown species can be observed for N8D RirA upon exposure to low iron conditions both aerobically and anaerobically. One potential benefit of the increased stability of the N8D RirA protein may be in the structural characterisation of RirA, which has not yet been possible for the wild type protein. This may be in part due to the fragility/lability of the [4Fe-4S] cluster. Thus, the artificial stabilisation of the [4Fe-4S] cluster may be useful for obtaining a uniform stable sample for crystallisation trials.

6.6. References

1. Andrews, S.C., A.K. Robinson, and F. Rodriguez-Quinones, *Bacterial iron homeostasis.* FEMS Microbiol Rev, 2003. **27**(2-3): p. 215-37.
2. Winterbourn, C.C., *Toxicity of iron and hydrogen peroxide: the Fenton reaction.* Toxicol Lett, 1995. **82-83**: p. 969-74.
3. Hantke, K., *Regulation of ferric iron transport in Escherichia coli K12: isolation of a constitutive mutant.* Mol Gen Genet, 1981. **182**(2): p. 288-92.
4. Troxell, B. and H.M. Hassan, *Transcriptional regulation by Ferric Uptake Regulator (Fur) in pathogenic bacteria.* Front Cell Infect Microbiol, 2013. **3**: p. 59.
5. Merchant, A.T. and G.A. Spatafora, *A role for the DtxR family of metalloregulators in gram-positive pathogenesis.* Mol Oral Microbiol, 2014. **29**(1): p. 1-10.
6. Gonzalez de Peredo, A., et al., *Conformational changes of the ferric uptake regulation protein upon metal activation and DNA binding; first evidence of structural homologies with the diphtheria toxin repressor.* J Mol Biol, 2001. **310**(1): p. 83-91.
7. Todd, J.D., et al., *RirA, an iron-responsive regulator in the symbiotic bacterium* Rhizobium leguminosarum*.* Microbiology, 2002. **148**(Pt 12): p. 4059-4071.
8. Johnston, A.W., et al., *Living without Fur: the subtlety and complexity of iron-responsive gene regulation in the symbiotic bacterium* Rhizobium *and other alpha-proteobacteria.* Biometals, 2007. **20**(3-4): p. 501-11.
9. Pellicer Martinez, M.T., et al., *Sensing iron availability via the fragile [4Fe-4S] cluster of the bacterial transcriptional repressor RirA.* Chem Sci, 2017. **8**(12): p. 8451-8463.
10. Crack, J.C., M.Y.Y. Stewart, and N.E. Le Brun, *Generation of ^{34}S-substituted protein-bound [4Fe-4S] clusters using ^{34}S-L-cysteine.* Biology Methods and Protocols, 2019. **4**(1).
11. Pellicer Martinez, M.T., et al., *Mechanisms of iron- and O_2-sensing by the [4Fe-4S] cluster of the global iron regulator RirA.* Elife, 2019. **8**.
12. Bhubhanil, S., et al., *Cysteine desulphurase-encoding gene* sufS2 *is required for the repressor function of RirA and oxidative resistance in* Agrobacterium tumefaciens*.* Microbiology, 2014. **160**(Pt 1): p. 79-90.
13. Santos, J.A., P.J. Pereira, and S. Macedo-Ribeiro, *What a difference a cluster makes: The multifaceted roles of IscR in gene regulation and DNA recognition.* Biochim Biophys Acta, 2015. **1854**(9): p. 1101-12.
14. Tucker, N.P., et al., *There's NO stopping NsrR, a global regulator of the bacterial NO stress response.* Trends Microbiol, 2010. **18**(4): p. 149-56.
15. Crack, J.C., A.J. Thomson, and N.E. Le Brun, *Mass spectrometric identification of intermediates in the O_2-driven [4Fe-4S] to [2Fe-2S] cluster conversion in FNR.* Proc Natl Acad Sci U S A, 2017. **114**(16): p. E3215-E3223.
16. Crack, J.C. and N.E. Le Brun, *Mass spectrometric identification of [4Fe-4S](NO)$_x$ intermediates of nitric oxide sensing by regulatory iron-sulfur cluster proteins.* Chemistry, 2019. **25**(14): p. 3675-3684.
17. Rodrigues, A.V., et al., *Iron loading site on the Fe-S cluster assembly scaffold protein is distinct from the active site.* Biometals, 2015. **28**(3): p. 567-76.

18. Hulme, E.C. and M.A. Trevethick, *Ligand binding assays at equilibrium: validation and interpretation.* Br J Pharmacol, 2010. **161**(6): p. 1219-37.
19. Crack, J.C., et al., *NsrR from* Streptomyces coelicolor *is a nitric oxide-sensing [4Fe-4S] cluster protein with a specialized regulatory function.* J Biol Chem, 2015. **290**(20): p. 12689-704.
20. Keyer, K. and J.A. Imlay, *Superoxide accelerates DNA damage by elevating free-iron levels.* Proc Natl Acad Sci U S A, 1996. **93**(24): p. 13635-40.

Chapter 7. General discussion and further work

This thesis details studies of Fe-S cluster proteins which function as transcriptional regulators, focusing primarily on the *S. venezuelae* Wbl proteins involved in *Streptomyces* development, WhiB and WhiD. The decision to explore Wbl proteins in *S.venezuelae* follows its emergence as a model developmental system for *Streptomyces* research. The advantage of this organism is its ability to sporulate to near completion in liquid media, which facilitates *in vivo* studies of *Streptomyces* development using techniques such as ChIP-seq [1, 2]. This thesis also provides further insights into the function of an Fe-S cluster dependent global regulator of iron metabolism, RirA from *R. leguminosarum*.

Studies of *Sv*WhiB and *Sv*WhiD focused on biophysical characterisations of the proteins and clusters, and their interactions with corresponding protein interaction partners. Both WhiB and WhiD were over-produced in *E. coli* and purified anaerobically. Characterisation of as isolated proteins confirmed that WhiB and WhiD both coordinate a [4Fe-4S] cluster. This is consistent with previously characterised Wbl proteins from *S. coelicolor* and *M. tuberculosis* and supports this as a universal feature of Wbl proteins. Although both *Sv*WhiB and *Sv*WhiD can coordinate a [4Fe-4S] cluster, cluster incorporation differed drastically between the two proteins. WhiB was isolated with average ~40% cluster loading, whilst WhiD was isolated with average ~90% cluster loading. WhiB and WhiD also exhibited different sensitivities to oxygen. Whilst WhiB showed signs of cluster degradation immediately after exposure to 230 µM O_2, WhiD remains relatively unchanged for >15 minutes after exposure. Indeed, aerobic purification of WhiD results in weakly coloured fractions, whilst aerobic purification of WhiB results in colourless apo-protein. These indicate that, out of the two Wbl proteins, the [4Fe-4S] cluster of WhiD appears to be more stable. For both WhiB and WhiD, interaction with the primary σ-factor σ^{HrdB} significantly protects the [4Fe-4S] cluster from O_2-mediated degradation for at least 60 minutes. Since the interaction is dependent upon the [4Fe-4S] cluster, the eventual degradation of the cluster due to O_2 then results in the disassembly of the complex.

Previous research showed that Wbl proteins react slowly with oxygen, but very rapidly with NO [3-6]. The high cluster load of as isolated *Sv*WhiD made it well suited for NO sensitivity experiments. NONOates were used to release known concentrations of NO, and nitrosylation of [4Fe-4S] WhiD was observed by non-denaturing ESI-MS, and UV-visible absorbance spectroscopy. These experiments showed that the reaction of *Sv*WhiD with NO was complete at ~9-10 NO per cluster, consistent with data previously reported for *Sc*WhiD [6]. However, in comparison to *Sc*WhiD, the nitrosylation intermediates/products of *Sv*WhiD were considerably less stable. A stepwise titration with PROLI-NONOate resulted in mild precipitation of the *Sv*WhiD sample, and no nitrosylated forms of the WhiD [4Fe-4S] cluster, nor any other iron-nitrosyl products, were detected by non-denaturing mass spectrometry, which were previously detected for *Sc*WhiD [7]. Stopped-flow kinetic studies of the reaction of [4Fe-4S] *Sv*WhiD with NO were carried out on the protein alone, and in the presence of σ^{HrdB}_4. Although the instability of the [4Fe-4S] cluster in *Sv*WhiD made a complete kinetic analysis problematic due to precipitation, this did not occur until after ~500 ms which allowed for the characterisation of the initial 2 reaction phases as first order with respect to NO for *Sv*WhiD alone. The derived rate constants are consistent with those reported for the equivalent phases of nitrosylation of *Sc*WhiD and *M. tuberculosis* WhiB1 [4]. Thus, the nitrosylation of *Sv*WhiD most likely occurs via a mechanism that is like that of other Wbl proteins. Interestingly, the interaction with σ^{HrdB}_4 alters the reaction of [4Fe-4S] WhiD with NO. Although the reaction still occurs in a multi-step process reminiscent of the reaction of NO with WhiD independently, in the presence σ^{HrdB}_4, step 1 of WhiD alone becomes separated into two distinct steps. Importantly, although these steps still occur rapidly, they are independent of NO and occur on a slower timescale than step 1 of the reaction with WhiD. This may be due to a shielding effect of σ^{HrdB}_4 to NO accessibility to the cluster. The independence from NO concentration suggests that a conformational flexibility or reversible dissociation, which allows NO access, occurs more slowly than step 1 of the reaction of NO with [4Fe-4S] WhiD alone. Thus, step 1 in the complex could be interpreted as the dissociation of σ^{HrdB} or a conformational change, which must occur prior to NO attack on the cluster. Step 2 in the complex is distinct from step 1, which suggests that a second conformational change is dependent upon the completion of the first step.

Although the role of the WhiD: σ^{HrdB}_4 interaction remains unknown, it is clear that the *Sv*WhiD: σ^{HrdB}_4 complex is optimally arranged to distinguish between O_2 and NO as the reaction of [4Fe-4S] WhiD with O_2 and NO in association with σ^{HrdB}_4 become more distinct than for [4Fe-4S] WhiD alone. A well-established example of the physiological significance of O_2 and NO sensitivity in Wbl proteins can be found in *M. tuberculosis* WhiB1. WhiB1 is an essential transcriptional regulator for reprogramming gene expression when exposed to the NO produced within the lung macrophage environment, as the DNA binding ability of WhiB1 is affected after exposure to NO [3, 8, 9]. Notably, WhiB1 regulates the *espA* operon, which codes for proteins essential for the function of ESX-1, a major *M. tuberculosis* virulence factor involved in invasion of host cells, phagosome escape and forming extensive tissue lesions [9]. A similar physiological significance of the oxygen and NO sensitivity is likely for *S. venezuelae* Wbl proteins. Like in most bacteria, intracellular NO is highly regulated in *Streptomyces*, in particular the dedicated NO sensor NsrR regulates the expression of detoxifying enzymes [10]. Furthermore, a link has been established between NO signalling and various metabolic pathways that Wbl proteins are involved in, including antibiotic production and morphological differentiation [10, 11].

An interesting observation, specific to *Sv*WhiD, was its ability to dimerise. Analytical gel filtration revealed that both holo-WhiD and apo-WhiD existed in a monomer/dimer equilibrium. The same characteristic was not observed for *Sv*WhiB, nor previously for *Sc*WhiD, with which *Sv*WhiD share 78% overall sequence identity. The two proteins mostly differ in the C-terminus, as *Sv*WhiD has a C-terminal extension of 18 residues compared to *Sc*WhiD. Strikingly, the two proteins are 100% identical from residues 1-95. To test whether these additional residues may be responsible for the dimerization of *Sv*WhiD, a truncated form of WhiD which lacked 33 residues at the C-terminus was generated. The truncated form of WhiD was able to bind a [4Fe-4S] cluster and interact with σ^{HrdB}_4. Furthermore, the UV-visible absorbance and CD spectra revealed no significant differences between truncated and full length WhiD. However, the truncated form of WhiD eluted from an analytical gel filtration column at a volume indicative of a monomer. Thus, the C-terminal part of WhiD is essential for dimerization but not for cluster incorporation nor σ^{HrdB}_4 interactions. The function of dimerization remains

unclear. However, Blast analysis revealed that WhiD-like proteins exist with a comparable C-terminal extension in some other *Streptomyces* species, indicating the ability to dimerization likely exist for other Wbl proteins.

As mentioned above, an important finding in these studies was the specific interaction between *S. venezuelae* WhiB and WhiD and the primary σ factor σ^{HrdB}, and specifically with σ factor domain 4. This is in line with previous studies of mycobacterial Wbl proteins with the primary σ factor in mycobacteria (σ^{A}) [9, 12-14]. Non-denaturing ESI-MS and analytical gel filtration were used to confirm both that WhiB and WhiD interact with σ^{HrdB}_4 and the lack of interaction between WhiD and the alternative sigma factor σ^{HrdD}_4. The dependence of the Wbl : σ interaction upon the [4Fe-4S] cluster was previously shown for *M. tuberculosis* WhiB1 and σ^{A} and, in line with this, no complex formation was observed between apo-WhiD and σ^{HrdB}_4. Non-denaturing ESI-MS was also utilised to demonstrate that *Sv*WhiD forms a tight complex with σ^{HrdB}_4 (K_d < 1 μM). This observation that *Streptomyces* Wbl proteins can also interact specifically with the primary σ factor further confirms this interaction as a conserved feature of at least some Wbl proteins throughout the actinomycetes. Although both WhiB and WhiD have been observed to bind to σ^{HrdB}, the physiological relevance of this, and mechanism by which the two proteins function as transcriptional regulators, requires more study. It was established from mutagenesis studies that WhiD in *Streptomyces* regulate gene expression involved in the late stages of sporulation, and furthermore that the [4Fe-4S] cluster is likely to be crucial for this activity as substitutions of the conserved cysteines result in the *whi(te)* mutant phenotype. However, the regulon of *Sv*WhiD has not yet been characterised. Therefore, the role of holo-WhiD may be to recruit to σ^{HrdB} to specific subsets of promoters to initiate transcription of genes involved in late sporulation. Alternatively, WhiD may act as an anti-σ factor and function by sequestering σ^{HrdB} to allow for alternative σ factors, specific to sporulation to function.

For WhiB, ChIP-seq analysis of its regulon revealed many genes involved in the transition to sporulation initiation [15]. Direct binding of WhiB to DNA was a observed in this study. Specifically, WhiB was shown here to bind the promoter regions of *ftsW*, a septation gene. Therefore, WhiB may in part, recruit σ^{HrdB} to specific subsets of promoters to recruit the core RNAP and initiate transcription of genes involved in sporulation. The

WhiB regulon also includes genes involved in the arrest of aerial growth, which are repressed upon sporulation initiation. These genes include *filP*, for which direct binding of WhiB was also observed [15]. Further investigation into the WhiB: DNA interaction revealed the importance of the nature of the cluster and the oxidation state of the protein. Both holo-WhiB and reduced apo-WhiB, but not oxidised apo-WhiB, could bind DNA directly. The effect of the cluster and oxidation state of Wbl proteins for function has been previously documented in studies in *M. tuberculosis*. Holo-WhiB1 was not observed to bind DNA. However, upon cluster loss/nitrosylation the subsequent apo/nitrosylated-WhiB1 was found to bind and repress transcription from its own promoter, as well as promoters of *groEL2* and the *espA* operon [3, 8, 9]. Equally, *in vitro* studies of *M. tuberculosis* WhiB3 showed that holo-WhiB3 binds DNA weakly, but oxidised apo-WhiB3 binds DNA very strongly [16]. Here, the affinity difference between *S. venezuelae* [4Fe-4S] WhiB and apo-WhiB for DNA binding was not explored, due to the low cluster incorporation of as isolated WhiB. Regardless, it is likely that *Sv*WhiB functions in line with these previous observations, whereby the oxygen and NO sensitive [4Fe-4S] cluster functions as an environmental sensor. With its cluster is intact, [4Fe-4S] WhiB is capable of both interacting with σ^{HrdB} and binding specifically to DNA. The loss of cluster within a reducing environment allows apo-WhiB to retain some DNA-binding abilities, whereby exposure to an oxidising environment may then result in complete loss of the WhiB: DNA interaction.

An important component to consider for deducing the mechanism of function of WhiB is its putative interaction with the transcriptional regulator WhiA. *In vivo* ChIP-seq studies suggested that neither *Sv*WhiB or *Sv*WhiA function independently, as mutations in either protein abolishes the other's regulatory function, subsequently inhibiting sporulation [15]. In line with previous *in vivo* ChIP-seq and *in vitro* DNA footprinting studies, EMSA experiments confirmed binding of *Sv*WhiA to promoter regions of both genes encoding sporulation machinery (*ftsW*) and genes encoding proteins involved in aerial growth (*filP*) [15]. Interestingly, initial characterisations of *Sv*WhiA revealed an unexpected metal cofactor, not reported for WhiA orthologues studied previously. Strikingly, *Sv*WhiA overexpression in *E. coli* yielded 90% zinc bound WhiA. Non-denaturing ESI-MS then confirmed the capability of zinc bound WhiA for DNA-binding.

Non-denaturing ESI-MS also revealed the ability of WhiA to bind to three GACAC sites within the promoter region of *ftsW.* Since the occurrence of the GACAC sequence within the *S. venzuelae* genome is drastically mismatched with the number of binding sites identified in the WhiA-WhiB regulon (~250 out of ~15,000 copies), one possible mechanism of function may require WhiA to scan the genome, displaying weak, unspecific binding to GACAC recognition sites [15, 17]. Previous observations revealed that WhiA expression is consistent throughout both the vegetative and developmental stages, whilst WhiB expression becomes upregulated upon the initiation of sporulation [18]. It then follows that the cooperativity of WhiA and WhiB likely relies on WhiB (which itself must exhibit the correct cluster and oxidation state) to target WhiA to specific promoter regions involved in sporulation. Direct interaction between *Sv*WhiA and *Sv*WhiB is anticipated for their function, notably *in vitro* studies in *C. glutamicum* has revealed direct interaction between WhiA and the *C. glutamicum* WhiB orthologue WhcD. However, the same interaction has yet to be observed between *Sv*WhiA and *Sv*WhiB, and no evidence for such an interaction was obtained in this work. Although direct interaction is likely, the novel observation that both WhiB and WhiA can independently bind to specific promoter regions of sporulation genes *in vitro* may provide an alternative mechanism. In the presence of both proteins, WhiB binding is lost and WhiA binding becomes enhanced, thus the direct binding of WhiB to specific DNA targets may induce a conformational change in the DNA backbone. This could allow for a tighter and more specific interaction between WhiA and the DNA, and subsequent dissociation of WhiB from the DNA.

The interaction between [4Fe-4S] WhiB and σ^{HrdB} is also likely to have significance in the WhiA-WhiB mechanism of function. As was proposed for WhiD, one possibility may involve [4Fe-4S] WhiB functioning as an anti- σ factor, sequestering the housekeeping sigma factor to allow for sporulation specific σ factors to function. Equally, the WhiA-WhiB interaction may require another protein component, for which σ^{HrdB} becomes an obvious candidate. Attempts to identify this potential tripartite interaction were un-successful. However this may be due to these studies involving only domain 4, and not the full-length σ^{HrdB}. Indeed, if the interaction requires the primary sigma factor σ^{HrdB}, another potential component to consider is RbpA: a small, non-DNA binding

transcriptional factor that associates with the primary σ factor [19, 20]. RbpA is specific to, but widely found in actinobacteria. In *M. tuberculosis*, RbpA is essential and appears to have a general function in transcription initiation from the primary σ factor as it stabilised the RNAP holoenzyme and stimulated transcription. In *S. coelicolor*, although mutants lacking RbpA were viable, they grew slower and RbpA was shown to be present in the σ^{HrdB}–RNAP transcription initiation complex *in vivo.* Thus, RbpA may also be required to stabilise the theoretical σ^{HrdB}: WhiB: WhiA interaction and will be worth exploring in future studies.

Another Fe-S cluster protein investigated in this thesis was RirA from *R. leguminosarum*. As with Fe-S cluster studies in [4Fe-4S] WhiD, the application of non-denaturing ESI-MS application to RirA demonstrated the value of this technique to Fe-S cluster proteins. Unlike in WhiD, in which cluster degradation species upon nitrosylation were too unstable to observe, the RirA cluster breakdown in low iron conditions readily yielded numerous cluster species that could be detected in high resolution, including those previously unobserved via spectroscopic experiments. The experiments detailed in this thesis provide supporting data for the characterisation of the RirA cluster breakdown in low iron conditions. The ^{34}S-substituted cluster-bound RirA experiments were crucial for unambiguous assignment of the cluster species. These experiments confirmed that in addition to cluster species previously identified via UV-visible and EPR spectroscopic methods, such as the [2Fe-2S] and [3Fe-4S] clusters, the latter of which is EPR-active in its +1, $S=\frac{1}{2}$ state). Other cluster species identified included [4Fe-3S], [3Fe-3S], [3Fe-2S], [3Fe-S] and [2Fe-S] forms [21, 22]. The confirmation of the [3Fe-3S] cluster was important as this is a novel intermediate, first observed in the cluster degradation reaction of FNR upon exposure to oxygen [23]. An inorganic model $[3Fe\text{-}3S]^{3+}$ cluster was recently also described for the first time, in which all iron and sulfide ions were in the same molecular plane, forming a hexagonal arrangement [24]. Strikingly, the [3Fe-3S] intermediate may be a key feature of the conversion in Fe-S cluster proteins from [4Fe-4S] to [2Fe-2S], in which the coordinating ligands transition from tetrahedral coordination (for [4Fe-4S] cluster) to planar (for [2Fe-2S] cluster) [21].

The lability of the fourth iron is crucial in the iron sensing mechanism of RirA. The high sensitivity of the [4Fe-4S] cluster in RirA to low iron conditions is atypical, compared to

conventional [4Fe-4S] cluster proteins. Unlike more conventional [4Fe-4S] cluster proteins, such as the *Sv*WhiB and *Sv*WhiD described in these studies, RirA has only 3 highly conserved cysteines to coordinate the cluster; a fourth ligand has not been identified. One possibility is that RirA lacks an amino acid ligand to the 4th iron. Mutagenesis studies were based on Asp8, the fourth coordinating ligand of NsrR, and corresponding N8D and N8C variants were produced [25]. Characterisation of the N8D variant resulted in the RirA cluster becoming insensitive to low iron conditions and exhibiting the spectroscopic profile of a conventional [4Fe-4S] cluster protein and, strikingly, a CD spectrum reminiscent of NsrR. This suggests that the RirA has evolved a labile iron mechanism for sensing iron by having its cluster coordinated by only 3 cysteines, with the fourth iron likely coordinated a transient ligand such as water or hydroxide. The binding constant of the fourth, labile iron was also studied by a chelator competition assay. If the reversible [4Fe-4S] ⇌ [3Fe-4S] equilibrium is a key part of the mechanism, then the binding constant would be expected in the range of cellular free iron. Although the free cheatable iron within *R. leguminosarum* has not been determined, it is known for *E. coli* to be in the range of ~10 μM [26]. The competition assay was set up using the metal chelator mag-fura-2, and a binding constant was determined as ~3 μM, consistent with sensing of free iron in the cell.

In summary, this work provides new insights into *Streptomyces* Wbl proteins and their functions which rely on specific protein-protein interactions. The unusual characteristic observed for *Sv*WhiD to form a dimer via the C-terminal extension region was novel, but likely conserved in many WhiD homologues. Studies of the reaction of the WhiD: σ^{HrdB}_4 complex with O_2 and NO demonstrated that the interaction is well adapted to distinguish between the two signalling molecules. The unique collaborative nature of WhiB and WhiA was also explored and fundamental characterisation experiments of SvWhiA revealed a zinc-bound form that was competent for DNA binding. The direct binding of WhiB to DNA and its ability to enhance WhiA: DNA binding, provides a likely mechanism for which WhiA and WhiB specifically target genes involved in sporulation. Finally, this work further demonstrates the power of non-denaturing ESI-MS for the study of Fe-S cluster proteins, specifically here for both characterising the protein-

protein interaction of WhiD: σ^{HrdB}, and exploring the cluster breakdown reaction of RirA, in combination with ^{34}S-isotope substitution.

7.1. References

1. Glazebrook, M.A., et al., *Sporulation of* Streptomyces venezuelae *in submerged cultures.* J Gen Microbiol, 1990. **136**(3): p. 581-8.
2. Flardh, K. and M.J. Buttner, Streptomyces *morphogenetics: dissecting differentiation in a filamentous bacterium.* Nat Rev Microbiol, 2009. **7**(1): p. 36-49.
3. Smith, L.J., et al., Mycobacterium tuberculosis *WhiB1 is an essential DNA-binding protein with a nitric oxide-sensitive iron-sulfur cluster.* Biochem J, 2010. **432**(3): p. 417-27.
4. Crack, J.C., et al., *Mechanistic insight into the nitrosylation of the [4Fe-4S] cluster of WhiB-like proteins.* J Am Chem Soc, 2011. **133**(4): p. 1112-21.
5. Crack, J.C., et al., *Differentiated, promoter-specific response of [4Fe-4S] NsrR DNA binding to reaction with nitric oxide.* J Biol Chem, 2016. **291**(16): p. 8663-72.
6. Crack, J.C., et al., *Iron-sulfur clusters as biological sensors: the chemistry of reactions with molecular oxygen and nitric oxide.* Acc Chem Res, 2014. **47**(10): p. 3196-205.
7. Crack, J.C. and N.E. Le Brun, *Mass spectrometric identification of [4Fe-4S](NO)x Intermediates of nitric oxide sensing by regulatory iron-sulfur cluster proteins.* Chemistry, 2019. **25**(14): p. 3675-3684.
8. Stapleton, M.R., et al., Mycobacterium tuberculosis *WhiB1 represses transcription of the essential chaperonin GroEL2.* Tuberculosis (Edinb), 2012. **92**(4): p. 328-32.
9. Kudhair, B.K., et al., *Structure of a Wbl protein and implications for NO sensing by* M. tuberculosis*.* Nat Commun, 2017. **8**(1): p. 2280.
10. Sasaki, Y., et al., *Nitrogen oxide cycle regulates nitric oxide levels and bacterial cell signaling.* Sci Rep, 2016. **6**: p. 22038.
11. Crack, J.C., et al., *NsrR from* Streptomyces coelicolor *is a nitric oxide-sensing [4Fe-4S] cluster protein with a specialized regulatory function.* J Biol Chem, 2015. **290**(20): p. 12689-704.
12. Casonato, S., et al., *WhiB5, a transcriptional regulator that contributes to Mycobacterium tuberculosis virulence and reactivation.* Infect Immun, 2012. **80**(9): p. 3132-44.
13. Feng, L., et al., *Genome-wide characterization of monomeric transcriptional regulators in* Mycobacterium tuberculosis*.* Microbiology, 2016. **162**(5): p. 889-897.
14. Wan, T., et al., *Structural basis of non-canonical transcriptional regulation by the sigmaA-bound iron-sulfur protein WhiB1 in* M. tuberculosis*.* Nucleic Acids Res, 2020. **48**(2): p. 501-516.
15. Bush, M.J., et al., *Genome-wide chromatin immunoprecipitation sequencing analysis shows that WhiB Is a transcription factor that cocontrols its regulon with WhiA to initiate developmental cell division in* Streptomyces*.* mBio, 2016. **7**(2): p. e00523-16.
16. Singh, A., et al., Mycobacterium tuberculosis *WhiB3 maintains redox homeostasis by regulating virulence lipid anabolism to modulate macrophage response.* PLoS Pathog, 2009. **5**(8): p. e1000545.
17. Bush, M.J., et al., *Genes required for aerial growth, cell division, and chromosome segregation are targets of WhiA before sporulation in Streptomyces venezuelae.* mBio, 2013. **4**(5): p. e00684-13.
18. Bush, M.J., et al., *Multi-layered inhibition of* Streptomyces *development: BldO is a dedicated repressor of whiB.* Mol Microbiol, 2017. **104**(5): p. 700-711.
19. Hubin, E.A., et al., *Structural, functional, and genetic analyses of the actinobacterial transcription factor RbpA.* Proc Natl Acad Sci U S A, 2015. **112**(23): p. 7171-6.
20. Tabib-Salazar, A., et al., *The actinobacterial transcription factor RbpA binds to the principal sigma subunit of RNA polymerase.* Nucleic Acids Res, 2013. **41**(11): p. 5679-91.
21. Pellicer Martinez, M.T., et al., *Mechanisms of iron- and O2-sensing by the [4Fe-4S] cluster of the global iron regulator RirA.* Elife, 2019. **8**.

22. Pellicer Martinez, M.T., et al., *Sensing iron availability via the fragile [4Fe-4S] cluster of the bacterial transcriptional repressor RirA.* Chem Sci, 2017. **8**(12): p. 8451-8463.
23. Crack, J.C., et al., *Influence of the environment on the $[4Fe\text{-}4S]^{2+}$ to $[2Fe\text{-}2S]^{2+}$ cluster switch in the transcriptional regulator FNR.* J Am Chem Soc, 2008. **130**(5): p. 1749-58.
24. Lee, Y., et al., *A $[3Fe\text{-}3S]^{(3+)}$ cluster with exclusively mu-sulfide donors.* Chem Commun (Camb), 2016. **52**(6): p. 1174-7.
25. Volbeda, A., et al., *Crystal structures of the NO sensor NsrR reveal how its iron-sulfur cluster modulates DNA binding.* Nat Commun, 2017. **8**: p. 15052.
26. Keyer, K. and J.A. Imlay, *Superoxide accelerates DNA damage by elevating free-iron levels.* Proc Natl Acad Sci U S A, 1996. **93**(24): p. 13635-40.